TRANSPORTATION RESEARCH
RECORD

No. 1293

Pavement Design, Management, and Performance

Backcalculation of Pavement Moduli 1991

A peer-reviewed publication of the Transportation Research Board

TRANSPORTATION RESEARCH BOARD
NATIONAL RESEARCH COUNCIL
WASHINGTON, D.C. 1991

Transportation Research Record 1293
Price: $17.00

Subscriber Category
IIB pavement design, management, and performance

TRB Publications Staff
Director of Publications: Nancy A. Ackerman
Senior Editor: Naomi C. Kassabian
Associate Editor: Alison G. Tobias
Assistant Editors: Luanne Crayton, Kathleen Solomon, Norman Solomon
Graphics Coordinator: Diane L. Ross
Production Coordinator: Karen S. Waugh
Office Manager: Phyllis D. Barber
Production Assistant: Betty L. Hawkins

Printed in the United States of America

Library of Congress Cataloging-in-Publication Data
National Research Council. Transportation Research Board.

Backcalculation of pavement moduli, 1991.
p. cm.—(Transportation research record, ISSN 0361-1981; no. 1293)
Research papers from the 70th Annual Meeting of the Transportation Research Board held 1991 in Washington, D.C.
ISBN 0-309-05101-0
1. Pavements—Testing. 2. Nondestructive testing. I. National Research Council (U.S.). Transportation Research Board. Meeting (70th: 1991: Washington, D.C.) II. Series: Transportation research record ; 1293.
TE7.H5 no. 1293
[TE250]
388 s—dc20
[625.8] 91-18043
CIP

Sponsorship of Transportation Research Record 1293

GROUP 2—DESIGN AND CONSTRUCTION OF TRANSPORTATION FACILITIES
Chairman: Raymond A. Forsyth, Sacramento, California

Pavement Management Section
Chairman: R. G. Hicks, Oregon State University

Committee on Strength and Deformation Characteristics of Pavement Sections
Chairman: J. Brent Rauhut, Brent Rauhut Engineering, Inc.
Mark Anderson, Gilbert Y. Baladi, Richard D. Barksdale, Stephen F. Brown, Albert J. Bush III, Yu T. Chou, George R. Cochran, Billy G. Connor, Mark P. Gardner, Amir N. Hanna, R. G. Hicks, Lynne H. Irwin, William J. Kenis, Thomas W. Kennedy, Robert L. Lytton, Michael S. Mamlouk, Frank Meyer, Lutfi Raad, Richard B. Rogers, Byron E. Ruth, Stephen B. Seeds, Roger E. Smith, R. N. Stubstad, Marshall R. Thompson, Per Ullidtz, Jacob Uzan, Thomas D. White

Frank R. McCullagh, Transportation Research Board staff

The organizational units, officers, and members are as of December 31, 1990.

Transportation Research Record 1293

Contents

Foreword

This Record contains 13 papers on backcalculation of pavement moduli. Hossain and Zaniewski have developed an alternative approach for characterizing the falling weight deflectometer (FWD) deflection basin in the form $Y = A*e^{BX}$. Graves and Drnevich provide an overview of the various procedures required to calculate pavement deflections caused by impulse loadings accurately. Nazarian et al. have developed a cost-effective, rugged, and accurate calibration system for the FWD devices that can be utilized by state departments of transportation. Touma et al. evaluate the assumption of circular loaded area and uniform stress distribution under that area that is currently being used in linear-elastic theory backcalculation programs. The analysis indicated that significant errors in backcalculated moduli can occur when this assumption is invalid. Parker conducted a study to develop methods for using FWD measurements to determine moduli of in situ pavement materials, and although some inconsistencies in input to thickness design procedures may result, FWD moduli are recommended for characterizing in situ granular base-subbase. Hugo et al. evaluate the mobile load simulator and the role of accelerated pavement testing in Texas. They also present a methodology for including environmental effects. Magnuson et al. demonstrate the extraction of engineering properties of pavement layers by dynamic analysis of FWD data. They conclude that good agreement between experimental and computer-predicted data was obtained. Chou and Lytton compared backcalculation results from different agencies using various procedures; although the discrepancies among agencies can be large, good agreement was reached in many cases. The sources of systemic errors and ways to reduce them are discussed and an expert system approach is described. Ong et al. discuss the results from a finite element backcalculation program developed to account for dynamic effects. Sivaneswaran et al. describe a nonlinear least squares convergence method and its ability to backcalculate both the layer moduli and thickness. Lenngren presents a comparison of recorded strain at an instrumented road section with the strain obtained from backcalculation based on FWD data and found that the agreement between the two methods was good. Hall and Mohseni describe a straightforward procedure for backcalculation of AC/PCC pavement layer moduli. Hossain and Zaniewski present a new approach to the detection of a rigid layer at a shallow depth below the pavement using FWD deflection data. They also verified the procedure with field and manual backcalculation analysis.

Characterization of Falling Weight Deflectometer Deflection Basin

A. S. M. MUSTAQUE HOSSAIN AND JOHN P. ZANIEWSKI

Deflection basins from any nondestructive testing device can be characterized by parameters that describe the structural characteristics of an existing pavement. An exponential curve of the form $Y = A * e^{BX}$, where Y is the deflection in mils and X is the radial distance in inches, approximates the deflection basins simulated from elastic layer theory and measured by the falling weight deflectometer (FWD). The coefficients A and B describe the structural characteristics of the pavement. Usually, a pavement with a stiffer upper layer or layers is indicated by a lower A value, whereas a stiff subgrade or the presence of a rigid bottom at a shallow depth (or both) is indicated by a higher B value. The value of the coefficient of determination for the exponential fit, R^2, was found useful for judging the suitability of an FWD-measured basin for backcalculation of layer moduli in a deflection-matching technique. Generally, a low value of R^2 for an exponential curve fitted to an FWD-measured basin indicates that there will be a high error in the backcalculation of layer moduli using elastic layer theory. Guidelines are presented for using the value of R^2 to indicate the error between measured and computed deflections that can be expected during a backcalculation analysis.

Early static deflection devices could measure deflection at only one point. This point deflection was successfully related to the structural performance of the pavement by many researchers and was the basis for a number of overlay design methods. Later, vibratory devices, such as Dynaflect and Road Rater, provided deflection measurements near the load and at fixed distances from the load, resulting in a measured deflection basin. Falling weight deflectometers (FWDs) can measure deflection under the load and at a number of locations away from the load, resulting in a much larger basin. Thus, more information is expected from the FWD basin than from other devices.

Work of other researchers on FWD basin parameters to characterize the pavement is available (*1*,*2*). An approach for characterization of the FWD basin has been developed during this research. The objective was to find new parameters from the deflection basin that define the structural characteristics of the pavement.

INTERPRETATION OF DEFLECTION BASIN

Deflection basin parameters are widely used for three major applications: (*a*) to check the structural integrity of in-service pavements, (*b*) to relate to critical pavement response, and (*c*) to calculate the in situ layer moduli of the pavements. A number of basin parameters, which are functions of deflection values at one or more sensors, are available for characterization of deflection basins produced by the Dynaflect, Road Rater, and FWD. Table 1 summarizes deflection basin parameters available in the literature (*1*,*3*–*8*). Figure 1 shows the Dynaflect deflection basin parameters. The area parameter for the Road Rater deflection basin is shown in Figure 2. Table 1 indicates that not much effort has been made to characterize the deflection basin of FWDs.

College of Engineering and Applied Sciences, Arizona State University, Tempe, Ariz. 85287.

CHARACTERIZATION OF DEFLECTION BASINS FROM ELASTIC LAYER THEORY

The surface deflection basins for pavement systems from elastic layer theory can be characterized by Boussinesq's theory of linear-elastic half-space. Jung (*9*) has shown that the deflections (Y) on the top of the half-space around a concentrated load are a simple hyperbola with a linear term for the distance (X) from the load in the denominator:

$$Y = Z/X \tag{1}$$

For the quasi-concentrated FWD test load, the constant (Z) is

$$Z = P * A(1 - \nu^2)/Em \tag{2}$$

where

P = concentrated load,
A = radius of the loaded area,
ν = Poisson's ratio of the subgrade, and
Em = elastic stiffness of the subgrade (assuming infinite depth of the subgrade).

The computed surface deflections' distance from the load axis will closely follow the hyperbola given by Equations 1 and 2. Unfortunately, the equations are not valid when the subgrade is of finite depth (i.e., when a rigid layer is encountered below the subgrade at a shallow depth, say 120 in.). The equations are also not valid for nonlinear behavior of bases and subgrades. This necessitates the characterization of the deflection basin by some other method.

An empirical approach was taken to characterize the deflection basins from elastic layer theory. The intent was to find a characteristic curve with a minimum number of parameters that closely approximates the deflection basin. Several functional forms of equations were evaluated for fitting the deflection basin. An exponential curve was found to have the

TABLE 1 SUMMARY OF DEFLECTION BASIN PARAMETERS

Parameters	Definition	NDT Device	Reference
Dynaflect Maximum Deflection, DMD	$DMD = W_1$	Dynaflect	3
Surface Curvature Index, SCI	$SCI = W_1 - W_2$	Dynaflect Road Rater 400	3,4 3
Base Curvature Index, BCI	$BCI = W_4 - W_5$	Dynaflect	3
Spreadability, SP	$SP = \frac{\sum_{i=1,5} W_i}{5W_i} X\ 100$ $SP = \frac{\sum_{i=1,4} W_i}{4W_i} X 100$	Dynaflect Road Rater 2008	3,5
Basin Slope, SLOP	$SLOP = W_1 - W_5$	Dynaflect	5
W_5	$W_5 = W_5$	Dynaflect	6
Area (inch), A	$A = 6\,(1+2W_1/W_0+2W_2/W_0+W_3/W_0)$	Road Rater 2008, FWD	1
Shape Factors, F_1, F_2	$F_1 = (W_1-W_3)/W_2$ $F_2 = (W_2-W_4)/W_3$	Road Rater 2008, FWD	1
Tangent Slope, TS	$TS = (W_m-W_x)/x$	None	7
Deflection Ratio, Q_r	$Q_r = W_r/W_o$	FWD	8

W = Deflection; subscripts: 1,2,.... 5 = sensor locations

0 = center of load

r = radial distance

m = maximum deflection

x = distance of the tangent point from the point of maximum deflection

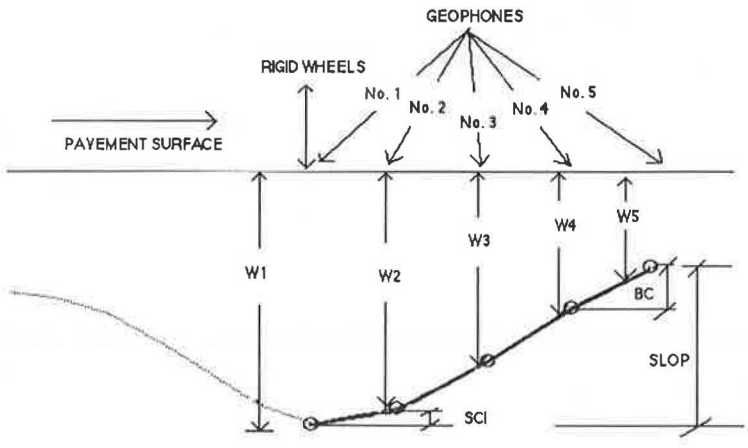

FIGURE 1 Dynaflect deflection basin parameters.

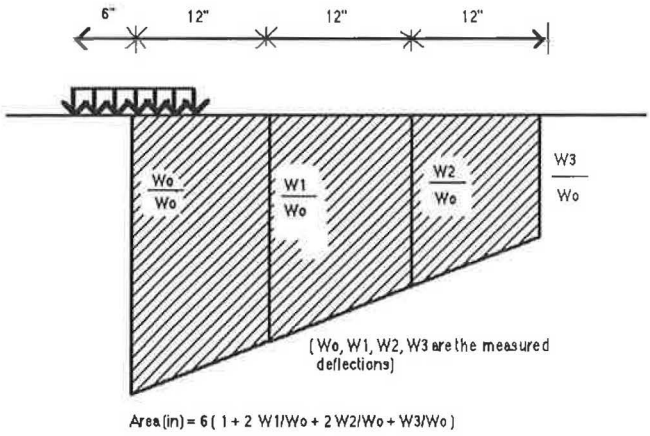

FIGURE 2 Road Rater deflection basin area parameter.

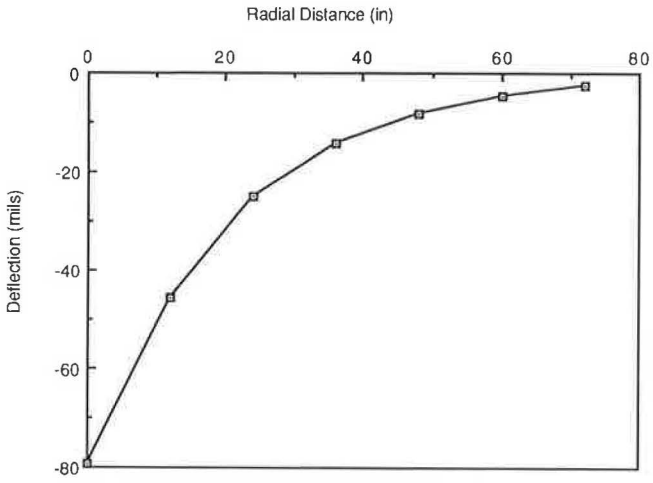

FIGURE 3 Typical exponential curve for fitting the deflection basin.

desired characteristics. The form of the equation is

$$Y = A * e^{BX} \tag{3}$$

where

Y = deflection value in mils,
X = radial distance from the load axis in inches, and
A, B = constants.

A typical shape for the exponential curve is shown in Figure 3.

Simulated deflection basins were generated by running the CHEVRON program (*10*), using a 9,000-lb load uniformly distributed over a circular area 11.8 in. in diameter and computing surface deflections at the load center and six other locations uniformly spaced at 12 in. The locations correspond to the typical sensor locations used by the Arizona Department of Transportation (ADOT) in FWD testing (*11*). The basins were generated by a combination of layer thickness and moduli in a matrix for five-layer pavement systems, as shown in Table 2.

In order to pick realistic pavement sections, the ADOT pavement management system data base was searched, and a frequency analysis of the structural number, SN (*12*), was done mile by mile to classify the pavements as stiff, medium, or weak. Table 3 gives the frequency analysis results. The target SNs selected on the basis of the frequency analysis corresponding to weak, medium, and stiff pavements were 3.0, 6.0, and 8.0, respectively. Layer thicknesses for 12 pavements from all roadway types in Arizona—Interstates, U.S. routes, and state routes—were statistically analyzed to find the representative thicknesses of layers corresponding to the target SNs. Because a sufficient number of pavement sections with a granular base and an SN of 8 were unavailable, the layer thicknesses of the stiff pavements were calculated to correspond to an SN of 8. Layer thicknesses for other pavements were selected on the basis of the statistical analysis shown in Table 4 and engineering judgment. Representative moduli values were selected on the basis of a literature search.

The matrix in Table 2 has eight factors each at three levels, yielding $3^8 = 6{,}561$ pavement structures having SNs between 1.51 and 7.98. The SNs were calculated by using the equation for SN in the *AASHTO Guide* (*12*). The drainage coefficients for the base and subbase layers were assumed to be unity, and the structural layer coefficients were computed from ADOT's *Materials Preliminary Engineering Design Manual* (*11*). An exponential curve with the form of Equation 3 was fitted to each deflection basin. Table 5 gives the summary statistics for A and B for each pavement type, and Table 6 shows the frequency distribution of R^2 for each pavement type. Figure 4 shows the CHEVRON and fitted basins for pavements of each category. These deflection basin shapes were qualitatively observed by Jung (*9*).

From Table 5, it is seen that the pavements fall into three distinct classes on the basis of the values of A. Again, the R^2 values indicate that exponential curves can be fitted to the CHEVRON deflection basins well.

The coefficient of determination, R^2, is an important diagnostic tool for judging the suitability of applying elastic layer theory for backcalculation of layer moduli. Figure 5 shows the CHEVRON and exponential curve–fitted deflection basins with low R^2. It is apparent that the deflection basin with a low R^2 will have a higher error in a deflection-matching technique. In general, the higher the value of the coefficient of determination, the lower will be the absolute sum of the percentage errors between the measured and the fitted deflection basin in a backcalculation routine. The absolute sum of the percentage errors between an exponential curve–fitted basin and the measured basin may be used as a limit for setting the lowest sum of percentage errors desired in the backcalculation process. Usually, the iteration should be carried out until the absolute sum of the percentage errors is less than or equal to that between the exponential curve–fitted and the measured deflection basins.

A high value of R^2 also indicates the suitability of modeling of pavements by elastic layer theory. Table 6 indicates that about 12 percent of pavements in the weak category have R^2 values less than 0.90, compared with less than 2.2 percent in the medium category and less than 1.1 percent in the stiff category. Thus, the frequency analysis of Table 6 indicates that, if an exponential curve of the form $Y = A * e^{BX}$ approximates the deflection basin closely, the application of

TABLE 2 PAVEMENT MATRIX USED FOR CHEVRON DEFLECTION BASIN GENERATION

	FACTORS							
LEVELS	T_{AC} (in)	T_{AB} (in)	T_{SM} (in)	D (in)	E_{AC} (ksi)	E_{AB} (ksi)	E_{SM} (ksi)	E_{SG} (ksi)
(1) LOW	3.0	4.0	9.0	120	100	15	10	3
(2) MED	6.0	4.0	12.0	240	450	30	20	7
(3) HIGH	10.0	6.0	18.0	s-i	850	50	30	14

Note: 1) D: Depth to Rigid Layer, s-i: semi-infinite subgrade

2) AC: Asphalt Concrete, AB: Aggregate Base, SM: Select Material/ Subbase, SG: Subgrade

TABLE 3 FREQUENCY ANALYSIS OF STRUCTURAL NUMBERS ON THE ARIZONA HIGHWAY SYSTEM

From	To Below	Frequency	Percent	Cumulative Percent
0.0	1.0	1144	16.37	16.37
1.0	2.0	1440	20.60	36.97
2.0	3.0	1353	19.36	56.33
3.0	4.0	2116	30.27	86.60
4.0	5.0	473	6.76	93.36
5.0	6.0	185	2.65	96.01
6.0	7.0	47	0.67	96.68
7.0	8.0	106	1.52	98.20
8.0	9.0	130	1.86	100.00

TABLE 4 REPRESENTATIVE THICKNESSES OF ARIZONA PAVEMENTS

SN	Statistic	T_{AC} (in)	T_{AB} (in)	T_{SM} (in)
3.0	Mean	4.0	4.0	9.0
	Std. Dev.	0.75	1.5	3.0
	Sample Size	12	12	12
6.0	Mean	7.25	4.0	13.5
	Std. Dev.	4.0	2.0	7.5
	Sample Size	12	12	12

Note: AC; Asphalt Concrete, AB; Aggregate Base, SM; Select Material/Subbase.

TABLE 5 SUMMARY STATISTICS FOR PARAMETERS OF THE CHEVRON BASINS

Pavement Type	Statistic	A	B	R^2
Weak	Mean	32.14	-.034	0.958
(3" AC)	Std. Dev.	12.12	-.009	0.048
	C.V. (%)	3.8	2.6	5.1
	Sample Size	2187	2187	2187
Medium	Mean	24.64	-.028	0.974
(6" AC)	Std. Dev.	9.52	-.008	0.021
	C.V. (%)	3.9	2.9	2.2
	Sample Size	2187	2187	2187
Stiff	Mean	18.07	-.020	0.976
(10" AC)	Std. Dev.	7.73	-.005	0.020
	C.V. (%)	4.3	2.5	2.0
	Sample Size	2187	2187	2187

TABLE 6 FREQUENCY ANALYSIS OF R^2 FOR SIMULATED DEFLECTION BASINS OF DIFFERENT PAVEMENT TYPES

Pavement Type	From	To Below	Frequency	%	Cumulative %
Weak	0.74	0.78	8	0.3	0.3
(3" AC)	0.78	0.82	45	2.1	2.4
	0.82	0.86	52	2.3	4.8
	0.86	0.90	156	7.1	11.9
	0.90	0.94	306	13.9	25.9
	0.94	0.98	730	33.3	59.3
	0.98	1.00	890	40.6	100.0
Medium	0.85	0.88	6	0.27	0.27
(6" AC)	0.88	0.91	42	1.92	2.19
	0.91	0.94	131	6.0	8.19
	0.94	0.97	342	15.63	23.82
	0.97	1.00	1601	73.2	97.02
	= 1.00		65	2.98	100.0
Stiff	0.85	0.88	2	0	0
(10" AC)	0.88	0.91	22	1	1.1
	0.91	0.94	102	4.66	5.76
	0.94	0.97	441	20.2	25.96
	0.97	1.00	1576	72.06	98.02
	= 1.00		44	1.98	100.0

elastic layer theory to thin pavements will result in a slightly higher error in backcalculation of layer moduli. The limitations of applying layer theory to thin pavements have also been demonstrated by Thrower et al. (*13*) and Yazdani and Scullion (*14*).

Low values of R^2 (e.g., less than 0.90) for CHEVRON basins are also indicative of other situations. Out of 308 deflection basins having R^2 values less than 0.90, 190 pavements are so-called "inverted" structures in which the modulus of an upper layer is smaller than the modulus of a lower layer. For 62 pavements the modulus of either the base or the subbase layer is close to that of the next layer, and others are extreme cases in which either a thin asphalt concrete (AC) layer of very low modulus exists in combination with stiff subgrades or a thick pavement with a high modulus is on a very weak subgrade. In general, these conditions may not be detected in a backcalculation process, but they can be used to explain some badly shaped deflection basins.

On the basis of the frequency analysis of R^2 in Table 6, the following guidelines are suggested for values of R^2 (corresponding to 99th percentile or greater values in the table) for deflection basins that can be backcalculated by elastic layer theory using an iterative technique without large errors:

If 3 in. $\leq$ AC thickness $<$ 6 in., R^2 should be greater than 0.78.

If 6 in. $\leq$ AC thickness, R^2 should be greater than 0.88.

Correlation tables were computed to investigate the relationships among *A*, *B*, SN, depth to rigid layer (D), and subgrade modulus (Esg), and *t*-tests were used to test significance. SN was assumed to quantify the stiffness of the upper layers. Table 7 is the correlation table for pavements with finite subgrade thicknesses of 120 and 240 in., and Table 8 shows the correlation table for pavements with semi-infinite subgrade. Table 7 indicates that for pavements with rigid layers at shallow depth, *A* is negatively correlated with both SN and Esg, but the correlation with SN is better. Thus, as SN or Esg increases, *A* decreases. *B* is positively correlated with SN (i.e., as the stiffness of the upper layers increases, *B* increases), whereas *B* is negatively correlated with Esg. *B* is also significantly correlated with D. As the depth decreases,

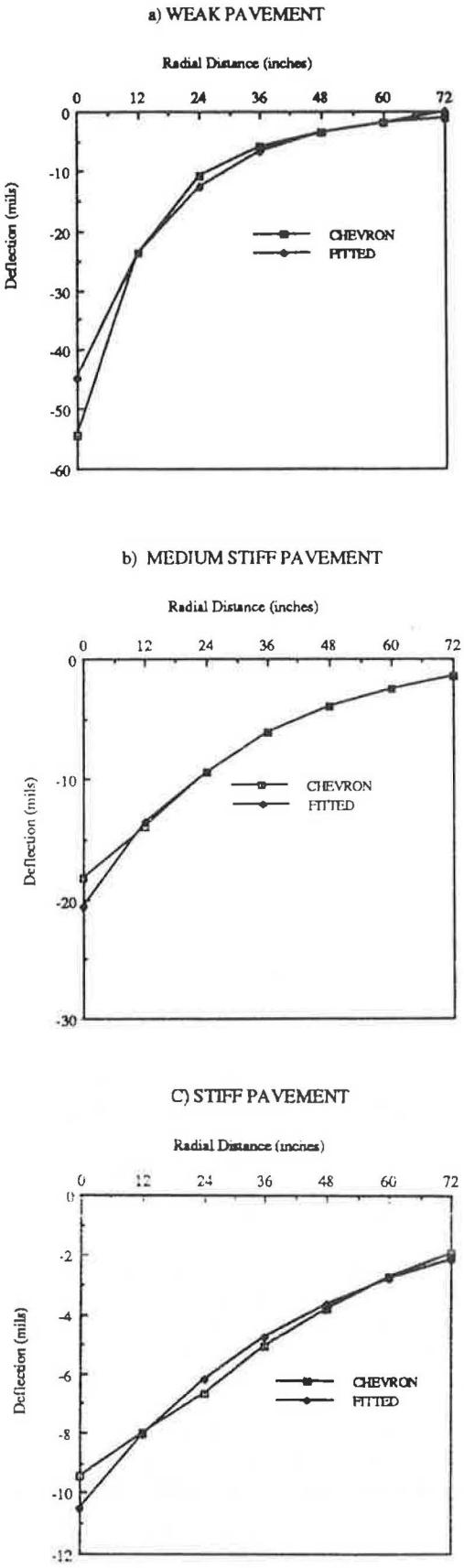

FIGURE 4 Actual and fitted deflection basins for different pavements.

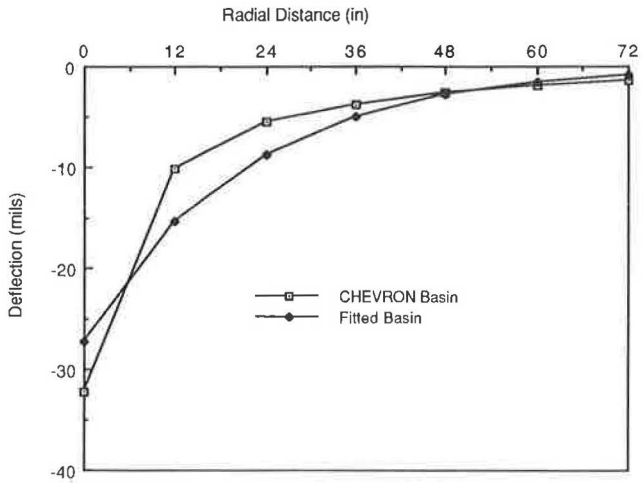

FIGURE 5 CHEVRON and exponential curve–fitted deflection basins with low R^2 (R^2 = 0.775).

B increases. For infinite subgrade, *A* is correlated with both SN and Esg. However, the subgrade modulus seems to be better correlated with *A* (Table 8). In this case, *B* is also correlated with SN and Esg. However, an increase in the stiffness of the upper layers results in an increase in the value of *B*, whereas an increase in Esg results in a decrease in the value of *B*.

Evidently these parameters describe the deflection basin structurally. They can be used to classify the pavements according to structural integrity for a network-level pavement management system. The combination of *A* and *B* is usually unique for a particular structural number when the subgrade characteristics are similar. Two pavements with similar structural numbers and subgrade moduli would yield deflection basins having identical *A* and *B* parameters. Figure 6 shows an example of such pavements from the matrix in Table 2. Because of the high correlation of *A* and *B* with Esg, they can be used in estimating Esg (see the companion paper in this Record by Hossain and Zaniewski).

VERIFICATION WITH FIELD DATA

Field deflection basins from sites in the Arizona State University overlay study (*15*) were used to verify the applicability

TABLE 7 CORRELATION AMONG *A*, *B*, SN, D, AND Esg FOR PAVEMENTS WITH FINITE DEPTH OF SUBGRADE

	A	B	SN	D	Esg
A	1.0	-.06	-0.68*	0.07	-0.60*
B		1.0	0.64*	0.33*	-0.63*
SN			1.0	0.0	0.0
D				1.0	0.0
Esg					1.0

* Significant at α = 5%

TABLE 8 CORRELATION AMONG *A*, *B*, SN, AND Esg FOR PAVEMENTS WITH INFINITE DEPTH OF SUBGRADE

	A	B	SN	Esg
A	1.0	0.09	-0.58*	-0.71*
B		1.0	0.68*	-0.68*
SN			1.0	0.0
Esg				1.0

* Significant at α = 5%

of the exponential curve–fitting technique in characterizing deflection basins. Table 9 gives the sites used in this study, and Table 10 shows the pavement sections of the sites. Deflection testing was done using the Dynatest Model 8002 FWD on the outer wheelpath of the travel lane at these sites. Deflections were measured at 10 stations at each site, spaced at 10-ft intervals. The target load was 9,000 lb, and seven sensors were arranged at a uniform spacing of 12 in., the first sensor being at the center of the load.

For each site, Table 11 shows Parameters *A* and *B*; the coefficient of determination, R^2, of the exponential curve–fitted deflection basins; and the structural number, subgrade modulus, and depth to rigid layer. Figure 7 shows the actual and fitted FWD basins for two sites. Figure 7 indicates that the fitted basins closely approximate the shapes of the FWD-measured basins.

Table 11 indicates that the exponential curve fits the FWD-measured deflection basins well, with R^2 values varying from 0.856 to 0.996. In order to find the relationships between *A*, *B*, SN, backcalculated subgrade modulus, and calculated depth to rigid layer, Tables 12 and 13 were formed for pavements having finite and infinite subgrade thicknesses, respectively. Student's *t*-tests were used to determine significance. Table 12 indicates that *A* is significantly correlated with SN and D. As SN (the stiffness of upper layers) increases, *A* decreases. Again, when the depth of the rigid layer increases, *A* increases. There is no significant correlation between *A* and the backcalculated subgrade modulus. However, the trend shows that as the subgrade modulus decreases, *A* increases. *B* is significantly correlated with SN and the backcalculated modulus of the subgrade. The trend is similar to that of the CHEVRON basins. *B* increases with increasing SN and decreases with increasing backcalculated subgrade modulus. For FWD basins, *B* is not significantly correlated with the depth to the rigid layer. But the trend suggests that as the depth to rigid layer increases, *B* decreases.

Table 13 indicates that when the subgrade is semi-infinite, *B* is significantly influenced by the subgrade modulus. As the subgrade modulus increases, *B* decreases. Though no significant correlation exists among *A*, SN, and backcalculated subgrade modulus, trends are similar to those observed for the CHEVRON basins. The relationship between *B* and SN follows the same trend as for the CHEVRON basins.

For FWD-measured basins, the backcalculated subgrade modulus is significantly correlated with SN for both finite and infinite subgrades. Because SN is largely influenced by the thickness of the layers above the subgrade, it is clear that the backcalculation of the subgrade modulus is influenced by the thickness of the upper layers.

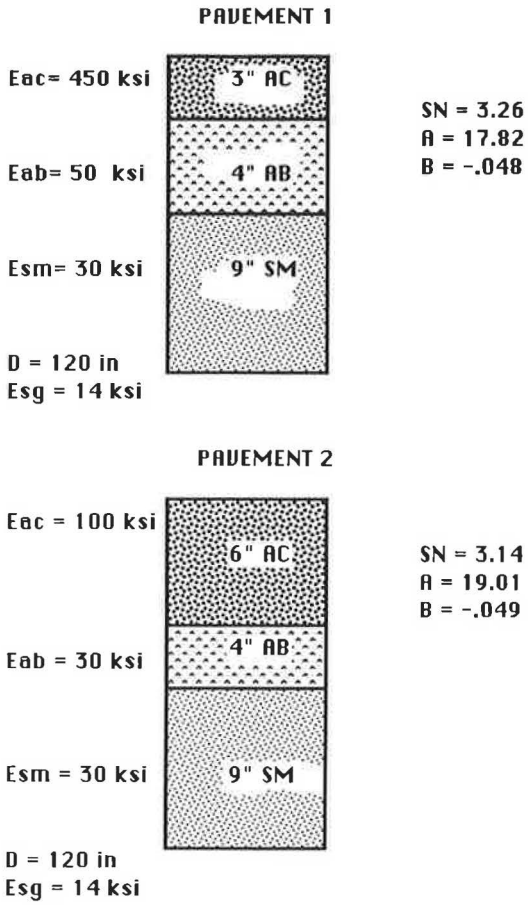

FIGURE 6 *A* **and** *B* **for pavements with similar SNs.**

A, *B*, and R^2 are important diagnostic tools for identifying the deflection basins. For example, Sites 3 and 4 are adjacent pavement sections with the same structural number and subgrade modulus. The pavements were tested at identical loads and temperatures. The *A* and *B* values for FWD deflection basins on these pavements are remarkably similar. Thus, *A* and *B* values of normalized deflection basins can be used to define the structural integrity of the pavements in a network-level pavement management system. The approach may also be useful in subsectioning a project when a rehabilitation is considered without backcalculating layer moduli for individual deflection basins. However, more study is needed to decide this point.

INTERPRETATION OF ERROR IN BACKCALCULATION

The sum of the absolute percentage errors between a measured basin and an exponential curve–fitted basin can be used as a guideline for how far the iteration should be carried or for setting the tolerance for the sum of absolute percentage errors in a backcalculation routine using elastic layer theory. The BKCHEVM (*16*) backcalculation program was used to backcalculate the layer moduli of a number of the sites of

TABLE 9 LOCATION OF TEST SITES AND PAVEMENT TYPES

Site	Location	Route	Mile Post	Pavement Type
1	Benson	I10W	300.07	5-layer
3	Winslow	I40E	260.21	4-layer
4	Minnetonka	I40E	261.78	4-layer
5	Dead River	I40E	317.06	4-layer
6	Flagstaff	I17N	337.00	4-layer
7	Crazy Creek	I40E	323.78	4-layer
9	Sunset Point	I17N	251.41	5-layer
10	Seligman	I40W	131.71	4-layer
12	Benson East	I10W	303.00	4-layer
14	Jacob Lake	US89AN	578.00	4-layer
18	Morristown	US60W	120.00	4-layer
19	McNary	US260E	369.00	5-layer
20	Kingman	I40E	59.00	4-layer

TABLE 10 LAYER TYPES AND THICKNESSES AT DIFFERENT SITES

Site/ Sta	Layer 1		Layer 2		Layer 3		Layer 4		Layer 5	
	Mat	Thk (in)	Mat	Thk (in)	Mat	Thk (in)	Mat	Thk (in)	Mat	Thk (in)
1/1	AC	7	BS	2.5	AB	2	SB	12	SC-SM*	
3/1	AC	12	BTB	3	SB	5	SM*	-	-	-
4/1	AC	11.5	BTB	2	SB	3	SM*	-	-	-
5/1	AC	8	CTB	4.5	SB	7	SM*	-	-	-
6/1	AC	9	AB	4	SB	12	-	-	-	-
7/1	AC	8	CTB	6	SB	6	SM*	-	-	-
9/1	AC	6	BS	4	SB	26	SGS	6	CL-CH*	-
10/1	AC	6	AB	6	SB	24	CH*	-	-	-
12/1	AC	6	AB	6	SB	18	SC-SM*	-	-	-
14/1	AC	9	BS	4	AB	4	SC-CH*	-	-	-
18/1	AC	4.25	AB	4	SB	15	-	-	-	-
19/1	AC	4.8	BS	2.2	AB	3	SB	6		
20/1	AC	9.5	AB	4	SB	15	-	-		

* Subgrade Classification based on Unified Method.

Note: AC: Asphalt Concrete, BS: Bituminous Surface, BTB: Bituminous Treated Base, CTB: Cement Treated Base, AB: Aggregate Base, SGS: Subgrade Seal, SB: Sub Base (Select Material)

TABLE 11 CHARACTERISTICS OF FITTED FWD DEFLECTION BASINS

Site/ Sta [1]	FWD Test Temp (^{O}F)	A	B	R^2	SN	Esg^2 (ksi)	D^2 (in)
1/1	70	17.79	-.0510	0.984	3.58	18	140
3/7	64	7.89	-.0221	0.994	5.30	20	>480 [3]
4/1	64	7.27	-.0211	0.986	5.30	20.5	>480 [3]
5/1	55	10.23	-.0261	0.977	5.32	7	85
6/1	43	7.55	-.0221	0.981	6.37	6.5	60
7/4	61	17.58	-.0296	0.985	5.24	13.5	>480 [3]
9/1	70	12.80	-.0334	0.996	3.94	8.5	72
10/1	48	16.18	-.0336	0.995	6.52	19	>480 [3]
12/1	62	15.46	-.0403	0.988	4.42	10.5	100
14/4	97	15.85	-.0539	0.856	0.97	25	120
18/1	71	9.74	-.0430	0.924	4.08	50	>480 [3]
19/1	31	19.03	-.0325	0.996	2.06	10	240
20/1	61	7.38	-.0413	0.948	4.30	45	150

Notes:
1. Station locations correspond to drilling and cone penetration test sites
2. Computed from manual matching of deflection basins (After Mamlouk et al. (15))
3. D > 480 in. signifies semi-infinite subgrade

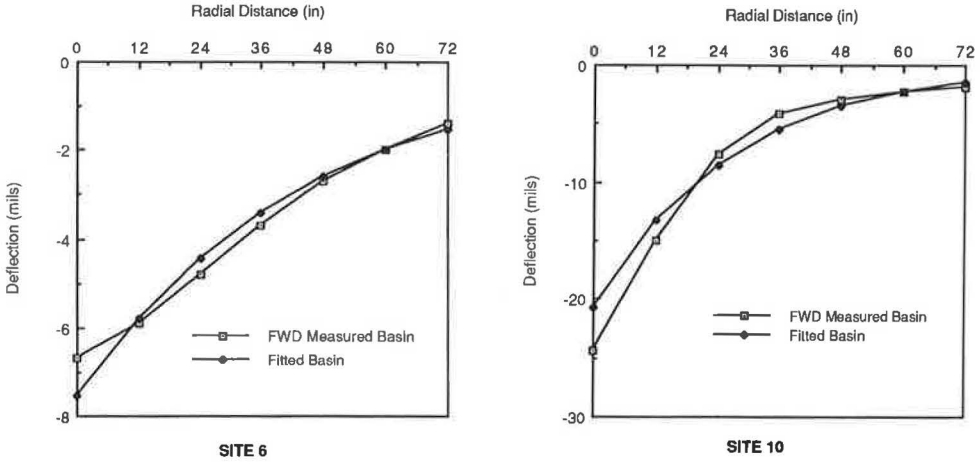

FIGURE 7 FWD-measured and fitted deflection basins for Sites 6 and 10.

TABLE 12 PAVEMENTS WITH FINITE DEPTH OF SUBGRADE—CORRELATION AMONG *A*, *B*, SN, D, AND Esg FOR FWD DEFLECTION BASINS

	A	B	SN	D	Esg
A	1.0	-.53**	-.73*	0.57*	-.24
B		1.0	0.68*	-0.26	-0.54**
SN			1.0	-0.61*	-0.27
D				1.0	0.29
Esg					1.0

* Significant at α = 5%
** Significant at α = 10%

TABLE 13 PAVEMENTS WITH INFINITE DEPTH OF SUBGRADE—CORRELATION AMONG *A*, *B*, SN, AND Esg FOR FWD DEFLECTION BASINS

	A	B	SN	Esg
A	1.0	-.33	-0.45	-0.36
B		1.0	0.37	-0.75*
SN			1.0	0.75*
Esg				1.0

* Significant at α = 10%

Table 9. Table 14 shows the sum of the absolute percentage errors from backcalculation and that from the exponential fit. It is evident that the better the exponential fit, the lower is the sum of absolute percentage errors. In all cases except two, the error in the BKCHEVM calculation is less than that from the exponential fit. Therefore, the iteration for deflection matching should be carried out until the error from backcalculation is less than that from the exponential fit; in other words, the tolerance should be based on the sum of the absolute error percentages in the exponential fit. However, the tolerance should also be based on the desired accuracy and the cost of computation.

The results from BKCHEVM also support the recommendation for values of R^2 presented earlier for deflection basins that are suitable for backcalculation with an iteration technique using the elastic layer theory without large error. For example, Site 14 has an AC thickness of 9 in. For this AC thickness, R^2 for an exponentially fitted basin should be greater than or equal to 0.88 if the backcalculation is to be done without large errors. But the R^2 value for the deflection basin at this site is 0.856, resulting in an absolute error of 214.3 percent. Figure 8 shows the actual FWD-measured and exponential curve–fitted deflection basins for this site. From the figure, it appears that the FWD-measured basin has an unusual shape that can be explained by judging the value of R^2 of the exponential fit. Thus, in the deflection-matching scheme, a high error tolerance should be used to terminate the iteration process for this basin.

CONCLUSIONS

An alternative approach was developed for characterizing the FWD deflection basin. An exponential curve of the form $Y = A * e^{BX}$, where Y is the deflection in mils and X is the radial distance in inches, was suggested for approximating deflection basins simulated from elastic layer theory and measured by the FWD. The coefficients A and B appear to describe the pavement structurally. Recommendations were made to classify pavements on the basis of the values of A and B for network-level pavement classification or subsectioning a project when a rehabilitation is considered. The value of the coefficient of determination of the exponential fit, R^2, was found useful for judging the suitability of an FWD-measured basin for backcalculation of layer moduli in a deflection-matching technique. Values of R^2 were suggested for back-

TABLE 14 SUM OF ABSOLUTE PERCENTAGE ERRORS FOR FWD DEFLECTION BASINS

Site/Station	R^2	BKCHEVM Error (%)	EXP. Fit Error (%)
4/1	0.986	28.0	37.5
5/1	0.977	90.0	51.0
7/4	0.985	16.1	54.7
9/1	0.996	8.4	31.5
10/1	0.995	8.3	34.1
12/1	0.988	16.7	77.68
14/4	0.856	214.3	329.76
18/1	0.924	42.9	192.4
19/1	0.996	39.2	28.4
20/1	0.948	39.6	142.9

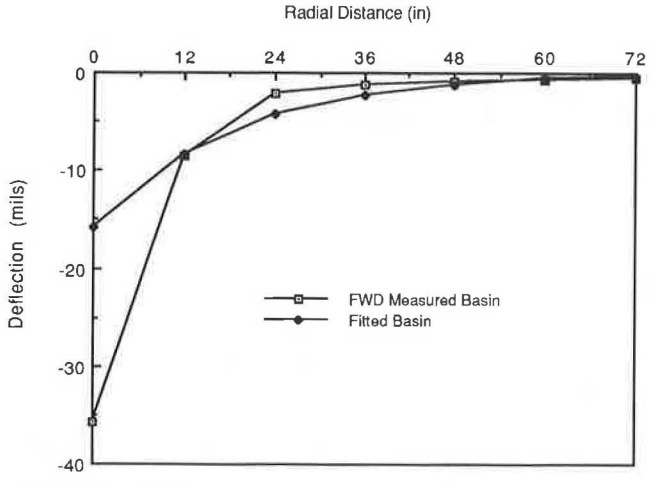

FIGURE 8 FWD-measured and fitted deflection basins for Site 14.

calculation of layer moduli in an iteration scheme using elastic layer theory. Guidelines were presented for using the value of R^2 to indicate the error between measured and computed deflections that can be expected during a backcalculation analysis.

REFERENCES

1. M. S. Hoffman and M. R. Thompson. Backcalculating Nonlinear Resilient Moduli from Deflection Data. In *Transportation Research Record 852*, TRB, National Research Council, Washington, D.C., 1982, pp. 42–51.
2. E. Horak. The Use of Surface Deflection Basin Measurements in the Mechanistic Analysis of Flexible Pavements. *Proc., 6th International Conference on Structural Design of Asphalt Pavements*, Ann Arbor, Mich., Vol. 1, 1987, pp. 990–1,001.
3. K. Majidzadeh. *Pavement Condition Utilizing Dynamic Deflection Measurements*. Research Report OHIO-DOT-13-77. FHWA, U.S. Department of Transportation, 1977.
4. W. P. Kilareski and B. A. Anani. Evaluation of In Situ Moduli and Pavement Life from Deflection Basin. *Proc., 5th International Conference on Structural Design of Asphalt Pavements*, Delft, the Netherlands, Vol. 1, 1982, pp. 349–366.
5. N. K. Vaswani. Method for Separately Evaluating Structural Performance of Subgrades and Overlaying Flexible Pavements. In *Highway Research Record 362*, HRB, National Research Council, Washington, D.C., 1971, pp. 48–62.
6. A. Taute, B. F. McCullough, and W. R. Hudson. *Improvements to the Material Characterization and Fatigue Life Prediction Methods of the Texas Rigid Pavement Overlay Design Procedure*. Research Report 249-1. Center for Transportation Research, The University of Texas at Austin, Austin, 1981.
7. A. F. Stock and J. Yu. Use of Surface Deflection for Pavement Design and Evaluation. In *Transportation Research Record 954*, TRB, National Research Council, Washington, D.C., 1984.
8. A. J. M. Classen, C. P. Valkering, and R. Ditmarsch. Pavement Evaluation with the Falling Weight Deflectometer. *Proc., Association of Asphalt Paving Technologists*, Vol. 45, 1976.
9. F. W. Jung. Interpretation of Deflection Basin for Real-World Materials in Flexible Pavements. Presented at 69th Annual Meeting of the Transportation Research Board, Washington, D.C., 1990.
10. L. J. Painter. *CHEVRON N-Layer Program—Improved Accuracy*. California Research Corporation, Richmond, Calif., 1980.
11. *Materials Preliminary Engineering Design Manual*, 3rd ed. Arizona Department of Transportation, Phoenix, 1989.
12. *AASHTO Guide for Design of Pavement Structures*. AASHTO, Washington, D.C., 1986.
13. E. N. Thrower, N. W. Lister, and J. F. Potter. Experimental and Theoretical Studies of Pavement Behavior Under Vehicular Loading in Relation to Elastic Theory. *Proc., 3rd International Conference on Structural Design of Asphalt Pavements*, London, 1972, pp. 521–535.
14. J. I. Yazdani and T. Scullion. Comparing Measured and Theoretical Depth Deflections Under a Falling Weight Deflectometer Using a Multidepth Deflectometer. In *Transportation Research Record 1260*, TRB, National Research Council, Washington, D.C., 1990, pp. 216–225.
15. M. S. Mamlouk, W. N. Houston, S. L. Houston, and J. P. Zaniewski. *Rational Characterization of Pavement Structures Using Deflection Analysis*. Report FHWA-AZ 88-254, Vol. 1. Arizona Department of Transportation, Phoenix, 1988.
16. BKCHEVM, Modified Microcomputer Version of CHEVDEF Backcalculation Program. Modified in the project *Rational Characterization of Pavement Structures Using Deflection Analysis*, Project HPR-PL-1(31)-254, Arizona Department of Transportation, Phoenix, 1988.

Calculating Pavement Deflections with Velocity Transducers

R. CLARK GRAVES AND VINCENT P. DRNEVICH

Pavement engineers and researchers agree that valuable information can be obtained from surface deflection basin measurements of pavements. Several methods of applying a load to the pavement to cause pavement deflections have been used for many years, including static, vibratory, and impulse types of loadings. Vibratory and impulse loadings typically use velocity transducers to measure the corresponding surface deflections. Methods used to calculate pavement deflections caused by impulse loadings are complex. A good understanding of signal analysis and the theory of vibration is needed to accurately calculate pavement deflections from the transducer outputs. An overview of the various procedures required to accurately calculate these deflections is provided. A three-part study has been conducted: theoretical modeling of the transducer response, laboratory calibration of the transducer response, and comparison of independently determined deflections with those from an impulse loading test, referred to as a falling weight deflectometer.

In the past few years, there has been increasing interest in the long-term monitoring of pavement performance. Nondestructive testing has proven to be a good tool for evaluating the structure of in-service pavements.

Pavement engineers and researchers agree (*1*) that pavement surface deflection basin measurements, nondestructive tests, provide valuable information on the structural condition of pavement systems. Pavement deflections depend on the magnitude and mode of loading (steady state, impulse, or vehicular). The ideal response measurements for structural evaluation are those produced under actual design traffic loads, but these are not practical now (*1*).

Several techniques have been used for nondestructive pavement testing. They are typically divided into three categories: static deflection measurements, steady-state vibration deflection measurements, and impulse deflection measurements.

The steady-state and impulse devices both use velocity transducers to calculate pavement deflections. However, the method of deflection calculation is considerably different for the impulse devices because of the nature of the loading. The steady-state devices operate at a fixed frequency, which is normally in the linear range of the transducers. Therefore, a direct integration of the transducer output provides the pavement deflection.

Impulse testing is generally conducted with a falling weight deflectometer (FWD). A weight is lifted a given height above the pavement and dropped onto a spring-buffer system. The spring-buffer system transfers the load to the pavement over approximately 30 msec. The load applied to the pavement and the vertical motions at various radial distances from the center of the load are measured by using velocity transducers. The load is adjusted by varying the drop height and the weight. The deflections at the radial distances are calculated from the outputs of the velocity transducers.

Impulse-testing devices generate a transient response, which has frequency components that are predominantly between 0 and 100 Hz. Because the response of the velocity transducer is not constant across the entire frequency range, a direct integration of the transducer output does not provide the displacement of the pavement. The response characteristics of the transducer across the entire frequency range are required to calculate accurate pavement deflection time histories.

The goal of this study was to gain a better understanding of the transducers typically used with FWD measurements, to evaluate their accuracy, and to develop a technique for obtaining accurate pavement displacement time histories. A three-phase study was conducted: theoretical modeling of the transducer response, laboratory calibration and validation of the transducer response, and comparison of independently determined deflections with those from an impulse loading test using an FWD (*2*). This research confirms and builds on the information presented by Nazarian and Bush (*3*) for the frequency response function approach.

PHASE 1: THEORETICAL TRANSDUCER RESPONSE

Background

Velocity transducers (geophones) may be modeled as damped single-degree-of-freedom (SDOF) systems. Geophones are typically coil-magnet systems, as shown in Figure 1. A mass having an attached magnetic coil (labeled "conductor" in Figure 1) is suspended from the case with a spring. On impact, the magnetic field moves and the mass remains relatively still. This causes a relative motion between the coil (mass) and the transducer case (magnetic field). The voltage generated by this motion is proportional to the velocity of the coil relative to the transducer case. Depending on the frequency range, the velocity of the coil relative to the case may or may not be the actual velocity of the transducer case. When measurements are obtained at either the low or the high end of the transducer's frequency range, the output is usually not the actual velocity response of the transducer case. However, for a range of frequencies, the transducer response is directly

R. C. Graves, Kentucky Transportation Center, University of Kentucky, 533 South Limestone Street, Lexington, Ky. 40506. V. Drnevich, Department of Civil Engineering, University of Kentucky, 212 Anderson Hall, Lexington, Ky. 40506.

proportional to the actual velocity response of the transducer case, and it is independent of frequency. This concept is better shown in Figure 2, in which a velocity transducer output divided by actual velocity is plotted versus frequency. Between the points labeled A and B in Figure 2, the response of the transducer does not significantly change with frequency. However, below Point A and above Point B, the response of the transducer is frequency dependent.

Because the response of the pavement usually occurs in the frequency range 0 to 100 Hz, the frequency-dependent response function must be used to calculate the actual velocity from the given transducer output if accurate velocities are desired for the entire time history (*2*,*3*).

Transducer Simulation

To properly describe the velocity transducer as an SDOF system, the following characteristics must be known: undamped natural frequency, f_n, mass of the suspended body, m, and the damping ratio (fraction of critical damping, ξ). From these parameters, others, such as critical damping, spring constant, and undamped natural angular frequency, may be calculated (*5*).

A typical spring-mass system representing a velocity transducer is shown in Figure 3. The following displacements may

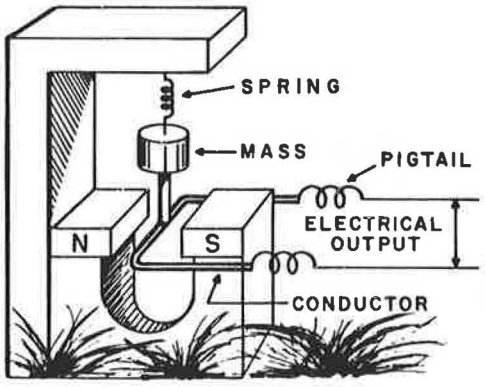

FIGURE 1 Typical transducer configuration (*4*).

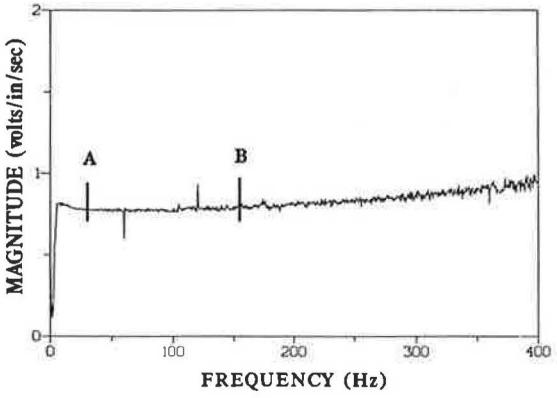

FIGURE 2 Typical transducer frequency response curve.

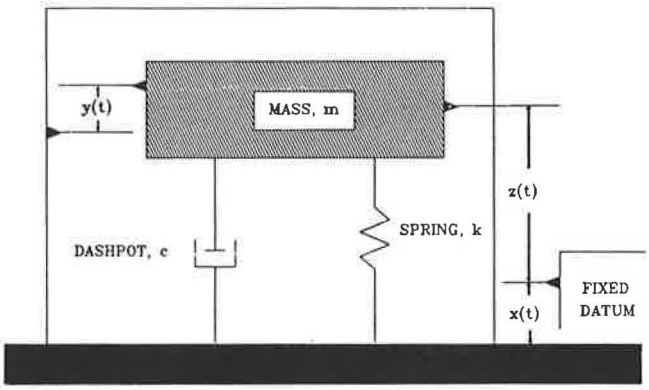

FIGURE 3 Typical spring mass system.

be defined: $y(t)$ is the displacement between the mass and the transducer case; $x(t)$ is the displacement of the pavement (with attached transducer case) relative to a fixed datum; and $z(t)$ is the absolute displacement of the mass, defined as follows:

$$z(t) = x(t) + y(t) \tag{1}$$

If the pavement undergoes a movement $x(t)$, the response to the system may be derived from the equation of motion stating that the summation of forces in the vertical direction (including inertial forces) must equal zero. From a free-body diagram the following forces may be determined: the inertial force $m \cdot \ddot{z}(t)$, the spring force $k \cdot y(t)$, and the damping force $c \cdot \dot{y}(t)$. Summation of these forces yields the following:

$$m \cdot \ddot{z}(t) + c \cdot \dot{y}(t) + k \cdot y(t) = 0 \tag{2}$$

Substituting Equation 1 into Equation 2 and dividing both sides by the mass yields

$$\ddot{x}(t) + \ddot{y}(t) + \dot{y}(t)\frac{c}{m} + y(t)\frac{k}{m} = 0 \tag{3}$$

This equation may be solved for the pavement acceleration, $\ddot{x}(t)$, in terms of the acceleration, velocity, and displacement of the mass relative to the case.

$$\ddot{y}(t) + \dot{y}(t)\frac{c}{m} + y(t)\frac{k}{m} = -\ddot{x}(t) \tag{4}$$

Substitution of the known transducer characteristics of damping and natural frequency into Equation 4 gives

$$\ddot{y}(t) + \dot{y}(t)2\xi\omega_n + y(t)\omega_n^2 = -\ddot{x}(t) \tag{5}$$

where $\omega = 2\pi f_n$.

Equation 5 is the time domain representation of the SDOF system in Figure 3. Using Fourier analysis as presented by Ramirez (*6*), an equivalent equation of motion may be determined in the frequency domain. Taking the Fourier transform of both sides gives

$$\ddot{Y}(\omega) + \dot{Y}(\omega)2\xi\omega_n + Y(\omega)\omega_n^2 = -\ddot{X}(\omega) \tag{6}$$

where ω is the circular frequency ($2\pi f$) and $Y(\omega)$, $\dot{Y}(\omega)$, and

$\ddot{Y}(\omega)$ are the Fourier transforms of the displacement, velocity, and acceleration, respectively. Integration in the frequency domain is accomplished by multiplying the function by $(j\omega)^{-1}$, where $j = \sqrt{-1}$. Differentiation may be accomplished by multiplying the function by $j\omega$. Performing these operations leads to

$$\ddot{Y}(\omega) = -\omega^2 Y(\omega) \tag{7}$$

$$\dot{Y}(\omega) = j\omega Y(\omega) \tag{8}$$

and

$$\ddot{X}(\omega) = -\omega^2 X(\omega) \tag{9}$$

Substitution of these equations into Equation 6 yields

$$-\omega^2 Y(\omega) + 2\xi j\omega\omega_n Y(\omega) + Y(\omega)\omega_n^2 = -\omega^2 X(\omega) \tag{10}$$

Solving for $X(\omega)$ in terms of $Y(\omega)$ gives

$$X(\omega) = Y(\omega)\left(\frac{-\omega^2 + \omega_n^2 + 2\xi j\omega\omega_n}{-\omega^2}\right) \tag{11}$$

which, on rearrangement, becomes

$$X(\omega) = Y(\omega)\left[1 - \left(\frac{\omega_n^2}{\omega^2}\right) - \frac{2\xi j\omega\omega_n}{\omega^2}\right] \tag{12}$$

The inverse of the term in brackets in Equation 12 is called a transfer function of the transducer, because it is the system output divided by the system input. It is denoted by $H(\omega)$. Thus,

$$H(\omega) = \left[1 - \left(\frac{\omega_n^2}{\omega^2}\right) - \frac{2\xi j\omega\omega_n}{\omega^2}\right]^{-1} \tag{13}$$

Pavement Response Simulation

The pavement motion, which is the input to the velocity transducer, also may be simulated by using another equivalent SDOF model. As mentioned earlier, several system parameters must be defined to characterize the SDOF system. The parameters used for the velocity transducer and for the pavement are given in the following table.

Parameter	*Velocity Transducer*	*Pavement*
Natural frequency, f_n (Hz)	4.5	100
Damping ratio, ξ	0.6	0.4
Spring constant, k (lb/in.)	0.0867	1,000,000

Computer Simulation of the SDOF System

The solution to both SDOF models has been completed using the computer program DIRECT developed by Paz (*7*). The method of solution is exact for excitations that may be described by linear segments between points defining the excitation function. This is accomplished by linear interpolation between the data points. The response of each time interval is calculated by considering the initial conditions and a linear excitation during the interval. The values calculated are the displacement, velocity, and acceleration time histories for the model given by the input parameters.

In this study, several types of forcing functions were applied to the pavement model (Figure 4). All the forcing functions have a duration of 0.025 sec and a maximum amplitude of 10,000 lb. Each forcing function, defined by 256 points, was entered into the computer program, and the resulting pavement displacement time histories were calculated.

In modeling the response of the velocity transducer on the pavement according to Equation 11, the acceleration of the pavement is used as the input excitation to the transducer. DIRECT was used again with the velocity transducer parameters and the pavement acceleration as input. A solution was determined for each of the forcing functions shown in Figure 4.

As indicated in Table 1, a change in shape of the forcing function changes the peak displacement response of the system, even when the duration and maximum input force are the same. This indicates that pavement deflection basins will vary somewhat from device to device for given peak force inputs. Although current convention (*1,3*) utilizes peak input force and peak displacements, better correlation among different devices could be obtained by using techniques such as root-mean-square (RMS) values (*8*) of both input force and measured displacement. In order to obtain RMS values of displacement, the entire time history must be accurately determined.

Pavement Displacement Determination from Velocity Transducer Model

A comparison of the pavement displacements from the pavement model with the integrated velocity transducer model outputs, which are the displacements of the mass relative to the transducer case, indicates that they are not the same. The results for the half-sine pulse are shown in Figure 5. The results for each forcing function are given in Table 1. Besides having different peak values, the integrated values are in error at all times and have peaks occurring at times different from the pavement model peak displacements.

Frequency Response Method for Displacement Calculations

The frequency response function given in Equation 13 is a true transfer function between pavement displacement and transducer displacement. It may be modified to calculate the pavement response (displacement) from the given transducer output.

Solving Equation 12 for the pavement response in terms of the velocity transducer output gives the following:

$$X(\omega) = \dot{Y}(\omega)\left[\frac{1}{j\omega} - \left(\frac{\omega_n^2}{\omega^2 j\omega}\right) - \frac{2\xi\omega_n}{\omega^2}\right] \tag{14}$$

A transfer function, $H_v(\omega)$, may be defined as the ratio between the velocity transducer output $\dot{Y}(\omega)$ and the pavement displacement $X(\omega)$.

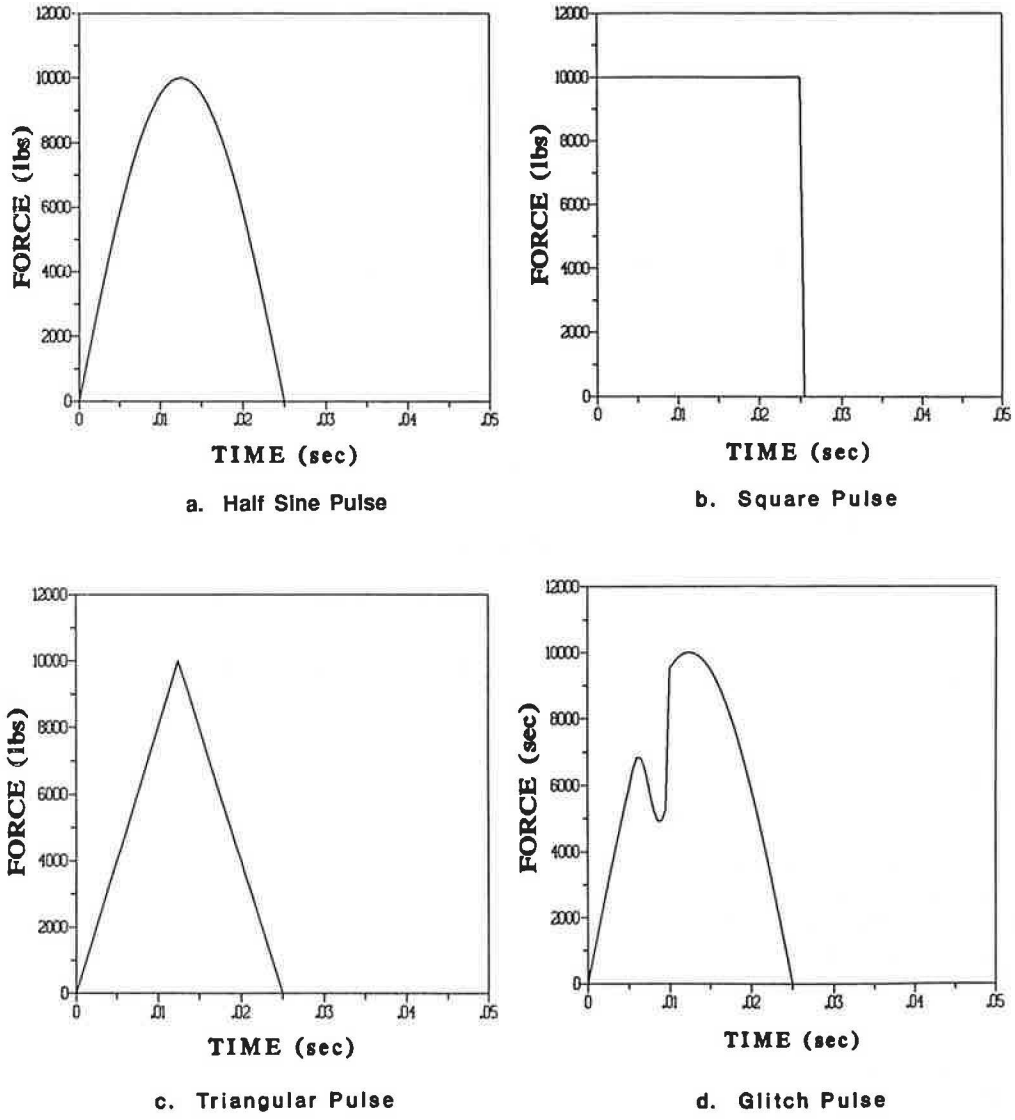

FIGURE 4 Forcing functions.

TABLE 1 COMPARISONS OF PEAK DEFLECTIONS OF PAVEMENT MODEL AND INTEGRATION OF VELOCITY TRANSDUCER MODEL OUTPUT

Type of Pulse	Deflection (mils)	
	Pavement	Transducer
Half Sine	10.22	7.98
Square	12.54	11.43
Triangle	9.93	7.75
Glitch	10.73	8.04

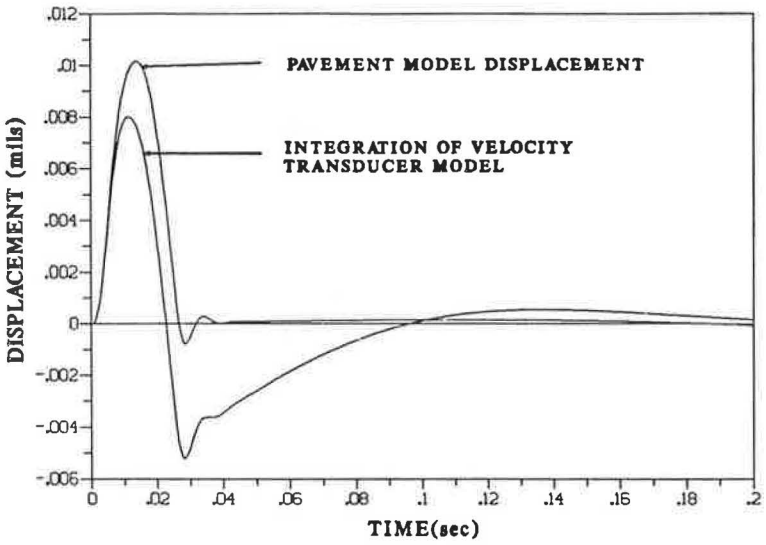

FIGURE 5 Displacement of pavement model and displacement calculated by integrating the transducer model output.

$$H_v(\omega) = \left[\frac{1}{j\omega} - \left(\frac{\omega_n^2}{\omega^2 j\omega}\right) - \frac{2\xi\omega_n}{\omega^2}\right]^{-1} \quad (15)$$

By using Equation 14, the pavement displacement may be calculated from the output of the velocity transducer (i.e., the velocity of the transducer mass moving relative to the transducer case).

Calculation of the pavement displacement has been accomplished by programming Equation 14 in QuickBASIC and convoluting it with the transformed velocity transducer output. The velocity transducer output (relative velocity) is transformed to the frequency domain by using a Fast Fourier Transform (FFT) (*6*). After conversion to the frequency domain, the velocity is convoluted with the frequency response function $H(\omega)$ defined in Equation 15 by using complex multiplication. The pavement displacement versus time is then calculated using the inverse FFT. The maximum calculated displacements from the velocity transducer outputs and the displacements of the pavement model are compared in Table 2. There is excellent agreement between the two.

TABLE 2 COMPARISON OF ACTUAL PAVEMENT MODEL AND TRANSDUCER-CALCULATED OUTPUT DISPLACEMENT USING FREQUENCY RESPONSE METHOD

Type of Pulse	Deflection (mils)	
	Actual	Calculated
Half Sine	10.22	10.22
Square	12.54	12.52
Triangle	9.93	9.87
Glitch	10.73	10.67

PHASE 2: LABORATORY CALIBRATION OF VELOCITY TRANSDUCERS

Background

The objective of calibrating velocity transducers is to determine their sensitivity, defined as the ratio of the electrical output to mechanical input applied to the specified axis (*9*). The relationship between the transducer sensitivity and frequency is commonly referred to as the calibration curve, transfer function, or frequency response function of the transducer. A typical one is shown in Figure 2.

Because the responses created by the FWD are transient, they contain frequency components that are predominantly in the range 0 to 100 Hz. The response of a typical velocity transducer is not linear throughout this range (see Figure 2). Therefore, for the analysis of these responses, the frequency response of the transducer must be established over this frequency bandwidth.

The theoretical representation of a transducer modeled as an SDOF system was developed in Equation 12. However, most velocity transducers do not behave as theory predicts; empirically developed frequency response functions are necessary to characterize them.

The fastest and most economical form of transducer calibration is the comparison method. This method involves simultaneous measurement of the outputs of the device under test and some reference device of known and stable conditions, with both devices subjected to the same excitation (*9*).

Most calibrations are conducted using an electrodynamic shaker that can produce various excitations depending on the voltage applied to its armature. The reference device is normally an accelerometer or a velocity transducer built into the shaker system. The frequency response function for this system may be defined as

$$H(f) = \frac{S_y}{S_x} \cdot \frac{S_x^*}{S_x^*} = \frac{G_{yx}}{G_{xx}} \quad (16)$$

where

S_y = linear Fourier spectrum of the output,
S_x = linear Fourier spectrum of the input,
S_x^* = complex conjugate of S_x,
G_{yx} = cross power spectrum, and
G_{xx} = auto power spectrum.

A velocity transducer can be considered to be a linear system up to limits defined by the travel of its coil. This means that the response of the transducer is proportional to its excitation (*9*). Because the transducer is considered a linear system, its response is independent of the excitation magnitude to which it is subjected (*10*). Therefore, any type of excitation of the shaker—swept-sine, random noise, or impulse—could be used to calibrate the transducer.

Frequency Response Curves for FWD Velocity Transducers

Calibration System

A velocity transducer of the type used in FWDs was mounted on an electrodynamic shaker that had an internal velocity transducer. An audio range oscillator was used to supply a single ramp function having a rise time of 24 msec to the shaker. The velocity of the shaker armature and the output of the FWD-type transducer were simultaneously recorded by the analyzer, a Hewlett Packard 3562A Dynamic Signal Analyzer. The use of the shaker velocity transducer to determine armature displacement was validated by attaching a displacement transducer, an LVDT, to the shaker armature and comparing the two. Excellent agreement was obtained to frequencies of 20 Hz, where the LVDT data became erratic because of vibration of the LVDT support system (*2*). For higher frequencies, a seismic accelerometer with linear range from 0.07 Hz to 800 Hz was used. It also provided excellent agreement. Details are given elsewhere (*2*).

The resulting displacement history of the shaker armature is shown as one of the curves in Figure 6. The shape of this curve is similar to that of the theoretical curve developed in Phase 1 and given in Figure 5.

Time Domain Integration of Data of the FWD-Type Transducer

Because the net displacement after applying the ramp function was zero, the output of the FWD-type transducer was corrected to zero by subtracting (or adding) the corresponding average values from (or to) all 2,048 data points. The signal was then converted to displacement by simple, time-domain integration. The resulting integrated time history displayed a very small negative value at time zero even though no displacement existed. This small value was added to all integrated values (i.e., the zero axis was shifted downward a small amount).

The resulting curve for the time-domain-integrated, FWD-type velocity transducer is also shown in Figure 6. It is clearly different from that of the shaker armature, which is the displacement applied to the transducer case. It differs not only in magnitude but also in times to the peak values. This is expected according to the theory for velocity transducers as discussed in Phase 1 and shown in Figure 5.

Generation of the Frequency Response Function for the FWD-Type Transducer

The frequency response function for the FWD-type velocity transducer was obtained directly by using the analyzer's frequency response function, which operates according to Equation 16. This is equivalent to transforming both curves shown in Figure 6 using the FFT function and then, in the frequency domain, dividing the FWD-type transducer curve by the curve for the actual displacement. The resulting curve is the frequency response function for the FWD-type transducer, which is shown in Figure 7. The curve is well defined at low frequencies but is not well defined at frequencies above 100 Hz.

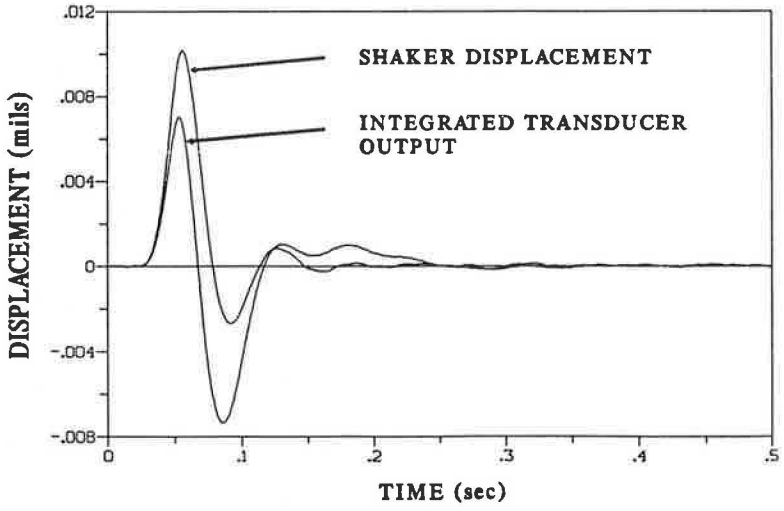

FIGURE 6 Actual displacement of the transducer case and displacement of transducer mass relative to the transducer case.

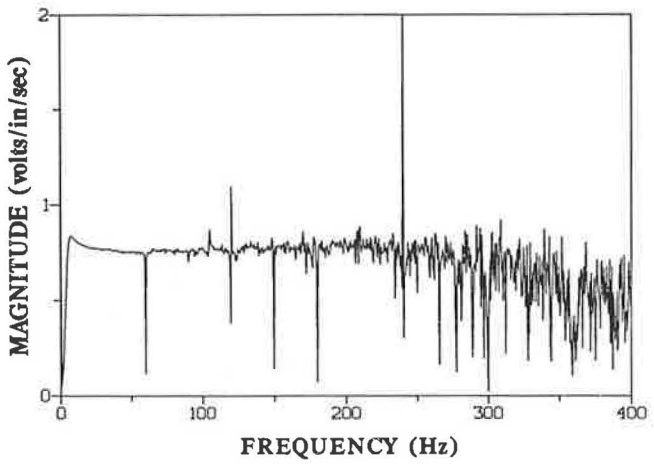

FIGURE 7 Frequency response function calculated using the ramp excitation.

The reason is that the displacement applied to the transducer was deficient in high-frequency components.

Hybrid Frequency Response Function for the FWD-Type Transducer

According to the theory discussed earlier, the frequency response function should be independent of the type of excitation. The FWD-type transducer was calibrated a second time with the excitation being random noise having a 0- to 400-Hz bandwidth. (The analyzer has a built-in random noise generator.) The same process was applied to these outputs as was applied to the one with the ramp excitation. The resulting curve is given in Figure 2. Comparison of the two indicates that they are similar in shape and magnitude. Closer examination reveals that the ramp-generated curve has more consistent values at frequencies less than 25 to 50 Hz, the random-noise-generated curve has more consistent values in frequencies above this range, and values in the 25- to 50-Hz range are practically identical. The two responses were combined to form a hybrid frequency response curve, as shown in Figure 8. The two response functions were combined at a specified frequency in the 25- to 50-Hz range to obtain a frequency response function that is accurate across the complete frequency bandwidth.

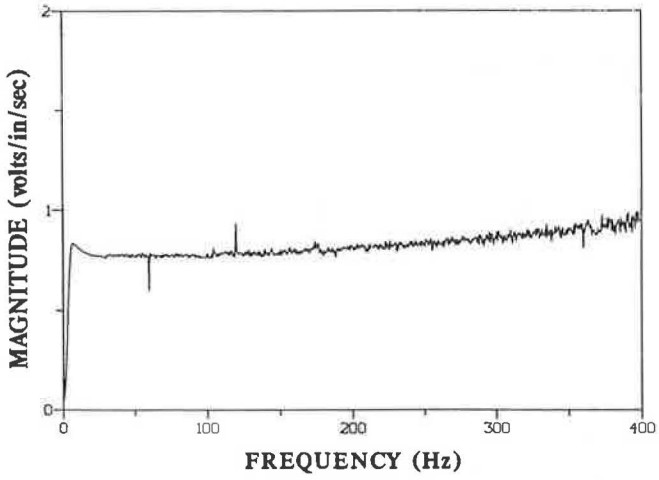

FIGURE 8 Hybrid frequency response function.

Checking the Hybrid Frequency Response Function

To check its accuracy, the hybrid frequency response function was used on the FWD-type transducer output to obtain a calculated displacement. The process involved the following steps:

1. Transform the transducer voltage output from the time domain to the frequency domain by use of the FFT.
2. Divide the transformed data by the FWD-type frequency response function.
3. Integrate the signal to obtain frequency domain values proportional to the displacement of the transducer case.
4. Inverse transform the result back to the time domain.
5. Check the initial displacement. It should be zero. If it is not, adjust all displacement values by the appropriate amount to obtain zero initial conditions.

The resulting displacement is plotted in Figure 9 along with the displacement determined by the shaker transducer. The two curves are not distinguishable. By use of the analyzer, it was established that the peak values differed by less than 1 percent and that the average difference in displacement over the time range 0 to 200 msec was less than 0.1 mil.

Behavior for Another Frequency Bandwidth

All of the above procedures were repeated for a frequency bandwidth of 0 to 100 Hz (which corresponds to the 8-sec data acquisition time). Similar results were obtained, and the differences between the measured and calculated displacements were even smaller (e.g., peak difference less than 0.25 percent). The improved accuracy was due to a combination of displacement time history curve smoothing caused by the longer interval between data points (4 msec versus 1 msec) and the increased accuracy of the frequency response function caused by more closely spaced frequency lines (0.125 Hz versus 0.5 Hz). The technical term for the latter phenomenon is reduced leakage (*6*), which is discussed subsequently.

In the frequency domain, data can only be determined at the frequency lines that are spaced Δf apart. Components with frequencies between the frequency lines are "leaked" to adjacent frequency line values. For the cases studied, very low frequency components between the first frequency line at 0 Hz and the second frequency line at $0 + \Delta f$ Hz are leaked to the 0 Hz and the Δf Hz lines. On performing the inverse transform to obtain the time domain data, the 0 Hz component registers as a DC offset.

Another possible cause of the DC offset is the periodicity of the input that is inherently assumed in Fourier transformations. Veletsos and Ventura described this phenomenon in detail (*11*). The assumption is that the time record repeats itself indefinitely (i.e., at the end of the time record, exactly the same signal recurs). Real FWD signals are transient and last less than 0.5 sec. The entire time record for a 400-Hz

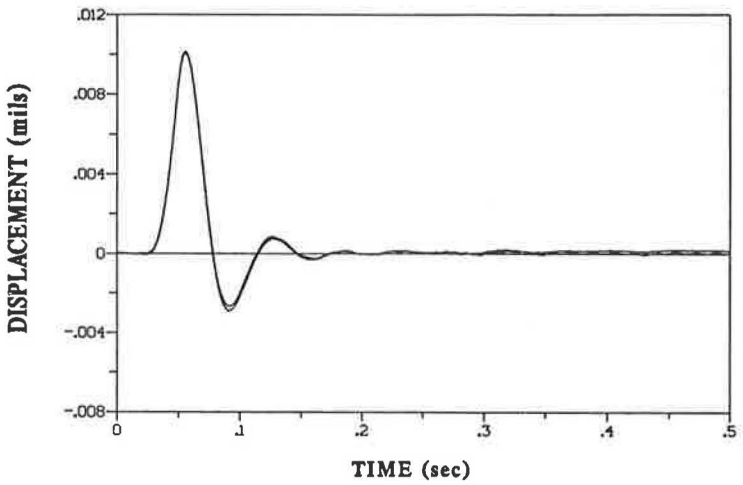

FIGURE 9 Comparison of shaker displacement and FWD-type transducer calculated displacement.

bandwidth is 2 sec. Hence, a "quiet time" that lasts 1.5 sec or longer follows the FWD signal. This problem is identified by values of both DC offset and nonzero slope at time zero on the inverse transformed signal. Close examination of the inverse transformed signals showed the DC offset but zero slope, and it was concluded that the DC offset was not caused by this phenomenon. The fact that vertically loaded pavements exhibit high damping also supports this conclusion.

PHASE 3: COMPARISON OF DEFLECTIONS WITH THOSE FROM AN FWD DEVICE

FWD Apparatus and Location of Verification Site

The FWD used in this study was a JILS-20, manufactured by Foundation Mechanics, El Segundo, California. The test location, referred to as the garage, was in the garage adjacent to the research building. The pavement structure there consisted of 6 in. of portland cement concrete over 4 in. of crushed stone over a compacted subgrade. Bedrock is located approximately 10 ft below the surface.

Comparison Setup

Two FWD-type velocity transducers, which were calibrated during Phase 2, were used for this testing and were independent of those used as sensors on the FWD. The comparison process, similar to the process used by Nazarian and Bush (*3*), consisted of rigidly attaching the independent, FWD-type transducers to the pavement as close to the actual FWD sensors as possible. The FWD sensors were located at distances of 0, 1, 2, 3, 4, 5, and 6 ft and were labeled Locations 1 through 7. To ensure that the independent transducers remained securely attached in this location, they were screwed to aluminum disks that were glued to the pavement. The FWD sensors were held in place by springs attached to the sensor boom. For the displacement comparison, one transducer was used as a reference and remained at Location 2 while the other was moved to Locations 3 through 7. It was not possible to place a transducer adjacent to the transducer at Location 1 because of the loading plate surrounding it.

The recording device was a Hewlett Packard 3562A Dynamic Signal Analyzer. Because it is a two-channel analyzer, a new set of data must be obtained as the transducer is moved to each new position. The output from the reference transducer is connected to Channel 1 while the output of the other transducer is connected to Channel 2. All data were taken over a 2-sec time record, as in Phase 2.

Test Procedure

Both single- and multiple-drop tests were performed. The JILS-20 FWD can take up to four successive measurements at a given location before the boom and loading plate are raised from the pavement. Because the analyzer can average the measurements, tests were conducted using both a single drop and a four-drop series. For the four-drop tests, the voltage time histories taken by the analyzer were averaged using time domain averaging. The displacement was then calculated from the averaged velocity signal. For the FWD data, four peak displacements were calculated by the FWD software. The four peak displacements were averaged and then compared with the average displacement calculated by the analyzer. This test procedure was carried out at the site for loads of 7,000 and 14,000 lb.

Displacement Determination

Calculation of the displacements using the analyzer with signals from the independent transducers was done in the same manner as for Phase 2. Typical results for each step are given below for one sensor location with a 7,000-lb load with a single drop.

The raw voltage output of the independent transducer at Location 4 (3 ft from the center of the load) is shown in Figure 10. This signal, transformed to the frequency domain, is given

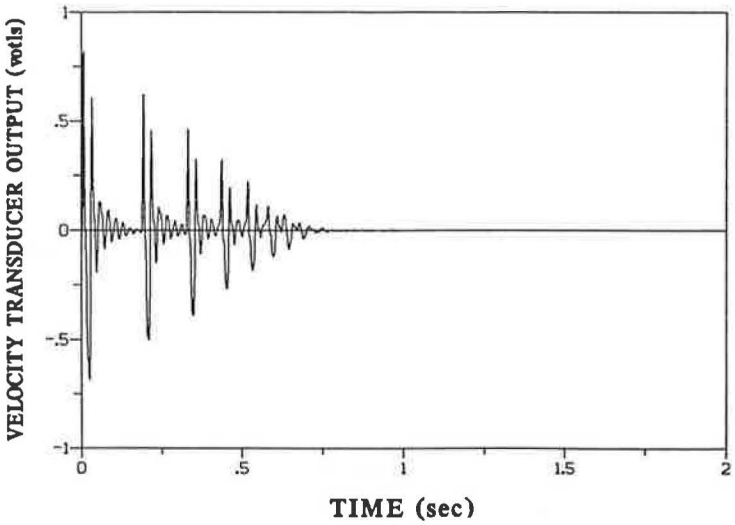

FIGURE 10 Raw velocity output of independently calibrated transducer at Location 4.

in Figure 11. Integration in the frequency domain is carried out by multiplying by $j\omega^{-1}$, and convolution is accomplished by dividing the integrated signal by the frequency response function for that transducer. The result is the pavement displacement in the frequency domain shown in Figure 12. An inverse transform is then performed to obtain the pavement displacement in the time domain, that is, the pavement displacement time history. The time history is then corrected for DC offset. The final pavement displacement is given in Figure 13.

Examination of the displacement in Figure 13 indicates some interesting features. First, multiple hits have occurred, and multiple displacement responses are observed. They are identified as such because each subsequent response has diminished amplitude and occurs at a shorter interval. (Bedrock reflections would occur at constant intervals.) The traces also indicate that motion at the sensor consists of multiple cycles of vibration that are highly damped. Because the entire time history should be accurate, these characteristics present some powerful possibilities, such as determining pavement response to multiple force levels from a single test and obtaining pavement damping characteristics.

Displacement Comparisons

FWD deflections are used to determine deflection basins for each location. The deflection basin is a plot of maximum displacement versus radial distance from the center of the load. Deflections at each sensor location for a single test and for a four-test average are included in Figures 14 and 15, respectively. Both the FWD-calculated and the analyzer-calculated deflections are shown.

The difference in the deflections for each basin is calculated as the difference between the analyzer- and FWD-calculated deflections. The differences are shown as the percentage of

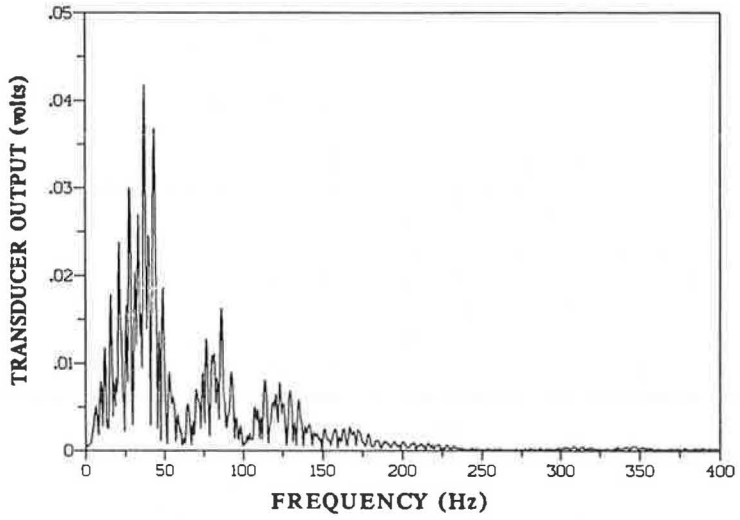

FIGURE 11 Frequency domain representation of transducer output.

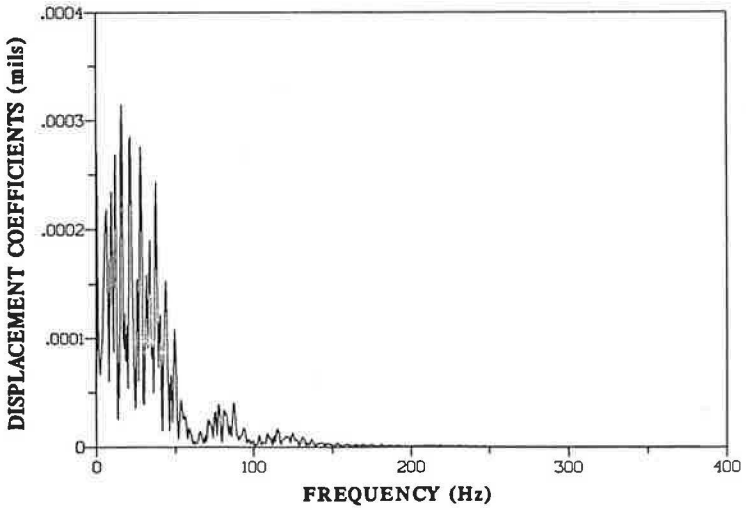

FIGURE 12 Frequency domain representation of calculated displacement.

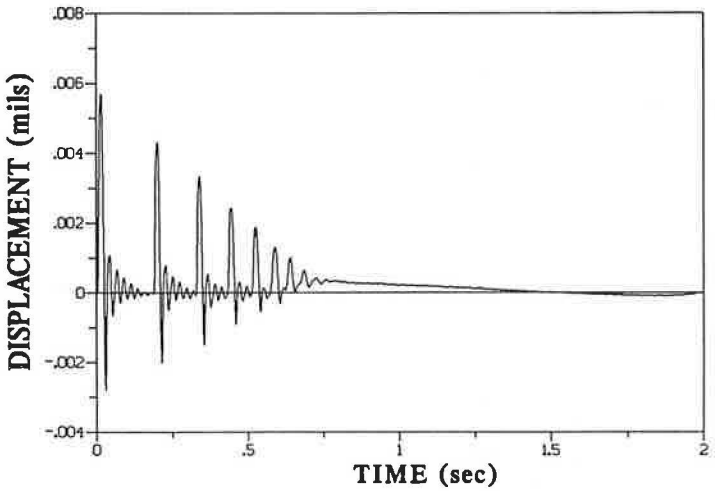

FIGURE 13 Calculated deflection time history of pavement.

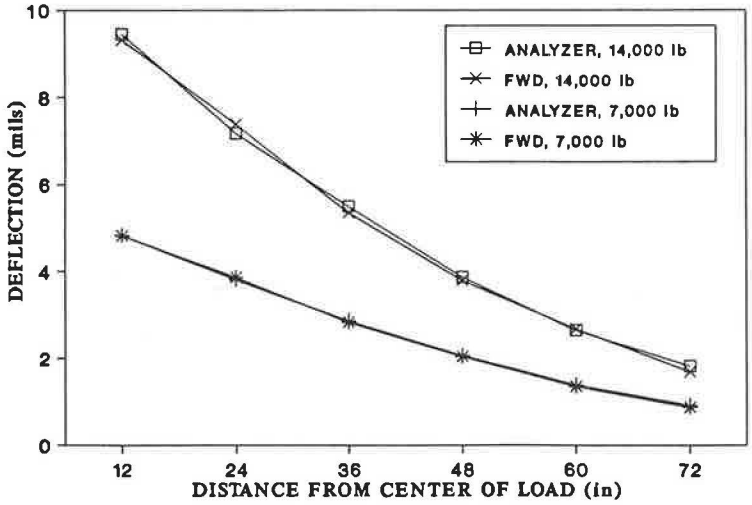

FIGURE 14 Deflection basin, garage floor, single test, 7,000 and 14,000 lb.

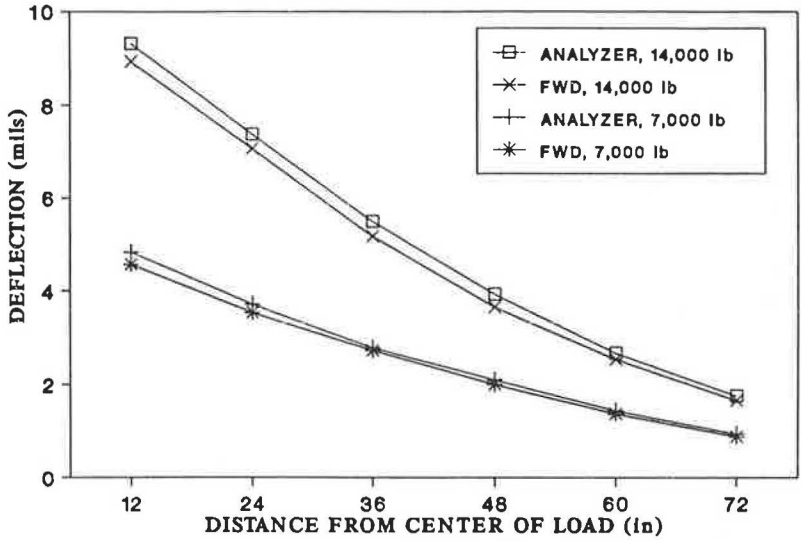

FIGURE 15 Deflection basin, garage floor, four-test average, 7,000 and 14,000 lb.

the maximum analyzer-calculated deflection. Tables 3 and 4 summarize the results for the single drop tests at two different loads, and Tables 5 and 6 summarize the results for the multiple-drop tests. For perspective, other studies have noted that the precision of measurements with an FWD is generally within ±5 percent (*3*).

Discussion of Differences

Tables 3 through 6 indicate that, for the garage floor, the difference between the deflections determined by the two methods is greater for the four-test average than for the single-drop tests. The differences obtained from the single tests are generally between −3 and +7 percent, and the differences from the four-test average are between +2 and +8 percent. The deflections determined by the independent transducers tend to be larger than those determined by the JILS-20 FWD transducers and software. The reason for this is not known and is being studied. Some of the differences between the two types of tests may be attributed to the method of averaging. The analyzer averages the raw velocity trace before it is used to calculate the displacement. The average values of the FWD displacements are calculated from the average of the four individual peak displacements.

TABLE 3 DEFLECTION COMPARISON, 7,000 lb, GARAGE FLOOR, SINGLE TEST

Sensor Location	Displacements (mils)		Percent Diff.
	FWD	Analyzer	
3	3.87	3.82	-1.31
2	4.92	4.96	0.81
4	2.84	2.87	1.05
2	4.94	4.90	-0.81
5	2.04	2.06	0.97
2	4.82	4.84	0.41
6	1.36	1.39	2.16
2	4.78	4.84	1.24
7	0.87	0.92	5.43
2	4.81	4.87	1.23

TABLE 4 DEFLECTION COMPARISON, 14,000 lb, GARAGE FLOOR, SINGLE TEST

Sensor Location	Displacements (mils)		Percent Diff.
	FWD	Analyer	
3	7.39	7.18	-2.92
2	9.36	9.34	-0.21
4	5.36	5.50	2.54
2	9.46	9.47	0.10
5	3.79	3.87	2.07
2	9.32	9.45	1.37
6	2.68	2.65	1.12
2	9.54	9.52	0.21
7	1.69	1.82	7.14
2	9.57	9.58	0.10

TABLE 5 DEFLECTION COMPARISON, 7,000 lb, GARAGE FLOOR, FOUR-TEST AVERAGE

Sensor Location	Displacements (mils)		Percent Diff.
	FWD	Analyzer	
3	3.54	3.72	4.84
2	4.45	4.72	5.72
4	2.72	2.78	2.16
2	4.57	4.85	5.77
5	2.00	2.10	4.76
2	4.62	4.86	4.94
6	1.37	1.43	4.19
2	4.57	4.83	5.38
7	0.88	0.94	6.38
2	4.60	4.87	5.54

TABLE 6 DEFLECTION COMPARISON, 14,000 lb, GARAGE FLOOR, FOUR-TEST AVERAGE

Sensor Location	Displacements (mils)		Percent Diff.
	FWD	Analyzer	
3	7.07	7.38	4.20
2	9.03	9.48	4.75
4	5.17	5.49	5.82
2	8.93	9.32	4.18
5	3.65	3.92	6.89
2	8.86	9.23	4.01
6	2.54	2.67	4.87
2	8.75	9.16	4.47
7	1.66	1.76	5.68
2	8.97	9.36	4.17

The FWD software uses a single frequency response function for all seven velocity transducers, whereas the individual frequency response functions were used with the independent transducers. Variations among transducers could account for some of the observed differences, especially the variation from one transducer location to another.

As discussed in Phase 2, displacements determined by use of frequency response functions are sensitive to values of the frequency response functions at very low frequencies. Some of the consistent differences could be due to small differences in the frequency response functions at the low frequencies. A comparison of a typical field deflection calculated by the different frequency response curves is presented in Table 7 for the 7,000-lb load. Table 7 indicates that the difference in frequency response function may affect the calculated displacement.

SUMMARY AND CONCLUSIONS

The frequency response function method is a feasible approach to accurately calculating displacement time histories from measurements made with velocity transducers. This was verified by use of classical mathematical models to describe pavement and transducer behavior. The models also were used to demonstrate that the shape of the loading function influences the peak displacement even when the peak load and duration of loading are kept constant. The procedures were validated in the laboratory utilizing an electrodynamic shaker and an FWD-type velocity transducer. It was found that the accuracy of the method depends on obtaining accurate frequency response functions, especially in the very-low-frequency range, where the function varies greatly with frequency.

TABLE 7 FREQUENCY RESPONSE FUNCTION EFFECTS ON ACTUAL FIELD DEFLECTIONS, 7,000-lb LOAD, SINGLE TEST

Frequency Response Function	Displacement (mils)	Percent Diff. from FWD
Random Noise	5.42	1.10
Impulse	5.54	3.25
Hybrid	5.50	2.54
FWD	5.36	0.00

A comparison was made at one site with independent transducers used side by side with those of a JILS-20 FWD. Agreement between the two was generally good, but deflections determined by use of the independent transducers gave slightly larger deflections, on the average, than those from the FWD sensors and software. Reasons for these differences include methods of averaging and accuracy of the frequency response functions for specific transducers, especially in the low-frequency range.

The frequency response function approach gives accurate time histories for the entire time record. This is important because it allows for determining accurate deflection basins that account for different shapes of loading functions. It also may allow for calculating pavement response to multiple force levels from a single test, because data associated with the bounces could be used. This could mean a savings in both testing time and expense.

ACKNOWLEDGMENTS

The study reported herein was funded by the Federal Highway Administration and the Kentucky Transportation Cabinet through the University of Kentucky Research Foundation.

REFERENCES

1. M. S. Hoffman and M. R. Thompson. Comparative Study of Selected Nondestructive Testing Devices. In *Transportation Research Record 852*, TRB, National Research Council, Washington, D.C., 1983, pp. 32–40.
2. R. C. Graves. *Pavement Deflection Determination Using Velocity Transducers*. Master's thesis. University of Kentucky, Lexington, 1989.
3. S. Nazarian and A. J. Bush III. Determination of Deflection of Pavement Systems Using Velocity Transducers. In *Transportation Research Record 1227*, TRB, National Research Council, Washington, D.C., 1989, pp. 147–158.
4. *Mark Products Catalog*. Mark Products, Inc., Houston, Tex., 1989.
5. M. Paz. *Structural Dynamics Theory and Computation*. Van Nostrand Reinhold, New York, 1980.
6. R. W. Ramirez. *The FFT Fundamentals and Concepts*. Prentice-Hall, Inc., Englewood Cliffs, N.J., 1985.
7. M. Paz. *Microcomputer-Aided Engineering Structural Dynamics*. Van Nostrand Reinhold, New York, 1986.
8. V. P. Drnevich. Operating Characteristics of the WES 16-Kip Vibrator for the Nondestructive Testing of Pavements. *University of Kentucky Soil Mechanics Series*, No. 32, May 1985.
9. C. M. Harris. *Shock and Vibration Handbook* (3rd ed.). McGraw-Hill, New York, 1988.
10. *Application Note 243: The Fundamentals of Signal Analyses*. Hewlett Packard Company, 1985.
11. A. S. Veletsos and C. E. Ventura. Pitfalls and Improvements of DFT Method of Dynamic Analysis. *Structural Research at Rice*, Report 28, Department of Civil Engineering, Rice University, Houston, Tex., Aug. 1984, 37 pp.

Development of an Absolute Calibration System for Nondestructive Testing Devices

SOHEIL NAZARIAN, VIVEK TANDON, AND ROBERT C. BRIGGS

Many highway agencies use falling weight deflectometers (FWDs) for pavement evaluation. The primary function of the FWD is to measure a deflection basin due to a load imparted to the pavement. Deflection basins measured in the field are used to back-calculate modulus profiles of pavement sections. Accurate determination of deflection basins in the field is critical. Velocity transducers (geophones) are used to determine the deflections, and load cells are used to measure the applied loads. The accuracy of deflections and loads obtained from these devices is of much concern, and a system is needed to calibrate them. A recently developed absolute calibration system is described. The system consists of two well-calibrated geophones, three load cells, a signal-conditioning unit, a loading plate, an analog-to-digital (A/D) board, and a computer. Software was developed to control the A/D board and to reduce the data. Geophones were selected for the calibration of the FWD sensors after an evaluation of the accuracy and precision of five candidate sensors. An aluminum loading plate was constructed to allow mounting of the load cells in line with and below the FWD load cell. The calibration curves of all load cells were traceable to the National Bureau of Standards. The effects on the calibration factors of load cells of using the aluminum plate were small. The signal-conditioning unit was developed to condition the signals before acquisition. The system was used to calibrate an FWD device. The system was effective. A calibration process is proposed on the basis of an analysis of the data collected. The calibration system is cost-effective, accurate, and rugged, and it can be used by highway agencies to calibrate their FWD devices.

It has become increasingly important in recent years to evaluate the performance of deflection and load sensors of falling weight deflectometer (FWD) devices. A small error in deflections measured in the field may yield significantly erroneous modulus values (*1*). A reliable method for evaluating the accuracy of the sensors used for determining these deflections is necessary. An absolute calibration system is required for this purpose.

An absolute calibration consists of determining the accuracy with which the deflections and loads are measured by using an independent system. Such a system has been proposed by Richter and Irwin (*2*). At a minimum, the following criteria should be met: (*a*) the calibration of the load and deflection sensors should be traceable to the National Bureau of Standards, and (*b*) all sensors should be calibrated in place. In this manner, the decoupling of the loading and sensing mechanisms and the coupling of the sensing mechanism to the pavement can be verified. The device recommended by Richter and Irwin provided a good start, but it does not satisfy the two criteria. Low cost and portability are other desirable characteristics.

The development of an absolute calibration system and the procedure used to calibrate an FWD device are described. To identify the most accurate and practical sensors for the system, five commercially available sensors were investigated. Different types of motion were used to compare the performance of each sensor. The evaluation procedures, selection criteria, and recommendations regarding the most suitable sensor type are included.

The selected sensors were used to develop an absolute calibration system. The components of the calibration system are described in detail. A computer algorithm developed to collect and reduce the data obtained from the sensors is also described.

The data obtained from the calibration system were compared and analyzed with the data obtained simultaneously from an FWD device. The effects of different parameters, such as drop height and pavement type, on the deflections and loads obtained from both devices are discussed. On the basis of an evaluation of the data collected with the calibration system and the FWD device, a calibration process is proposed.

SELECTION OF SENSORS

The calibration system consists of several deflection sensors and load cells. The selection of proper sensors for each of the components was critical. Five deflection-measuring devices were evaluated, including an accelerometer, a linear variable differential transformer (LVDT), a proximeter probe, a laser optocator, and a geophone. These devices were selected because of their commercial availability and their effectiveness in deflection measurement (*3*).

Sensor characteristics considered in the evaluation were accuracy, precision, field worthiness, cost, and mounting. Amplitude of vibration, type of excitation, and frequency content of vibration were studied over a wide range to evaluate fully the five candidates. Tests were carried out in the laboratory so these variables could more closely be controlled. The setup used for the evaluation of accuracy and precision of each sensor type is shown in Figure 1.

A detailed account of the testing procedure and results is given by Tandon (*3*). In summary, the amplitude of vibration

S. Nazarian and V. Tandon, Department of Civil Engineering, The University of Texas at El Paso, El Paso, Tex. 79968. R. C. Briggs, Texas State Department of Highways and Public Transportation, Austin, Tex. 78701.

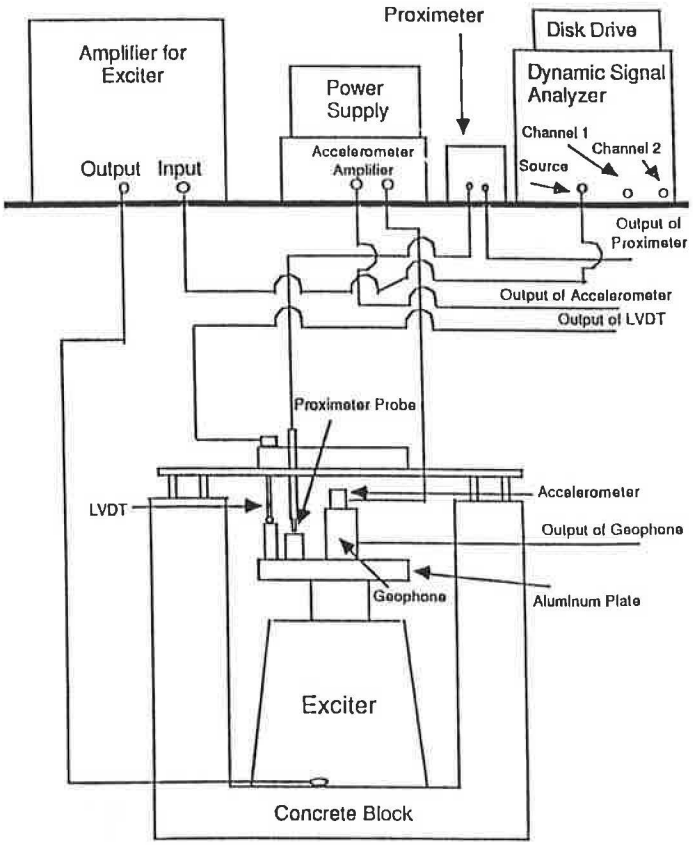

FIGURE 1 Schematic of setup used for evaluation of five sensors.

varied between 1 and 25 mils. Such a broad range was studied to ensure proper response of the sensors to small as well as large amplitudes. Different types of excitation were investigated to determine the appropriateness of each sensor type for use in calibrating the various types of nondestructive testing devices. Types of excitation included impulse (transient) motions and steady-state vibrations. Three type of impulses—half-sine, triangular, and square—were used. For the impulse tests, the duration impulse varied between 12.5 and 175 msec to cover the frequency ranges of interest in nondestructive testing methods. For the steady-state tests, the frequency of vibration varied between 5 and 100 Hz.

The accuracy of the sensor types was determined by comparing deflections measured with each device against those measured with a proximeter probe (Figures 2b and 3b). The proximeter is an accurate and precise deflection-measuring device in the laboratory because of its noncontact nature.

As an example, data obtained from a geophone and an LVDT under half-sine impulse motion are shown in Figures 2 and 3, respectively. The LVDT used was similar to that suggested by Richter and Irwin (*2*). The variances as a function of impulse width and deflection level are shown in Figures 2a and 3a. Each experiment was repeated 10 times to determine the variances. In all but a few cases, the variance was less than 0.5 percent, and it never exceeded 1.5 percent. Such a small variation can be attributed to background noise. The accuracy of geophones under steady-state motion, compared with the proximeter, is typically within 2.5 percent.

The advantages and disadvantages of all the sensors and their direct and indirect costs are given in Table 1, which indicates that geophones are the most practical of the sensors evaluated. They are rugged enough for the field testing, cost less than other sensors, and do not need a special type of mounting fixture because they can be attached to the pavement with the help of modeling clay. Tests indicate that the use of clay does not affect the response of the geophone in the frequency range of interest for FWD testing. No post- or preamplification or signal conditioning is needed for collection of data, resulting in large cost savings. The cost of calibration of each device is approximately the same.

The load-measuring sensor was selected on the basis of commercial availability and calibration curves traceable to the National Bureau of Standards. However, one of the load cells was calibrated in the laboratory to confirm the calibration factor.

DESCRIPTION OF CALIBRATION SYSTEM

The system developed consists of a load calibration component and a deflection calibration component. Figure 4 shows a block diagram of the fundamental components.

The load calibration component consists of three load cells and an aluminum plate. The deflection calibration component consists of two well-calibrated geophones and a signal-conditioning unit (SCU). A data acquisition system and a

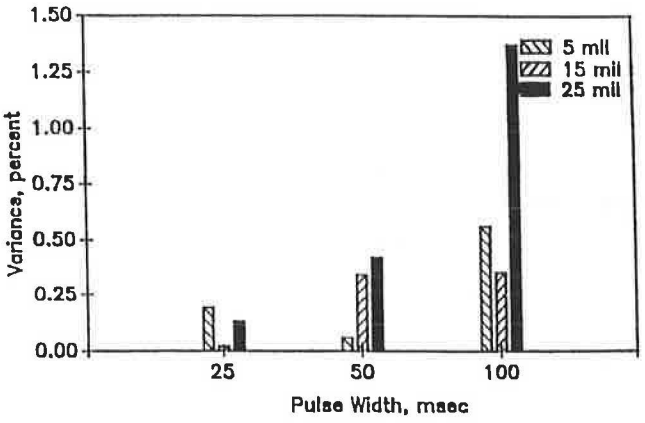

a) Variance

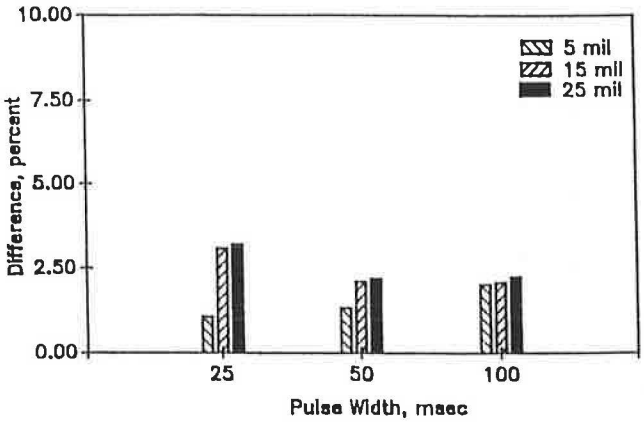

b) Difference from Proximeter Deflections

FIGURE 2 Evaluation of a geophone under half-sine impulse motion.

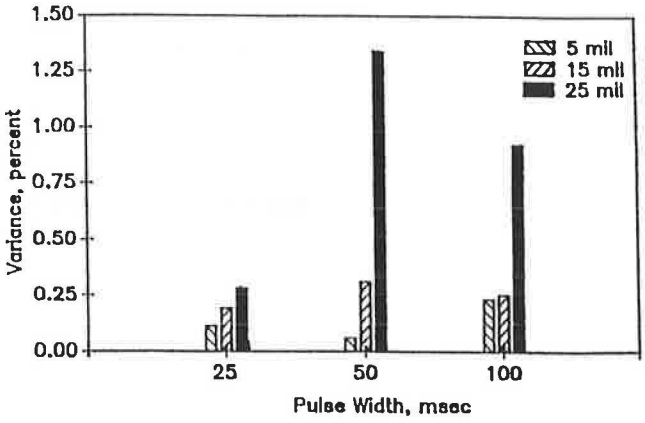

a) Variance

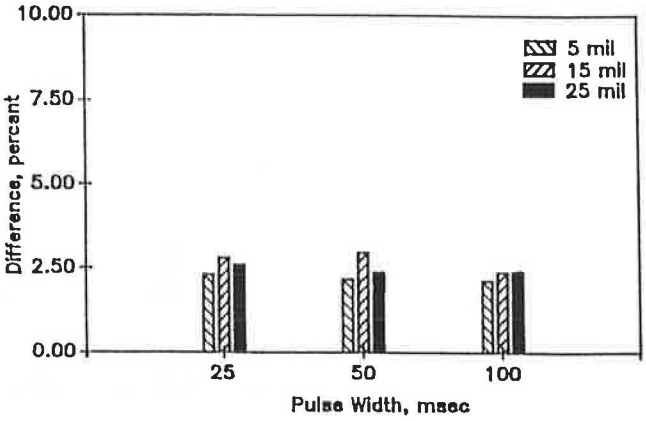

b) Difference from Proximeter Deflections

FIGURE 3 Evaluation of an LVDT under half-sine impulse motion.

TABLE 1 COMPARISON OF CHARACTERISTICS OF FIVE DEFLECTION SENSORS

	Sensor				
Characteristic	Accelerometer	LVDT	Geophone	Proximeter	Laser
Cost ($)	350	350	40	400	>10,000
Supporting devices	Power amplifier ($300)	Power supply ($400)	–	Power supply ($400)	–
Precision, steady state	Moderate	Good	Good	Very good	Excellent
Precision, impulse	Poor	Good	Good	Very good	Good
Accuracy, steady state	Moderate	Good	Good	Excellent	Excellent
Accuracy, impulse	Poor	Good	Good	Good	Good
Field worthiness	Good	Moderate	Very good	Moderate	Poor
Mounting	Very easy	Difficult	Very easy	Difficult	Difficult

computer are also used. The components are controlled and all collected data are reduced and presented through a computer algorithm. Figure 5 shows the entire system.

The FWD device imparts a load to the pavement by dropping a weight from different heights. The load is transferred to the pavement through a polyvinyl chloride (PVC) plate. An aluminum plate with the same thickness and diameter as the PVC plate was fabricated (Figure 6). A PVC plate cannot be used for calibration because the high flexibility of this material results in erroneous measured loads.

Six holes were drilled in the plate for fastening the load cells to the plate. Three holes, 120 degrees apart, each located halfway between two screws, were used for connecting the aluminum plate to the FWD device. The other three holes were made along a diametral line. The first three holes are used for calibration and the other three to study the variation

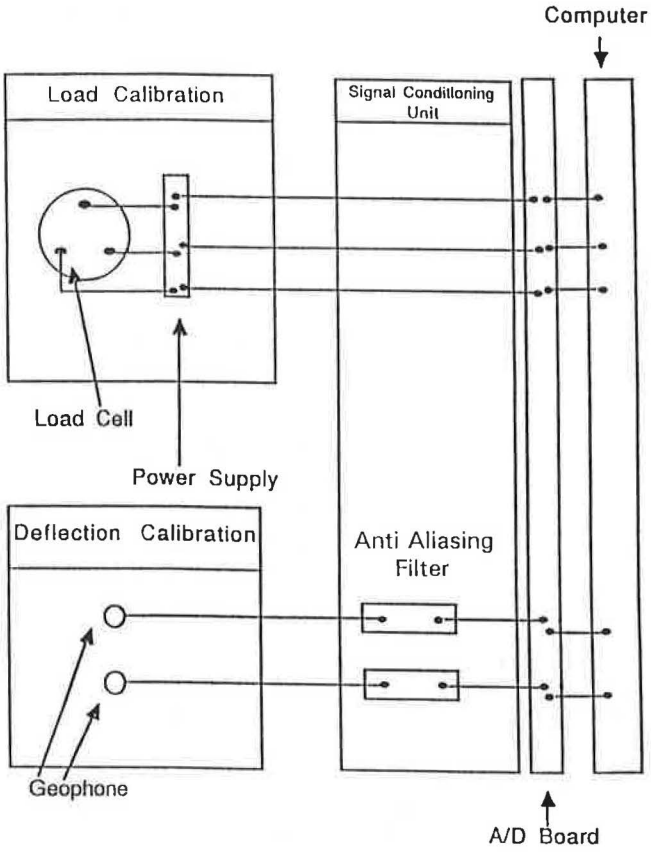

FIGURE 4 Diagram of calibration system.

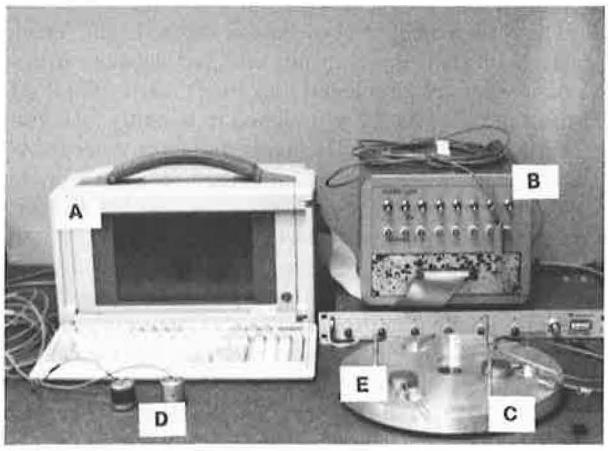

FIGURE 5 Components of calibration system: A, computer; B, SCU; C, aluminum plate; D, geophones; E, load cell.

of load along the diameter of the FWD plate. Grooves were cut in the plate to accommodate load cell cables. Three small holes were also provided for fastening the aluminum plate to the FWD device.

Three load cells with calibration curves traceable to the National Bureau of Standards were used. The nominal calibration factors for the load cells were 250 mV/kip with a capacity of 20 kips. The effect of mounting the load cells in the aluminum plate was found to be negligible (*3*).

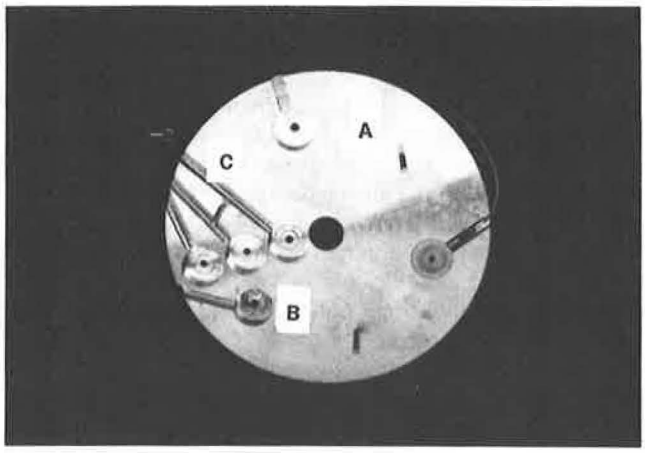

FIGURE 6 Aluminum plate developed for calibration system: A, aluminum plate; B, hole for load cell; C, slot provided for load cell cables.

The two geophones used in the calibration system have nominal natural frequencies of 4.5 Hz, nominal damping ratios of 70 percent, and nominal gain factors of 0.75 V/in./sec. For a typical pavement, the voltage output is on the order of 100 mV to 1 V.

The SCU, which was designed, built, and tested in house, consists of an eight-channel analog filter and a triggering mechanism, as shown in Figure 7. The filter is a fourth-order, low-pass filter with a cutoff frequency of 250 Hz. The unit is placed between the sensors and the analog-to-digital (A/D) board. Each load or displacement sensor is connected to one channel of the unit (see Figure 7). The signal can be filtered and output to the A/D board, or the filter can be bypassed and the output directed to the board. Each channel has a switch for directing or bypassing the signal through the filter. The SCU has eight BNC connectors for connecting the input signals. The output signals from the SCU were directed to the A/D board through a 50-pin connector. There are provisions in the unit for starting the A/D board through external triggering circuitry. The triggering sensor is a proxy sensor.

The A/D board used offers a dynamic range of 96 dB, which is well suited for calibration purposes. The throughput sampling rate of 50 kHz was used. The data at each channel are

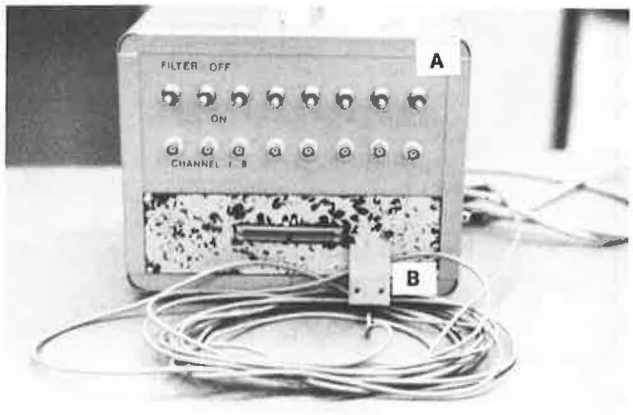

FIGURE 7 A, SCU; B, proxy switch.

measured at a rate of about 10 kHz. The A/D board is not equipped with a simultaneous sample-hold circuit. However, because most of the energy is concentrated below a frequency of 100 Hz, that deficiency is of little consequence.

Calibration system software was developed for an IBM PC–compatible computer. The program can control the acquisition and retrieval of the analog data captured by the sensors, reduce the collected data, and display and analyze the raw and reduced data. The program provides software-controlled initialization and identification of the A/D board and facilitates the collection of data using direct memory access. The acquired data are stored in a file for further processing. A flowchart of the program is shown in Figure 8. The program can be used in two modes: (*a*) to collect data through the board and process them or (*b*) to reduce previously collected data.

The software is programmed for calibration of either the Dynaflect or the FWD device. A third option is provided for flexibility. With this option, any other type of sensor reacting to either a steady-state sinusoidal load or an impulse load can be calibrated. If this option is selected, a table containing parameters for collection and reduction of data will appear on the screen. The parameters consist of the desired number of channels for collection of data, the type of sensor used with each channel, the calibration properties of each sensor, the time span for collection of data, and the number of data points per channel. The values of the parameters can be specified or default values chosen. The default values can also be read from a file previously saved.

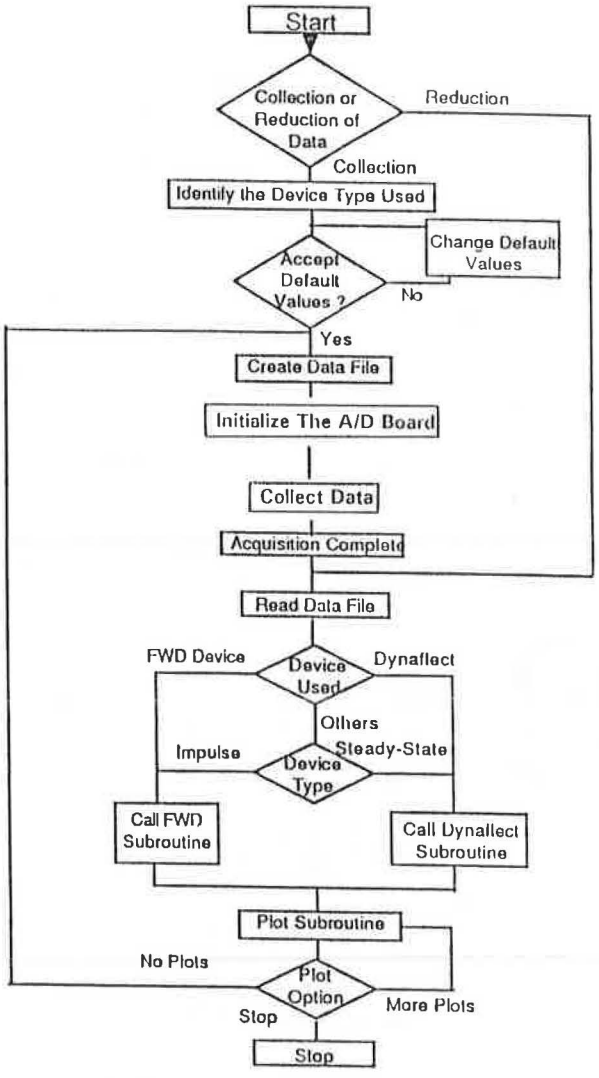

FIGURE 8 Flowchart of computer program.

The program saves the setup information and the collected data in one file. The program then reduces the collected data. The load obtained from each load cell and deflections measured with sensors are shown on the screen. The raw or reduced data can be plotted on the screen.

DESCRIPTION OF CALIBRATION PROCESS

The process for calibrating the FWD load cell is as follows. An appropriate site, consisting of a thick rigid pavement section, should be identified. Concrete thickness of 18 in. or greater is recommended; otherwise, the loss of strain energy in the paving material may result in large errors. The site should be reasonably flat to minimize the nonuniform distribution of loads among the three load cells. An asphaltic pavement section is not appropriate for load calibration.

The FWD's PVC loading plate should be replaced by the aluminum plate encasing the calibration load cells. The use of rubber padding between the loading plate and the pavement is not recommended. The padding will absorb part of the energy imparted by the drop weight to the FWD system, which will cause erroneous results.

The calibration process should be performed in two phases. Both consist of 10 drops. In the first phase the FWD load plate remains seated between successive drops. In the second phase the load plate is lifted and reseated between drops. Both phases should be repeated four times, each from a different drop height. Phase 2 is designed to quantify load variability due to plate seating. The loads should be recorded by the FWD and calibration system simultaneously. The average, standard deviation, and the coefficient of variation of all drops should be calculated for each device, drop level, and phase. A Student's *t*-test should be done to test for differences in recorded load between the FWD and calibration system.

The data from the four drop heights should be plotted using the FWD loads as the independent variables and the calibration system loads as the dependent variables. The least-squares best-fit regression line should then be determined. The upper and lower bounds corresponding to a confidence level of 95 percent should be included on the same plot. If the 95 percent interval confidence level encloses the line of equality, no action should be taken. Otherwise, the calibration factor of the FWD load cell should be adjusted.

If the coefficient of variation is more than 4 percent, the calibration process should be terminated. Some other factor, such as the mounting mechanism or a bad electrical connection, may be interfering with the sensors. The value of 4 percent is based on the precision of the sensors.

The calibration process to be followed for the deflection sensors is similar to that for the loads. A flexible pavement site is appropriate for calibrating the FWD sensors. Deflections of more than 25 mils should be obtained for sensors

close to the loading plate. Tests on concrete sites are not recommended unless the FWD is used extensively on rigid pavements.

The reference geophones are placed close to the FWD sensors. The weight is dropped, and the deflections are measured with both the FWD and the calibration system. The load imparted to the pavement is also measured with the calibration system. The measured loads are used to normalize the deflection, as described later. This process is repeated at least 10 times. The average, standard deviation, and coefficient of variation of deflections measured with the two devices and the load measured with the calibration system are calculated. A Student's *t*-test on the two samples should be carried out to verify whether means of the two samples are statistically the same.

This process is repeated for four representative drop heights. The results from the four drop heights are plotted using the deflections measured with the FWD as the independent variable and the deflections measured with the calibration system as the dependent variable. The least-squares best-fit line and the upper and lower bounds of a 95 percent confidence interval should be plotted. If the line of equality is enclosed within the 95 percent confidence interval, no change is necessary. Otherwise, the calibration values should be revised.

If the coefficient of variation measured with a sensor is more than 4 percent, the calibration process should be terminated. Some other factor, such as the mounting mechanism or a bad electrical connection, may be interfering with the sensors.

CALIBRATION EXAMPLE

An example is included to clarify the steps involved in the calibration of an FWD. The data used in the example were collected with an FWD device (*3*).

A calibration curve for the load cell of an FWD device is shown in Figure 9. Forty data points, corresponding to the 10 drops per drop height, are included in the figure. The data

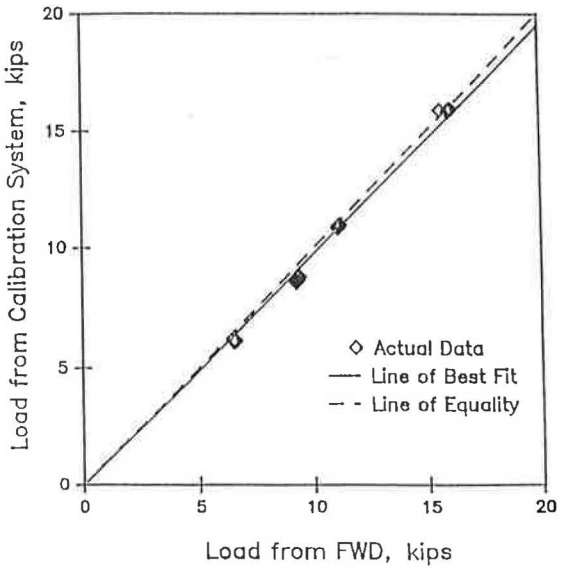

FIGURE 9 Calibration curve for FWD load cell.

are clustered in four groups corresponding to the four drop heights. The best-fit line and the line of equality are also shown. The two lines are close to one another, indicating the closeness of the calibration value to unity. The slope of the line (the calibration value) is actually 0.97.

The line of equality and upper and lower bounds corresponding to a confidence interval of 95 percent are shown in Figure 10. On the basis of this figure, a correction of the calibration value is necessary.

The calibration curve for Deflection Sensor 2 is shown in Figure 11. The data are clustered in three groups. Because of lack of time, only three load levels were used. The best-fit line and the line of equality are also shown in Figure 11. The best-fit line, line of equality, and upper and lower bounds of the 95 percent confidence interval are shown in Figure 12. Obviously, a significant difference exists between the FWD load cell and Deflection Sensor 2. There is no doubt that the calibration of Deflection Sensor 2 should be revised.

The calibration factors for all sensors are summarized in Table 2. The calibration factors for both the wraps and the repetitions are included. It can be seen that the effect on the calibration factors of lifting the loading pad after each drop is small.

SUMMARY AND CONCLUSIONS

A system was developed for the absolute calibration of FWD devices. The calibration system consists of two well-calibrated geophones and three load cells with calibration constants traceable to the National Bureau of Standards. An SCU was also developed to precondition the signals. The SCU consists of antialiasing filters and a triggering mechanism. A computer algorithm was coded for collection and reduction of data. Data

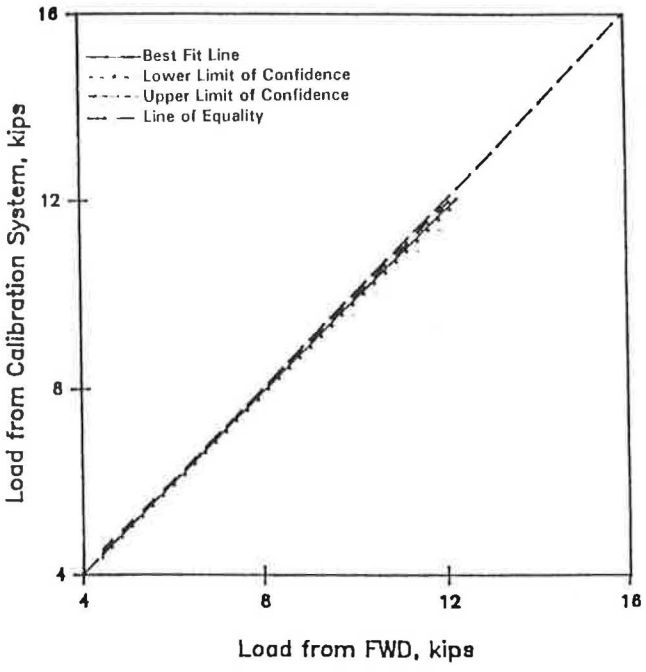

FIGURE 10 Ninety-five percent confidence interval obtained from load measurements.

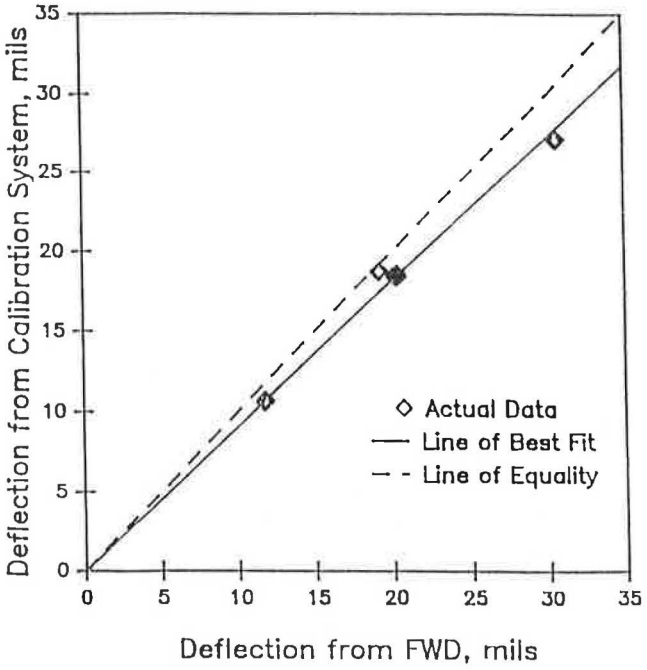

FIGURE 11 Calibration curve of Sensor 2 of FWD.

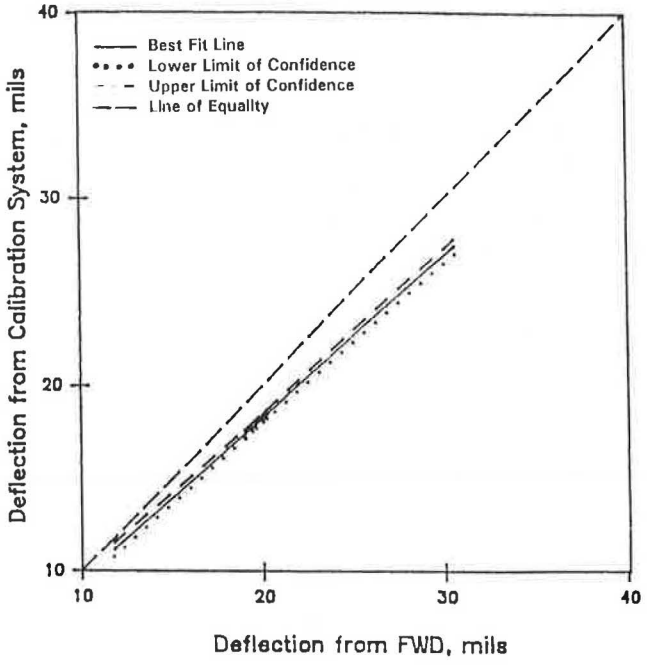

FIGURE 12 Ninety-five percent confidence interval obtained from deflection measurement of Sensor 2.

TABLE 2 CALIBRATION FACTORS FOR FWD SENSORS

Sensor	Calibration Factor	
	Repetition	Wraps
Load cell	0.97	0.97
Geophone 2	0.91	0.91
Geophone 3	0.99	0.99
Geophone 4	0.96	0.96
Geophone 5	0.98	0.98
Geophone 6	0.95	0.95
Geophone 7	0.95	0.95

can be collected from the load cells and geophones, reduced, and compared with the loads and deflections obtained simultaneously from the FWD. A calibration factor for both the FWD load cell and geophones can be determined on the basis of linear regression between data collected by the calibration system and those reported by the FWD device.

On the basis of field and laboratory investigations, the following conclusions can be drawn: (*a*) the calibration of FWD devices used by highway agencies is necessary; (*b*) geophones are feasible for use in the calibration; and (*c*) for the calibration of load cells, a portland cement concrete pavement should be used, whereas deflection sensors should be calibrated on an asphalt section.

ACKNOWLEDGMENTS

This work was funded by the Texas State Department of Highways and Public Transportation. The financial assistance and cooperation of this organization is gratefully acknowledged. Special thanks are extended to Richard Rogers, the initial project manager, for his trust and enthusiasm.

REFERENCES

1. S. Nazarian and R. C. Briggs. Determination of Structural Integrity of Secondary Roads Using Falling Weight Deflectometer. *Proc., 2nd International Conference on Bearing Capacity of Roads and Airfields*, Trondheim, Norway, 1990.
2. C. A. Richter and L. H. Irwin. SHRP Prototype Procedures for Calibrating Falling Weight Deflectometers. *Proc., State of the Art of Pavement Response Monitoring Systems for Roads and Airfields*, West Lebanon, N.H., 1989.
3. V. Tandon. *Development of an Absolute Calibration System for Nondestructive Testing Devices*. Master's thesis. The University of Texas at El Paso, El Paso, 1990.

Effect of Various Load Distributions on Backcalculated Moduli Values in Flexible Pavements

BASSAM E. TOUMA, JAMES A. CROVETTI, AND M. Y. SHAHIN

The structural adequacy of pavements is routinely evaluated by analyzing measured deflections collected with nondestructive testing devices such as the falling weight deflectometer (FWD). The FWD is an impulse loading device that closely simulates moving wheel loads in both magnitude and duration. The FWD is typically equipped with a circular loading plate and several deflection sensors positioned at discrete locations from the center of the loading plate. Virtually all available backcalculation programs that use linear elastic theory assume a circular loaded area and uniform stress distribution under the loaded area. Any deviation from these assumptions will introduce an error. To investigate the magnitude of this error, the multielastic layer computer program BISAR was used to calculate surface deflections for a limited factorial of pavement layer thicknesses and stiffnesses. Three contact stress distributions were considered: uniform (full contact), partial edge distribution (rutting), and partial circumferential distribution (weak pavement). The calculated deflections from each loading case were used to backcalculate layer moduli with the ELSDEF computer program. Results from the three cases were analyzed and the relative errors computed. The analysis indicated that if full contact is assumed when in reality it did not occur, significant errors in the backcalculated moduli values of the pavements analyzed may result.

The proliferation of nondestructive deflection testing devices has led to a dramatic increase in the use of deflection data for the structural analysis of flexible pavement systems. ("Flexible" describes conventional asphalt concrete pavement systems composed of an asphalt concrete surface layer over one or more layers of crushed aggregate resting on the natural subgrade.) Backcalculation of the elastic moduli of pavement layers is one such use. Programs based on linear elastic theory, such as ELSYM5, BISAR, ELSDEF, BISDEF, and so forth, are commonly used for this purpose.

In backcalculation of layer moduli, it is commonly assumed that the applied load is uniformly distributed over the pavement surface. Available loading plates used by falling weight deflectometers (FWDs) fall into two basic categories: segmented and nonsegmented. Both types are constructed of a semirigid upper portion with one or more layers of rubber membrane attached to the underside. It has been assumed that the rubber membranes transform the semirigid loading plate into a flexible loading plate, thus producing uniform pressure distributions over the pavement surface. To date, the authors know of no documentation that confirms this assumption.

ERES International, Inc., 1401 Regency Drive East, Savoy, Ill. 61874.

The objective of this study is to investigate the effect of various load pressure distributions on calculated surface deflections for a range of flexible pavement systems. The calculated deflections are then used to backcalculate layer moduli values, assuming a uniform load distribution. The error introduced in the backcalculated moduli due to the varying applied load distributions is determined. Finally, the relative error introduced because of the varying load distributions is determined.

PAVEMENT LOADING SIMULATION

Pressure distributions were selected to reflect potential field conditions (i.e., pavement irregularities) that preclude uniform stress distributions. Figure 1 shows loading conditions that may result from varying pavement surface conditions. The full contact case represents the assumed "control" condition, in which uniform pressure distribution is achieved under the loading plate. The rut condition assumes that surface rutting is such that the central portion of the loading plate will not come into contact with the pavement surface. The outer rim contact case assumes that the loading plate is significantly stiffer than the pavement being tested, resulting in a rigid rather than a flexible loading plate condition.

The computer program BISAR was used to calculate surface deflections that would result from each loading case over a number of pavement systems. The individual load locations selected for each load case were chosen to best simulate the load distributions while satisfying program constraints. For all program runs, the total applied load was kept constant at 9,000 lbf. Figure 2 shows the loading geometry used to simulate loading conditions for BISAR calculations for Cases 1, 2, and 3. Table 1 gives the pressure, radius, and coordinates of each discrete circle in the loaded areas.

Layer moduli were varied for the asphalt concrete pavement layer to produce a factorial experiment that encompassed a realistic range of in-service pavement systems. Figure 3 shows the cross sections investigated during this study.

To validate the assumption that discretization of the loaded area will yield valid results, trial runs were conducted using BISAR, in which Case 1 (full contact) loading was investigated. Deflection basins produced from the actual full contact were compared with those produced from the simulated full contact and were found to be in excellent agreement. Figure 4 shows a typical output. The basins are essentially the same except at D_0, where there is a difference of less than 1 percent.

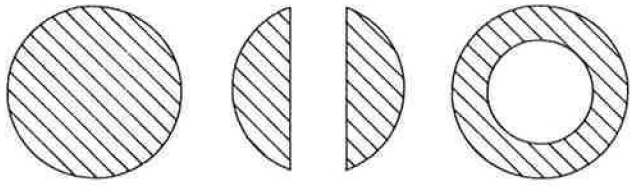

Case 1
Full Contact (control)

Case 2
Side Contact (rutting)

Case 3
Outer rim contact (weak pavement)

FIGURE 1 Possibilities for contact area shapes.

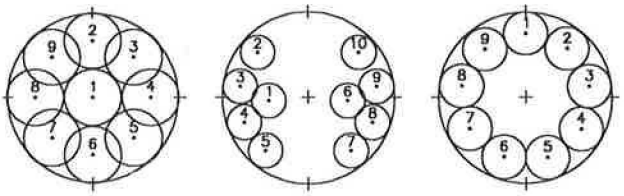

Case 1
Full Contact (control)

Case 2
Side Contact (rutting)

Case 3
Outer rim contact (weak pavement)

FIGURE 2 Approximations of contact areas for BISAR calculations.

TABLE 1 DISCRETIZED LOAD PARAMETERS FOR EACH LOADING CASE SHOWN IN FIGURE 2

Case No.	Circle No.	Pressure psi.	Radius in.	X-Y Coordinates in.	
1	1	82.02	1.97	0.00	0.00
	2	82.02	1.97	4.00	0.00
	3	82.02	1.97	0.00	4.00
	4	82.02	1.97	-4.00	0.00
	5	82.02	1.97	0.00	-4.00
	6	82.02	1.97	2.83	2.83
	7	82.02	1.97	2.83	-2.83
	8	82.02	1.97	-2.83	2.83
	9	82.02	1.97	-2.83	-2.83
2	1	233.56	1.108	-2.94	0.00
	2	233.56	1.108	-3.58	3.18
	3	233.56	1.108	-4.73	0.82
	4	233.56	1.108	-4.54	-1.49
	5	233.56	1.108	-3.43	-3.31
	6	233.56	1.108	2.87	-0.15
	7	233.56	1.108	3.36	-3.48
	8	233.56	1.108	4.59	-1.52
	9	233.56	1.108	4.69	0.73
	10	233.56	1.108	3.68	3.01
3	1	140.45	1.505	0.00	4.44
	2	140.45	1.505	2.37	3.45
	3	140.45	1.505	4.39	0.75
	4	140.45	1.505	3.79	-2.17
	5	140.45	1.505	1.36	-4.11
	6	140.45	1.505	-1.60	-4.06
	7	140.45	1.505	-3.80	-2.10
	8	140.45	1.505	-4.22	0.87
	9	140.45	1.505	-2.77	3.49

Asphalt Concrete Layer
H_{AC} = 4", 8", 12" u = 0.35
E_{AC} = 200 ksi, 600 ksi, 1000 ksi

Aggregate Base Course Layer
H_{BC} = 8" u = 0.40
E_{BC} = 30 ksi, 80 ksi

Subgrade
H_{SG} = semi infinite u = 0.40
E_{SG} = 15 ksi

FIGURE 3 Pavement cross sections investigated.

Table 2 gives the surface deflections calculated for each pavement system under each loading case. The full contact loading case (9,000-lbf load, 5.91-in. radius) defines the exact solution. Case 1 was used as the control to define the deflections that would have been expected with the FWD had a uniform distribution been modeled by discrete loads. The calculated deflections from Cases 2 and 3 represent the deflections that would have been measured by the FWD if the actual load distributions had been altered because of local conditions to resemble Case 2 and Case 3 model loadings.

BACKCALCULATION OF LAYER MODULI

The calculated deflections for Cases 1, 2, and 3 were used as inputs to ELSDEF to backcalculate the elastic modulus of each pavement layer, assuming a uniformly distributed load over a radius of 5.91 in. During program runs, the tolerance of deflection variation was set at 5 percent. Seed moduli values and allowable moduli ranges were varied as shown in Tables 3 through 6. The assumption of a uniformly distributed load was made to simulate the common practice of backcalculation using FWD deflections. Tables 7 through 10 give the backcalculated layer moduli for each system investigated.

The tables indicate that the backcalculated moduli values for each layer vary significantly from the exact solution for Cases 2 and 3. This behavior is shown in Figures 5 through 11, in which the backcalculated moduli values are plotted against the exact moduli values. It is evident that a trend exists. The surface moduli tend to be overestimated, whereas the second-layer moduli tend to be underestimated, and errors produced at the subgrade level were relatively smaller. The variation for Case 1 can be used to estimate the error introduced by discretizing the load.

Even if the exact moduli of the pavement system are provided as inputs during the backcalculation process (Tables 7 and 9), significant errors may still result for the backcalculated surface and base moduli. This impact is markedly reduced for backcalculated subgrade moduli.

FIELD LOADING CONDITIONS

To this point, this paper has been limited to a theoretical analysis of the pavement's response to varying loading

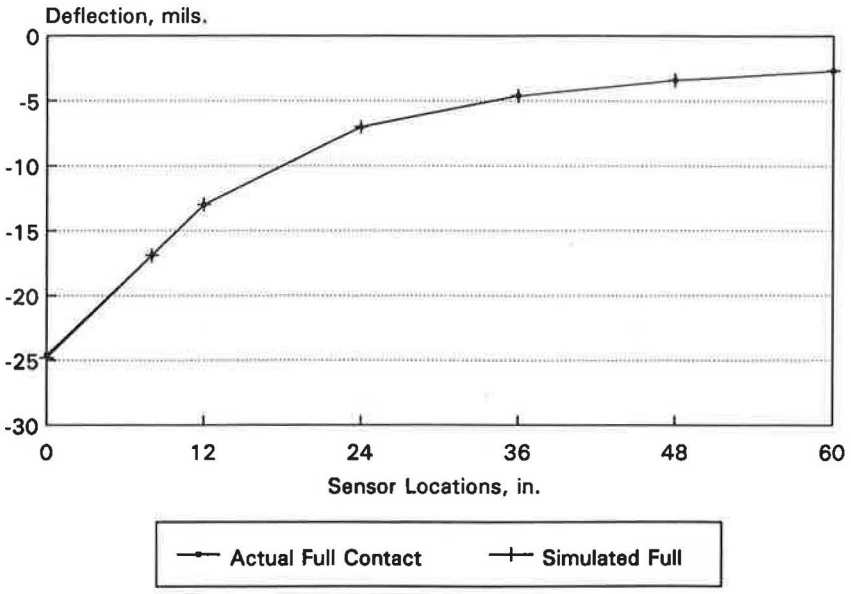

FIGURE 4 Deflection basins of uniform and simulated uniform contact pressures.

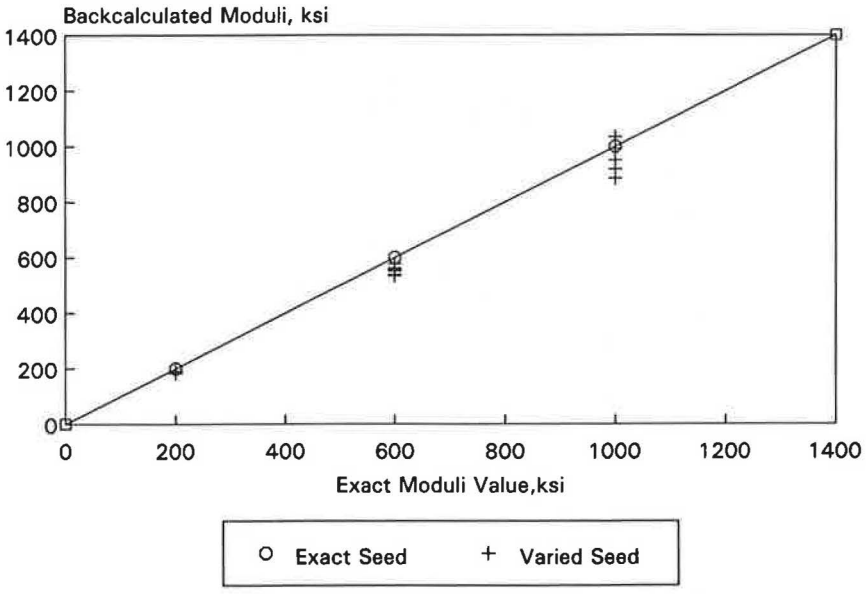

FIGURE 5 Asphalt concrete moduli comparison—full contact.

TABLE 2 CALCULATED SURFACE DEFLECTIONS FOR EACH LOADING CASE

Layer Moduli Values (ksi)			Layer Thickness (in.)		Case 1 - Full Contact Model							Case 2 - Side Contact Model							Case 3 - Rim Contact Model						
					Calculated Surface Deflections, (mils.)							Calculated Surface Deflections, (mils.)							Calculated Surface Deflections, (mils.)						
AC	Base	SG	AC	Base	D0	D6	D12	D24	D36	D48	D60	D0	D6	D12	D24	D36	D48	D60	D0	D6	D12	D24	D36	D48	D60
200	30	15	4	8	24.80	16.90	13.00	7.01	4.60	3.39	2.68	22.80	15.90	12.40	6.87	4.55	3.36	2.67	22.70	17.00	13.00	7.04	4.62	3.40	2.69
600	30	15	4	8	19.60	15.30	12.50	7.14	4.66	3.40	2.68	18.90	14.70	12.10	7.00	4.60	3.37	2.66	18.90	15.30	12.50	7.17	4.67	3.41	2.68
1000	30	15	4	8	17.50	14.30	12.00	7.21	4.73	3.43	2.68	17.00	13.80	11.70	7.08	4.67	3.40	2.66	16.90	14.20	12.00	7.23	4.74	3.43	2.69
200	30	15	8	8	16.90	12.80	10.90	6.99	4.79	3.52	2.75	15.40	12.30	10.60	6.88	4.74	3.49	2.73	15.30	12.80	10.90	7.01	4.80	3.53	2.75
600	30	15	8	8	12.00	10.30	9.28	6.71	4.88	3.65	2.84	11.50	10.10	9.14	6.64	4.83	3.62	2.82	11.50	10.30	9.28	6.72	4.89	3.66	2.85
1000	30	15	8	8	10.20	9.12	8.40	6.42	4.85	3.71	2.91	9.93	8.96	8.30	6.36	4.81	3.68	2.89	9.91	9.11	8.40	6.42	4.86	3.72	2.92
200	30	15	12	8	13.30	10.10	8.90	6.45	4.77	3.63	2.86	11.90	9.77	8.74	6.38	4.73	3.61	2.85	11.80	10.10	8.90	6.46	4.78	3.64	2.87
600	30	15	12	8	8.79	7.61	7.08	5.73	4.58	3.67	2.97	8.33	7.49	7.01	5.68	4.55	3.65	2.95	8.30	7.62	7.08	5.73	4.58	3.67	2.97
1000	30	15	12	8	7.33	6.60	6.24	5.26	4.37	3.60	2.98	7.06	6.52	6.20	5.23	4.34	3.59	2.97	7.04	6.60	6.24	5.27	4.37	3.61	2.98
200	80	15	4	8	18.40	13.30	11.10	7.02	4.81	3.53	2.75	16.80	12.70	10.80	6.92	4.77	3.50	2.74	16.70	13.40	11.10	7.04	4.82	3.54	2.75
600	80	15	4	8	15.50	12.30	10.50	6.88	4.80	3.55	2.77	14.80	11.90	10.30	6.78	4.76	3.53	2.76	14.80	12.40	10.50	6.89	4.81	3.56	2.77
1000	80	15	4	8	14.30	11.80	10.20	6.82	4.81	3.57	2.78	13.80	11.50	10.00	6.74	4.76	3.54	2.77	13.70	11.80	10.20	6.84	4.81	3.57	2.79
200	80	15	8	8	14.10	10.80	9.26	6.54	4.79	3.63	2.85	12.70	10.30	9.08	6.47	4.75	3.61	2.84	12.60	10.70	9.27	6.55	4.80	3.64	2.86
600	80	15	8	8	10.50	9.01	8.20	6.21	4.73	3.66	2.91	10.00	8.85	8.10	6.15	4.69	3.64	2.89	10.00	9.01	8.20	6.21	4.73	3.67	2.91
1000	80	15	8	8	9.23	8.21	7.60	5.97	4.66	3.67	2.94	8.93	8.09	7.53	5.93	4.63	3.65	2.92	8.90	8.20	7.60	5.97	4.66	3.67	2.94
200	80	15	12	8	11.80	8.79	7.79	5.93	4.60	3.63	2.92	10.40	8.50	7.67	5.88	4.57	3.61	2.91	10.30	8.84	7.80	5.93	4.61	3.63	2.92
600	80	15	12	8	8.08	6.96	6.49	5.34	4.37	3.58	2.95	7.63	6.85	6.43	5.31	4.35	3.56	2.94	7.60	6.97	6.49	5.34	4.37	3.58	2.95
1000	80	15	12	8	6.87	6.17	5.84	4.97	4.19	3.51	2.94	6.60	6.10	5.80	4.95	4.17	3.49	2.93	6.58	6.17	5.84	4.97	4.19	3.51	2.94

Case 1 Full Contact Load Modeling **Case 2 Partial Contact Load Modeling (Rutting Simulation)** **Case 3 Circumferential Load Modeling (Weak Pavement)**

TABLE 3 INPUT VALUES USED FOR ELSDEF PROGRAM RUNS WITH EXACT SEED MODULI (BASE COURSE MODULUS = 30 ksi)

Layer Thickness (in.)		"Exact" Moduli (Ksi.)			"Seed" Moduli (Ksi.)			Moduli Ranges, Ksi.					
								Asphalt Layer		Base Layer		Subgrade	
AC	Base	AC	BC	SG	AC	BC	SG	Min	Max	Min	Max	Min	Max
4	8	200	30	15	200	30	15	50	2000	10	75	5	30
4	8	600	30	15	600	30	15	50	2000	10	75	5	30
4	8	1000	30	15	1000	30	15	50	2000	10	75	5	30
8	8	200	30	15	200	30	15	50	2000	10	75	5	30
8	8	600	30	15	600	30	15	50	2000	10	75	5	30
8	8	1000	30	15	1000	30	15	50	2000	10	75	5	30
12	8	200	30	15	200	30	15	50	2000	10	75	5	30
12	8	600	30	15	600	30	15	50	2000	10	75	5	30
12	8	1000	30	15	1000	30	15	50	2000	10	75	5	30

Case 1 Full Contact Load Modeling
Case 2 Partial Contact Load Modeling (Rutting Simulation)
Case 3 Circumferential Load Modeling (Weak Pavement)

TABLE 4 INPUT VALUES USED FOR ELSDEF PROGRAM RUNS WITH SLIGHTLY VARYING SEED MODULI (BASE COURSE MODULUS = 30 ksi)

Layer Thickness (in.)		"Exact" Moduli (Ksi.)			"Seed" Moduli (Ksi.)			Moduli Ranges, Ksi.					
								Asphalt Layer		Base Layer		Subgrade	
AC	Base	AC	BC	SG	AC	BC	SG	Min	Max	Min	Max	Min	Max
4	8	200	30	15	200	50	10	50	2000	1	75	5	30
4	8	600	30	15	600	50	10	50	2000	1	75	5	30
4	8	1000	30	15	1000	50	10	50	2000	1	75	5	30
8	8	200	30	15	200	50	10	50	2000	1	75	5	30
8	8	600	30	15	600	50	10	50	2000	1	75	5	30
8	8	1000	30	15	1000	50	10	50	2000	1	75	5	30
12	8	200	30	15	200	50	10	50	2000	1	75	5	30
12	8	600	30	15	600	50	10	50	2000	1	75	5	30
12	8	1000	30	15	1000	50	10	50	2000	1	75	5	30

Case 1 Full Contact Load Modeling
Case 2 Partial Contact Load Modeling (Rutting Simulation)
Case 3 Circumferential Load Modeling (Weak Pavement)

TABLE 5 INPUT VALUES USED FOR ELSDEF PROGRAM RUNS WITH EXACT SEED MODULI (BASE COURSE MODULUS = 80 ksi)

Layer Thickness (in.)		"Exact" Moduli (Ksi.)			"Seed" Moduli (Ksi.)			Moduli Ranges, Ksi.					
								Asphalt Layer		Base Layer		Subgrade	
AC	Base	AC	BC	SG	AC	BC	SG	Min	Max	Min	Max	Min	Max
4	8	200	80	15	200	80	15	50	2000	10	125	5	30
4	8	600	80	15	600	80	15	50	2000	10	125	5	30
4	8	1000	80	15	1000	80	15	50	2000	10	125	5	30
8	8	200	80	15	200	80	15	50	2000	10	125	5	30
8	8	600	80	15	600	80	15	50	2000	10	125	5	30
8	8	1000	80	15	1000	80	15	50	2000	10	125	5	30
12	8	200	80	15	200	80	15	50	2000	10	125	5	30
12	8	600	80	15	600	80	15	50	2000	10	125	5	30
12	8	1000	80	15	1000	80	15	50	2000	10	125	5	30

Case 1 Full Contact Load Modeling
Case 2 Partial Contact Load Modeling (Rutting Simulation)
Case 3 Circumferential Load Modeling (Weak Pavement)

TABLE 6 INPUT VALUES USED FOR ELSDEF PROGRAM RUNS WITH SLIGHTLY VARYING SEED MODULI (BASE COURSE MODULUS = 80 ksi)

Layer Thickness (in.)		"Exact" Moduli (Ksi.)			"Seed" Moduli (Ksi.)			Moduli Ranges, Ksi.					
								Asphalt Layer		Base Layer		Subgrade	
AC	Base	AC	BC	SG	AC	BC	SG	Min	Max	Min	Max	Min	Max
4	8	200	80	15	200	50	10	50	2000	1	125	5	30
4	8	600	80	15	600	50	10	50	2000	1	125	5	30
4	8	1000	80	15	1000	50	10	50	2000	1	125	5	30
8	8	200	80	15	200	50	10	50	2000	1	125	5	30
8	8	600	80	15	600	50	10	50	2000	1	125	5	30
8	8	1000	80	15	1000	50	10	50	2000	1	125	5	30
12	8	200	80	15	200	50	10	50	2000	1	125	5	30
12	8	600	80	15	600	50	10	50	2000	1	125	5	30
12	8	1000	80	15	1000	50	10	50	2000	1	125	5	30

Case 1 Full Contact Load Modeling
Case 2 Partial Contact Load Modeling (Rutting Simulation)
Case 3 Circumferential Load Modeling (Weak Pavement)

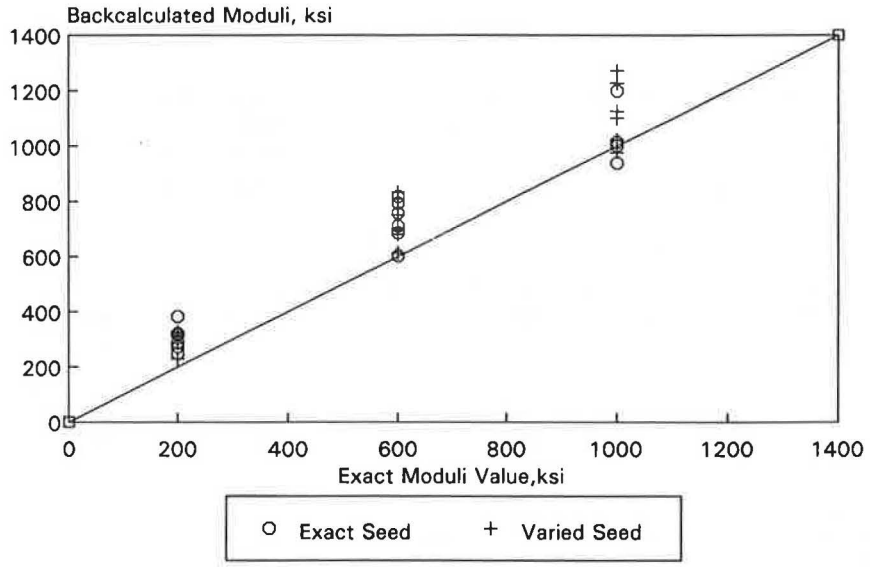

FIGURE 6 Asphalt concrete moduli comparison—rut condition.

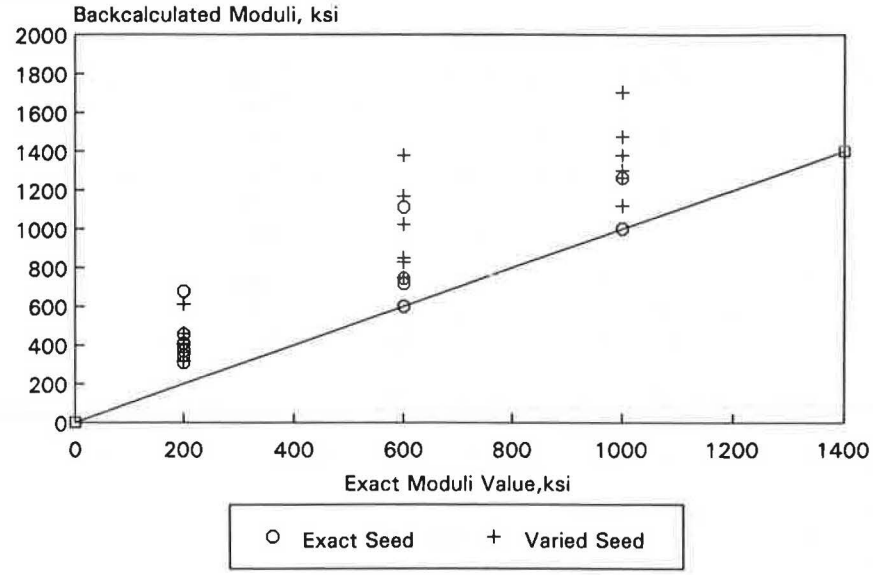

FIGURE 7 Asphalt concrete moduli comparison—rim contact.

TABLE 7 BACKCALCULATED LAYER MODULI FOR ELSDEF PROGRAM RUNS WITH EXACT SEED MODULI (BASE COURSE MODULUS = 30 ksi)

Layer Thickness (in.)		Backcalculated Pavement Moduli Values. Ksi.												Percent Difference from Exact Solution								
		Case 1				Case 2				Case 3				Case 1			Case 2			Case 3		
AC	BC	AC	BC	SG	% Err *	AC	BC	SG	% Err *	AC	BC	SG	% Err *	AC	BC	SG	AC	BC	SG	AC	BC	SG
4	8	200.0	30.0	15.0	1.21	247.6	32.8	15.5	2.03	370.9	24.6	15.2	3.32	0.0	0.0	0.0	23.8	9.3	3.3	85.4	-18.0	1.3
4	8	600.0	30.0	15.0	1.12	602.1	34.1	15.3	1.61	600.0	30.0	15.0	4.46	0.0	0.0	0.0	0.4	13.7	2.0	0.0	0.0	0.0
4	8	1000.0	30.0	15.0	0.72	938.0	36.3	15.2	1.20	1000.0	30.0	15.0	3.88	0.0	0.0	0.0	-6.2	21.0	1.3	0.0	0.0	0.0
8	8	200.0	30.0	15.0	1.22	286.7	22.4	15.5	0.78	345.9	10.0	16.8	3.94	0.0	0.0	0.0	43.3	-25.3	3.3	72.9	-66.7	12.0
8	8	600.0	30.0	15.0	1.10	756.9	14.7	16.0	0.38	600.0	30.0	15.0	4.07	0.0	0.0	0.0	26.1	-51.0	6.7	0.0	0.0	0.0
8	8	1000.0	30.0	15.0	0.93	1198.0	19.7	15.4	4.42	1000.0	30.0	15.0	2.55	0.0	0.0	0.0	19.8	-34.3	2.7	0.0	0.0	0.0
12	8	200.0	30.0	15.0	1.47	272.8	13.7	16.4	4.82	308.7	10.0	15.9	5.71	0.0	0.0	0.0	36.4	-54.3	9.3	54.3	-66.7	6.0
12	8	600.0	30.0	15.0	2.09	710.7	10.0	16.2	1.29	716.0	10.0	15.8	3.98	0.0	0.0	0.0	18.5	-66.7	8.0	19.3	-66.7	5.3
12	8	1000.0	30.0	15.0	2.09	1000.0	30.0	15.0	4.16	1000.0	30.0	15.0	4.69	0.0	0.0	0.0	0.0	0.0	0.0	0.0	0.0	0.0

* Absolute Error of Convergence from ELSDEF Program Runs

Case 1 Full Contact Load Modeling.
Case 2 Partial Contact Load Modeling (Rutting Simulation).
Case 3 Circumferential Load Modeling (Weak Pavement).

TABLE 8 BACKCALCULATED LAYER MODULI FOR ELSDEF PROGRAM RUNS WITH SLIGHTLY VARYING SEED MODULI (BASE COURSE MODULUS = 30 ksi)

Layer Thickness (in.)		Backcalculated Pavement Moduli Values. Ksi.												Percent Difference from Exact Solution								
		Case 1				Case 2				Case 3				Case 1			Case 2			Case 3		
AC	BC	AC	BC	SG	% Err *	AC	BC	SG	% Err *	AC	BC	SG	% Err *	AC	BC	SG	AC	BC	SG	AC	BC	SG
4	8	186.5	30.4	15.0	1.02	229.1	34.2	14.3	1.83	403.6	23.8	15.0	4.69	-6.8	1.3	-0.3	14.5	14.0	-4.7	101.8	-20.6	-0.2
4	8	561.8	31.1	14.9	0.67	612.8	33.6	15.2	0.79	827.8	26.7	14.7	4.72	-6.4	3.5	-0.5	2.1	12.0	1.3	38.0	-11.2	-1.9
4	8	992.0	29.8	15.0	0.86	976.1	34.7	15.1	0.75	1378.6	19.1	15.5	2.08	-0.8	-0.5	-0.3	-2.4	15.6	0.7	37.9	-36.5	3.3
8	8	191.2	31.3	14.9	0.60	284.3	23.8	15.3	1.34	362.1	8.2	17.6	4.04	-4.4	4.3	-0.4	42.2	-20.7	2.0	81.1	-72.8	17.0
8	8	551.3	35.8	14.9	0.51	750.1	14.0	16.1	1.21	1378.6	19.1	15.5	2.08	-8.1	19.3	-0.7	25.0	-53.3	7.3	129.8	-36.5	3.3
8	8	918.2	39.6	14.8	0.38	1124.7	19.5	15.5	0.20	1300.9	5.2	17.8	0.43	-8.2	31.9	-1.3	12.5	-35.1	3.3	30.1	-82.6	18.8
12	8	183.6	36.1	14.8	0.96	311.0	8.3	16.8	1.59	317.5	7.9	16.7	4.96	-8.2	20.4	-1.1	55.5	-72.2	11.7	58.8	-73.6	11.1
12	8	537.3	44.6	14.8	0.81	698.6	7.6	16.8	2.62	747.0	2.9	20.3	2.33	-10.5	48.6	-1.3	16.4	-74.8	12.3	24.5	-90.5	35.3
12	8	950.8	27.4	15.3	1.11	1099.4	7.5	16.4	3.68	1118.9	3.5	18.7	3.53	-4.9	-8.8	2.0	9.9	-74.9	9.3	11.9	-88.3	24.4

* Absolute Error of Convergence from ELSDEF Program Runs

Case 1 Full Contact Load Modeling.
Case 2 Partial Contact Load Modeling (Rutting Simulation).
Case 3 Circumferential Load Modeling (Weak Pavement).

TABLE 9 BACKCALCULATED LAYER MODULI FOR ELSDEF PROGRAM RUNS WITH EXACT SEED MODULI (BASE COURSE MODULUS = 80 ksi)

Layer Thickness (in.)		Backcalculated Pavement Moduli Values. Ksi.												Percent Difference from Exact Solution								
		Case 1				Case 2				Case 3				Case 1			Case 2			Case 3		
AC	BC	AC	BC	SG	% Err *	AC	BC	SG	% Err *	AC	BC	SG	% Err *	AC	BC	SG	AC	BC	SG	AC	BC	SG
4	8	200.0	80.0	15.0	1.44	382.2	77.0	15.1	2.73	678.2	54.5	14.9	1.83	0.0	0.0	0.0	91.1	-3.8	0.7	239.1	-31.9	-0.7
4	8	600.0	80.0	15.0	1.04	684.4	84.5	15.2	1.25	1111.7	64.4	15.0	2.04	0.0	0.0	0.0	14.1	5.6	1.3	85.3	-19.5	0.0
4	8	1000.0	80.0	15.0	1.32	1013.2	85.9	15.2	0.73	1000.0	80.0	15.0	3.83	0.0	0.0	0.0	1.3	7.4	1.3	0.0	0.0	0.0
8	8	200.0	80.0	15.0	1.39	320.7	63.4	15.2	0.69	455.6	33.8	15.7	4.28	0.0	0.0	0.0	60.3	-20.8	1.3	127.8	-57.8	4.7
8	8	600.0	80.0	15.0	1.28	816.5	55.5	15.3	1.26	600.0	80.0	15.0	4.54	0.0	0.0	0.0	36.1	-30.6	2.0	0.0	0.0	0.0
8	8	1000.0	80.0	15.0	1.84	1000.0	80.0	15.0	4.98	1000.0	80.0	15.0	2.89	0.0	0.0	0.0	0.0	0.0	0.0	0.0	0.0	0.0
12	8	200.0	80.0	15.0	1.95	316.3	44.5	15.5	2.39	407.8	5.4	19.5	3.20	0.0	0.0	0.0	58.2	-44.4	3.3	103.9	-93.3	30.0
12	8	600.0	80.0	15.0	1.99	792.5	22.3	16.1	1.78	744.0	28.4	15.9	4.50	0.0	0.0	0.0	32.1	-72.1	7.3	24.0	-64.5	6.0
12	8	1000.0	80.0	15.0	1.69	1000.0	80.0	15.0	4.90	1262.7	4.6	18.3	3.95	0.0	0.0	0.0	0.0	0.0	0.0	26.3	-94.3	22.0

*** Absolute Error of Convergence from ELSDEF Program Runs**

Case 1 Full Contact Load Modeling.
Case 2 Partial Contact Load Modeling (Rutting Simulation).
Case 3 Circumferential Load Modeling (Weak Pavement).

TABLE 10 BACKCALCULATED LAYER MODULI FOR ELSDEF PROGRAM RUNS WITH SLIGHTLY VARYING SEED MODULI (BASE COURSE MODULUS = 80 ksi)

Layer Thickness (in.)		Backcalculated Pavement Moduli Values. Ksi.												Percent Difference from Exact Solution								
		Case 1				Case 2				Case 3				Case 1			Case 2			Case 3		
AC	BC	AC	BC	SG	% Err *	AC	BC	SG	% Err *	AC	BC	SG	% Err *	AC	BC	SG	AC	BC	SG	AC	BC	SG
4	8	188.9	81.2	15.0	1.06	328.1	87.9	15.0	3.13	611.8	56.1	15.0	2.82	-5.5	1.5	0.0	64.1	9.9	0.0	205.9	-29.9	0.0
4	8	534.4	84.2	15.0	0.73	680.4	87.0	15.1	1.90	1168.8	66.5	14.9	4.32	-10.9	5.3	0.0	13.4	8.8	0.7	94.8	-16.9	-0.7
4	8	885.5	83.8	15.0	0.82	1022.3	86.7	15.2	1.67	1703.0	58.9	15.1	2.52	-11.5	4.7	0.0	2.2	8.4	1.3	70.3	-26.4	0.7
8	8	183.7	86.7	15.0	0.74	323.1	62.6	15.2	0.54	459.9	33.2	15.6	3.68	-8.2	8.4	0.0	61.6	-21.8	1.3	130.0	-58.5	4.0
8	8	556.3	87.8	15.0	1.13	832.5	65.8	15.0	4.47	1023.1	15.8	16.5	1.87	-7.3	9.7	0.0	38.8	-17.8	0.0	70.5	-80.3	10.0
8	8	885.5	97.0	14.9	1.77	1226.1	60.9	15.1	1.94	1474.0	14.6	16.5	1.07	-11.5	21.3	-0.7	22.6	-23.9	0.7	47.4	-81.8	10.0
12	8	185.6	87.9	15.0	0.72	316.0	45.5	15.4	1.97	407.6	5.4	19.4	3.19	-7.2	9.9	0.0	58.0	-43.1	2.7	103.8	-93.3	29.3
12	8	576.7	81.8	15.2	2.43	808.3	23.7	15.7	3.15	848.9	6.2	18.1	3.01	-3.9	2.2	1.3	34.7	-70.4	4.7	41.5	-92.3	20.7
12	8	1034.5	52.3	15.4	1.21	1271.2	8.5	16.9	2.30	1263.1	4.5	18.3	4.17	3.5	-34.6	2.7	27.1	-89.4	12.7	26.3	-94.4	22.0

*** Absolute Error of Convergence from ELSDEF Program Runs**

Case 1 Full Contact Load Modeling.
Case 2 Partial Contact Load Modeling (Rutting Simulation).
Case 3 Circumferential Load Modeling (Weak Pavement).

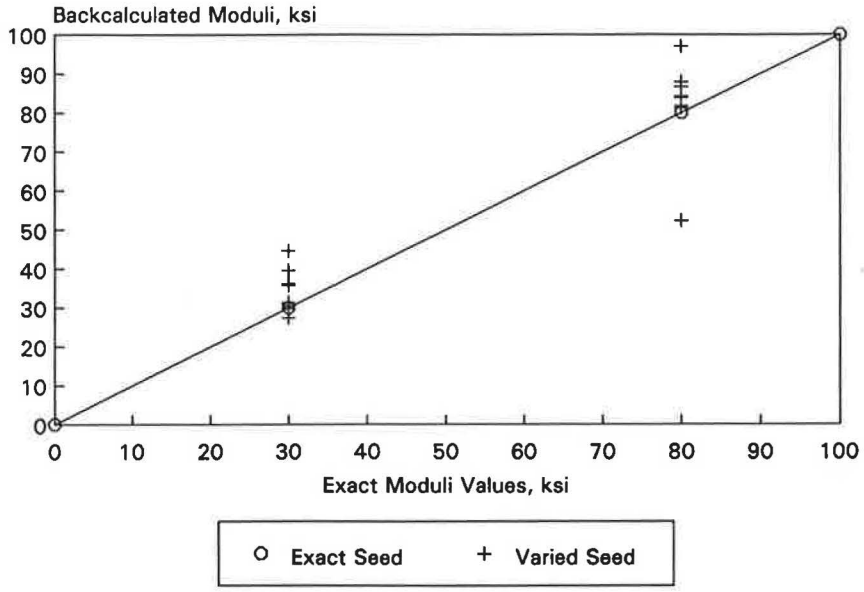

FIGURE 8 Base course moduli comparison—full contact.

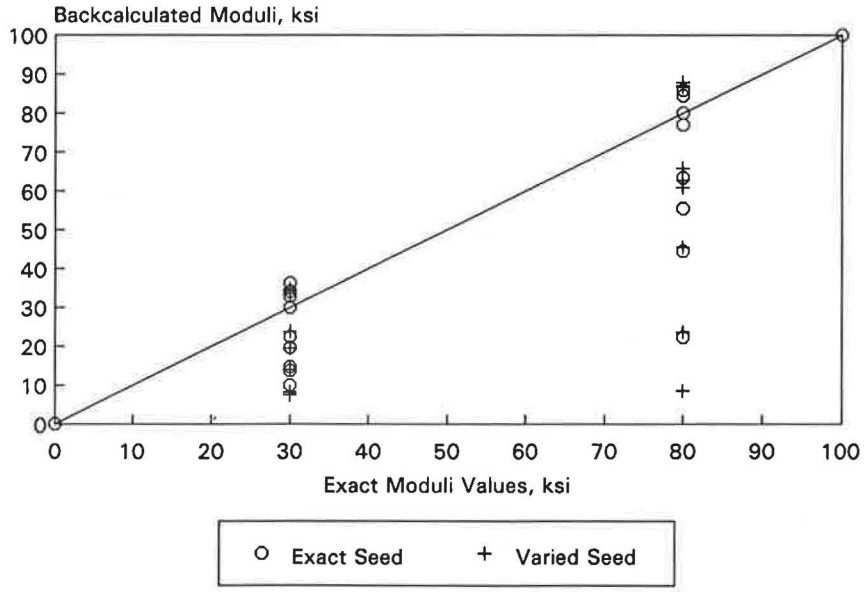

FIGURE 9 Base course moduli comparison—rut condition.

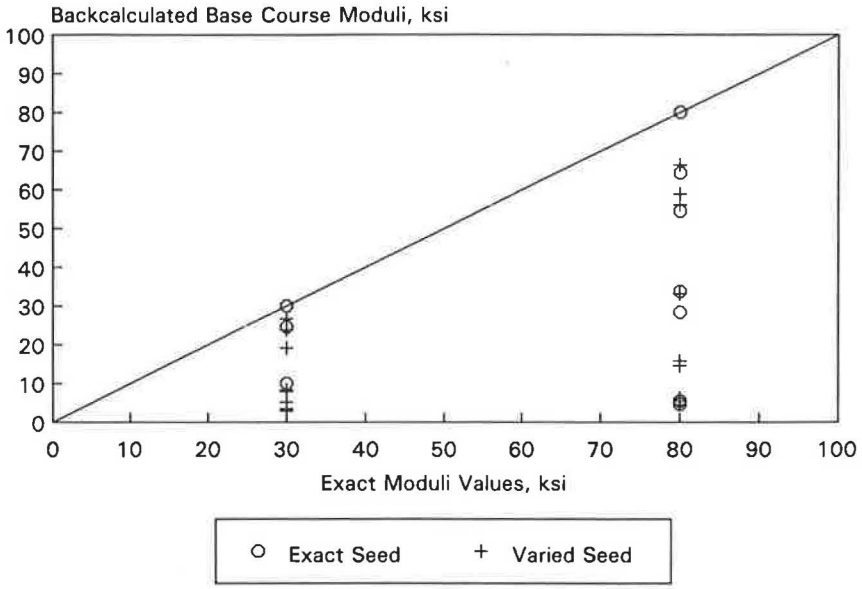

FIGURE 10 Base course moduli comparison—rim contact.

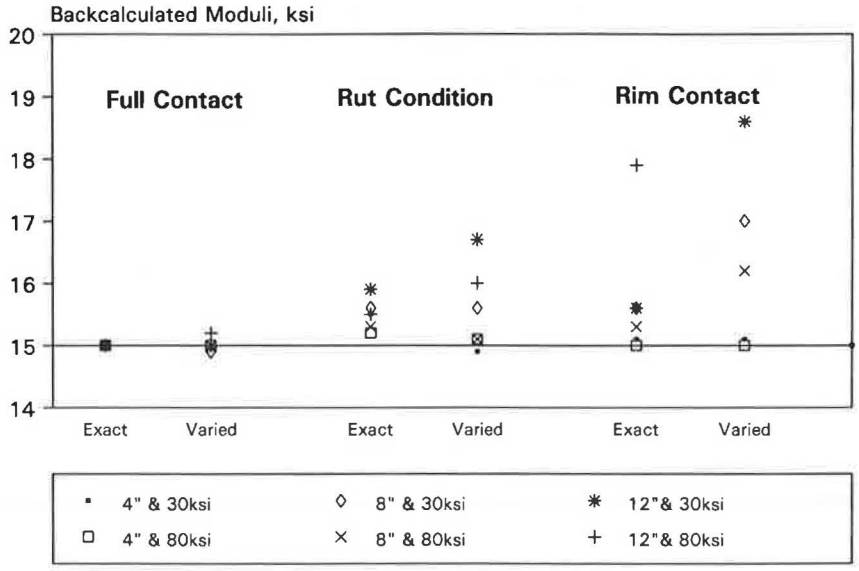

FIGURE 11 Average subgrade moduli comparison—all cases.

conditions. It has been generally assumed by the pavement community that all FWD loading systems produce relatively uniform stress distributions under the entire loading plate for all but severely rutted pavements. Data that significantly alter this viewpoint have been collected.

Two FWD loading plates, segmented and nonsegmented, were used under field testing conditions. Pressure-sensitive film, manufactured by Fuji Film I & I, was used to obtain a footprint of the pressure distribution under each loading plate at an applied load of approximately 14,000 lbf. The Fuji Prescale Film is available in widths of 270 mm on continuous rolls 5 m long and sensitive in the range of 70 to 350 psi. This film is composed of an A-film, featuring a layer of microencapsulated color-forming material in between, and a C-film, featuring a layer of color-developing material. When pressure is applied, the microcapsules on the A-film are broken, and the noncolored, color-forming material is released and absorbed by the color-developing material of the C-film, which in turn reacts with the color-developing material to generate the colors of the C-film. The microcapsules of color-forming material are designed to break at different pressure levels, thus allowing for determination of the pressure distribution throughout the material. The intensity of the color indicates the pressure applied; darker color indicates higher pressure.

Tests were conducted on three different pavement types, as follows:

1. A smooth, newly paved asphalt pavement that had received very few traffic loadings;
2. A relatively strong, heavily trafficked asphalt pavement with a rut depth of ⅛ in. measured across the radius of loading (Figure 12); and
3. A relatively weak, lightly trafficked chip-seal pavement with a flat profile under the loading plate.

Before pavement testing, 18-in. strips of A-film and C-film were cut from the film rolls and taped together to form a sandwich of prescale film with approximate dimensions of 18 × 10.6 in. The segmented loading plate was positioned on the pavement surface so that a spray-painted outline of the loading plate could be made. Next, the prescale film sandwich was taped onto the pavement surface to cover the loading plate outline (11.81-in. diameter) as completely as possible. The FWD was switched to computer operation to produce one load at approximately 14,000 lbf (127 psi). The prescale sandwich was removed and the FWD driven off the pavement surface.

The second FWD, equipped with a nonsegmented loading plate, was positioned so that the loading plate would fall within the previously painted loading plate outline. A second prescale film sandwich was taped to the pavement surface. A single load at approximately 14,000 lbf was applied to the pavement using the nonsegmented loading plate. The prescale sandwich was removed, and the FWD was driven off the pavement surface.

Figure 13 shows digitized copies of the original pressure distributions obtained for each field loading condition. The nonsegmented loading plate produces variable stress distributions depending on the type of pavement tested. A rut depth as small as ⅛ in. produced significant alteration of the stress distribution applied with the nonsegmented plate. Conversely, the segmented loading plate provided relatively uniform stress distributions regardless of the pavement's surface condition.

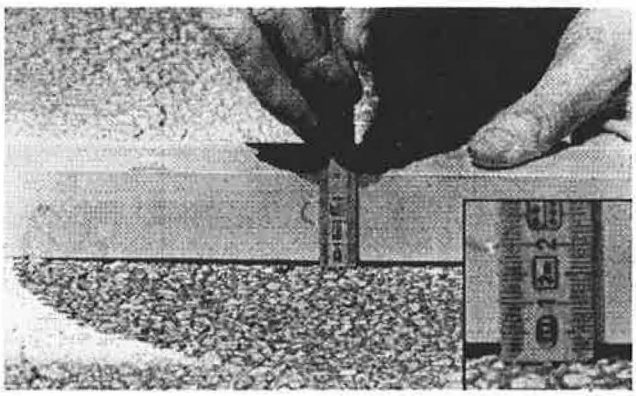

FIGURE 12 Rut measurement (3 mm) on a relatively strong, heavily trafficked asphalt pavement.

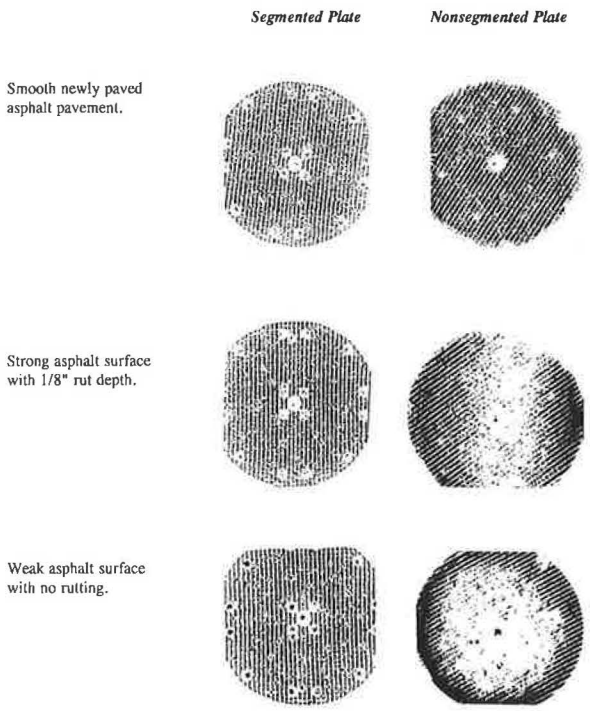

FIGURE 13 Actual pressure distribution under rigid and segmented plates.

SUMMARY AND CONCLUSIONS

A theoretical analysis of deflection variation as a function of load shape for a variety of asphalt pavement systems has been presented. The calculated deflections were used as input to determine the backcalculated layer moduli of the pavement systems. It has been demonstrated that significant error can be introduced into the pavement analysis process if measured deflections are obtained with anything but a uniform stress distribution. The error stems from one of the assumptions used by the analysis programs—uniform pressure distribution over the pavement surface. The error is present even if the exact moduli of the pavement system are provided as inputs during backcalculation.

Field tests covering a variety of pavement surface conditions have been made. The results indicate that the pressure distributions obtained from the nonsegmented plate were neither uniform nor consistent for all cases considered. However, consistently uniform distributions were obtained from the segmented plate. The implication is that a significant source of error may be introduced into a detailed pavement analysis that uses FWD deflections if the exact pressure distribution at the time of loading was unknown.

Estimation of Paving Materials Design Moduli from Falling Weight Deflectometer Measurements

FRAZIER PARKER, JR.

The emergence of mechanistic pavement thickness design procedures or semiempirical design procedures, as contained in the 1986 *AASHTO Guide for Design of Pavement Structures*, has created a need for methods of evaluating elastic moduli of paving materials and subgrade soils. A study was conducted to develop methods for using falling weight deflectometer (FWD) measurements to determine moduli of in situ pavement materials and to compare FWD-estimated moduli with laboratory-measured values in order to achieve consistent input to thickness design procedures. A three-layer pavement model was used to characterize typical Alabama flexible pavements. Simple procedures were developed to account for seasonal variations and to estimate average or effective moduli values for granular base-subbase and subgrade soils from limited FWD measurements. A procedure for adjusting asphalt-aggregate moduli to standard design temperature (70°F) was developed. Laboratory moduli for asphalt-aggregate mixtures measured with indirect tension tests (ASTM D4123) produce moduli that compare well with moduli backcalculated from FWD pavement deflection basin measurements. As expected, characterization of granular base-subbase was most difficult. There were large differences between FWD moduli and laboratory moduli from triaxial testing (AASHTO T274). Although some inconsistencies in input to thickness design procedures may result, FWD moduli are recommended for characterizing in situ granular base-subbase. In general, good agreement was demonstrated between FWD and laboratory (AASHTO T274) moduli for subgrade soils.

The emergence of mechanistic or semiempirical design procedures, as contained in the 1986 *AASHTO Guide for Design of Pavement Structures* (*1*), has created a need for methods of evaluating elastic moduli of paving materials. In addition, the emphasis on pavement rehabilitation and maintenance activities has increased the need for in situ evaluation. After years of utilization and evaluation of in situ testing devices, beginning with the static Benkelman beam and progressing through various vibratory loading devices, the falling weight deflectometer (FWD) has gained widespread acceptance.

The Alabama Highway Department, preparing for implementation of the 1986 *AASHTO Guide* and utilization of the FWD, funded a study of methods for evaluating elastic moduli of paving materials. Portions of that study are described, with emphasis on methodology for selection of moduli values for use in thickness design procedures. The study was limited to flexible (asphalt-aggregate surfaced) pavements with granular or asphalt base courses and granular subbase courses. No pavements with lime- or cement-treated base, subbase, or subgrade were considered.

Highway Research Center, Auburn University, Auburn, Ala. 36849-5337.

The moduli of paving materials backcalculated from FWD load–deflection basin measurements reflect pavement conditions at the time of measurement and stress conditions induced by the applied load. The moduli values must be modified to average or design conditions for use in pavement thickness design procedures. Some backcalculation programs can modify moduli on the basis of preset criteria. For example, ELMOD (*2*) can adjust asphalt-aggregate modulus for temperature and granular base and subgrade for seasonal variations.

For asphalt-aggregate mixtures, temperature dramatically affects modulus, and most design procedures require adjustment to a standard design temperature (usually around 70°F). The procedure considered for temperature adjustment follows that suggested in the 1986 *AASHTO Guide*. Rate of loading also influences asphalt-aggregate modulus. The procedure considered for adjusting FWD moduli to values for comparable laboratory testing load rates follows that suggested by Lee et al. (*3*).

Granular base-subbase is the most difficult paving material to characterize. The modulus is sensitive to the state of stress, and there may be seasonal variations. In Alabama, where there is no significant frost action, seasonal variations are caused primarily by moisture content variations. Procedures for estimating average moduli were considered. Comparisons were made with typical granular material constants (k_1 and k_2) contained in the 1986 *AASHTO Guide* for dry, damp, and wet conditions and with values presented by other researchers.

Subgrade moduli must be adjusted for seasonal variations. As with granular base-subbase, this variation is due primarily to moisture. The magnitude of the expected variation does not appear to warrant application of a procedure as complex as the one recommended in the 1986 *AASHTO Guide* for computing an effective roadbed soil resilient modulus. Because there is no significant frost action in Alabama, the relative damage factors are rather uniform, and the use of average moduli for design is considered adequate.

The sensitivity of moduli of all materials (asphalt-aggregate mixtures, granular base-subbase, and subgrade) to stress levels was considered. The magnitude of the FWD load was varied, and backcalculated moduli were compared.

STUDY PLAN

To develop procedures for estimating design moduli of paving materials from FWD measurements, a program of sampling and testing was conducted. Eight seasonal sites, Locations 1 through 8 in Figure 1, were selected. Beginning in fall 1985, FWD data were collected at approximately 2-month intervals for a period of about 3 years. In addition, four sites on the Interstate system, Locations A through D in Figure 1, were selected for limited testing.

Site Selection

Sites were selected to include as many variables as possible. The test sites were distributed geographically from north to south to cover the limited climatic variability within the state. They were located in three geologic regions: Appalachian Plateau, piedmont, and coastal plains. To ensure a range in pavement structure, sites were selected on the Interstate, primary, and secondary road systems. Pavement structures are described in Table 1.

FWD Testing

Deflection basins were measured with a Dynatest 8000 FWD by the Bureau of Materials and Tests of the Alabama Highway Department. Dynamic loads of 9, 12, and 15 kips were applied. Asphalt-aggregate temperature was measured periodically during FWD testing. All FWD testing was conducted in outside lanes.

At each seasonal site there were 10 test points spaced approximately 200 ft apart. Interstate sites consisted of 2.4- to 5-mi-long sections with test points spaced at approximately 400 ft.

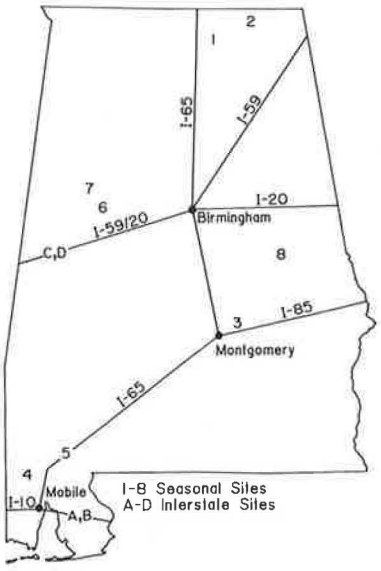

FIGURE 1 Locations of test sites.

TABLE 1 PAVEMENT STRUCTURES AT TEST SITES

Site	Structure	Model
	Seasonal Sites	
1	5.5" asphalt -aggregate 10" crushed aggregate base 14" select soil	t_1 = 5.5" t_2 = 24"
2	4" asphalt -aggregate 3" sand gravel base 12" select soil	t_1 = 4" t_2 = 15"
3	9" asphalt -aggregate 6" soil aggregate base 12" select soil	t_1 = 9" t_2 = 12"
4	3.5" asphalt -aggregate 8" granular soil base 12" select soil	t_1 = 3.5" t_2 = 20"
5	10" asphalt -aggregate 5" roadmix reef shell base 12" select soil subbase 12" improved roadbed	t_1 = 10" t_2 = 24"
6	4.8" asphalt -aggregate 4" soil aggregate base 6" soil aggregate subbase	t_1 = 4.8" t_2 = 10"
7	3.2" asphalt -aggregate 10" soil aggregate base and subbase 12" improved roadbed	t_1 = 3.2" t_2 = 22"
8	4.5" asphalt -aggregate 8" soil aggregate base	t_1 = 4.5" t_2 = 8"
	Interstate Sites	
A & B	7.6" asphalt -aggregate 5" soil aggregate (shell) base 6" select soil subbase 12" improved roadbed	t_1 = 7.6" t_2 = 23"
C	9.3" asphalt -aggregate 5" soil aggregate base 6" select soil subbase 12" improved roadbed	t_1 = 9.3" t_2 = 11"
D	8.8" asphalt -aggregate 5" soil aggregate base 12" select soil subbase 12" improved subgrade	t_1 = 8.8" t_2 = 17"

Improved roadbed included in pavement structure where indicated from available as constructed information, or where sampling indicated dramatic differences (density and/or water content) between top 12 inches and remainder of subgrade.

Backcalculation of Moduli

Moduli were backcalculated with the program ELMOD (*2*). The rigid subgrade boundary option of ELMOD, in which the depth to a rigid boundary is computed on the basis of an analysis of the outer deflections, was used.

Typical pavement structures consisted of asphalt-aggregate surface, granular base, granular subbase, and, usually, a processed subgrade layer. Within layers there were often additional layers creating a more complex layered system. For estimation of moduli from FWD data, such a complex system is neither practical (because of computation time required) nor necessary (in terms of characterization). Simplified models are normally used, but no generally accepted recommendations for the number of layers required to adequately model flexible pavements were found in a literature review. In the literature three layers were most often used, and four were used occasionally. When four were used, the moduli for the

third and fourth (subgrade) layers were often quite close. Bush and Alexander (*4*) indicate that best results are obtained when not more than three layers with unknown moduli are used. Husain and George (*5*) recommend that pavements with four or more layers be reduced to three-layer models.

For this study pavement structures were modeled with three layers, not including the rigid boundary placed by the ELMOD program. Thicknesses for Layers 1 and 2 are given in Table 1.

Asphalt-aggregate layers included several different types of asphalt concrete, but some also included tack, flush, or seal coats, as well as chip seals. All asphalt-aggregate layers, including asphalt base course, were combined into Layer 1 of the model.

Base and subbase layers were composed of granular unbound soil-aggregate materials. They were combined into Layer 2 of the model.

Determining where to place the processed subgrade (upper portion of subgrade) in the model presents the most problems. Select material, with possibly stabilizing additives, is included in this layer to improve or modify its properties. The decision is whether the processed subgrade should be included in Layer 2 because it is more like the base-subbase or in Layer 3 because it is more like the subgrade. The location of the processed subgrade layer was based on in situ density and moisture content measurements, which in this study usually resulted in inclusion in Layer 2. A sensitivity analysis indicated that inclusion of the processed subgrade in Layer 2 or 3 of the model had little effect on E_1, some effect on E_3, and significant effect on E_2.

Sampling and Laboratory Testing

Cores of asphalt-aggregate layers and disturbed samples of unbound granular base-subbase layers and subgrade soils were obtained at six of the eight seasonal sites and the four Interstate sites. The asphalt-aggregate cores were sawed along layer interfaces, where possible, to produce specimens for indirect tension testing. The specimens were tested at 41°F, 77°F, and 104°F, in accordance with ASTM D4123. A weighted composite modulus was computed for the entire asphalt-aggregate layer from the moduli of individual layers.

Specimens (8 × 4 in.) for triaxial testing were recompacted from disturbed samples of base-subbase and subgrade soils. Specimens were compacted with a kneading compactor in accordance with AASHTO T190 to densities and moisture contents approximating those measured in situ. The recompacted specimens were tested for resilient modulus in accordance with AASHTO T274.

ANALYSIS OF TEST RESULTS

Data from the FWD and laboratory testing were analyzed to develop procedures for selecting design modulus. The effects of temperature and load rate on asphalt-aggregate modulus, the effects of seasonal variations on unbound granular base-subbase and subgrade modulus, and the effects of load or stress intensity on the modulus of all materials were examined.

Asphalt-Aggregate Modulus

To study the effects of temperature, plots were made of asphalt-aggregate moduli backcalculated from FWD measurements versus temperature. Figure 2 shows a plot for Site 1 with data for all three FWD load levels. Linear and power curves were fitted to the data using least squares criteria. The power curves more accurately modeled the variation in asphalt-aggregate moduli with temperature and were similar to relationships suggested by Lee et al. (*3*) and Witczak (*6*).

The data for all eight seasonal sites were combined and the following composite power curve was developed:

$$E_1 = 322{,}000/T^{1.591} \quad (1)$$

The composite curve is shown in Figure 3 with curves for the individual sites and in Figure 4 with relationships suggested by Lee et al. (*3*) and Witczak (*6*).

The wide range of moduli exhibited in Figure 3 reflects the wide range of asphalt-aggregate materials encountered. The asphalt-aggregate layer at Site 5 is composed of 10 in. of high-quality surface, binder, and base course hot mix, whereas Site 2 is composed of road mix, seal coats, and lower-quality hot mix. Comparison of the composite curve with the curves suggested by Lee et al. (*3*) and Witczak (*6*) indicates that, on the average, the asphalt-aggregate mixtures were less sensitive to temperature. At 70°F the composite curve also agrees with the curve suggested by Witczak (*6*).

To provide a way to adjust asphalt-aggregate modulus backcalculated with FWD data to standard design temperature,

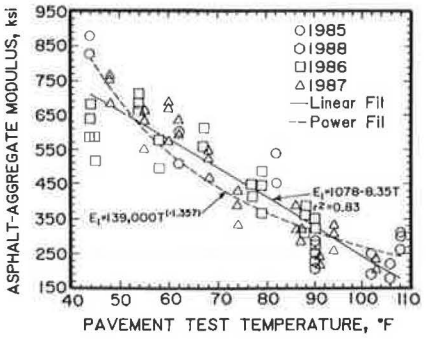

FIGURE 2 Asphalt-aggregate modulus versus temperature, Site 1.

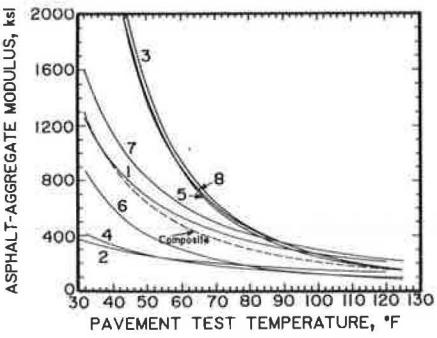

FIGURE 3 Composite and individual curves for eight seasonal sites.

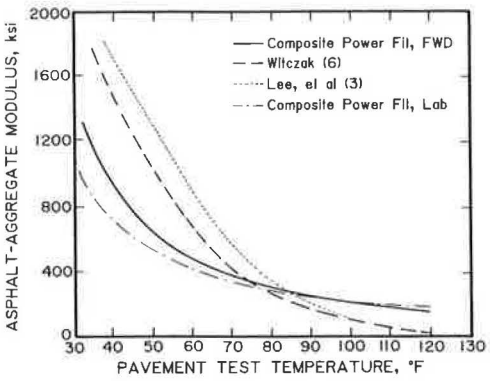

FIGURE 4 Relationships between asphalt-aggregate modulus and temperature.

the moduli-temperature relationships in Figure 3 were used. Moduli were computed using Equation 1 for various temperatures, and the ratios of those moduli to the moduli at 70°F were computed as

$$F_a = E_{1(70)}/E_{1(T)} \quad (2)$$

These ratios were used to develop the curve shown in Figure 5. Also shown in Figure 5 are the correction curve provided in the 1986 *AASHTO Guide* and modular ratios for the eight individual seasonal sites at 40°F and 100°F. Although there will be some inaccuracies for particular sites, the composite correction curve provides criteria for adjusting asphalt-aggregate moduli measured at temperatures between 30°F and 120°F to 70°F design temperature.

Figure 6 shows the variable influence of FWD load magnitude. At Site 1, modulus increased as FWD load increased. This trend was also observed at Sites 2, 4, 6, and 7. At Site 3, FWD load had virtually no effect on asphalt-aggregate

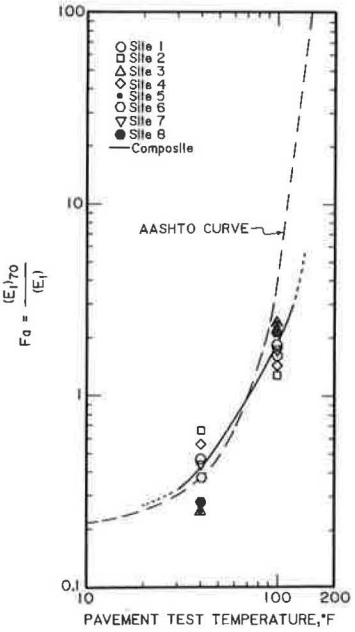

FIGURE 5 Asphalt-aggregate modulus temperature adjustment factor.

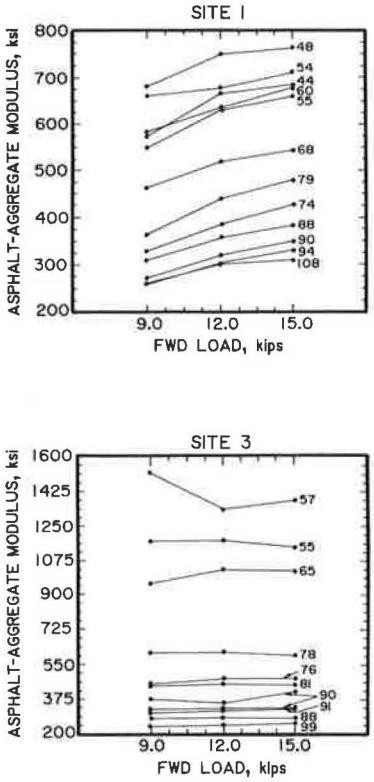

FIGURE 6 Effects of FWD load level on asphalt-aggregate modulus.

modulus. This trend was also observed at Sites 5 and 8. The reasons for the observed differences in response are not clear but are probably due to the stiffness of the asphalt-aggregate layers in relation to that of the overall pavement structure. As indicated in Figure 3, the asphalt-aggregate moduli at Sites 3, 5, and 8 are higher (at temperatures below about 80°F) than at the other seasonal sites. The asphalt-aggregate layers at Sites 3 and 5 are also the thickest.

The implication is that the overall state of stress induced in the asphalt-aggregate layer influences the modulus. However, the nature of the influence is unclear, and laboratory testing provided no clarification. Indirect tension testing was conducted on samples from six of the eight seasonal sites and the four Interstate sites. Three levels of indirect tension stress were applied, ranging from 5 to 30 percent of the indirect tensile strength at 77°F. Modulus increased for six of the sites and decreased for four sites as the stress intensity increased. There was no correlation between field and laboratory trends, although, as shown in Figure 4, there is good agreement between the composite FWD curve and a similar composite curve developed from laboratory data.

After considering plots similar to Figure 6 for all sites and the laboratory data, it was concluded that the stress (load) sensitivity would not be sufficient to alter the relationship between the average moduli at the various sites, as shown in Figure 3. However, load level apparently influences estimated asphalt concrete modulus and, therefore, justifies testing at multiple levels and using average values. Selection of loads for testing should be based on the anticipated operation of critical vehicles (trucks). A 9-kip FWD load may be representative

of standard 18-kip axle loads, but larger loads should be considered to account for heavier trucks. For low-volume roads, FWD loads smaller than 9 kips might also be considered.

A correction for differences in the rate of loading was necessary to compare laboratory moduli with FWD moduli. The FWD rate of loading is faster than the laboratory rate and, therefore, FWD moduli will be inherently larger than laboratory moduli. The following adjustment factor suggested by Lee et al. (*3*) was used:

$$R = 0.791 + 0.00813T \quad (3)$$

where R is the ratio of FWD modulus to laboratory-determined resilient modulus and T is the temperature (°F). FWD and laboratory moduli at 77°F, the midrange temperature for laboratory testing, are shown in Table 2. As indicated by the means and standard deviations of the unadjusted and adjusted modular ratios, the adjustment for load rate improves the mean ratio from 1.36 to 0.96 and the standard deviation from 0.63 to 0.44.

Unbound Granular Base-Subbase Modulus

Figure 7 is a typical plot showing seasonal variations in base-subbase modulus. Average monthly temperature and rainfall, as percentages of maximum average monthly temperature and rainfall, are also shown. The correlation between base-subbase modulus and temperature and rainfall shown in Figure 7 was generally observed at all sites. Heavy rainfall provides a source of water and low temperatures prevent rapid evaporation, which results in low values in winter and spring and high values in summer and fall.

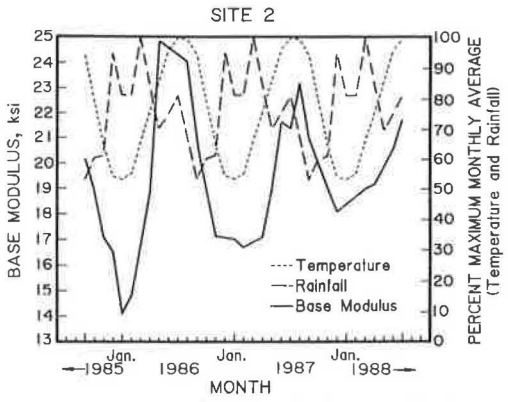

FIGURE 7 Typical variation in base moduli with temperature and rainfall.

To develop factors for adjusting base-subbase modulus for seasonal variations, average monthly moduli values and their ratios to the maximum monthly values were computed. Plots of these ratios, as shown in Figure 8a, were made for each site. Two groups (winter/spring and summer/fall) were apparent from the plots. The beginning and ending months for both groups varied from site to site, but an analysis of average ratios indicated that the most consistent were January to June and July to December. Yearly average ratios and average ratios by group are given in Table 3.

Ratios of minimum to maximum modulus (E_{min}/E_{max}) are another indicator of seasonal variability. They are shown in Table 3 and range from 0.58 to 0.85. These ratios and the average monthly to maximum moduli ratios do not indicate dramatic seasonal variations.

TABLE 2 COMPARISON OF LABORATORY AND FWD MODULI FOR ASPHALT-AGGREGATE AT 77°F

Site	FWD Moduli,E (ksi)	Unadjusted Laboratory Moduli M_R (ksi)	Laboratory Moduli, M_R, Adjusted for Load Duration (ksi)	Unadjusted E/M_R[1]	Adjusted E/M_R[2]
1	380	397	563	0.96	0.67
3	500	329	466	1.52	1.07
5	470	336	476	1.40	0.99
6	190	181	256	1.05	0.74
7	440	162	230	2.72	1.91
8	490	319	452	1.54	1.08
A	530	257	364	2.06	1.46
B	600	481	682	1.25	0.88
C	160	321	455	0.50	0.35
D	230	380	538	0.61	0.43

[1] E/M_R Mean = 1.36
Std Deviation = 0.63

[2] E/M_R Mean = 0.96
Std Deviation = 0.44

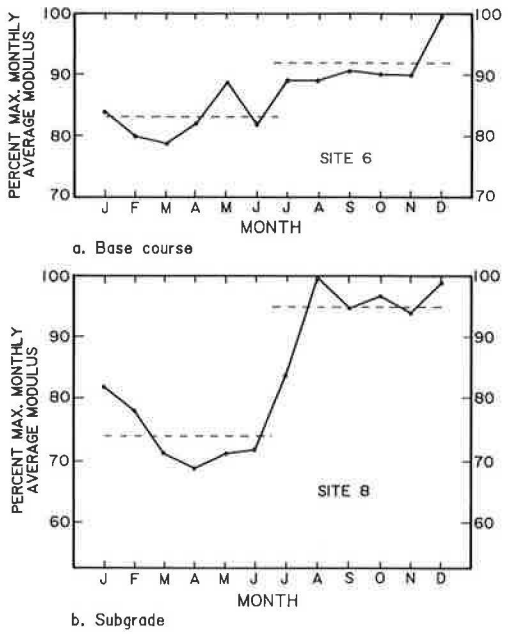

FIGURE 8 Typical variations in base and subgrade modulus.

The analysis of yearly modulus variability indicated that characterization with average values would be adequate for design and suggested a simple procedure for converting moduli backcalculated from particular FWD measurements to average values. The average of the modular ratios in Table 3 was 0.82 for January to December, 0.78 for January to June, and 0.86 for July to December. Correction factors were obtained by dividing the yearly average ratio by the average ratio for each group. To convert to average conditions, moduli backcalculated from FWD measurements made during January through June should be multiplied by 0.82/0.78 = 1.05, and those backcalculated from measurements made during July through December should be multiplied by 0.82/0.86 = 0.95.

Figures 9a, 9b, and 9c show the effects of FWD load on base-subbase modulus for Sites 5, 4, and 1, respectively. Load magnitude had essentially no effect for Sites 5 and 6 (see Figure 9a). Moduli increased with increasing load for Sites 3, 4, and 7 (see Figure 9b). Differences between 9- and 15-kip loads were 2 to 3 ksi (less than 10 percent) for Sites 4 and 7. Differences were 8 to 12 ksi (10 to 15 percent) for Site 3. Moduli decreased with increasing load for Sites 1, 2, and 8 (see Figure 9c). The effect of load magnitude was somewhat erratic for Site 1, and the differences between 9- and 15-kip loads were 4 to 8 ksi (about 10 percent). The differences were more uniform, only 2 to 4 ksi (less than 10 percent), for Sites 2 and 8.

As shown in Figure 9, load effects are smaller than seasonal effects and are not a major consideration. However, as with asphalt-aggregate, the variation that may occur at individual sites justifies testing at representative multiple FWD load levels and averaging the results.

To compare laboratory and FWD moduli, the effects of the state of stress must be considered. Using material coefficients (k_1 and k_2) in Table 4 and first stress invariant at midlayer for a 15-kip FWD load, base course laboratory moduli were calculated with the familiar equation

$$M_{R(BS)} = k_1\Theta^{k2} \quad (4)$$

where Θ is the first stress invariant, $\sigma_1 + 2\sigma_3$ for triaxial test.

Moduli calculated with Equation 4 are compared with average FWD moduli in Table 5. The modular ratios in the last column of Table 5 range from 0.80 to 8.57 and indicate good to poor correlation between FWD and laboratory moduli. The mean value of the ratios is 3.03, which indicates that FWD moduli are consistently higher than laboratory moduli. The standard deviation is 1.99, which indicates considerable variability.

There are several possible causes of the poor correlation between FWD and laboratory moduli. Laboratory moduli were measured on specimens recompacted to densities and moisture contents as close as possible to those measured in the field. Field sampling operations, which involved wet sawing through asphalt-aggregate layers, may have increased water contents above actual in situ values. Disturbance during sampling surely destroyed any cementation or thixotropic strengthening that may have existed. Removal of 0.75-in. particles for 4-in. diameter laboratory specimen preparation would also have caused decreased moduli.

Finally, the characterization of the state of stress in the unbound granular base-subbase layers may not have been adequate. The first stress invariant (Θ) was calculated at midlayer directly beneath the center of the FWD load with an elastic layered model (ELSYMS5). It did not include the influence of overburden confinement or, probably more important, the influence of horizontal residual confining stresses developed during compaction and traffic application. The use of this single value for computing modulus from laboratory equations may not have been adequate and probably contributed to the poor correlations. This explanation is more appealing when values of material coefficients (k_1 and k_2) are compared with typical values recommended in the 1986 *AASHTO Guide*. The typical range for k_1 is 4 to 6 ksi and for k_2 is 0.5 to 0.7 for damp base course. The mean value for k_1 is 6.1 ksi (standard deviation = 3.3) and for k_2 is 0.43 (standard deviation = 0.14) for the data in Table 4. The mean values are on the high end of the typical range for k_1 and are low for k_2. The typical range for k_2 is 4 to 6 ksi and for k_2 is 0.4 to 0.6 for damp subbase course. The mean value for k_1 is 8.3 ksi (standard deviation = 3.1) and for k_2 is 0.38 (standard deviation = 0.18) for the data in Table 4. Again the mean values are higher than the typical range for k_1 and on the low end for k_2. However, natural soil aggregate type materials widely used in Alabama tend to have high cohesion (indicating high k_1) and low friction (indicating low k_2).

A second comparison strengthens the contention that the poor correlation between FWD and laboratory moduli is the result of the representation of the state of stress with a single value (Θ). Values of k_1 and k_2 and their relationship are compared with results reported by Rada and Witczak (*7*) in Figure 10. Rada and Witczak's results were for 271 granular materials and compare reasonably well with the 18 materials tested in this study.

TABLE 3 BASE-SUBBASE DATA FROM SEASONAL SITES

Site	Material Classification		Description	Avg. E	Avg. E/E_{max}			E_{min}/E_{max}
	Unified	AASHTO			J - D	J - J	J - D	
1	GW	A-1-a	10" Crushed Agg Base (w = 3%)	58 ksi	0.93	0.90	0.96	0.85
	SP-SC	A-2-6	14" Select Soil (w = 22%)					
2	–	–	3" Sand Gravel Base	20 ksi	0.82	0.79	0.85	0.68
	SW-SM	A-1-b	12" Select Soil (w = 21%)					
3	SP	A-1-b	6" Soil Aggregate Base (w = 9%)	80 ksi	0.76	0.77	0.76	0.70
4	–	–	8" Granular Soil Base	27 ksi	0.82	0.76	0.87	0.67
5	SP	A-3	5" Sandy Shell Base (w = 7%)	34 ksi	0.74	0.72	0.76	0.63
	SP	A-3	12" Select Soil (Sand Clay) Sub-base (w = 11%)					
6	SP	A-1-a	4" Sandy Gravel Base (w = 6%)	31 ksi	0.87	0.83	0.92	0.80
	SP	A-1-b	6" Clayey Sand Subbase (w = 8%)					
7	GP	A-1-a	4" Soil Aggregate Base (w = 3%)	32 ksi	0.86	0.81	0.90	0.73
	SP	A-1-b	6" Soil Aggregate Subbase (w = 4%)					
8	SP-SC	A-2-4	8" Soil Aggregate Base (w = 11%)	60 ksi	0.77	0.65	0.90	0.58

1. Moisture contents as sampled.
2. Average modulus and modular ratio for 3 year period. Ten (10) locations, spaced at approximately 200', tested at approximately 2 month intervals.

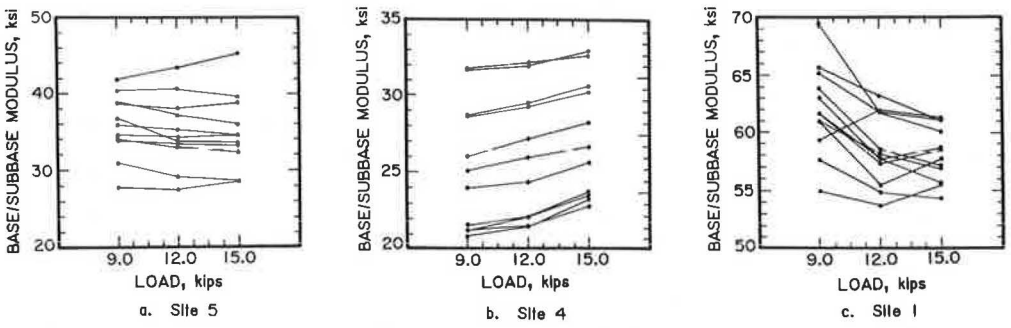

FIGURE 9 Effects of FWD load level on base-subbase modulus.

TABLE 4 MATERIAL COEFFICIENTS (k_1 AND k_2) FOR UNBOUND GRANULAR BASE-SUBBASE FROM TRIAXIAL TESTING

Site	Layer	k_1	k_2
1	Base	11.9	0.21
	Subbase	11.6	0.14
3	Base	3.0	0.58
5	Base	2.1	0.71
	Subbase	5.7	0.27
6	Base	6.7	0.29
	Subbase	4.5	0.46
7	Base	5.6	0.37
	Subbase	4.1	0.62
8	Base	1.0	0.57
A	Base	10.2	0.39
	Subbase	9.3	0.27
B	Base	6.4	0.47
	Subbase	3.7	0.55
C	Base	6.1	0.37
	Subbase	25.5	0.12
D	Base	8.0	0.33
	Subbase	2.3	0.64

Base: Average k_1 = 6.1 ksi, Average k_2 = 0.43
Subbase: Average k_1 = 8.3 ksi, Average k_2 = 0.38
Omitting Site C Average k_1 = 5.9 ksi, Average k_2 = 0.42

Subgrade Modulus

Plots similar to Figure 7 were made for subgrade modulus. The same trends were exhibited—low modulus in winter and spring, when rainfall is high and temperature low, and high modulus in summer and fall, when rainfall is low and temperature high. Plots of modular ratios (Figure 8b) were made for each site. The plots indicated that consistent groupings were January to June and July to December. Yearly average ratios and average ratios by group are given in Table 6.

Ratios of minimum to maximum (E_{min}/E_{max}) are also shown in Table 6. They range from 0.70 to 0.84. The ratios do not indicate dramatic seasonal moduli variations.

The analysis indicated that characterization with average values would be adequate for design. Moduli measured during January through June were to be multiplied by a correction factor of 1.06, and those measured during July through December were to be multiplied by 0.96.

An example will demonstrate that yearly average subgrade modulus is close to effective roadbed soil resilient modulus computed with the procedure recommended in the 1986 *AASHTO Guide*. The calculations are summarized in Table 7 for Site 8, which had the smallest E_{min}/E_{max} ratio. The average subgrade modulus is 17.9 ksi. The relative damage factors shown in Table 7 were computed using methods outlined in the 1986 *AASHTO Guide*. Using the average relative damage factor of 0.018, an effective roadbed soil resilient modulus

TABLE 5 COMPARISON OF FWD AND LABORATORY MODULUS FOR UNBOUND GRANULAR BASE-SUBBASE

Site	Layer	FWD Modulus, E (ksi)	Lab. Modulus, M_R (ksi)	E/M_R
1	Base	58	24	2.42
	Subbase	58	18	3.22
	Subgrade	27	16	1.68
3	Base	80	15	5.33
	Subgrade	19	12	1.58
5	Base	34	10	3.40
	Subbase	34	10	3.40
	Subgrade	13	10	1.30
6	Base	31	18	1.72
	Subbase	31	22	1.41
	Subgrade	9	6	1.50
7	Base	32	22	1.45
	Subbase	32	40	0.80
	Subgrade	15	11	1.36
8	Base	60	7	8.57
	Subgrade	18	7	2.57
A	Base	25	29	0.86
	Subbase	25	19	1.32
	Subgrade	10	16	0.62
B	Base	45	17	2.65
	Subbase	45	12	3.75
	Subgrade	18	10	1.80
C	Base	50	17	2.94
	Subbase	50	34	1.47
	Subgrade	15	13	1.15
D	Base	45	15	3.00
	Subbase	45	7	6.43
	Subgrade	15	21	0.71

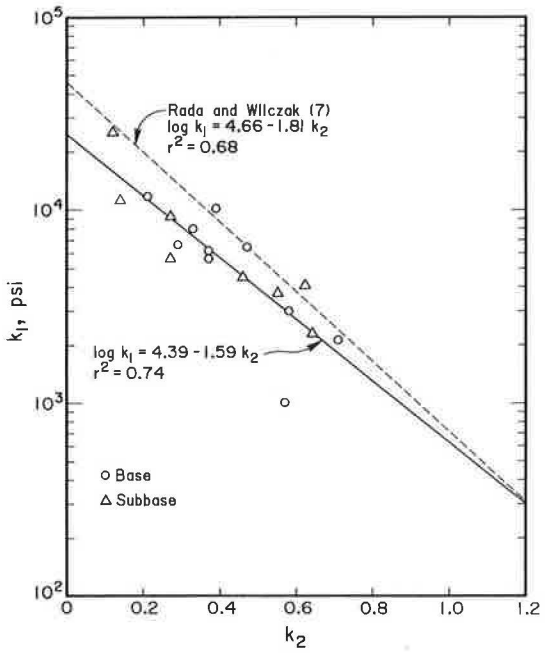

FIGURE 10 Comparison of material coefficients.

TABLE 6 SUBGRADE DATA FROM SEASONAL SITES

Site	Material Classification Unified	AASHTO	Description	Avg. E	Avg. E/E_{max} J - D	J - J	J - D	E_{min}/E_{max}
1	SC	A-2-6	Brown Silty Clay (w = 20%)	27 ksi	0.92	0.87	0.96	0.80
2	SC	A-2-6	Reddish Black Clay (w = 22-25%)	7.5 ksi	0.84	0.80	0.87	0.72
3	SP	A-2-6	Clayey Sand (w = 5%)	19 ksi	0.87	0.84	0.90	0.78
4	–	–	Red Sandy Clay	9.5 ksi	0.91	0.86	0.96	0.84
5	SP-SM	A-3	Red Clayey Sand (w = 13%)	13 ksi	0.85	0.83	0.86	0.72
6	SP	A-3	Tan Sandy Clay (w = 15%)	9 ksi	0.92	0.87	0.96	0.82
7	SP	A-3	Red Sandy Clay (w = 9%)	15 ksi	0.88	0.83	0.93	0.73
8	SW-SM	A-1-b	Red Sandy Clay (w = 14%)	18 ksi	0.84	0.74	0.95	0.70

1. Moisture contents as sampled.
2. Average modulus and modular ratio for 3 year period. Ten (10) locations, spaced at approximately 200', tested at approximately 2 month intervals.

TABLE 7 EXAMPLE CALCULATION OF EFFECTIVE ROADBED SOIL RESILIENT MODULUS

Month	Average Modulus, ksi	Relative Damage Factor (u_f)
J	17.4	0.017
F	16.6	0.020
M	15.1	0.024
A	14.7	0.027
M	15.0	0.024
J	15.3	0.023
J	17.8	0.016
A	21.1	0.012
S	20.1	0.012
O	20.5	0.012
N	19.9	0.012
D	20.9	0.012
Average	17.9	0.018

of 17.3 ksi is computed, which is only 3.5 percent smaller than the average subgrade modulus.

Figure 11 shows three effects of FWD load magnitude on subgrade modulus. For Sites 1 and 5, FWD load had essentially no effect on moduli (Figure 11a). For Sites 3, 4, and 7, moduli increased with load (Figure 11b). Moduli differences between loads of 9 and 15 kips ranged from 1 to 2 ksi for Sites 4 and 7 to 2 to 4 ksi for Site 3. These represent differences of 10 to 20 percent. For Sites 2, 6, and 8, moduli decreased with load (Figure 11c). Moduli differences ranged from 0 to 1 ksi for Sites 2 and 6 to 2 to 3 ksi for Site 8. Again, these represent differences of 10 to 20 percent.

As with base-subbase modulus, load magnitude does not appear to be an important consideration for subgrade modulus. However, the percentage differences that occur over a load range of 9 to 15 kips justify testing at representative multiple loads and using average values. For the subgrade, simulation of heavier vehicles with loads that may be applied over a large area is critical. Large FWD loads may be required to obtain similar stresses in the subgrade.

To compare laboratory and FWD moduli, the effects of the state of stress (confinement of triaxial specimens) must be considered. The first stress invariant (Θ) and the deviator stress (σ_d) were calculated at the top of the subgrade beneath the center of a 15-kip FWD load. These parameters were used in either Equation 4 or the equation below, as appropriate, to compute subgrade modulus.

$$M_{R(SG)} = k_3(\sigma_d)^{k4} \quad (5)$$

The moduli thus computed, as well as modular ratios, are given in Table 5. Modular ratios ranged from 0.62 to 2.57 with a mean value of 1.42 and a standard deviation of 0.53. FWD moduli were consistently higher than laboratory moduli, although much less than base-subbase. As with unbound granular base-subbase, disturbance of cementation bonds or thixotropic strengthening may have been a cause of the observed differences. However, the use of one parameter at a single location in the subgrade to represent the state of stress probably contributes more to the observed differences.

CONCLUSIONS

Reasonable estimates of pavement material and subgrade soil moduli may be backcalculated by using pavement surface deflection basins obtained with an FWD. Deflection basins should

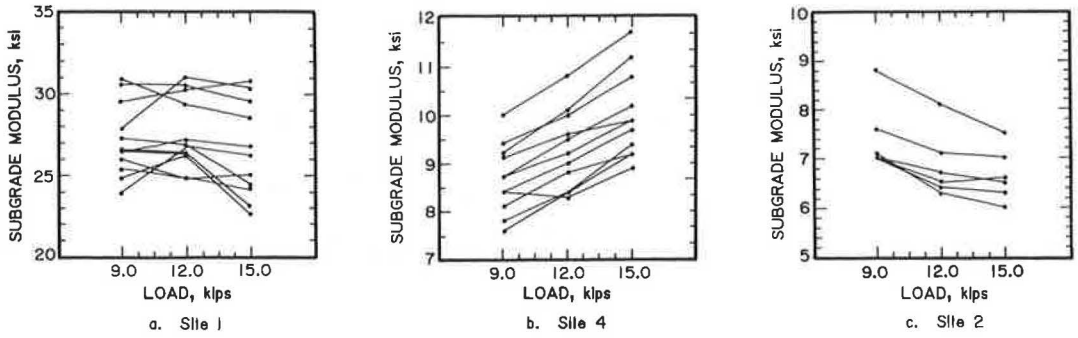

FIGURE 11 Effects of FWD load level on subgrade modulus.

be measured at multiple loads representative of anticipated truck traffic. The average temperature at middepth of asphalt-aggregate surface layers should be obtained during FWD testing. A limited number of small test pits should be excavated to determine layer thicknesses as well as moisture content and density data for modeling base and subgrade layers.

A three-layer pavement structure model was relatively simple, efficient, and provided reasonable moduli estimates. Base, subbase, and, where density and moisture content measurements indicate they are applicable, improved roadbed layers should be included in Layer 2. Subgrade and, where density and moisture content measurements indicate they are applicable, improved roadbed layers should be included in Layer 3. A stiff boundary layer should be used to limit subgrade depth.

To adjust the asphalt-aggregate modulus backcalculated from FWD data to a standard design temperature, a modified version of a curve recommended in the 1986 *AASHTO Guide* was developed. Load rate should also be considered in selecting asphalt-aggregate design modulus. Seasonal variations have only a limited influence on base-subbase and subgrade moduli. A simplified procedure was developed to convert values backcalculated from FWD measurements to average conditions.

Laboratory moduli for asphalt-aggregate measured with indirect tension tests (ASTM D4123) compared well with FWD moduli. As expected, characterization of unbound granular base-subbase was most difficult, and FWD and laboratory values correlated poorly. In general, fair agreement was demonstrated between FWD and laboratory (AASHTO T274) moduli of subgrade soils.

ACKNOWLEDGMENTS

This research was sponsored and supported by the Alabama Highway Department through the Highway Research Center of Auburn University. FWD measurements and test pits for material sampling were provided by the Alabama Highway Department. The author is grateful for the sponsorship, assistance, and cooperation of the Alabama Highway Department.

REFERENCES

1. *AASHTO Guide for Design of Pavement Structures*. AASHTO, Washington, D.C., 1986.
2. P. Ullidtz and R. N. Stubstad. Analytical-Empirical Pavement Evaluation Using the Falling Weight Deflectometer. In *Transportation Research Record 1022*, TRB, National Research Council, Washington, D.C., 1985, pp. 36–44.
3. S. W. Lee, J. P. Mahoney, and N. C. Jackson. Verification of Backcalculation of Pavement Moduli. In *Transportation Research Record 1196*, TRB, National Research Council, Washington, D.C., 1988, pp. 85–95.
4. A. J. Bush III and D. R. Alexander. Pavement Evaluation Using Deflection Basin Measurements and Layered Theory. In *Transportation Research Record 1022*, TRB, National Research Council, Washington, D.C., 1985, pp. 16–29.
5. S. Husain and K. P. George. In Situ Pavement Moduli from Dynaflect Deflection. In *Transportation Research Record 1043*, TRB, National Research Council, Washington, D.C., 1985, pp. 102–112.
6. M. W. Witczak. Design of Full Depth Air Field Pavements. *Proc., 3rd International Conference on the Structural Design of Asphalt Pavements*, 1972.
7. G. Rada and M. W. Witczak. Comprehensive Evaluation of Laboratory Resilient Moduli Results for Granular Material. In *Transportation Research Record 810*, TRB, National Research Council, Washington, D.C., 1981, pp. 23–33.

Full-Scale Accelerated Pavement Testing for the Texas State Department of Highways and Public Transportation

FREDERICK HUGO, B. FRANK MCCULLOUGH, AND BARRY VAN DER WALT

In 1988 the Texas State Department of Highways and Public Transportation initiated a study to develop a strategy to acquire a mobile accelerated pavement testing device. Many methods were evaluated, and the mobile load simulator (MLS) was selected for future application on pavements in Texas. The MLS, for which a provisional patent exists, incorporates a method of accelerated load application different from existing mobile accelerated pavement testers. A higher degree of traffic simulation and much higher production rates are attainable with the proposed MLS. The role of accelerated pavement testing in Texas and the degree of real traffic simulation of the proposed MLS are evaluated. A methodology for including environmental effects in accelerated pavement testing is presented.

Complexities in pavement engineering have led authorities to conclude that accelerated pavement testing devices should be used in pavement engineering. Provision for accelerated testing is made in one form or another all over the world, from plate-loading devices to full-scale test tracks. This new commitment is easily understood when the investment in pavement structures and the need for testing them in a cost-effective way are considered.

In 1988 the Texas State Department of Highways and Public Transportation (SDHPT) initiated a study at the Center for Transportation Research at The University of Texas at Austin to explore the feasibility of accelerated testing in the state. A steering committee was convened, and guidelines for the requirements of the proposed systems were established. The purpose of the study was to formulate a strategy for acquiring, operating, and managing a mobile accelerated pavement testing machine that satisfies the needs of the SDHPT. Attention was given to the role of accelerated pavement testing in pavement engineering, methods of accelerated pavement testing, data acquisition and handling, and the projected operational impact. Recommendations regarding the scheduling of a plan for accelerated pavement testing were made on the basis of information from the investigation. The ability of presently used simulators to satisfy the requirements of the SDHPT was considered. The feasibility of developing an innovative accelerated pavement testing machine was explored, and the proposed design of this machine was evaluated. The machine, called the mobile load simulator (MLS), for which a provisional patent exists, is expected to improve on existing machines.

Center for Transportation Research, The University of Texas at Austin, Austin, Tex. 78705.

PAVEMENT TESTING

Use of so-called mechanistic design procedures provides engineers with a well-established method for effective pavement design. In these mechanistic-empirical methods, theoretical models are used to analyze stress, strain, and deformation (response or behavior) for given loadings in a pavement structure, whereas the development of roughness, rutting, and cracking (performance) are empirically related, or calibrated, to the response. Pavement behavior is modeled through transform functions as a multilayered elastic or viscoelastic structure. The models are subject to uncertainty stemming from inexact descriptions of inputs such as traffic, environment, subgrade properties, and material characteristics. Researchers recognize that pavement performance prediction will also be influenced by factors that are not included in the models or that are not accurately modeled by mechanistic methods; thus the necessity of calibration through so-called shift factors.

Many test methods are used for the calibration of models, and there is a wide range in the reliability and the costs of these methods. Depending on the availability of funding, engineering parameters can be estimated, or more appropriate results can be obtained by testing batches of individual material samples. The total pavement structure can also be tested by using one of the available methods. From these results, the pavement can be mathematically evaluated by simulation. The available methods, which are essentially the decision tools of the engineer, are

- Computer simulation,
- Direct sampling methods and laboratory testing,
- Nondestructive evaluation or field testing,
- Test roads,
- Accelerated pavement testing, and
- Condition monitoring of in-service pavements.

Engineering judgment is vital in using the available decision tools.

TEST FACTORS PROVIDING THE BUILDING BLOCKS OF PAVEMENT ENGINEERING

Many factors affect the behavior of pavement structures under load and environmental conditions. Figure 1 gives the most important. Most problems experienced in pavement engi-

MAT & CONST FACTORS	PAVEMENT MANAGEMENT AND PERFORMANCE
1)Material Layer System 2)Micro Material Structure 3)Material Anisotropy 4)Subgrade Compaction 5)Subgrade Stiffness 6)Subgrade Plastic Behavior 7)Friction Between Layers 8)Application of Rejuvenators 9)New Materials/Mixtures 10)D-Cracking 11)Construction Variation 12)Flexible bases 13)Lime treated bases 14)Cement treated bases 15)Recycled Asphalt	1)Maintenance Strategies 2)Rehabilitation Strategies 3)Load transfer in joints 4)Percent Steel 5)Stripping of Asphalt 6)Rutting 7)Skid Resistance 8)Wear of Aggregate 9)Steel Concrete Bond 10)Concrete Joint Behavior 11)Fatigue cracking 12)Structural condition of Pavement 13)Surface condition of Pavement 14)Residual life 15)Delamination 16)Pavement performance (PSI)
STRUCTURAL FACTORS	**LOAD FACTORS**
1)Structural Systems 2)Voids Beneath Concrete 3)Effect of Shoulders 4)Balanced structural composition	1) Vehicle Speed 2)Dynamic Wheel Loads 3)Multi-Axle Loads 4)Actual Traffic loads 6)Selected Traffic Loads 7)Selected Tire Type 8)Selected Tire Pressure 9)Lateral Wheel Distribution 10)Axle Equivalency 11)Suspension Type 12)Overloads
ENVIRONMENTAL FACTORS	
1)Surficial water (artificial) 2)Sub surface water 3)Artificial Environment and Accelerated Load 4) Wind 5)Temperature 6)Humidity	
PERIPHERAL PAVEMENT ENG	
1)Traffic monitoring Devices 2)Durability of Road Markings	3)Effects of Gradients 4)Tire types

FIGURE 1 Testing factors forming the basis of engineering knowledge.

neering today are related to these factors. Any pavement test method should be evaluated on its ability to account for these factors in a cost-effective yet reliable way. Although they are well known in 1990, their extent has only gradually become known during the past 60 years. Initially, most of the problems were solved by three basic tools—engineering judgment, field trials and observations, and limited laboratory experimentation using material classification. Essentially, the physical characteristics of the materials were used to compare materials. In this way successful field experiences were related to new applications.

The road tests introduced the concept of accelerated testing to pavement engineers. Accelerated pavement testing, in which the rest periods of the pavement are reduced or overloads are used, or both, exists in many forms. The AASHO Road Test is an example of accelerated pavement testing using real traffic. The construction of test roads for accelerated testing was soon found to be prohibitively costly. Furthermore, the results obtained were limited in geographical application and extrapolation. However, pavement engineers accepted accelerated pavement testing as a way to establish results of pavement performance quickly and reliably. By the early 1970s, developments in heavy machinery manufacturing led to mobile accelerated test machines that use simulated traffic loading, such as the heavy vehicle simulator (HVS) in South Africa and, later, the accelerated loading facility (ALF) in Australia. Further details are discussed later.

Several agencies use observation of in-service pavement behavior to gain knowledge of traffic and environmental influences. In the mid-1980s a combined data base for the United States was established through long-term pavement performance studies as part of the Strategic Highway Research Program. Observation of in-service pavement behavior is generally considered to be the ultimate evaluation method, in which the real loading condition (traffic and environment) of the pavement is evaluated in real time.

SELECTION OF PAVEMENT ENGINEERING DECISION TOOLS

Decision tools available to engineers are shown subjectively in Figure 2 relative to cost and associated knowledge. The range and types of decision tools selected to give an agency the knowledge to design, construct, and manage highways depend largely on the agency's ability to finance a particular combination of tools. In Figure 2b the rectangle defined by the affordable cutoff line and the horizontal line linking it to the vertical axis from the turn line defines the extent of usage of the respective tools. (See the area mapped relative to the total for each method.) The horizontal line defines the achievable knowledge. For optimal results, a range of tools should be selected encompassing all those to the left of the affordable cutoff line.

The shape of the turn line in Figure 2b (shown as straight) depends on factors such as labor costs and technological development, which vary from agency to agency. The shape of the turn line in Figure 2b determines the position of the s-curve band in Figure 2a. The s-curve is obtained from a summation of the enclosed test method areas in Figure 2b. The band represents a range of knowledge that stems from a high or low utilization of the test methods.

Engineering judgment forms an important part of any selection and is supplemented by the other methods to various degrees. Some agencies rely solely on this knowledge to provide a pavement infrastructure. This is often adequate and may be the only method an agency can afford. To increase the dependability of a pavement system, however, more reliable and expensive methods must be used to predict the likelihood of distress occurrences.

After the selection of distress criteria for pavements in a specific area, a plan must be developed and equipment acquired to obtain the input information, such as moduli, that relate the distress criteria to pavement performance. Figure 2 indicates that computer simulation is an inexpensive evaluation method; however, obtaining accurate input through testing and then deriving or improving the models for greater reliability are relatively expensive.

Laboratory testing covers a wide range of costs with a relatively small increase in reliable knowledge. The so-called one-way testing method is usually used, in which all variables except the one to be evaluated are kept constant. An example is stabilometer testing of asphalt concrete mixtures, in which only the asphalt content is varied. Field testing can range from simple penetration tests to obtaining samples for testing in the conventional manner in a laboratory. It attempts to evaluate changes in the pertinent properties due to environmental and traffic influences and includes in situ destructive and nondestructive testing and evaluation. It may also include short-term evaluation of behavior, such as early-age cracking of

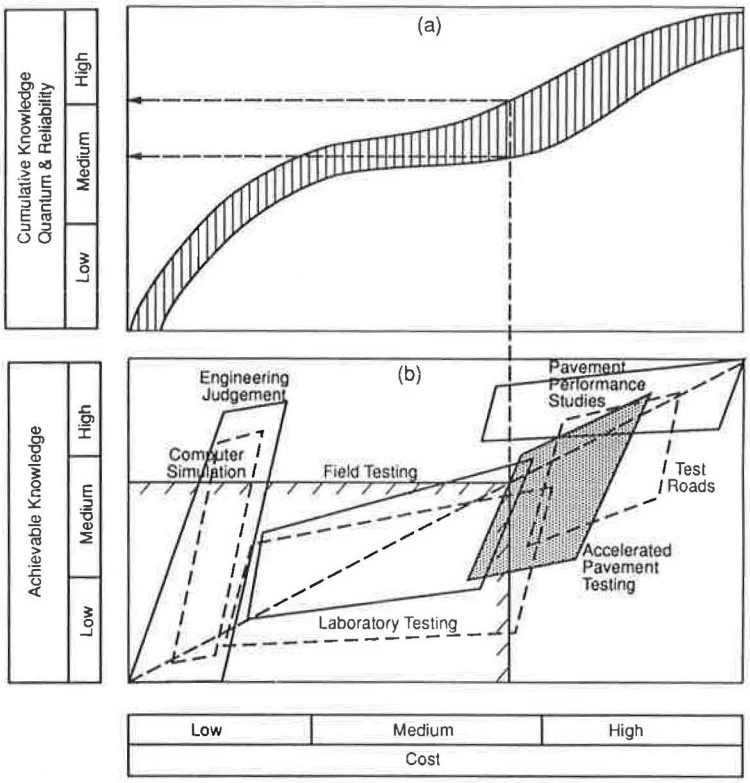

FIGURE 2 Financial investment and associated knowledge.

portland cement concrete pavements and static load deflection measurements. The objective is to evaluate more of the system so that the effective parameters can be used in the analysis of pavement behavior. Accelerated pavement testing is used in many forms to provide the information to develop and evaluate distress criteria. It has increased in popularity in the last 20 years because of the high attainable benefit-to-cost ratios [examples of 10 to 1 have been reported (*1*)] and its ability to test pavement responses that cannot be tested in other ways.

The cost of testing a section of pavement with an MLS is estimated to vary between $100,000 and $120,000 for 15,000,000 ESALs. This compares favorably with the present value of cost per test section of the AASHO Road Test as shown in the following table. The main difference is that the latter had a limited number of load applications and was limited to one geographic location.

Cost Component	*Value*
Number of load applications	1,114,000
Duration	2 years
Number of test sections	836
Lengths of test sections	160–260 ft
Total cost of test (1962)	$27,114,220
Present value of cost (4%)	$81,307,501
Present value of cost/test section	$97,257

An FHWA-sponsored pavement testing conference (*2*) concluded that a national pavement testing program was needed together with a rehabilitation program. Simultaneously, a long-term nationwide in-service pavement monitoring system using both existing and new pavements with untrafficked loops needed to be introduced. Accelerated pavement testing using vehicle simulators and laboratory testing were considered necessary to provide fast answers that could be calibrated against long-term performance of pavements. It was evident that none of the methods shown in Figure 2 offered a complete solution and that all the methods had to supplement each other.

ACCELERATED PAVEMENT TESTING FACILITIES

The testing facilities evaluated by SDHPT were those developed for studying problems associated with pavement design (i.e., those facilities having wheel loads in the typical range of trucks and operating on complete pavement structures). Subgrades could be either natural or imported. Lighter wheel load facilities, intended for studying the behavior of single layers, were not included.

Test facilities were divided into four categories according to their design and method of load acceleration: full-scale test tracks (AASHO Road Test, etc.), circular testing devices, linear testing devices (fixed location), and linear testing devices (mobile). Only the linear testing devices with mobile features will be discussed.

Apart from the proposed MLS, which is in the development phase, only two types of linear, mobile machines have been built to apply accelerated wheel loads to pavement sections at any location. (The Corps of Engineers has built and used mobile testing machines at its test site in Vicksburg, Mississippi, but they have not been deployed.) One of the two is the HVS, developed at the end of the 1960s in South Africa. Three improved HVSs are still operational. The other ma-

chine is the ALF, in use in Australia since 1984 and operational in the United States since October 1986.

The HVS has the dimensions of an oversized heavy vehicle. It can be pulled over long distances like a trailer by hooking the goose neck to a three-axle truck tractor and transporting it on two axles with 12 wheels total. Steerable wheels and a drive train allow movement of the machine over short distances without a tractor. The test wheel applies bi- or unidirectional loading over a length of 32.8 ft. Successive passes are distributed over a track width of up to 5 ft at a top speed of 9 mph. Although the wheel is normally variable up to 22.5 kips, loadings of 45 kips have been achieved for the testing of airport pavements. The working, features, and applications of the HVS are described elsewhere (*1*,*3*).

The ALF is owned by the Australian Road Research Board and has been operational since February 1984. FHWA interest in the machine stemmed from the March 1984 International Pavement Conference in McLean, Virginia (*2*). In mid-1984 the plans and authority to build the U.S. ALF were acquired, and the machine was delivered in August 1986. The ALF is patented in 20 countries. Using dual truck tires with loads ranging from 9,000 to 22,500 lb, the ALF applies accelerated loading to the pavement at a rate of 9,200 applications per day at 12 mph on a test section 33 ft long. The load is carried with the load wheel. The use of gravity in the start-up procedure and allowing gravity to provide the acceleration and deceleration of the load are energy efficient. Electric motors are used for replacing energy lost because of friction. Lateral load distribution is provided, with various loading patterns to select from. The manufacture of the U.S. ALF is documented in a 1987 FHWA report (*4*).

The MLS, the prototype of which is to be developed over 2 years starting in September 1990, is a new type of vehicle simulator based on a concept for improving the rate of real load application. The concept was evaluated through the construction of a 1-in-10 scale working model shown in Figure 3. The model version was constructed to serve as a basis for the design and construction of the full-scale prototype and will also be used in the establishment of a modeled pavement testing program for SDHPT. A comparison of the features and performance of the three systems is given in Table 1, and the differences in the method of load application are shown in Figure 4. Because the MLS method of load application can incorporate four, six, or eight undercarriages of trucks, a mixture of load magnitudes is easily incorporated by varying the spring stiffnesses or types of suspensions.

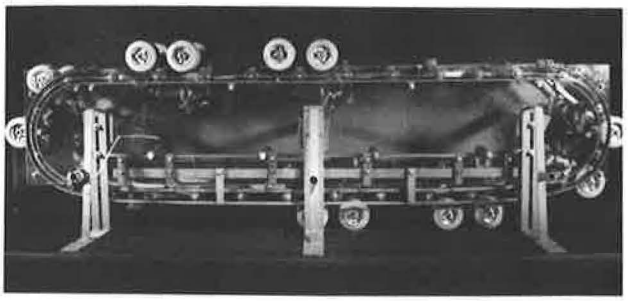

FIGURE 3 One-in-10 scale model of MLS.

TABLE 1 COMPARISON OF MOBILE LINEAR ACCELERATED PAVEMENT TESTERS

	ALF	HVS	MLS
Test Loads/Axle(kip) Single/Dual Wheel	9.4 - 37.9	4.5 - 45	6 - 25
Test Wheel Size Single/Dual	11 x 22.5	14 x 20	11 x 22.5
Wheel Speed(mph)	12	8	20
Rep/Hour	380	1200	10 920
Trafficked Length	40	32.8	35
Lateral Displacement of Test Wheels(ft)	2.65	4.9	3
Other Lengths(ft)			
Testing	92.6	74.15	60
Transportation	98.4	74.15	48 + 48
Overall Width(ft)	13.8	12.2	11
Overall Height(ft)			
Testing	22	13.8	17
Transportation	14.4	n/a	13.5
Total Mass(kip)	123	125	130

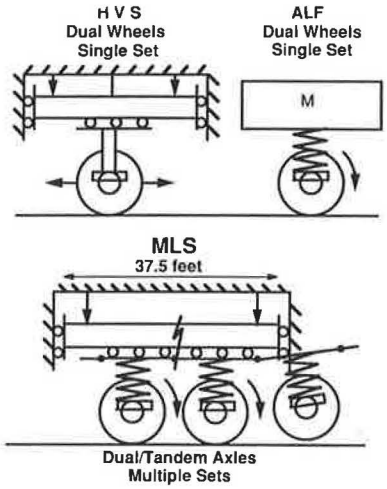

FIGURE 4 Comparison of methods of load application among HVS, ALF, and MLS.

PROPOSED MLS DESIGN

To increase the degree of real load simulation, the intention is to use standard truck components, including axles, tires, and suspension systems, as far as possible. Because there are many variations in the designs of each of these components, the MLS will have to be as adaptable as possible. The adaptability of the MLS may interest manufacturers of such components in testing new developments in their respective fields with the proposed MLS and will enhance use of the MLS.

Criteria to be met in the design of the proposed MLS fall under either overall dimensions or performance. The first determines transportation limitations, and the second determines the rate of load application or the production rate.

Specific design criteria (axle spacing and speed) were selected on the basis of practical considerations. A schematic configuration is shown in Figure 5. This was evaluated by comparison with real traffic. Mechanical features that will be the same in both the MLS and trucks, so-called off-the-shelf items, were not evaluated for accuracy of simulation. These include features such as springs, wheels, and resistance trans-

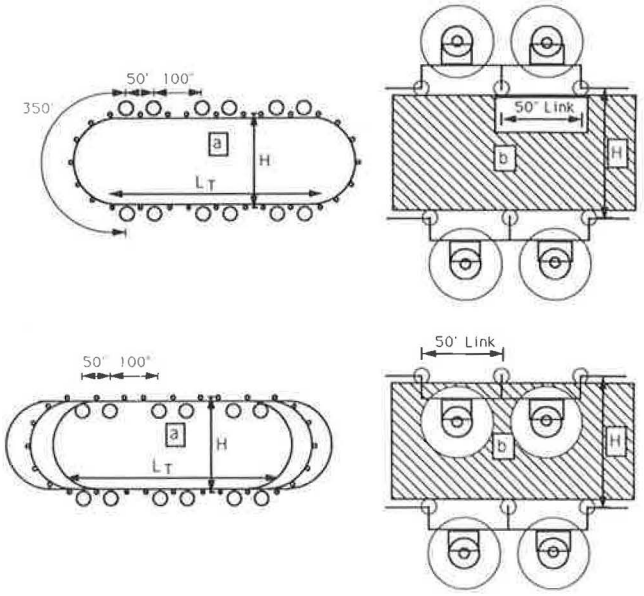

FIGURE 5 Proposed MLS dimensions and axle configurations.

mitted as a force to the surface of the pavement. Criteria evaluated were thus speed, sprung weight (mass riding on top of suspension), unsprung weight (mass riding beneath suspension), load intervals, lateral load distribution of undercarriages, and deflection bowl influences midway between axles of a tandem bogie and midway between two tandem bogies. (Undercarriages of trucks are commonly referred to as bogies and consist of single, tandem, tridem, or steering axles plus wheels and suspensions.)

Axle Spacing

Axle spacing in the system was an important consideration because

- Recovery time and residual stresses for viscoelastic materials should represent real conditions;
- Deflection bowls between axle bogies should not overlap, leading to excessive superposition of stresses and strains; and
- Electrical motors to drive the system must be able to produce relatively high speeds and should be placed in the system to provide combinations of driving and tagging axles without excessive fluctuations in speed.

Speed

The design speed of the MLS is being limited to 20 mph. This should ensure stability and improve on other linear accelerated pavement testing machines. Power requirements will be based on achieving this speed within 2 min.

In the literature (*5*), the dynamic effect of traffic loading is based on estimates of the dynamic loading coefficient, which is the standard deviation of the dynamic load/static load and a function of the sprung mass acceleration. Because mechanical aspects such as unsprung mass, spring stiffness, tire stiffness, and suspension types are the same in the MLS as in real trucks, these need not be evaluated. However, speed and sprung mass will differ considerably.

A Transport and Road Research Laboratory theoretical study evaluated the dynamic behavior of a wheel of a single-axle vehicle suspension system. The impact factor (IF), which is the common name for the ratio of dynamic force to the static wheel force applied to the road, was used in the study.

Figure 6 shows an evaluation of axle hop at speeds varying from 10 to 60 km/hr (6 to 37 mph) over a 40 × 250 mm (1⅝ × 10 in.) bump. The figure indicates that the first, second, and third IFs, or hops, increase with speed, but that the second and third maximum IFs are expected at 33 km/hr (21 mph). For the first peak, an IF maximum of 3.0 is calculated at a speed of 100 km/hr (62.5 mph) with a theoretical maximum of 3.33. Figure 6 shows that a 17 percent reduction for the first peak can be expected for the MLS operating at 20 mph, compared with a truck traveling at 60 mph. Overestimates of 17 and 9 percent, respectively, are expected for the second and third peaks.

Sprung Weight

The sprung weight per axle on the MLS will be in excess of (and may be double) typical sprung weights of trucks because of provision for overloading of the structure to reduce dynamic effects. However, this will not affect the bogie system, because the MLS superstructure will be supported on retractable legs resting on the pavement.

Unsprung Weight

Depending on the design of the load transfer bogies translating around the frame, the unsprung weight (axle components) can either be similar to or in excess of actual truck unsprung weights; the first is preferable. This can be done only through detailed design of the positioning as far as the electrical motor and transmission are concerned. A typical electric motor of 120 to 150 hp with the transmission could add from 1,500 to 2,000 lb to the unsprung weight if it is placed below the suspension.

Load Intervals

Evaluation of the load intervals in Figure 7 indicates that there is a similarity in the loading patterns of the pavement material. For modulus of rupture testing, stresses are generally applied at the same level and frequencies, which may not be the case for real pavement loading, because of variations in traffic loading conditions. For all four situations, the longer resting periods are similar; however, the intervals between axles on the same bogie for the MLS and axles on the same bogie for a truck differ by the ratio of truck speed to machine speed, which is two and three times smaller for the truck. This is due to the selected machine design, which features actual truck bogies for economy and better mechanical simulation.

Increasing the speed of the machine would greatly improve the accuracy of the simulation of resting periods for tandem

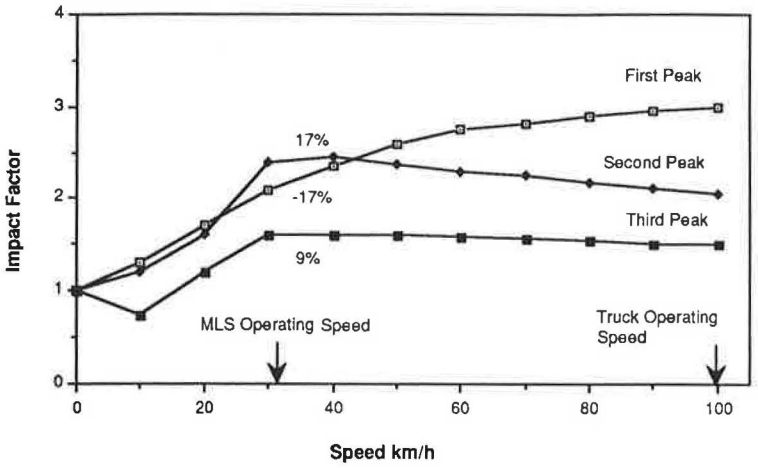

FIGURE 6 IF versus speed.

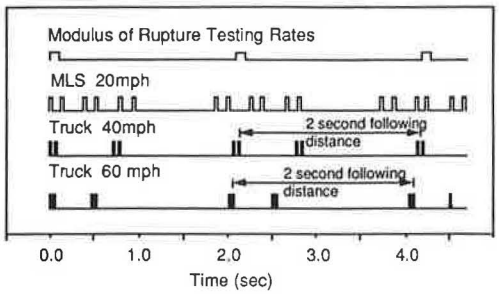

FIGURE 7 Typical load intervals for a point on a pavement.

axles but would lead to a decrease in resting periods for the longer sections. An alternative would be the removal of the middle bogie in each set of three bogies. This reduces the total number of axles to eight, which will reduce the rate of achievable acceleration considerably. Problems may also arise with irregular rotation speeds because of fewer axles on the pavement to provide translation.

Lateral Load Distribution

The previously discussed intervals of loading will also be influenced by the effect of lateral load distribution of actual traffic. Accordingly, it was decided to obtain similar variance by spacing the different bogies randomly within a total lateral width of 36 in.

Deflection Bowl Influences Between Bogies due to Closer Spacing of Axles on the MLS

Using the linear elastic multilayer program ELSYM5 (*6*), two pavement types were evaluated to examine the influences of the deflection bowls created by the tandem axles of a stationary truck and by the MLS. For the three-layer system, modulus values were taken that were comparable with material properties expected in portland cement concrete pavements. For the four-layer system, material properties were used that were comparable with those of asphalt concrete pavements. The systems are shown in Figure 8.

Circular loads were assumed in the analysis, representing a set of dual wheels and carrying a load of 9,000 lb at 75 psi wheel pressure. The simplification was made because ELSYM5 evaluates a maximum of 10 uniform loads. The analysis is also subject to the usual assumptions of layered theory.

Deflection profiles were drawn for loading situations in which the distance between bogies was varied (see Figure 9). According to *A Factbook of the Mechanical Properties of the Components for Single-Unit and Articulated Heavy Trucks* (*7*), corresponding offsets (x-distances) for trucks are on the order of 33 to 45 ft. The effect of steering axles was not taken into account. The MLS will have two discrete x-distances of 36 ft and four x-distances of 16 ft, as shown in Figure 5.

To establish an upper limit for x-distances to be evaluated, 2-sec following distances for trucks traveling at 45 mph were taken. Analysis at longer x-distances was not done in view of the trends of the results.

Figure 10 shows the findings of the three-layer analysis. Similar results were found for the four-layer system. The following deductions can be made from the deflection graphs:

1. At the 36-ft x-distance, surface deflections experienced with MLS loading are comparable with and fall within the

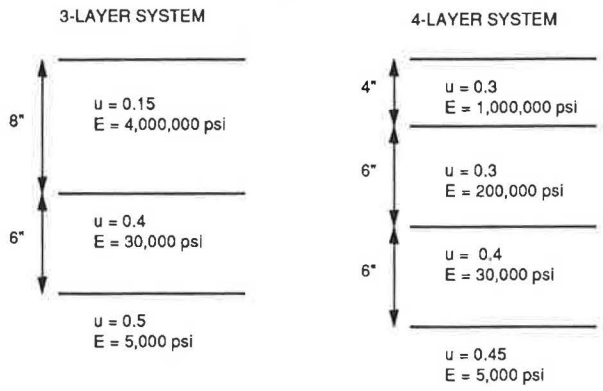

FIGURE 8 Pavement systems evaluated with ELSYM5.

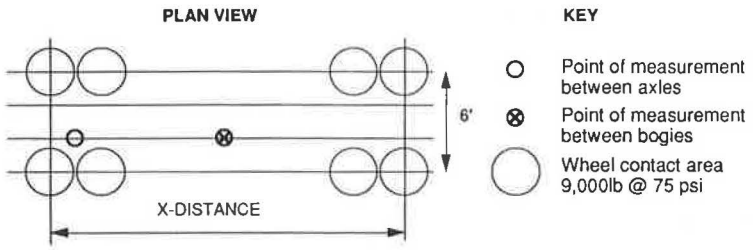

FIGURE 9 Diagram for computer analysis.

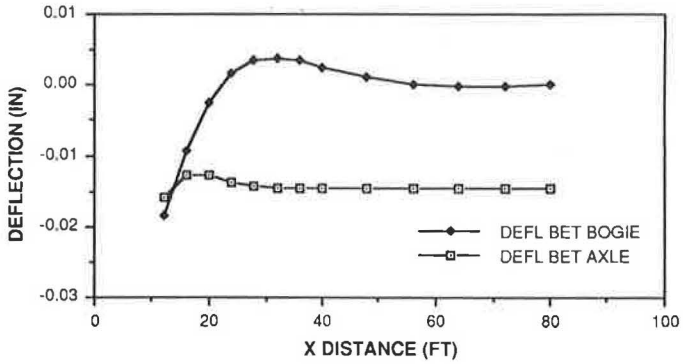

FIGURE 10 Deflections for three-layer system (9,000 lb, z = 0 in.).

range of truck deflections for measurements between axles and between bogies.

2. For both types of pavements, measurements of deflections between axles of a bogie show little sensitivity to the x-distance up to 25 ft.

3. The offset at the 16-ft x-distance indicates significant influence from the respective deflection bowls. Depending on the pavement type, a difference of up to 0.015 in. can be experienced.

On the basis of this analysis, superposition of deflection bowls can be expected for axle spacings corresponding to x-distances less than 16 ft. The effect of undercarriage spacing on test section performance is therefore an important variable to be analyzed, and variable undercarriage spacing must be a feature of the system.

EVALUATION OF CLIMATIC FACTORS USING ACCELERATED PAVEMENT TESTING

In the following discussion, it is assumed that environmental effects cause a reduction of pavement life. This need not be true throughout the pavement life; however, the same principles apply when environmental influences cause an increase in pavement life or a mixture of beneficial and detrimental effects.

The traditional relationships between distress and time are shown in Figure 11a. The figure shows that a certain distress occurs in a pavement because of the combined effects of load and environment. The distress occurs at an increasing rate, especially toward the end of the structure life, because of dynamic loading due to rougher pavement. At any given time, the relative contributions of the environment and loading to the total distress manifestation are not assessable. However, when accelerated loading is used to hasten the distress to a limiting level, the rate at which distress occurs (slope of D_1 and D_2 in Figure 11a) is an indication of the relative positions of t_1 and t_2 on the time scale and the degree of distress caused by the environment. Conceptually, it can be shown that an infinite distress accumulation rate would be reached at the distress limit, when the structure is tested without acceleration. Therefore, the rate of distress occurrence at a given time, using statistically based data, can be used to estimate the remaining life of a structure.

Figure 11b shows how two similar pavement sections are tested to failure under the same environmental conditions but at different times during the life of the pavement. The difference between the number of accelerated load applications (N_1 and N_2) can be attributed to two factors: the additional traffic that used the second section and aging or environmental effects. Because the traffic between testing of the first and second sections, $N_{traffic}$, can easily be measured, the reduction (or, in some cases, increase) in N_2, the remaining life, must be attributable to environmental effects, as given in Equation 2.

$$N_1 = N_2 + N_{traffic} + N_{environment} \quad (1)$$

$$N_{environment} = N_1 - N_2 - N_{traffic} \quad (2)$$

This relationship can be used to evaluate the effect of procedures designed to counteract environmental distress and to estimate the remaining life of a pavement structure.

A plot of the number of load applications versus time is shown in Figure 11b. A locus of failure points is given, from

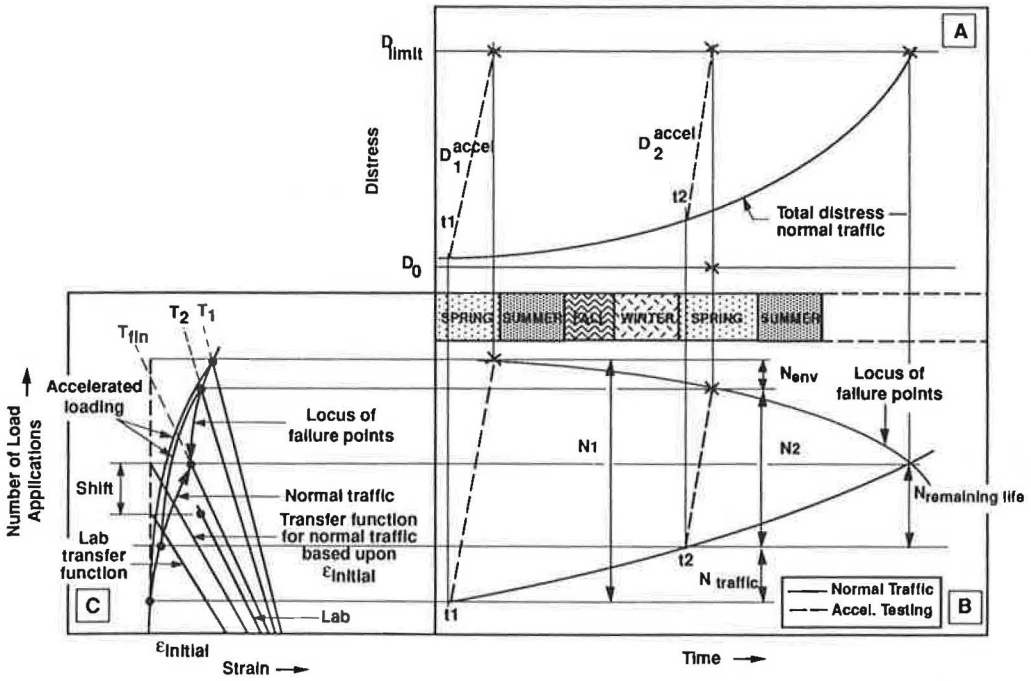

FIGURE 11 Conceptual application of accelerated pavement testing to evaluate environmental effects on pavements.

an interpolation of accelerated failure points at different times (t_1, t_2), as well as the failure point of the unaccelerated structure. Accelerated loading occurs at a constant rate, resulting in parallel lines that lead to a certain failure mode at different numbers of load applications, as given in Equation 2.

Two families of curves are presented in Figure 11c. The straight lines represent the transfer functions relating strain to the number of load applications at failure that can be expected at a given constant stress level. Currently, laboratory results are used to determine these relationships. Laboratory results often underestimate fatigue life of the material under real traffic and environmental conditions, which necessitates the use of shift factors to prevent costly overdesign of pavement structures. Great uncertainty exists about the magnitude of these shift factors, given that the goal is to determine T_{fin} (see Figure 11c).

The second family is the curved relationships that depict the strain path versus number of load applications followed by a material under constant stress loading. For constant strain, these paths are represented by straight vertical lines. Strain is shown as the dependent variable in Figure 11c. Because strain is not easily derived or determined in in-service pavements, surface deflections are usually used instead of strain.

Accelerated testing allows the researcher to locate T_{fin} by testing at different times during the life of a pavement structure. For a specific structure, defining the position of the transfer functions at T_1 and T_2 will define the coinciding origin for the relationships at one load application. All transfer functions, including T_{fin}, for that structure will originate from this point, thus establishing one point on the straight line. The transfer functions at T_1 and T_2 can be established by accelerated testing at different levels of constant stress, leading to different times to failure. Connecting the failure points will result in the two accelerated load transfer functions.

Establishing the other point on T_{fin} requires the strain paths for at least three accelerated test periods, the accelerated strain paths at t_1, t_2, and t_3 (t_3 not shown in Figure 11c), and the application of the same load magnitudes. Because of the mixture of traffic, the strain path for traffic can be represented by a weighted average strain caused by the traffic, which in turn defines the load to be used for the accelerated testing.

Plotting the strain paths for t_1, t_2, and t_3 will result in failure points on each respective transfer function after a certain number of applications. The strain path for the normally trafficked pavement between t_1 and t_3 can also be plotted, and it serves as the point of origin for accelerated testing strain paths. The traffic strain path is then extrapolated to the T_3 transfer function (not shown). To establish the second point on T_{fin}, which lies on the traffic strain path, the locus of accelerated failure points can be extrapolated until it coincides with the normal traffic strain path.

In this way, a family of transfer functions relating strain to the number of load applications can be established for different combinations of environment and load. This can be done in considerably less time than would normally be required using long-term pavement performance studies.

CONCLUSIONS AND RECOMMENDATIONS

A concept for an accelerated pavement testing machine has been presented as a first step. Operation of the machine has been described in a technical brochure, and a working model of the MLS was constructed as proof of the mechanical fea-

sibility of the concept. The model shown in Figure 3 will also be used for model pavement studies. The next step, design and construction of a full-scale prototype, has been completed. The development and use of the machine will be done within the budget constraints of SDHPT. Manufacture of subsequent machines will be undertaken only after a performance evaluation of the prototype has been completed and good experimental results have been obtained.

Use of accelerated pavement testing is to be expected and encouraged by agencies such as SDHPT. The cost of this type of testing, estimated at about $530,000 per year per machine (five tests per year), may necessitate alternative funding to guard against encroaching on other research programs. Maximization of benefits from accelerated pavement testing will require dedicated funding to support a long-term test program. At this stage, out-of-state participation in the program has been limited to an advisory capacity.

The MLS is expected to be operational in 18 months. Ultimately the MLS program could be viewed in one of two ways. It could be used as the main indicator of the behavior of pavement structures, which implies an extensive fleet of MLSs with a dedicated work force for many years to come. Alternatively, the MLS program could be considered as a means by which less expensive, faster, but still reliable methods can be developed and evaluated long after most of the MLS testing has been phased out. This decision will have to be made on the basis of a benefit-cost analysis.

ACKNOWLEDGMENTS

This paper is published with the permission of SDHPT. The authors gratefully acknowledge the support of the department, particularly R. G. Welsch, who recognized the capabilities of the MLS and guided its development as chairman of the project steering committee.

REFERENCES

1. R. N. Walker. The South African Heavy Vehicle Simulator. Annual Transportation Convention, Pretoria, South Africa, 1985.
2. G. B. Byrd and R. L. Hutchinson. *Pavement Testing Conference*. FHWA, May 1984.
3. National Institute for Transport and Road Research. *Symposium on Recent Findings of Heavy Vehicle Simulator Testing*. Annual Transportation Convention, Pretoria, South Africa, 1984.
4. H. K. Berry and R. C. Panuska. *Manufacture of an Accelerated Loading Facility (ALF)*. Report FHWA-RD-87-071. FHWA, U.S. Department of Transportation, April 1987.
5. J. Page. *Dynamic Behavior of a Single Axle Vehicle Suspension System: A Theoretical Study*. TRRL, LR 580, 1973.
6. G. Ahlborn. *ELSYM5, Computer Program for Determining Stresses and Deformation in Five Layer Elastic Systems*. University of California, Berkeley.
7. P. S. Fancher, R. D. Ervin, C. D. Winkler, and T. D. Gillespie. *A Factbook of the Mechanical Properties of the Components for Single-Unit and Articulated Heavy Trucks*. Transportation Research Institute, The University of Michigan, Ann Arbor, 1986.

Comparison of Computer Predictions and Field Data for Dynamic Analysis of Falling Weight Deflectometer Data

ALLEN H. MAGNUSON, ROBERT L. LYTTON, AND ROBERT C. BRIGGS

The extraction of engineering properties of pavement layers by dynamic analysis of falling weight deflectometer (FWD) data is demonstrated. FWD data from two in-service highway sections were analyzed. The FWD data consist of time records of surface loading and surface deflections at a range of distances. A Texas Transportation Institute pavement dynamics computer program, SCALPOT, was used to generate predicted responses. Physical properties of the pavement were generated by a trial-and-error backcalculation and a Systems Identification computer program. The pavement surface vertical deflections were characterized by using frequency response functions in the form of magnitude and phase angle plots as a function of frequency. The magnitude plots represent vertical pavement surface deformations resulting from a steady-state sinusoidal surface loading. The phase angle data represent the lag angle between the loading and the surface deflections. The asphaltic concrete surface layer was represented as a three-parameter viscoelastic medium. The base course, subgrade layers, and bedrock layers, if any, were treated as damped elastic solids. These physical properties were backcalculated by matching approximately the frequency-analyzed field data with computed values by varying the SCALPOT input data set. Good agreement between experimental and computer-predicted responses was obtained using the backcalculated pavement layer properties. One site with near-surface bedrock was analyzed and good agreement was obtained.

Dynamic analysis is governed by various forms of Newton's second law. In continuum mechanics Newton's law is usually expressed as the Navier vector field equation. For an axisymmetric, horizontally layered, viscoelastic medium (a highway pavement section), the vector field equation can be separated into two scalar reduced wave equations, each having its own scalar potential. The equations can be solved readily by using separation of variables and a suitable orthonormal eigenfunction expansion. The expanded solution can be evaluated numerically with specially formulated computer algorithms, which may be implemented in one or more computer programs. This process has been completed for the pavement dynamics problem, and some initial results are presented.

Dynamic analysis requires understanding of creep compliance functions, complex moduli, wave phenomena, dynamic vector field equations, compressional waves, shear waves, layered media, and many other physical phenomena, as well as various applied mathematics disciplines and numerical methods. By contrast, static analysis is usually formulated using the biharmonic operator, which is a special case (zero frequency) of the two reduced wave operators in the corresponding dynamic formulation.

A. H. Magnuson and R. L. Lytton, Texas Transportation Institute, Texas A&M University System, College Station, Tex. 77843. R. C. Briggs, Texas State Department of Highways and Public Transportation, Austin, Tex. 78701.

NEED FOR PAVEMENT DYNAMIC ANALYSIS

One may well ask, Why use dynamic analysis when static analysis methods are readily available? What, if anything, is wrong with existing static analysis procedures? These questions can be answered as follows:

- Dynamic analysis is more accurate and physically realistic, because it takes into account transient (time-dependent) wave phenomena in the pavement layers.
- More information on pavement layer properties can be extracted, because all the information in the falling weight deflectometer (FWD) time-pulse data is used in the backcalculation procedure (as opposed to only peak values of the pulses, as is currently done in elasto-static analysis).
- With dynamic analysis, the viscoelastic properties of the asphaltic concrete (AC) surface layer can be characterized by creep compliance functions in the time domain and complex moduli in the frequency domain. Static analysis is limited to elastic modeling because viscoelastic phenomena are inherently dynamic.
- More physical insight into the pavement section (e.g., the presence of bedrock, modal responses, and reflection and refraction between layers) can be obtained from dynamic analysis.
- Dynamic analysis is more sensitive to pavement layer properties because of the additional data available. This means that, in principle, more accurate backcalculation results can be obtained.

Dynamic analysis potentially offers the following benefits: cost savings, fast response time, and additional engineering information. Among the inherent advantages of FWD dynamic analysis are nondestructive testing of the pavement surface and inexpensive, fast automated data acquisition and analysis.

BACKGROUND

In September 1987 the Materials, Pavements and Construction Division of Texas Transportation Institute (TTI) started

work on a 4-year research project, "Dynamic Analysis of Falling-Weight Deflectometer Data." The project is administered by the Texas State Department of Highways and Public Transportation as part of FHWA's Cooperative Research Program. The project's purpose is to develop a computer model of pavement dynamic response and to apply it in the prediction and evaluation of pavement performance.

The division is using mechanistic approaches to characterize pavement failure and aging associated with cracking and rutting. The dynamic analysis of FWD data can, in principle, be used to backcalculate pavement layer properties related to remaining pavement life.

FWD (or drop weight force impulse) devices are in widespread use for in-service pavement evaluation and backcalculation of moduli. However, pavement response data are currently analyzed with static models.

In static analysis the dynamic deflection basin caused by the FWD is assumed to be static, whereby the instantaneous pavement deflection at a given point is assumed to be proportional to the instantaneous force on the pavement surface. In static analysis, therefore, only the peak values of the force and deflection pulses are used.

The FWD time-pulse data contain much more information on the pavement layers; however, this information cannot be extracted without a working pavement dynamic analysis program. Static analysis methods are used because no one has yet developed a practical working dynamic analysis program for pavements.

RELATED WORK

Pavement impulse testing is described by Lytton et al. (*1*) and Uzan et al. (*2*). Dynamic response of geophysical and geotechnical systems started with the work of Lamb (*3*), who solved the problem of the dynamic response of a uniform half-space to describe the main features of earthquake tremors. Ewing et al. (*4*) is a standard reference in seismology for dynamic analysis of multilayered elastic media. The analysis used in TTI's SCALPOT computer program is a direct extension of this work.

Magnuson (*5,6*) developed a matrix recurrence relation to solve the multilayered viscoelastic problem for another application. The recurrence relation reduced the matrix relations to a series of 4 × 4 matrix manipulations that could easily be programmed on a computer. He also introduced viscoelastic complex moduli into the multilayer problem by using the correspondence principle. Each layer's response was characterized by two scalar potentials, one for the compressional wave and the other for the vertical shear wave. The solution is expressed as a Fourier-Bessel integral expansion. This expression is an improper integral having one or more pole singularities near the path of integration and an infinite upper limit. The integral is particularly difficult to evaluate accurately because of the slow convergence as the upper limit approaches infinity. Magnuson (*7*) describes an integration algorithm developed for the pavement dynamics problem. The algorithm is an extension of Zhongjin's analysis (*8*). The multilayered medium's matrix algebra (*6*) and the integration algorithm (*7*) have been incorporated into the SCALPOT computer program, which was developed for the dynamic analysis of pavement responses.

SCALPOT AND FWD-FFT

The SCALPOT (scalar potential) program developed at TTI computes the dynamic response of a horizontally layered viscoelastic half-space to a time-dependent surface pressure distribution. Vertical surface deflections resulting from the oscillatory surface pressure distribution can be obtained for a range of frequencies and distances from the surface pressure distribution.

SCALPOT has been modified to incorporate a surface layer. Additional modifications were made to treat pavement sections with stiff layers and near-surface bedrock. The input data set for SCALPOT consists of the geometrical configuration of the FWD apparatus and the physical properties of each pavement layer. The properties of each layer include thickness, weight density, viscoelastic parameters, Young's modulus, damping ratio, and Poisson's ratio. SCALPOT is currently programmed to treat each layer as a damped elastic solid or as a three-parameter viscoelastic medium.

Another computer program developed at TTI, FWD-FFT, was used for analyzing the FWD data. The methods used to analyze the FWD data are described elsewhere (*9*). The program scans the time series data, makes the pulse "tail correction," computes averages, and performs a Fast Fourier Transform (FFT) of the corrected and averaged pulse data. FWD frequency response functions are then computed by performing a complex division of the FFT of the surface deflections by the FFT of the surface loading. The frequency response functions are computed for the seven displacements at each site, and the results are written to data files and plotted.

FREQUENCY DOMAIN ANALYSIS

FWD time pulses are transformed to the frequency domain by using the superposition principle. The transient pulses are expressed as a sum of time-harmonic functions interfering with each other in such a way as to closely replicate the original pulse shape. This process is performed efficiently using FFTs, which are based on an algorithm formulated by Cooley and Tukey in the 1960s.

This study was conducted using frequency domain analysis, whereby the pavement surface vertical deflections were characterized with steady-state frequency response functions. At a given frequency, the vertical surface deflections are represented as the response to a sinusoidal vertical surface loading. The data are presented in the form of magnitude and phase angle plots as a function of frequency. The phase angle represents the lag angle (at a given frequency) between the loading and the surface deflections.

PAVE-SID

PAVE-SID, a computer program based on the System IDentification (SID) methodology, was developed to extract pavement properties by using FWD data and dynamic analysis techniques. PAVE-SID is described by Torpunuri (*10*). The inputs to the program are the FWD experimental frequency response functions and computed responses generated by the

SCALPOT program. The SID method is described in detail elsewhere (*11,12*). PAVE-SID uses SCALPOT to generate a data base for constructing a sensitivity matrix. Increments in pavement layer properties are computed from the field data and the sensitivity matrix. The updated parameters are input into SCALPOT, and the response is computed and compared against the field data. The process is repeated until convergence is obtained.

PAVEMENT VISCOELASTIC PROPERTIES

An early study of viscoelastic properties of AC materials was conducted by Papazian (*13*). Papazian performed laboratory creep tests on AC core samples and used a linear Voigt-chain-Maxwell viscoelastic representation (*14*) to model the strain data in both the time and frequency domains. Lai and Anderson (*15*) used a nonlinear Voigt-chain-Maxwell viscoelastic representation to model the creep and recovery of AC material.

Paris's law governing crack propagation in a viscoelastic medium provides a direct link between pavement cracking and physical properties of the AC material. Schapery (*16*) put Paris's law on a sound mechanistic footing and developed a nonlinear fracture theory for viscoelastic composite materials applicable to AC pavements.

Pavement rutting resulting from permanent deformation of the AC layer is characterized by Kenis's viscoelastic system (VESYS) mu-alpha formulation (*17*). The VESYS formulation can be applied to the viscoelastic characterization of the pavement to estimate remaining life before failure from rutting.

ANALYSIS OF FWD DATA

Figure 1 is a time plot of the FWD forces and surface deflections for the District 1, Site 3 (D01S3) pavement section near Paris, Texas. Figure 2 is a similar plot for the District 8, Site 4 (D08S4) section (Interstate 20) near Abilene, Texas. The FWD data in Figures 1 and 2 are in the form of digitized time series with a sampling rate of 0.2 msec over a 60-msec duration. Figures 1 and 2 are working plots used in data reduction and preprocessing. They are screen dumps of a VGA 640- × 480-pixel color video display from an IBM AT-compatible computer with an Intel 30386 microprocessor. The forces and deflections are scaled from the pixel plots by dividing by the "fconst" and "dconst" values shown for each figure. The headers for each figure site give the load, highway section data, date of test, thickness of AC surface course, and surface temperature. The inverted curves at the tops of the figures show the drop weight force on the pavement surface as a function of time. The seven surface deflections are shown for sensors spaced 0, 1, 2, 3, 4, 5, and 6 ft from the center of the drop weight. The deflections decrease with distance, so the largest deflection is for the sensor at $r = 0$. The deflections in Figure 2 for D08S4 show an overshoot or zero-crossing at the tail of the pulse. The zero-crossings of the deflections indicate that near-surface bedrock is present.

CREEP COMPLIANCE DATA FROM AC SAMPLES

Core samples for the sections were taken in an earlier study. Information on the sections is given in Table 1, which indicates that they are both relatively stiff pavements having a thick AC surface course. Figure 3 shows recently obtained creep data for three AC core samples for the D01S3 and D08S4 sections. The data in Figure 3 show longitudinal strain response of the AC surface course samples subjected to a suddenly applied constant stress (step function) uniaxial compression. The data were taken using a materials testing system machine at TTI. The strain data in Figure 3 are presented in the form of log-log plots of millistrain as a function of time.

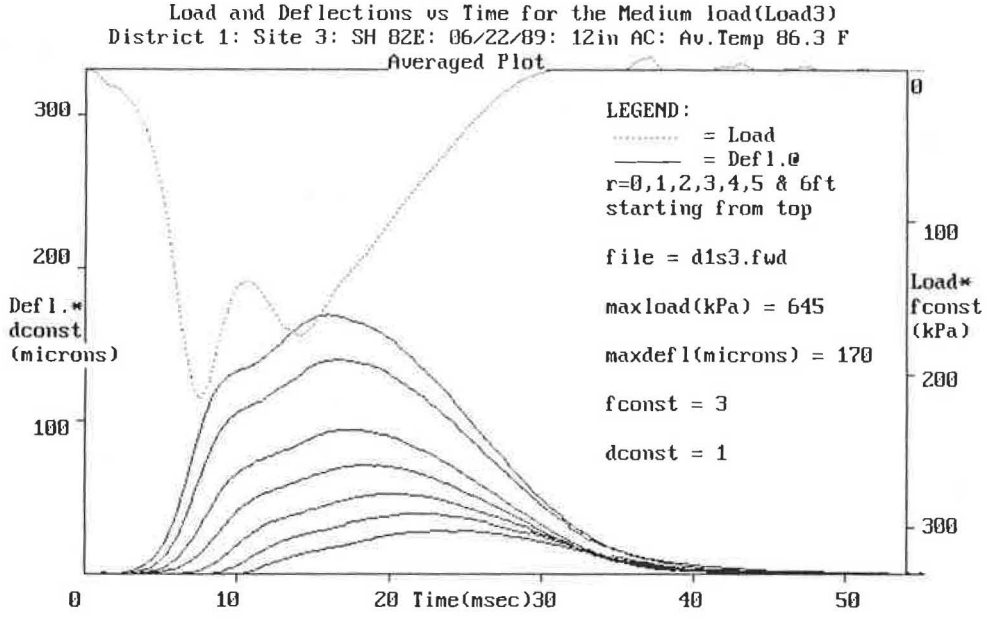

FIGURE 1 FWD time-pulse data, D01S3—drop weight force and seven displacement sensors versus time.

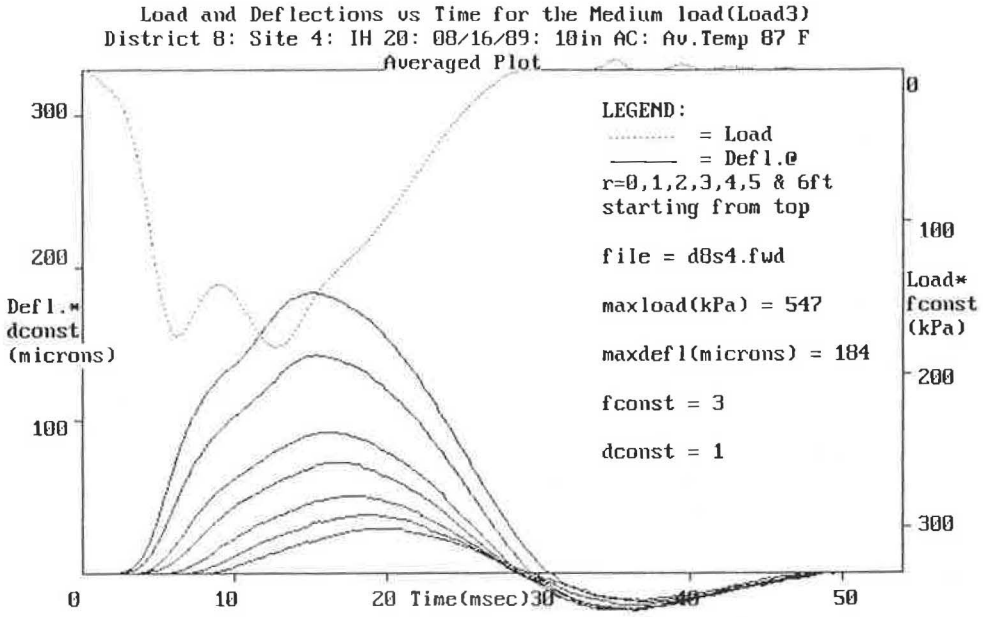

FIGURE 2 FWD time-pulse data, D08S4—drop weight force and seven displacement sensors versus time.

TABLE 1 PAVEMENT SECTION CHARACTERISTICS (FROM CORE SAMPLING LOG)

Section	Surface Course	Base Course	Subgrade
D01-S3	12 in thk AC	22 in (Sandy)	Clay
D08-S4	10 in thk AC	11 in LS CR	Clay:Rock @ 9.75 ft

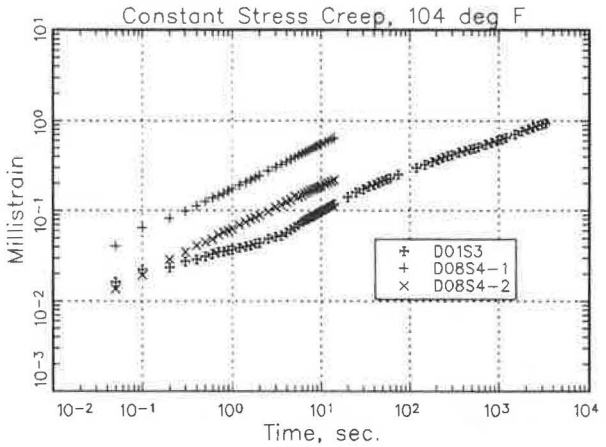

FIGURE 3 Log-log plots of millistrain from laboratory compressional creep tests—one sample from D01S3 and two samples from D08S4.

PAVEMENT FREQUENCY RESPONSE FUNCTIONS

Figures 4 and 5 represent the frequency response functions for pavement vertical surface deflections resulting from a vertical surface pressure distribution caused by the FWD apparatus. For convenience, the magnitude responses are given in units of mils per 10 kips in Figures 4a, 4c, 5a, and 5c. Figure 4 shows D01S3 frequency response functions computed from FWD data using the FWD-FFT computer program. Data are shown for displacements at r = 0, 1, 2, 3, 4, 5, and 6 ft. Magnitude responses for the inner sensors, phase angles for the inner sensors, magnitudes for the outer sensors, and phase angles for the outer sensors are shown in Figures 4a, 4b, 4c, and 4d, respectively. The magnitudes in Figures 4a and 4c decrease with r, so the r = 0 curve is on top, the r = 1 ft curve is immediately below it, and so on. The phase angle curves in Figures 4b and 4d start with the smallest r on top and work down as r increases.

These FWD frequency response curves behave the same for all the sections examined so far; the general arrangement of the response curves in Figure 4 is the same for other sections. The magnitude curves decrease with frequency because of the effect of the mass through Newton's law. Similarly, the phase angles increase with frequency.

The D01S3 phase angle curves for r = 5 and 6 ft show a jump at the higher frequencies. The jump coincides with a dip or partial null in the corresponding magnitude curves. This behavior indicates wave interference, or possibly modal response caused by repeated back reflection off lower layers.

Figure 5 shows D08S4 frequency response functions computed from FWD data using the FWD-FFT computer program. Data, which are shown for the same displacements as for Figure 4, are arranged in the same way as the data in

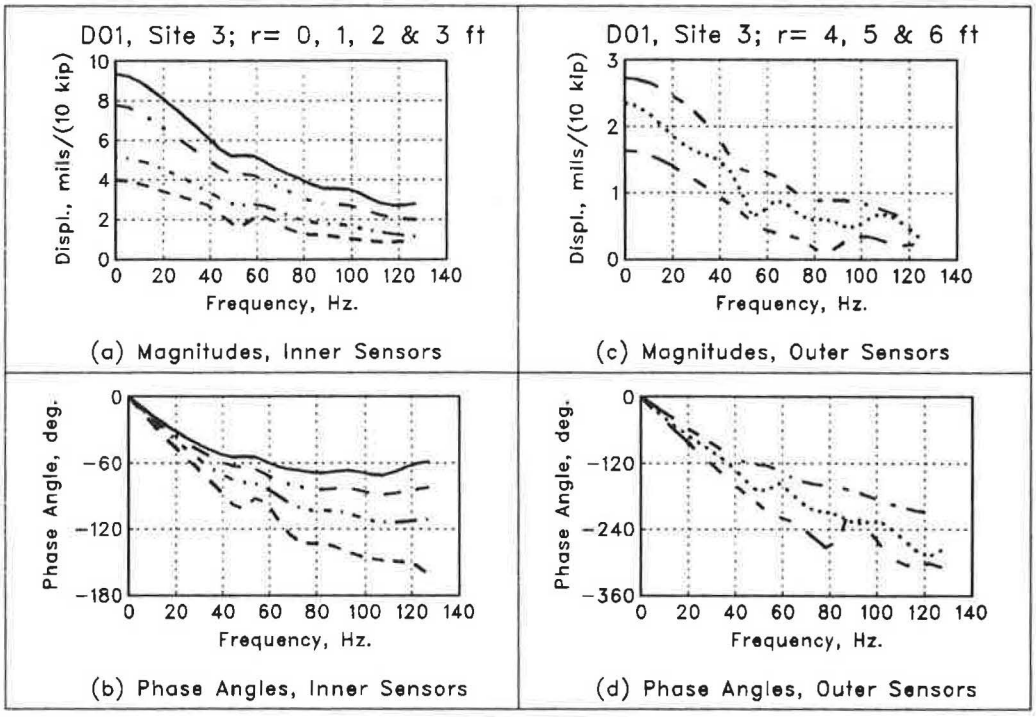

FIGURE 4 D01S3 frequency response functions (computed from FWD data).

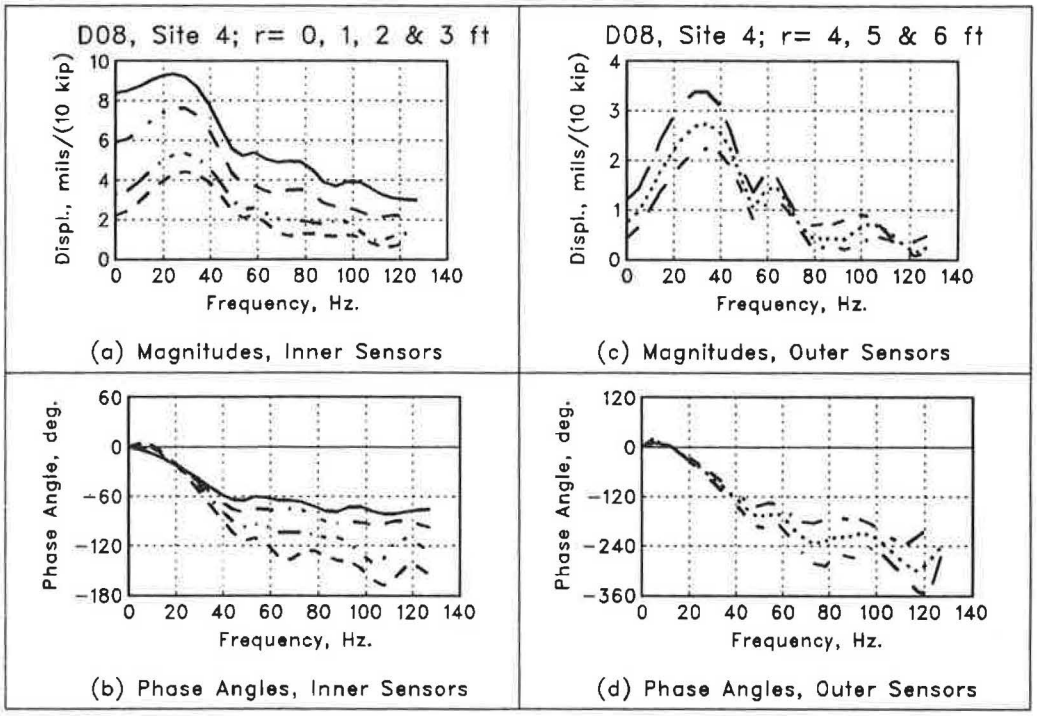

FIGURE 5 D08S4 frequency response functions (computed from FWD data).

Figure 4. The magnitude and phase angle curves differ considerably from the D01S3 responses because of the near-surface bedrock. The magnitude responses have a pronounced peak at about 30 Hz. The peaking increases for increasing distance r. There are two or three partial nulls in magnitude and corresponding jumps in phase angle. In addition the phase angles of the inner sensors show a crossover at about 25 Hz followed by a lead angle for lower frequencies. There is apparently a connection between the unusual behavior of the frequency response curves in the presence of bedrock and the time-pulse overshoot or zero-crossing seen in Figure 2.

VISCOELASTIC REPRESENTATION OF AC MATERIAL

The simplest way to interpret the data in Figure 3 is to use a two-parameter power-law representation, as follows:

$$D(t) = At^n \tag{1}$$

where n is the log-log slope and A is the intercept at $t = 1$ sec. A three-parameter representation, a generalized time-domain power-law representation, is also in extensive use. The generalized power-law or three-parameter representation separates the viscoelastic part from the (assumed) elastic response, and may be written as follows:

$$D(t) = D_0 + D_1t^n \tag{2}$$

where D_0 is the elastic compliance and D_1 is the viscoelastic term evaluated at $t = 1$ sec.

Because of the reciprocal relationship between compliances and moduli, the first and second compliances in Equation 2 can be written as follows:

$$D_0 = E_0^{-1} \tag{3a}$$

and

$$D_1 = E_1^{-1} \tag{3b}$$

where E_0 is the elastic modulus and E_1 is the viscoelastic modulus at $t = 1$ sec.

Expressing Equation 2 in terms of the moduli in Equation 3 gives

$$D(t) = 1/E_0 + t^n/E_1 \tag{4}$$

This representation, when evaluated at $t = 1$ sec, is equivalent to two springs in series.

FREQUENCY DOMAIN REPRESENTATION OF AC CREEP COMPLIANCE

The time-domain creep compliance functions (Equations 1 and 2) must be transformed into the frequency domain for use in pavement dynamic analysis programs. The frequency-domain representation is called the complex compliance because it can be expressed as a complex number having a real part and an imaginary part. Performing a Fourier integral transform on Equations 1 and 2 gives the following for the two- and three-parameter complex compliances, respectively:

$$D(\omega) = A\Gamma(1 + n)\omega^{-n}[\cos(n\pi/2) - i\sin(n\pi/2)] \tag{5a}$$

$$D(\omega) = D_0 + D_1\Gamma(1 + n)\omega^{-n}[\cos(n\pi/2) - i\sin(n\pi/2)] \tag{5b}$$

where $i = \sqrt{-1}$, ω is the radian frequency, and Γ represents the gamma function.

Equation 5b, for the three-parameter representation, has been coded into the SCALPOT program.

LABORATORY CREEP COMPLIANCE DATA

The D01S3 and D08S4 creep data in Figure 3 were used to obtain the viscoelastic parameters for the three-parameter model shown in Equation 2. For that representation, the constant D_0 for the elastic component is an assumed value. The viscoelastic component was obtained by subtracting out the assumed elastic term from the total creep data in Figure 3 and replotting the remaining strain on a log-log scale. The viscoelastic parameters n and D_1 are obtained from the slope and intercept, respectively, of the log-log plots.

DESCRIPTION OF COMPARISON STUDY

The comparison study presented here was conducted on Sections D01S3 and D08S4 because core samples from these sections were left over from a previous investigation. The samples were tested in uniaxial constant stress in compression. This allowed the investigators to compare backcalculated viscoelastic parameters obtained from FWD data with laboratory test results.

The frequency response functions shown in Figures 1 and 2 were compared with corresponding computed values generated by the SCALPOT program. The backcalculation study was performed by estimating the SCALPOT data set using creep data for AC materials and modulus data generated from static backcalculation efforts. The estimated data set was used in the SCALPOT program to obtain a first approximation to the surface deflections. Following the initial estimates, the moduli, viscoelastic constants, and unknown layer thicknesses for each layer were adjusted one at a time on a trial-and-error basis until satisfactory agreement with field data was achieved.

Generally speaking, the responses at the low frequencies are dominated by the lowest layer. This observation led to the introduction of new sublayers by splitting the subgrade or the bedrock, or both, into two sublayers, with modulus increasing with depth. This subdivision improved the correlation at low frequencies.

Section D01S3 was further subjected to an automated backcalculation procedure using the PAVE-SID computer program. The SID study significantly improved agreement of the field data with computed responses. The SID study used frequencies from approximately 10 to 130 Hz in 10-Hz steps.

RESULTS OF COMPARISON STUDY

D01S3 Results

Figure 6 compares SCALPOT-computed values using the backcalculated three-parameter viscoelastic representation with frequency-analyzed FWD data. The symbols represent computed values and the solid line represents the FWD data. The FWD data are the same as in Figure 4. Figures 6a, 6b, 6c, and 6d show the magnitude response at $r = 1$ ft, the phase angle response at $r = 1$ ft, the magnitude response at $r = 4$ ft, and the phase angle response at $r = 4$ ft, respectively. There is good correlation of phase angle at both $r = 1$ ft and $r = 4$ ft. Magnitude correlation is good for $r = 1$ ft; however, some discrepancy is apparent at $r = 4$ ft. Nevertheless, the discrepancy is within 1 mil per 10 kips.

Figure 7 compares, for all displacement sensors at Section D01S3, the SCALPOT-computed values and the frequency-analyzed FWD data shown in Figure 4. It appears here to show the full data set used in the actual backcalculation process. The symbols represent computed values, and the solid lines represent the FWD data. Figures 7a and 7b show the magnitude and phase angle responses, respectively, at $r = 0$, 1, 2, and 3 ft; Figures 7c and 7d show the magnitude and phase angle responses, respectively, at $r = 4$, 5, and 6 ft. There is good agreement for both magnitude and phase angle at all values of r. At a given frequency the magnitudes are larger for smaller values of r, and the phase angles increase with r.

The agreement of the outer sensors in Figure 7c does not appear to be as good as the inner sensors' correlation. This is because the magnitudes are shown on an expanded scale. The absolute correlation for all the magnitudes is within 0.5 to 1 mil per 10 kips, which is the limit of resolution of the geophones. The good overall agreement can be attributed to the use of the PAVE-SID program in the backcalculation.

Table 2 shows pavement layer thicknesses, including the backcalculated thickness of the upper subgrade layer. Table 3 shows viscoelastic parameters E_0, E_1, and n for the AC surface course; backcalculated values for Young's modulus; and damping for the base course and both subgrade layers. Table 4 compares viscoelastic parameters obtained from laboratory tests with those obtained from backcalculation.

D08S4 Results

Figures 8 and 9, respectively, show information for Section D08S4 corresponding to that shown in Figures 6 and 7 for Section D01S3. Again there is good agreement for both magnitude and phase angle for all values of r. Agreement at frequencies below approximately 10 Hz is poor, apparently because of the hyperbolic behavior of the complex modulus in Equation 5b. To avoid this, a four-parameter model for the AC surface course would be necessary.

From coring data, this section was known to have a near-surface bedrock layer at a depth of 9.75 ft (see Table 1). For this reason, the section was initially treated as a four-layered section, with a three-parameter viscoelastic AC layer, a base course, a subgrade layer, and the infinitely deep bedrock layer. In addition to the moduli of the top three layers, the depth to bedrock and the bedrock's modulus were backcal-

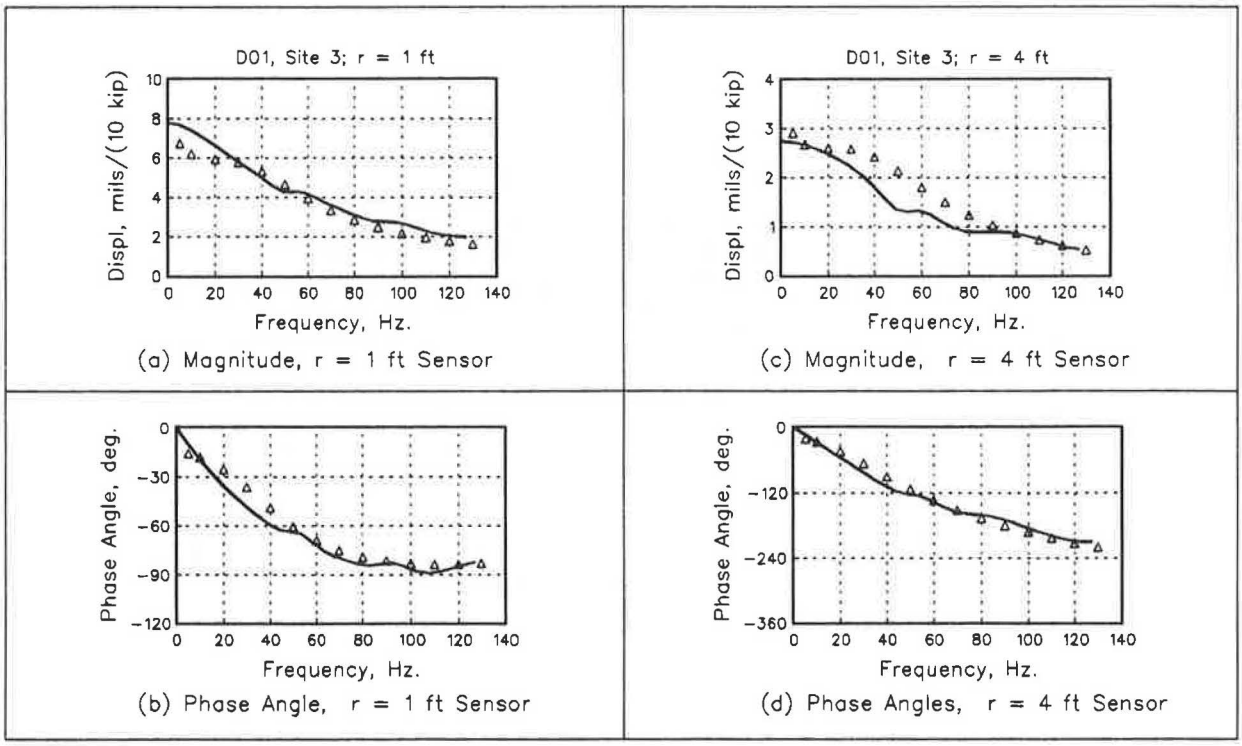

FIGURE 6 D01S3 frequency response functions for $r = 1$ ft and $r = 4$ ft: comparison between computed values (*symbols*) using backcalculated three-parameter viscoelastic representation and frequency-analyzed FWD data (*lines*).

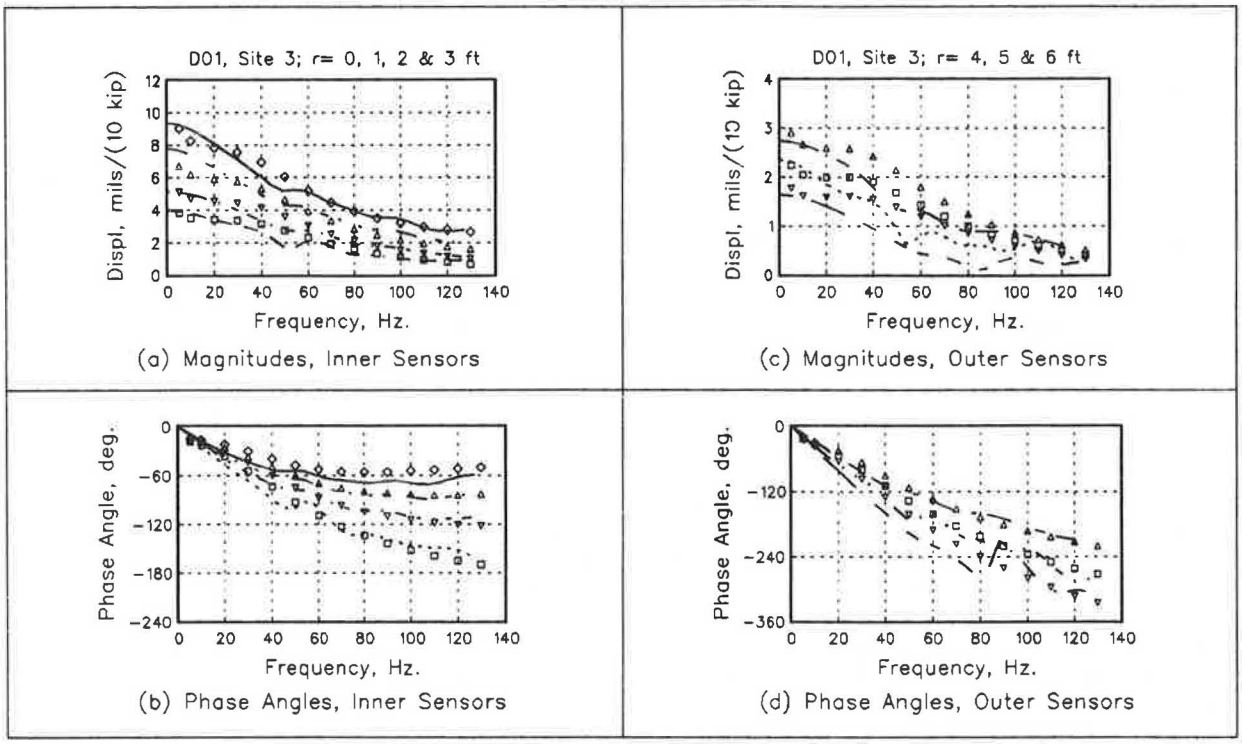

FIGURE 7 D01S3 frequency response functions for all displacement sensors: comparison between computed values (*symbols*) using backcalculated three-parameter viscoelastic representation and frequency-analyzed FWD data (*lines*).

TABLE 2 PAVEMENT LAYER THICKNESS (INCHES)

Site	D01S3		D08S4	
Layer	Thickness	Depth	Thickness	Depth
AC Surface	12	12	10	10
Base	22	34	11	21
Subgrade	20*	54	72*	93
SG-2/BR-1	∞	-	48*	141
Bedrock-2	-	-	∞	-

* Back-Calculated Value

Note: SG indicates subgrade; BR indicates bedrock.

TABLE 3 BACKCALCULATED PAVEMENT LAYER MODULI AND DAMPING

Site	D01S3		D08S4	
Layer	Modulus (KSI)	Damping	Modulus (KSI)	Damping
AC Surf.(3-Par)		0.296*		0.30*
E0	834.0		1250.0	
E1	1516.4		1250.0	
E @ 10 msec	731		999.0	
Base Course	45.11	0.015	104.2	0.015
Subgrade 1	20.17	0.015	31.3	0.075
SG2/BR-1	48.61	0.075	83.33	0.015
Bedrock-2	-	-	111.1	0.015

* Slope of Log-Log Creep Curve

Note: SG indicates subgrade; BR indicates bedrock.

TABLE 4 AC SURFACE COURSE VISCOELASTIC PARAMETERS— LABORATORY DATA AND BACKCALCULATED VALUES

Site	E0 (KSI)	E1 (KSI)	n(slope)
D01S3			
a) Lab, 104°F	2000.0	1666.67	0.5407
b) Back-Calculated	834.0	1516.4	0.296
D08S4			
a) Lab, 104°F	1250.0	312.5	0.6029
b) Back-Calculated	1250.0	1250.0	0.30

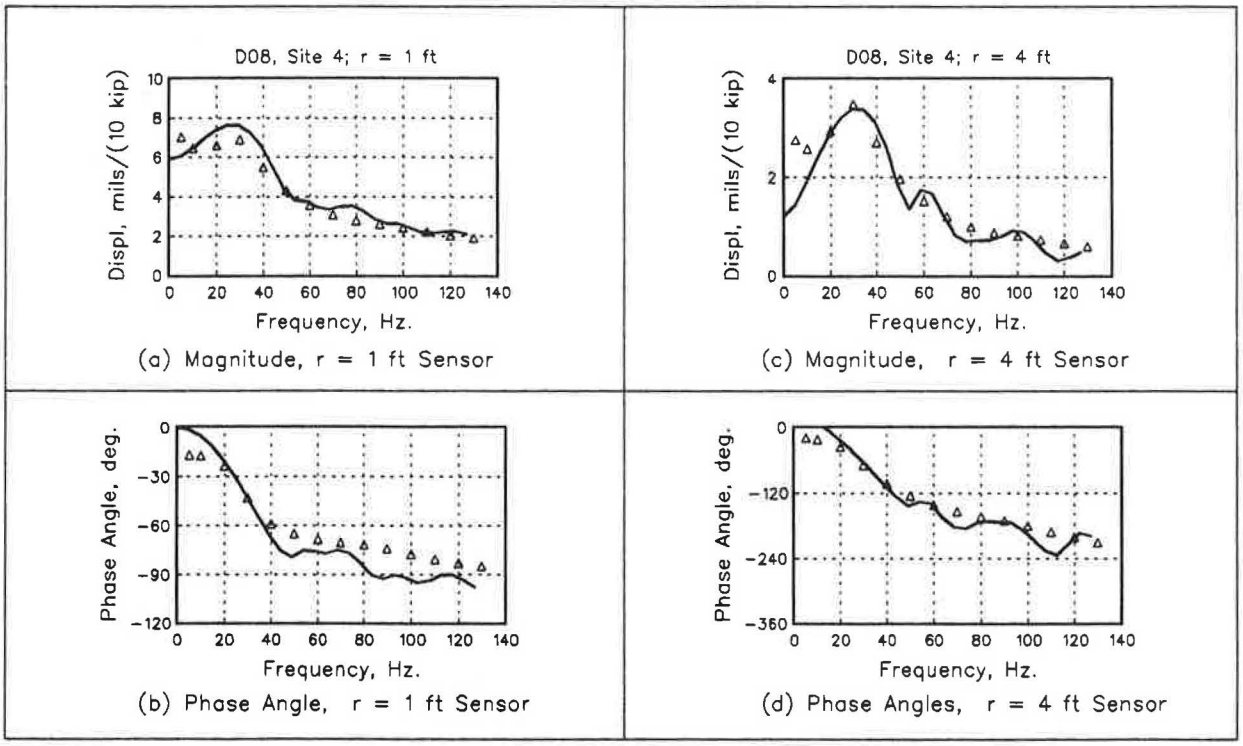

FIGURE 8 D08S4 frequency response functions for $r = 1$ ft and $r = 4$ ft: comparison between computed values (*symbols*) using backcalculated three-parameter viscoelastic representation and frequency-analyzed FWD data (*lines*).

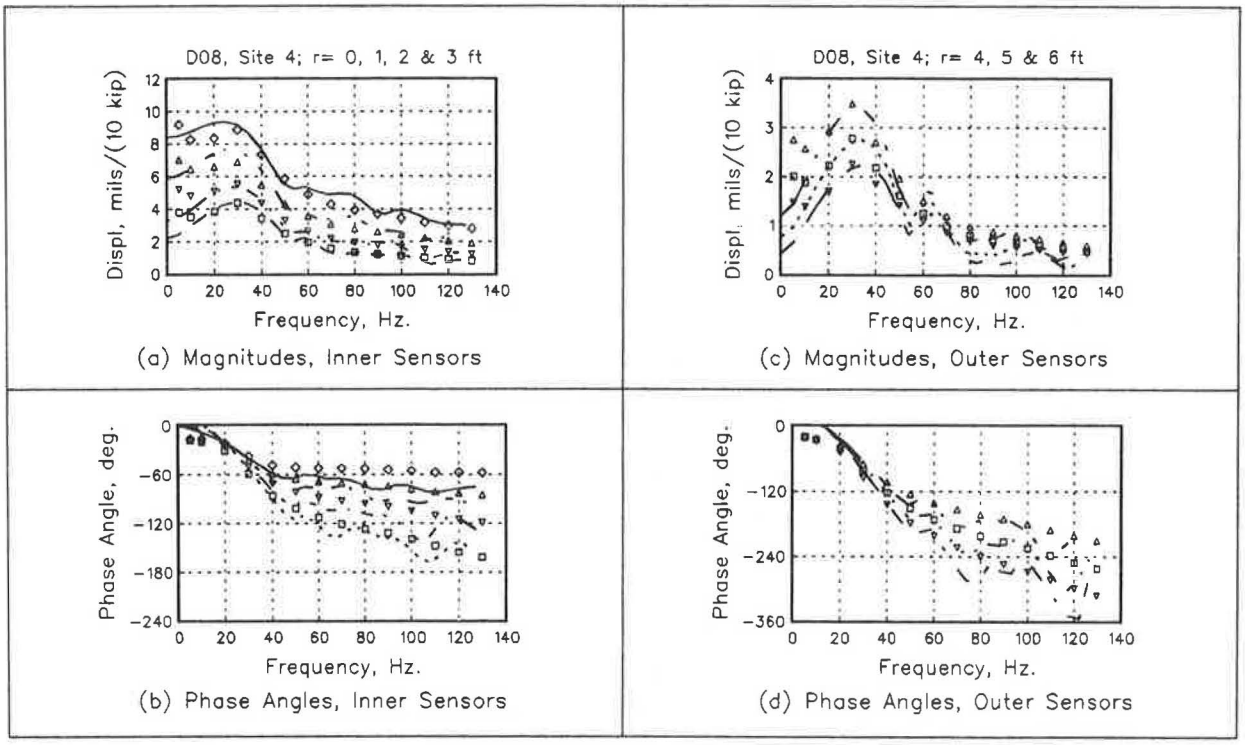

FIGURE 9 D08S4 frequency response functions for all displacement sensors: comparison between computed values (*symbols*) using backcalculated three-parameter viscoelastic representation and frequency-analyzed FWD data (*lines*).

culated. To improve low-frequency agreement, the bedrock half-space was then divided into two layers, as indicated in Table 2. The improved agreement (except at the very low frequencies) is evident in Figures 8 and 9. The good agreement indicates that dynamic analysis can be used to backcalculate pavement layer physical properties, even in the presence of near-surface bedrock. It is clear from the values of the bedrock moduli in Table 3 that any attempt to backcalculate layer properties for this section without taking into account the shallow bedrock would lead to erroneous results.

Comparison Between Laboratory Data and Backcalculated Values

Table 4 compares backcalculated AC viscoelastic parameters and laboratory creep data. The log-log slope (n) for the laboratory data was about twice the backcalculated value for both sections. The backcalculated elastic modulus E_0 was about half the laboratory data value for D01S3, whereas the backcalculated and laboratory data were the same for D08S4. The backcalculated viscoelastic modulus E_1 was about equal to the laboratory data value for D01S3, whereas the backcalculated value was about four times the laboratory data value for D08S4.

Two Versus Three Parameters

The three-parameter viscoelastic model was used instead of the two-parameter model because agreement between laboratory data and backcalculated values was poor for the two-parameter model. The backcalculated slope (n) was typically one-half to one-fifth of the laboratory data value. The backcalculated intercept (A in Equation 1) was typically 1/10th to 1/20th of the laboratory data value. Such large disagreement indicates that the two-parameter model is not physically realistic.

Effective Modulus for AC Surface Layer

The time domain three-parameter complex modulus in Equation 2 may, for comparative purposes, be evaluated at some representative time. The time can be taken at the peak of the FWD drop weight time pulse, which occurs at approximately 10 msec, or 0.01 sec after the start of the pulse (see Figures 1 and 2). Table 3 shows a modulus denoted as "E @ 10 msec" for the AC layer. This representative modulus at the pulse peak can be used to compare with resilient moduli obtained from cyclic loading and resonant column tests.

CONCLUSIONS

The TTI-developed SCALPOT program using a viscoelastic model for the AC surface course has been shown to describe or predict accurately the dynamic responses of the two pavement sections under study, D01S3 and D08S4. For both sections, the program backcalculated pavement layer properties, including moduli, lower layer thicknesses, and, for the AC surface course, the three viscoelastic parameters. On Section D01S3 the subgrade was split into two sublayers for which stiffness increased with depth. This was done to achieve better correlation with the low-frequency FWD data.

The dynamic analysis procedure was used successfully on a pavement section known to have near-surface bedrock, Section D08S4. The FWD responses were shown to be strongly affected by the presence of the near-surface bedrock layer. Nevertheless, the backcalculation produced realistic values for the moduli and the viscoelastic parameters for each layer (including the bedrock layers). The bedrock layer was divided into two sublayers to improve agreement between FWD field data and computed responses at the lower frequencies.

The results described indicate that this dynamic analysis method shows promise for use in the testing and evaluation of AC pavements. The comparison study indicates that pavement dynamic responses can be accurately modeled by adjustment of the physical properties of each layer in the SCALPOT program's input data set.

RECOMMENDATIONS

An extensive validation study is needed to establish the range of pavement types that can be treated by dynamic analysis and the amount and form of engineering information that can be extracted for each type. In such a study laboratory data from samples should be compared with backcalculated pavement layer properties obtained from FWD data, as in Table 4.

Backcalculation studies of 25 Texas pavement sections in the TTI dynamic analysis project are now in progress. The TTI PAVE-SID program will be used to perform automated backcalculations for these sections.

Creep compliance and creep recovery data for AC samples are needed for time scales down to the tens of milliseconds range. These data are required for the three-parameter complex compliance model defined in Equation 5b. The elastic component must be separated from the viscoelastic component. In addition, recoverable deformation must be separated from permanent deformation. The shorter time scales are needed because they are the time scales of the pavement design axle loads at speed. It is not known whether the power-law exponent (n) at the smaller time scales is the same as the exponent at the long time scales customarily used in laboratory creep and creep recovery tests.

This dynamic analysis procedure must be evaluated on its ability to predict layer moduli and viscoelastic parameters, layer thicknesses, and cracking and rutting as they relate to viscoelastic linear and nonlinear properties.

ACKNOWLEDGMENTS

The first author wishes to acknowledge the enthusiastic support, on both technical and financial matters, of his coauthor, the project's technical coordinator, R. C. Briggs of the Texas State Department of Highways and Public Transportation. The first author also wishes to acknowledge his other coauthor, R. L. Lytton, head of TTI's Materials, Pavements and Construction Division, for his guidance on technical matters, encouragement, and support.

George J. Bakas performed the creep tests and provided the creep compliance data. Ajay R. Karkala performed the FWD data reduction and computed the pavement section frequency response functions using the FWD-FFT computer program he developed. Vikram Torpunuri computed the pavement layer properties for Section D01S3 using the PAVE-SID computer program he developed.

REFERENCES

1. R. L. Lytton, F. P. Germann, Y. J. Chou, and S. M. Stoffels. *NCHRP Report 327: Determining Asphaltic Concrete Pavement Structural Properties by Nondestructive Testing*. TRB, National Research Council, Washington, D.C., 1990.
2. J. Uzan, R. L. Lytton, and F. P. Germann. General Procedure for Backcalculating Layer Moduli. *First Symposium on Nondestructive Testing of Pavements and Backcalculation of Moduli*, ASTM, Baltimore, Md., 1988.
3. H. Lamb. On the Propagation of Tremors over the Surface of an Elastic Solid. *Philosophical Transactions of the Royal Society*, Vol. 203, 1904, pp. 1–42.
4. W. M. Ewing, W. S. Jardetzky, and F. Press. *Elastic Waves in Layered Media*. McGraw-Hill Book Company, Inc., New York, 1957.
5. A. H. Magnuson. The Acoustic Response in a Liquid Layer Overlying a Multilayered Viscoelastic Half-Space. *Journal of Sound and Vibration*, Vol. 43, No. 4, 1975, pp. 659–669.
6. A. H. Magnuson. *Sound Propagation in a Liquid Overlying a Viscoelastic Halfspace*. Ph.D. thesis. University of New Hampshire, Durham, 1972.
7. A. H. Magnuson. *Computer Analysis of Falling-Weight Deflectometer Data, Part I: Vertical Displacement Computations on the Surface of a Uniform (One-Layer) Half-Space due to an Oscillating Surface Pressure Distribution*. Research Report 1215-1F. Texas Transportation Institute, Texas A&M University, College Station, Nov. 1988.
8. Y. Zhongjin. A Method of Finite Integrals of Oscillating Functions. *Communications in Applied Numerical Methods*, Vol. 3, 1987, pp.1–4.
9. A. H. Magnuson. *Dynamic Analysis of Falling-Weight Deflectometer Data*. Research Report 1175-1. Texas Transportation Institute, Texas A&M University, College Station, Nov. 1988.
10. V. S. Torpunuri. *A Methodology To Identify Material Properties in Layered Viscoelastic Halfspaces*. M.S. thesis. Texas A&M University, College Station, 1990.
11. W. Menke. Geophysical Data Analysis: Discrete Inverse Theory. *International Geophysics Series*, Vol. 45, 1989.
12. H. G. Natke and J. T. P. Yao. Structural Safety Evaluation Based on System Identification Approaches. *Proceedings of the Structural Safety Evaluation Based on System Identification Approaches*, Lambrecht, Germany, 1988.
13. H. S. Papazian. *The Response of Linear Viscoelastic Materials in the Frequency Domain*. Report 172-2. Transportation Engineering Center, Engineering Experiment Station, Ohio State University, Columbus, 1961.
14. Y. C. Fung. *Foundations of Solid Mechanics*. Prentice-Hall, Inc., Englewood Cliffs, N.J., 1965.
15. J. S. Lai and D. Anderson. Irrecoverable and Recoverable Nonlinear Viscoelastic Properties of Asphalt Concrete. In *Highway Research Record 468*, HRB, National Research Council, Washington, D.C., 1973, pp. 73–88.
16. R. A. Schapery. Nonlinear Fracture Analysis of Viscoelastic Composite Materials Based on a Generalized J Integral Theory. *Proc., Japan-U.S. Conference on Composite Materials*, Tokyo, Jan. 1981.
17. W. J. Kenis. *Predictive Design Procedures, VESYS Users' Manual—An Interim Design Method for Flexible Pavement Using the VESYS Structural Subsystem*. Report FHWA-RE-77-154. FHWA, U.S. Department of Transportation, 1978.

Accuracy and Consistency of Backcalculated Pavement Layer Moduli

Y. J. Chou and Robert L. Lytton

Backcalculation of pavement layer moduli from deflection measurements has been a focus of recent pavement research because of the need to adopt mechanistic design and analysis methods and the widespread use of nondestructive testing devices such as the falling weight deflectometer and Dynaflect. A number of pavement structural models and computerized procedures have been developed to perform backcalculation. However, the results often vary among analysts because of the assumptions made in each procedure and the different input assigned by individual analysts. Such variation causes concern because engineers will not have confidence using the backcalculated moduli in pavement evaluation or design if the size of the error associated with the backcalculated moduli values is unknown. To better understand the accuracy and consistency of the available backcalculation procedures, backcalculation results from different agencies using various procedures were compared. The results indicate that discrepancies among agencies can be large; however, a few agencies reached good agreement in many cases. The sources of systematic errors and ways to reduce them are discussed. Finally, an expert system approach that uses a specific analyst's knowledge to prepare input for the mechanistic backcalculation program and to interpret results is described.

Backcalculation of pavement layer moduli from nondestructively measured deflection basins has become the state-of-the-art method in pavement structural evaluation (*1*). A number of backcalculation computer procedures are available, for example, MODCOMP2 (*2*), BISDEF (*3*), CHEVDEF (*4*), ELSDEF (*4*), MODULUS (*5*), and ELMOD (*6*). Most of these programs model the pavement structure with a layered elastic system and use an iteration scheme to find the set of layer elastic moduli that best matches the computed theoretical deflections with the measured pavement deflections. The iteration process may require a large amount of computer time. Many programs use the influence zone concept to reduce the iterations.

Only two material parameters (Young's modulus and Poisson's ratio) are needed to describe the possible deformation in linear elastic theory, which is one of the major reasons why layer elastic theory is used by many backcalculation programs (*7*). In backcalculation, the less important parameter, Poisson's ratio, is usually assumed, and only the Young's modulus of each layer must be calculated to match the surface deflections. Because each layer is represented by only one unknown, the number of surface deflection readings needed in backcalculation is equal to the number of layers with unknown moduli. This reduces the number of variables to be solved for and allows a direct search technique to be used in converging to the effective layer moduli values.

Other methods of modeling pavement structures include the finite element method and the elastic-dynamic method. The finite element method is considered more accurate in its ability to model stress-sensitive materials. However, the increase in accuracy is usually accompanied by a greater number of unknown parameters, which makes backcalculation more difficult. In addition, the finite element method usually demands much greater computing power, and still it is not entirely successful in dealing with granular materials. The elastic-dynamic method may provide a better representation of the dynamic loading, but it is also more complicated in its analysis and, hence, in backcalculation. This study focuses on backcalculation by static, linear elastic analysis.

The basic assumption of backcalculation is that when the computed surface deflections match the measured deflections, the resulting layer moduli values represent the material moduli in the field. In other words, a unique set of layer moduli exists such that the theoretically computed deflection basin is equivalent to the measured basin. In nondestructive testing (NDT) backcalculation, only a few discrete surface deflection readings represent the deflection basin. The number of readings sampled must be at least equal to the number of layer moduli to be backcalculated to avoid a nonunique solution. Because of the rounding and truncation errors introduced during backcalculation, it may not even be possible to reproduce exactly the original layer moduli from a basin generated by the linear elastic solution.

In reality, inaccurate layer thicknesses and subgrade depth input and, more important, the deviation of material behavior from linear elastic modeling, prevent the use of a small tolerance for surface matching error, because no theoretical solution may exist with the given model that matches the measured basin perfectly. The increased tolerance introduces other nonuniqueness of the backcalculated moduli values.

Thus, dividing a pavement structure model into many layers may produce nonunique solutions, whereas assuming fewer layers may not produce solutions that match the measured deflection readings. This dilemma leads to the following understanding: the objective of backcalculation is not to match surface deflections perfectly, but to obtain a reasonably good assessment of the underlying structure. Such an assessment can usually be achieved if other pertinent information (e.g., layer thickness, subgrade depth and component, layer material type, pavement construction history, and existing distresses, if any) is used. Without a thorough knowledge of the pavement structure, achieving a good match of the surface deflection may not be meaningful in pavement evaluation.

Y. J. Chou, Department of Civil Engineering, University of Toledo, Toledo, Ohio 43606. R. L. Lytton, Texas Transportation Institute, Texas A&M University, College Station, Tex. 77843.

The error of backcalculation methods here means the accuracy in estimating the in situ layer moduli, not the error in matching the surface deflections.

Because backcalculation relies solely on measured pavement surface deflection under a given load, it is difficult to backcalculate moduli of thin layers and material properties other than moduli. Simultaneous measurement of impulse loads and dynamic deflections generated by the falling weight deflectometer (FWD) may provide more information, but this technique is still under development (*1*).

With the available layer elastic solution, several things can still be done to improve the backcalculation process. They include reduction of the errors caused by convergence schemes and better estimation of the given input parameters, such as Poisson's ratio, effective layer thickness, and depth to bedrock. The latter is a significant contributor to the size of errors and is more difficult to assess because it varies with each problem. Experience, engineering judgment, and accurate data must be relied on for every backcalculation problem.

MODULUS—A NONITERATIVE BACKCALCULATION PROCEDURE

The computer time required to perform backcalculation for a single deflection basin depends on the complexity of the problem, the efficiency of the convergence scheme, and the type of computer. For most iterative-type backcalculation programs, the initial moduli values (or "seed" moduli) given by the analyst also affect convergence speed. In general, on an IBM-PC type of computer, 30 min to 1 hr or more is needed to perform a single backcalculation. This does not include time for preparing input data, interpreting the result, or possibly rerunning the backcalculation with modified input data. Most highway agencies have limited computer resources, so the discussion is based on microcomputers—the most widely owned computers in highway communities.

In both network- and project-level testing, hundreds of deflection basins usually must be analyzed. The computing time can be prohibitive. Sometimes a few selected "typical" deflection basins are backcalculated instead of backcalculating every basin. However, the typical basin is difficult to determine, and much information about the variability of pavement materials is lost by doing so. Backcalculation of layer moduli from every deflection basin measured is desirable. To achieve this despite limited time and manpower, two approaches have been used. One is to replace the layer elastic solution by a simpler and faster scheme (e.g., Odemark's solution, as in the ELMOD program). The result is an approximation to the layer elastic solution.

The other approach is to store many generated deflection basins and corresponding layer moduli in a data base. When a measured basin is given, the data base can be searched and interpolated to find a deflection basin that best resembles the measured basin. The corresponding layer moduli are then determined. This method eliminates the iteration process and greatly speeds backcalculation. The overhead time needed to generate the deflection data base is often offset by the saving of time in analyzing individual basins when dozens of basins must be analyzed.

One of the data base backcalculation programs is called MODULUS (*5*). MODULUS uses a unique method to reduce the size of the data base so that the time to generate it and the time to find the solution from it are greatly reduced.

The generated deflection data base is based on the ratio of layer moduli to subgrade moduli; thus the size of the data base is reduced by an order. The pattern search algorithm developed by Hooke and Jeeves (*8*) and the Lagrange interpolation technique (*9*) are used to find the layer moduli that minimize the error between measured and computed basins. Figure 1 shows a typical error surface that the MODULUS program searches to find the least error. The solution found may only be a local minimum, and a global minimum may not exist in the given ranges if the problem is not modeled correctly.

MODULUS can backcalculate up to four unknown layer moduli (including subgrade modulus). Backcalculating more than four unknown moduli is not recommended because of possible nonuniqueness. Furthermore, none of the available design methods uses more than four layer moduli. The calculated surface deflections and matching errors reported by the MODULUS program are obtained by interpolation of the pregenerated data base; thus, the values are not exact. Nevertheless, the backcalculated moduli compare well with the results of BISDEF, an iterative program that takes much longer to run, and MODULUS can essentially reproduce input moduli when a forward-calculated deflection basin is given. When comparing a backcalculated modulus with laboratory test results, the actual field condition plays an important role. A case study is described later. MODULUS is used as the target program in the following comparative study.

COMPARATIVE STUDY OF BACKCALCULATIONS

Different backcalculation programs often give different results for the following reasons:

1. The numerical routine used to calculate pavement surface deflections may be different.

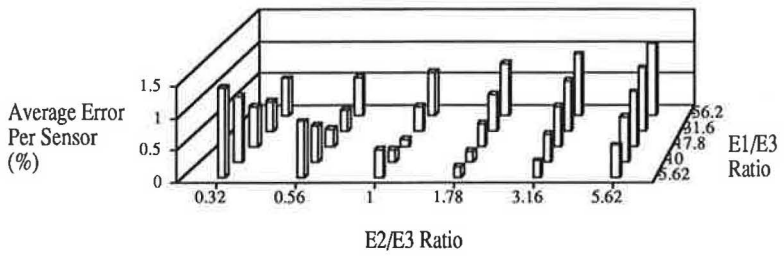

FIGURE 1 Typical error surface (bars show interpolation points).

2. The method of searching for new values of the layer moduli may be different.
3. Some methods try to correct for the stress dependency of the layer moduli; others do not.
4. Criteria for determining convergence (e.g., minimize surface deflection matching error) may be different.
5. Moduli ranges set by individual analysts may be different.

It was believed that a comparison of solutions from different programs would give an idea of the range of solutions that can be expected. Furthermore, it would be interesting to see how the experience and knowledge of the individual analyst contribute to the range of solutions for identical problems. Such an exercise was conducted as an activity of TRB's Committee on Strength and Deformation Characteristics of Pavements.

A total of 26 deflection basins were included in the study. Three types of NDT device (FWD, Dynaflect, and Road Rater 2000) were compared on two pavement sections. Deflections from three FWD load levels were also obtained from the same two sections for comparison. The deflection data are shown in Tables 1 and 2.

Four FWD basins were measured on different in-service pavement sections, and seven were measured on sections at the Texas Transportation Institute (TTI) Pavement Test Facility. In addition, four deflection basins were generated by using the layer elastic program BISAR, and four were generated by using the nonlinear finite element program ILLI-PAVE.

The NDT pavement deflection data, with their thickness and material information, were submitted to participating pavement research agencies in the United States and Britain. They were asked to report their backcalculation results. Thirteen results, with varying degrees of completeness, were obtained. The results were denoted anonymously as those of Agency A, B, . . . , M. Ten were based on the theory of elasticity. The other three, which found their solutions on the basis of a layer equivalency concept, used ELMOD. The backcalculation procedures used included MODULUS, BISDEF, PADAL, ELMOD, ELSDEF, MODCOMP2, CHEVDEF, and a BISAR-based procedure developed at Purdue University. BISDEF and ELMOD were each employed by three agencies, and MODCOMP2 was employed by two agencies.

The backcalculation results indicate a wide dissimilarity among agencies. Figure 2 shows the relative closeness of the modulus values backcalculated by other agencies to those of Agency A. The closer the plotted data are to the diagonal line, the more closely the results from the two agencies agree. For example, Agency A's results agree well with those of Agencies B and C but differ widely from those of Agencies G, H, and I. Agencies A, B, C, F, and I employed BISAR-based procedures, whereas Agencies E, J, and L used ELMOD. Agencies using the same procedure can produce very different results. Figure 2 is intended only to show the size of the dissimilarities among agencies. It should not be used to judge the success of backcalculation, because the selection of Agency A's result as a standard was arbitrary.

Device Comparison

The results of backcalculation comparing three NDT devices are shown in Table 3. Only three agencies completed this part of the exercise. The following observations may be made:

1. The backcalculated moduli were generally in the "reasonable" range for the given layer materials, although the values are quite different among NDT devices.
2. Because modes of loading are different among NDT devices, the relationship of backcalculated layer modulus values among various NDT devices depends on the individual pavement's structure and layer materials.
3. The three agencies produced similar results for each device. The differences may be attributed to the different modulus range set by individual analysts, because most of the backcalculated asphalt concrete layer moduli reached the upper limits.
4. The averaged deflection matching errors were larger for Test Section 10.1, which has a thin (1-in.) surface layer, than for Test Section 19.4, which has a thicker (5-in.) surface layer. This is true for all three agencies, which indicates that the

TABLE 1 DEFLECTION DATA COMPARING THREE NDT DEVICES

SECTION ID	FWD								ROADRATER						DYNAFLECT LOAD = 1000lbs Hz = 8			
	LOAD (lb)	DEFLECTIONS (mils) Radii (inches) 0"	7.87"	11.8"	23.6"	35.4"	49.2"	63"	FREQ	LOAD (lb)	DEFLECTION (mils) Radii (inches) 0"	12"	24"	36"	DEFLECTION (mils) Radii (inches) 0"	12"	24"	36"
19*- 1	9224	14.32	9.95	7.10	4.15	2.96	2.22	1.79	10.3	2040	3.14	1.73	0.99	0.75	0.81	0.55	0.39	0.29
19*- 4	9504	5.5	5.20	4.95	4.23	3.52	2.76	2.16	10.2	2010	1.65	1.27	1.11	0.96	0.56	0.52	0.45	0.38

*Refer to TTI PAVEMENT TEST FACILITY Tables for layer thicknesses and materials

1 mil = 0.001 inches

TABLE 2 DEFLECTION DATA COMPARING THREE FWD LOAD LEVELS (SURFACE TEMPERATURE = 100°F)

Section 10*- 1

LOAD (lb) \ SPACING (inches)	Deflections (mils) 0	7.87	11.8	23.6	35.4	49.2	63.0
6312	10.04	6.71	4.62	2.63	1.96	1.48	1.10
9224	14.32	9.95	7.10	4.15	2.96	2.22	1.79
14928	21.97	15.56	11.76	6.91	4.92	3.65	2.89

Section 19*- 4

LOAD (lb) \ SPACING (inches)	Deflections (mils) 0	7.87	11.8	23.6	35.4	49.2	63.0
6440	3.50	3.32	3.09	2.71	2.32	1.75	1.34
9504	5.55	5.20	4.95	4.23	3.52	2.76	2.16
14848	9.67	9.09	8.54	7.47	6.17	4.78	3.82

*Refer to TTI PAVEMENT TEST FACILITY Tables for layer thicknesses and materials
1 mil = 0.001 inches

layer elastic backcalculation procedures have difficulty dealing with thin surface pavement structures.

5. Results from Agencies A and B indicate that both base and subgrade moduli backcalculated from FWD sections are larger than from Dynaflect. This may be attributed to the stress-stiffening effect caused by the higher load of FWD, but it was not apparent in Agency C's result. The compensation of base and subgrade moduli during backcalculation may prevent identification of such a trend.

Load Comparison

Results of backcalculations comparing three FWD load levels are shown in Table 4. The relationship of backcalculated layer modulus values under different load levels depends on the individual pavement structure and layer materials. For example, the calculated granular base modulus values of Test Section 10.1 are higher at higher load levels (stress stiffening), whereas the sandy clay subgrade of Test Section 19.4 has decreasing modulus with increasing load (stress softening). Backcalculated lime-stabilized base modulus values of Test Section 19.4 are lower at higher load levels. The sandy gravel (coarse-grained) subgrade of Test Section 10.1 shows a stress-stiffening effect. Different results may be reached for other pavement structures, depending on the state of stresses (i.e., mean principal stress and deviator stresses) to which the materials are subjected.

The different load level does not change the averaged deflection matching error significantly. Again, it is more difficult to match measured deflection basins for thin pavement (Test Section 10.1) than for thicker pavement (Test Section 19.4).

Backcalculation of Generated Basin

Comparisons of backcalculated moduli from generated basins with moduli used in forward calculations are shown in Figures 3 to 8. Two forward-calculation methods, BISAR (a linear elastic program) and ILLI-PAVE (a nonlinear elastic finite element program), were employed to generate the deflection basins. Figures 3 to 5 show the moduli used in BISAR (the heavy vertical line) compared with the range of values backcalculated by each agency. For ILLI-PAVE, the modulus values at the middle of each layer and under the center of the load, obtained by substituting the computed stresses at that location into the modulus-stress relationship, are used as the basis (Figures 6 to 8).

Ideally, backcalculation should reproduce the layer moduli used to generate the theoretical basin. However, it can be

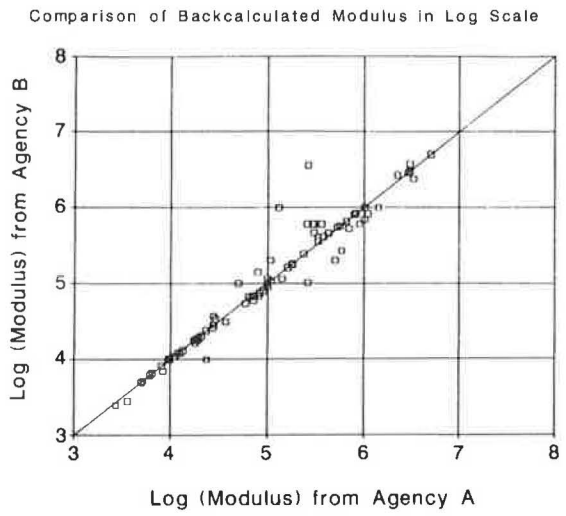

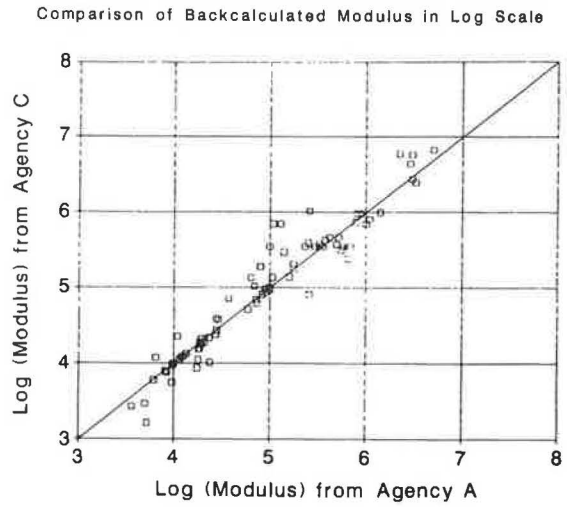

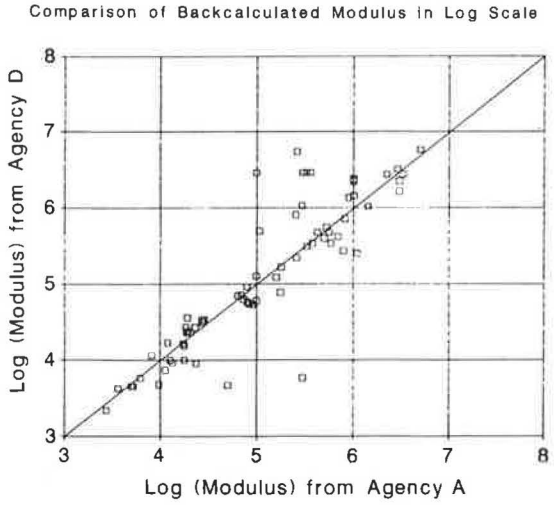

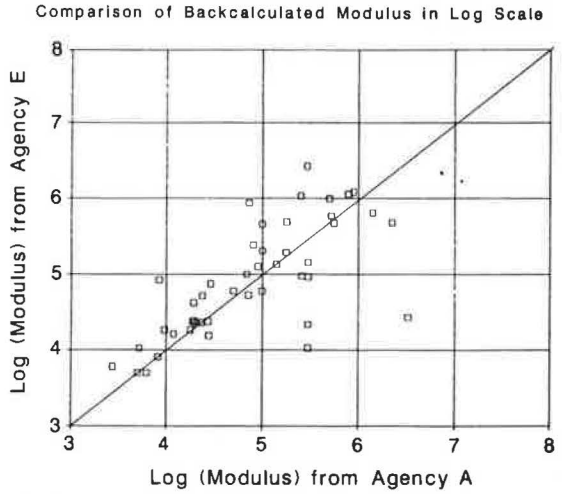

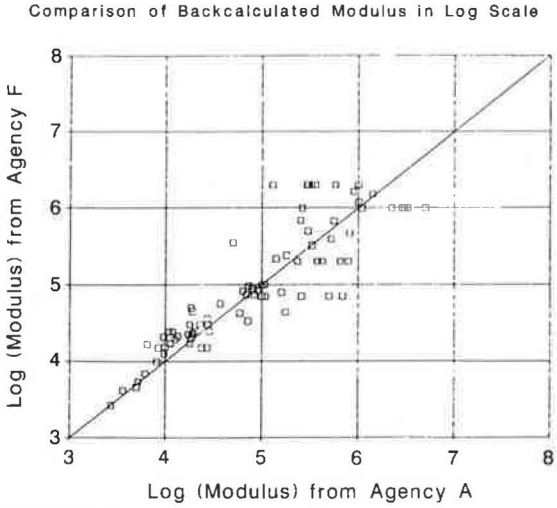

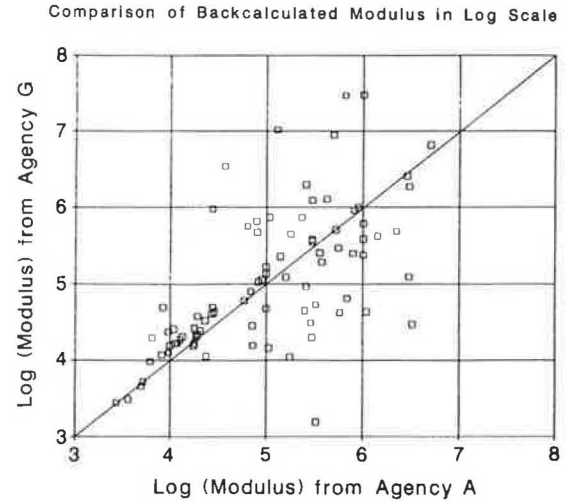

FIGURE 2 Closeness of modulus values backcalculated by other agencies to those of Agency A. (*continued on next page*)

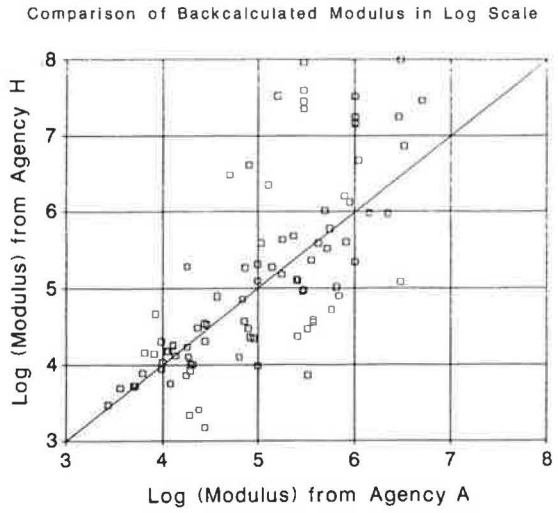

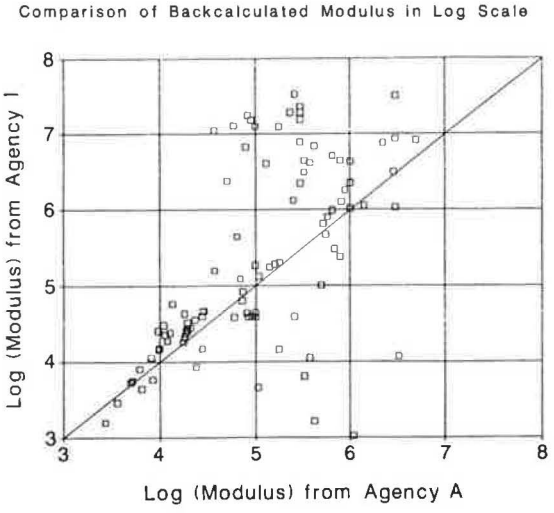

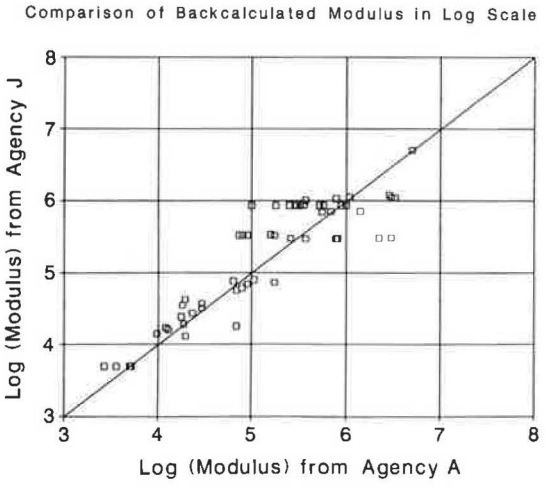

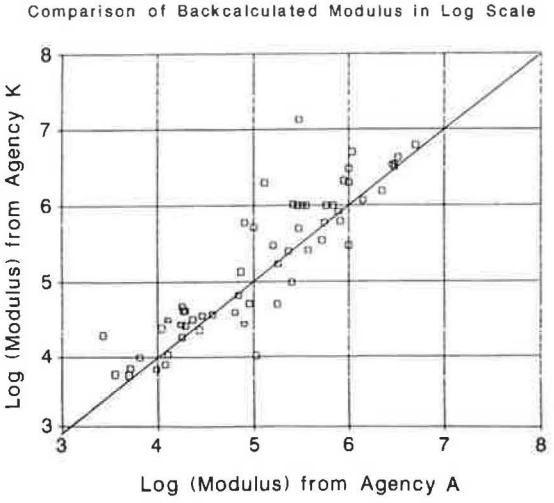

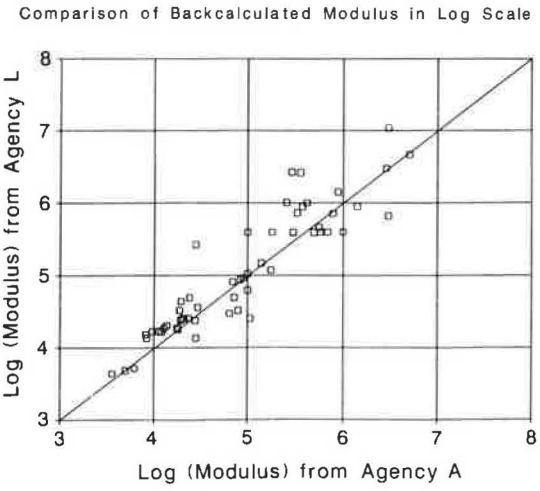

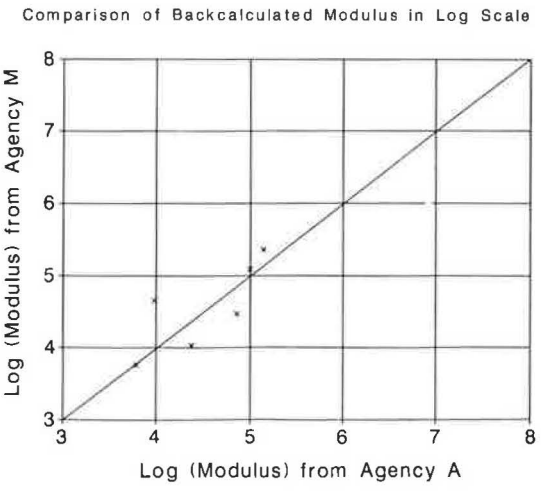

FIGURE 2 (*continued*)

TABLE 3 NDT DEVICE COMPARISON

Section 10.1		A (MODULUS)	B (BISDEF)	C (BISDEF)
FWD				
1" AC	E1	300,000	600,000	350,000
16" Cr Limestone	E2	90,000	80,509	93,790
Sandy Gravel	E3	19,600	18,706	17,661
		(7.8%)*	(6.7%)	(6.3%)
Road Rater				
1" AC	E1	300,000	600,000	350,000
16" Cr Limestone	E2	58,800	54,575	51,330
Sandy Gravel	E3	18,800	18,624	18,986
		(4.2%)	(3.7%)	(5.1%)
Dynaflect				
1" AC	E1	300,000	600,000	350,000
16" Cr Limestone	E2	37,000	31,442	70,832
Sandy Gravel	E3	11,000	10,879	22,469
		(4.7%)	(3.9%)	(4.9%)
Section 19.4				
FWD				
5" AC	E1	1,000,000	1,000,000	700,000
16" LimeStabilized	E2	375,100	409,642	429,101
Sandy Clay	E3	12,800	12,448	12,513
		(3.8%)	(4.7%)	(3.5%)
Road Rater				
5" AC	E1	108,600	107,017	700,000
16" LimeStabilized	E2	650,000	655,088	242,896
Sandy Clay	E3	9,900	9,906	9,918
		(0.1%)	(0.4%)	(3.7%)
Dynaflect				
5" AC	E1	130,000	1,000,000	700,000
16" LimeStabilized	E2	232,200	241,983	351,421
Sandy Clay	E3	6,500	6,548	11,884
		(0.2%)	(0.2%)	(1.1%)

* Numbers in parenthesis are the average deflection matching errors reported by each agency

TABLE 4 FWD LOAD LEVEL COMPARISON

Section 10.1		A (MODULUS)	B (BISDEF)	C (BISDEF)	D* (PADAL)
(312lb					
16" Cr.L.S.	E2	83,500	75,000	80,751	54,969
Sandy Grav	E3	20,700	20,060	19,220	23,061
		(8.0%)	(7.1%)	(8.7%)	
9224LB					
1" AC	E1	300,000	600,000	350,000	2,900,755
16" Cr.L.S.	E2	90,000	80,509	85,584	53,954
Sandy Grav	E3	19,600	18,706	17,998	24,076
		(7.8%)	(6.7%)	(8.0%)	
14928LB					
1" AC	E1	300,000	600,000	350,000	2,900,755
16" Cr.L.S.	E2	99,800	89,422	93,790	59,756
Sandy Grav	E3	19,100	18,137	17,661	23,061
		(7.0%)	(6.1%)	(6.3%)	
Section 19.4		A	B	C	D
6440lb					
5" AC	E1	1,000,000	1,000,000	700,000	2,215,451
16" LimeSta	E2	419,500	456,009	469,705	477,319
Sandy Clay	E3	13,600	13,244	13,402	9,137
		(4.9%)	(5.4%)	(4.5%)	
9540lb					
5" AC	E1	1,000,000	1,000,000	700,000	2,295,077
16" LimeSta	E2	375,100	413,159	429,101	340,259
Sandy Clay	E3	12,800	12,390	12,513	9,863
		(3.8%)	(4.3%)	(3.5%)	
14848lb					
5" AC	E1	1,000,000	1,000,000	700,000	2,402,695
16" LimeSta	E2	330,900	358,206	374,154	308,205
Sandy Clay	E3	11,300	10,999	11,047	7,397
		(3.9%)	(4.3%)	(3.5%)	

* Did not report deflection matching errors

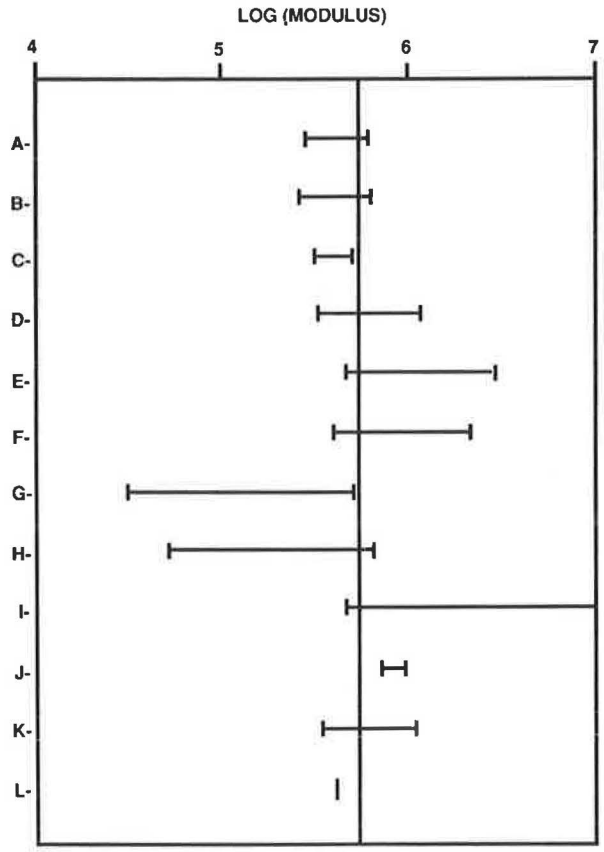

FIGURE 3 Comparison of backcalculated asphalt concrete modulus with modulus used in forward calculation.

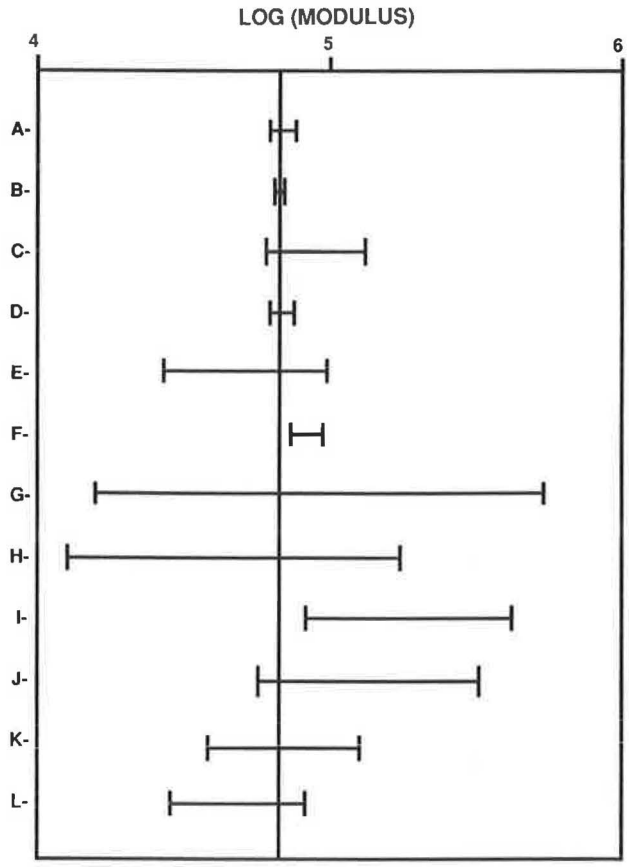

FIGURE 4 Comparison of backcalculated crushed limestone modulus with modulus used in forward calculation.

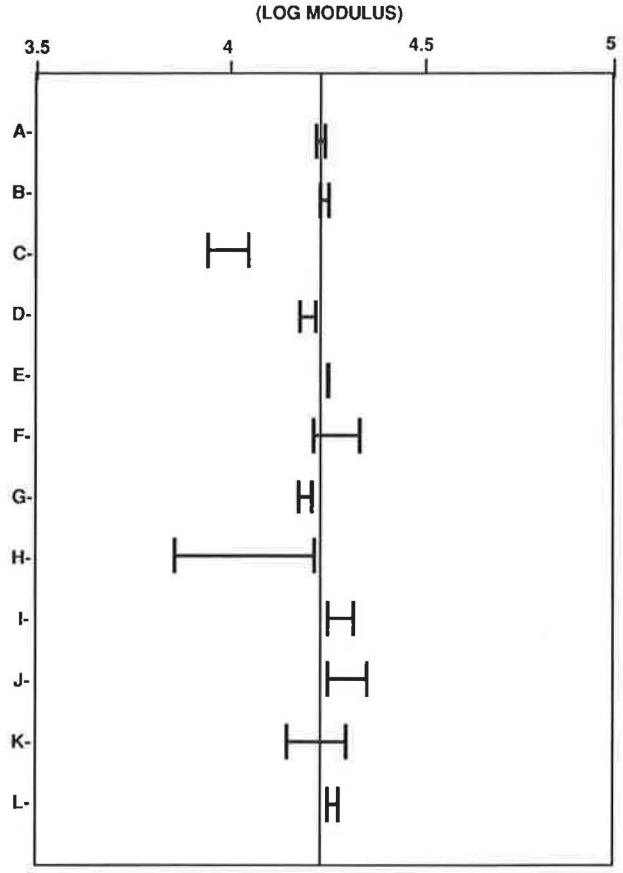

FIGURE 5 Comparison of backcalculated sandy gravel modulus with modulus used in forward calculation.

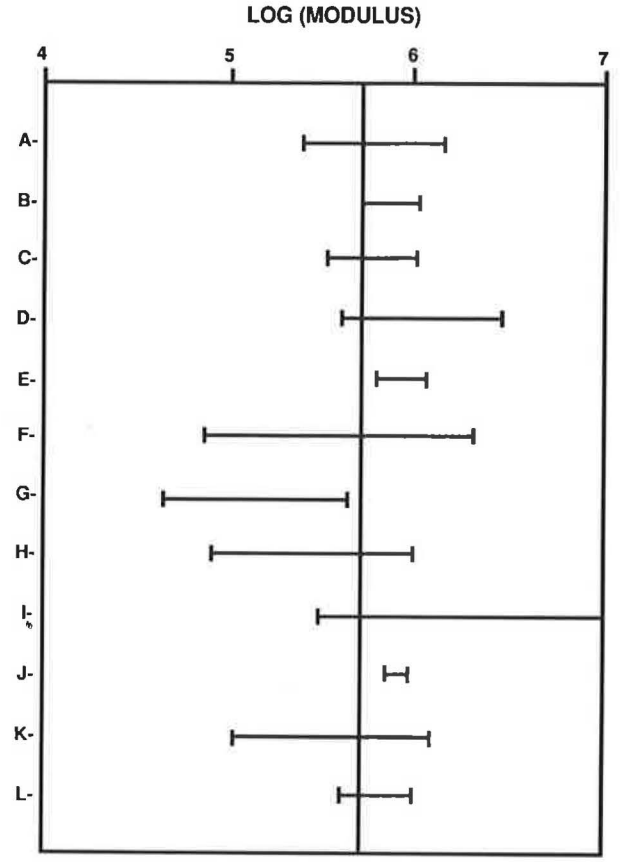

FIGURE 6 Comparison of backcalculated asphalt concrete modulus with averaged modulus in ILLI-PAVE forward calculation.

seen from these figures that the ranges of moduli backcalculated from theoretically generated deflection basins can be large due to different analysis methods and input parameters. Several agencies backcalculate accurately from the BISAR-generated basin, particularly the subgrade moduli. Much poorer results are obtained, as expected, when backcalculating from the nonlinear ILLI-PAVE–generated basins.

Backcalculation of Measured Basin

Comparison of backcalculated layer moduli at the TTI Research Annex included the following seven materials: asphalt concrete, cement-stabilized crushed limestone, lime-stabilized crushed limestone, crushed limestone, plastic clay subgrade, sandy clay subgrade, and sandy gravel subgrade. The results of backcalculation from measured surface deflection basins are shown in Figures 9 to 12. No datum value is given in the figures for these in situ materials because the correct value is unknown. Because each material is present in more than one pavement section, a range of backcalculated modulus values for the same material is given. Considering the scale factor of these figures, it is clear that much smaller (i.e., more consistent) ranges are obtained compared with the asphalt concrete moduli. Agreement of the backcalculated moduli for base layer materials (cement-stabilized, lime-stabilized, and crushed limestone) is better than for asphalt concrete but worse than for subgrade materials. A numerical representation of this observation is shown in Table 5, in which Agency A is chosen as the basis for calculating the average absolute relative difference (AARD) because of its consistent accuracy with the calculated basin. The AARD of backcalculated moduli for a specific material is defined as follows:

$$\text{AARD} = \frac{\sum_{i=1}^{n} |E_k^i - E_a^i|}{n}$$

where

E_k^i = the modulus of the specific material backcalculated by Agency k at Section i,
E_a^i = the modulus of the specific material backcalculated by Agency a at the same Section i, and
n = the number of pavement sections that have the specific material in their structures.

Statistical tests of significance by analysis of variance indicate that significant differences exist between several agencies. There are significant differences between materials within each agency. When results of the three agencies (G, H, and I) that compared poorly with those of other agencies are neglected, there are also significant differences between BISAR- and non-BISAR-based methods in average values of AARD.

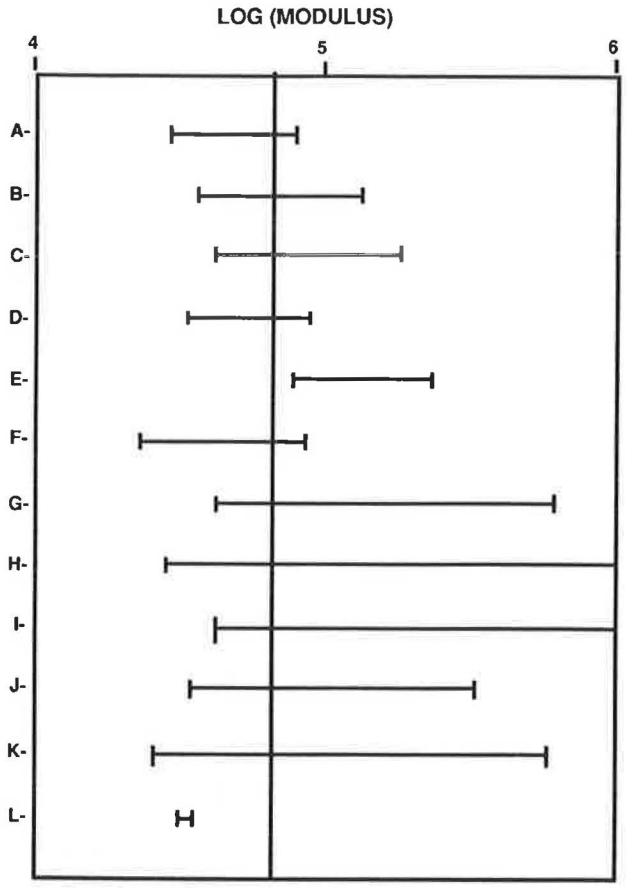

FIGURE 7 Comparison of backcalculated crushed limestone modulus with averaged modulus in ILLI-PAVE forward calculation.

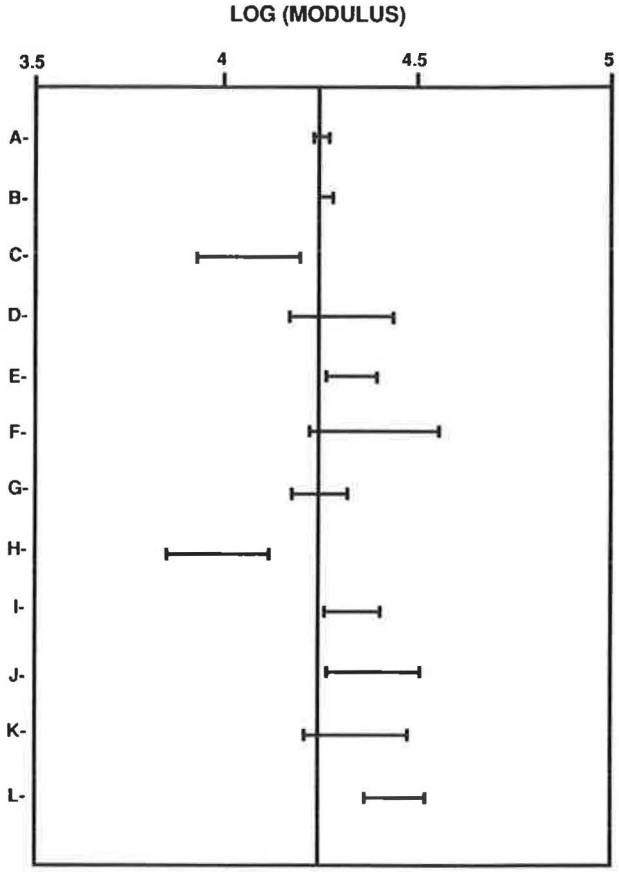

FIGURE 8 Comparison of backcalculated sandy gravel modulus with averaged modulus in ILLI-PAVE forward calculation.

Even agencies using the same backcalculation program produce considerably different backcalculated moduli values. This can be attributed to the various degrees of experience of and differing assumptions used by the individual analysts. Such inconsistency shows why the analysis of NDT data is difficult for practicing pavement engineers. Unlike researchers, practicing engineers usually do not have the time or resources to experiment with the many possible assumptions that may change backcalculation results.

It is difficult to assess the errors in each analyst's results. The comparisons show the relative affinities among solutions from different agencies. No solution can be considered correct, because each is associated with an error of unknown size. However, it is clear that several agencies produced solutions that were more reasonable than others, and the same agencies performed better in backcalculating theoretically generated deflection basins. Hence, it is reasonable to infer that these agencies have better knowledge in backcalculation of moduli values than the others.

The backcalculated moduli should not be expected to match the laboratory test results, because in situ field conditions are difficult to reproduce in the laboratory. Many of today's pavement design procedures (especially the AASHTO Guide) depend on laboratory estimates of moduli. Direct use of backcalculated moduli in these procedures can result in a systematic error that is not conservative because backcalculated moduli, especially for soils, are generally higher than laboratory-based resilient moduli. Furthermore, pavement materials often have large variations in their properties. Backcalculated layer moduli from NDT devices are averaged estimates instead of absolute measurements. If cautiously performed, however, laboratory results do provide a basis for assessing the reasonableness of backcalculated moduli.

NEED FOR EXPERT SYSTEMS IN BACKANALYSIS

Backcalculation programs appear to work well in many cases but do not produce good results in others. The reasons for this may be summarized into the following two categories.

First, pavement materials have a wide range of possible properties that do not always comply well with the linear elastic, homogeneous, and isotropic assumptions used inelasticity theory. The loading conditions of some NDT devices may be modeled incorrectly. The accuracy of deflection measurements may be affected by the accuracy of sensors and how they rest on the rough pavement surface. These are problems associated with the mechanistic modeling.

Second, to backcalculate layer moduli from surface deflections, the thickness of each layer, the Poisson's ratio of layer materials, and the depth of the subgrade must be known, or at least susceptible to close estimation. The moduli of thin

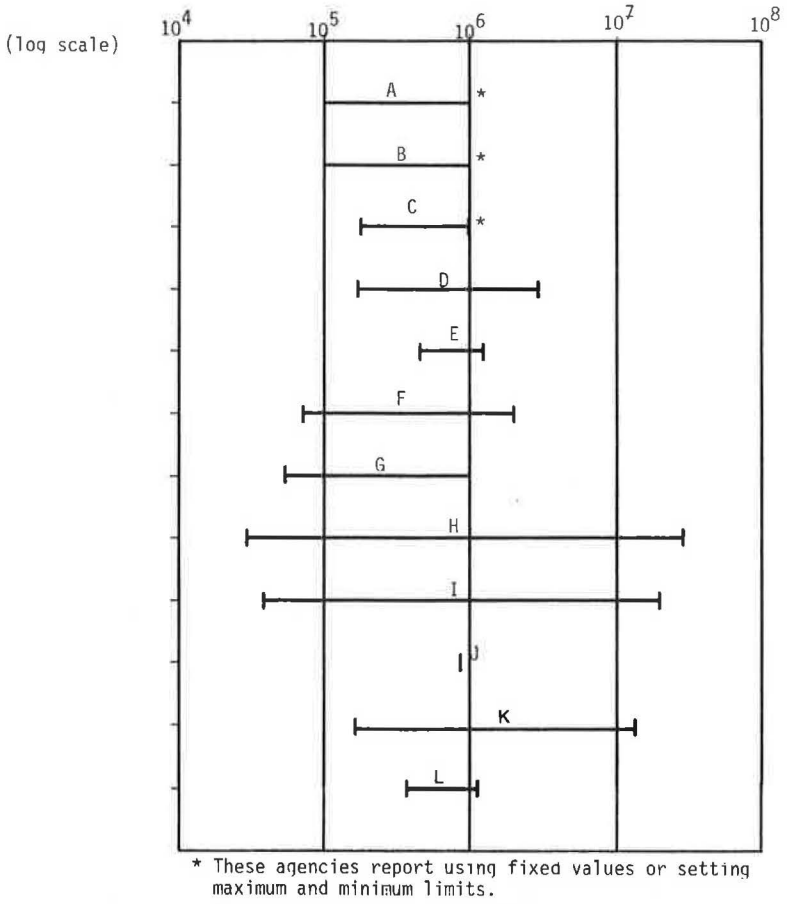

FIGURE 9 Comparison of backcalculated asphalt concrete modulus (deflection measured at TTI Pavement Test Facility).

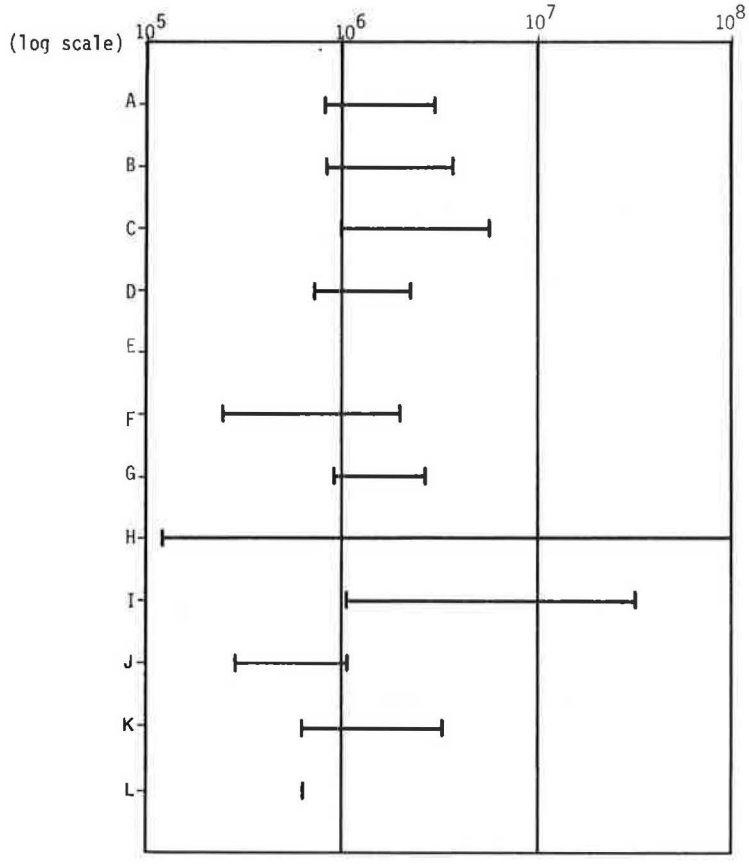

FIGURE 10 Comparison of backcalculated 4 percent cement-stabilized crushed limestone modulus (deflection measured at TTI Pavement Test Facility).

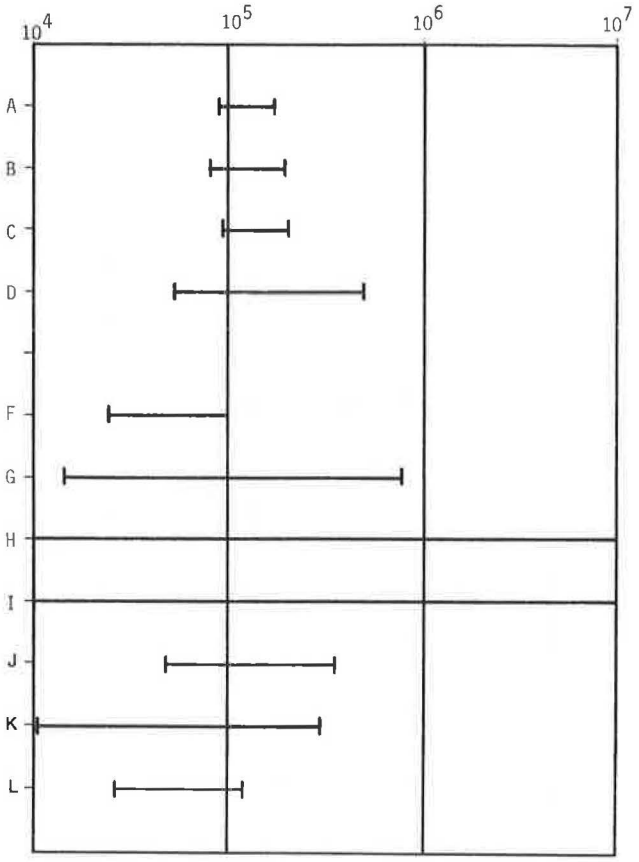

FIGURE 11 Comparison of backcalculated crushed limestone modulus (deflection measured at TTI Pavement Test Facility).

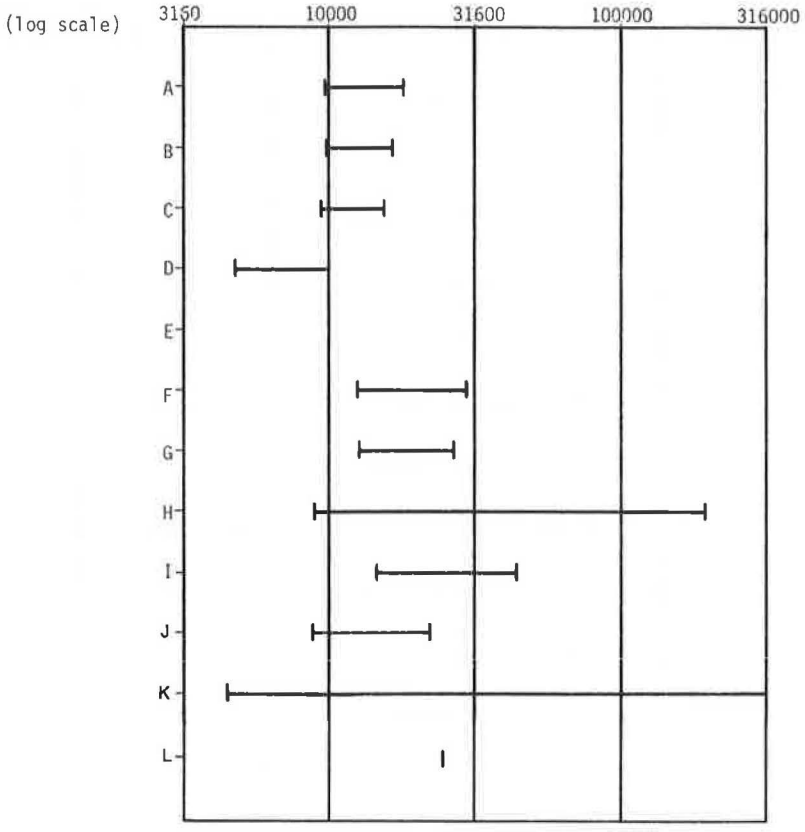

FIGURE 12 Comparison of backcalculated plastic clay modulus (deflection measured at TTI Pavement Test Facility).

TABLE 5 AARD OF BACKCALCULATED MODULI COMPARED WITH RESULTS OF AGENCY A

	Agencies									
Materials	B	C	D	E	F	G	H	I	K	L
Asphalt Concrete	.263	.494	6.701	1.890	2.038	.623	20.646	11.269	7.644	.379
Cement Stab. Limestone	.091	.400	.272	.836	.586	.393	59.116	3.178	.140	.217
Lime Stab. Limestone	.065	.098	.372	.463	.605	.530	15.055	4.101	.188	.867
Crushed Limestone	.249	.157	1.214	.099	.424	.997	259.446	40.290	.914	.292
Sandy Gravel	.032	.083	.428	.606	.603	.509	.452	.538	.610	.148
Sandy Clay	.022	.011	.322	.358	.768	.433	.481	.740	.229	.456
Plastic Clay	.044	.083	.475		.484	.393	4.915	.953	.965	.217
Average	.109	.189	1.398	.709	.787	.554	51.444	8.724	1.527	.368

surface layers or sandwiched layers are usually difficult to obtain, because surface deflections are often insensitive to changes in the moduli of these layers. Changes in the moduli of subgrade or other thick layers may mask changes in thin layers. These are difficulties resulting from the uncertainty of input parameters and the limitations of the basin-matching algorithms.

Any of these nonideal situations may render the results of purely numerical backcalculation schemes unreliable. Analysis error may be divided into two types: random and systematic. Random errors include load and deflection measurement errors, variation of layer thickness from mean thickness, and spatial variations of material properties. Systematic errors include deviation of the theoretical model from actual pavement behavior (e.g., using a linear elastic layer system to describe real pavement that may be nonlinear, viscoelastic, anisotropic, and nonhomogeneous, and using static analysis to characterize dynamic impulse loading); incorrectly assumed material parameters, such as Poisson's ratios; and incorrectly assumed layer thickness and subgrade depth.

The sizes of random errors may be estimated by replications of the test and reduced by averaging over several tests, but the sizes of systematic errors are often confounded and difficult to estimate. Some systematic errors cannot be eliminated without a better analysis method than current layer elastic theory, but some systematic errors can be reduced with a better knowledge of actual pavement behavior and limitations of the analysis method. The use of an expert system technique provides a means to convey the knowledge and experience possessed by an expert analyst to a less-experienced analyst so that systematic errors are kept to a minimum.

Sensitivity of Input Parameters

One of the main reasons for the variation of backcalculation results produced by different analysts, given the same backcalculation program, is the difference in assigning input parameters. Input parameters needed by most backcalculation programs include layer thickness, Poisson's ratios, load configuration, error tolerance, maximum number of iterations, seed moduli, and depth to bedrock. Sensitivity analyses of some of these parameters have been conducted by several researchers on different backcalculation programs (*6,10–12*). Results from the studies indicate that, except for seed moduli, all these parameters have significant effects on the values of backcalculated layer moduli. Surface layer moduli are the most sensitive, followed by base and subbase layer moduli. Subgrade moduli are relatively stable regarding variation of input parameters. The reason for this is the influence of layer moduli on surface deflection. This has been pointed out by Ullidtz (*13*):

> The subgrade usually contributes 60% to 80% of the total center deflection. A small error in the determination of the subgrade modulus will, therefore, lead to very large errors in the moduli of the other pavement layers.

Layer thickness is one of the crucial inputs that can change the backcalculation result drastically. The thinner the layer, the more accurate the thickness input must be to backcalculate accurate layer moduli. It is prudent to perform a few field borings to verify the actual layer thickness. However, layer thickness of constructed pavement may vary along the road depending on the contractor's quality control and local topography.

Poisson's ratios for pavement materials are seldom determined from experiment; they are usually estimated. Poisson's ratios of unbound materials are not well defined and may be different because of different confining pressure, moisture content, and gradation.

The load configuration depends on the NDT device being used and can affect the backcalculation results significantly. A uniformly distributed circular load is usually assumed. However, the actual loading applied to the pavement surface

may not be uniformly distributed and depends on the relative rigidity of the loading plate and surface layer.

A small error tolerance is usually better in obtaining an accurate backcalculation result, but a very small error tolerance may prevent convergence to a solution, particularly when backcalculating from a measured deflection basin, as has been explained previously. A small error tolerance must be accompanied by a larger number of allowed iterations, which can increase the time required to backcalculate each basin. The analyst must compromise between accuracy and efficiency of backcalculation.

The depth to bedrock can have a significant effect on the resulting backcalculated moduli, especially when the depth is shallow (e.g., less than 20 ft). The depth to bedrock can vary considerably according to local topography. If the assumed depth to bedrock is substantially different from the actual depth, backcalculation usually results in large errors in matching the surface deflections.

Role of Judgmental Knowledge

Results from the comparative study also indicate that analysts with specialized knowledge can often produce similar and more reasonable results than less-experienced analysts. When these "experts" encounter deflection basins that do not give reasonable layer moduli through backcalculation, they usually make judgments of the validity of assumptions, correctness of input, and usefulness of results on the basis of their knowledge. This knowledge may be gained from experience with a particular pavement section, research reports, textbooks, general experience, common sense, and engineering rules of thumb. These sources of knowledge are often called upon during analysis, especially when results from numerical backcalculations do not seem reasonable and when input parameters must be estimated.

Drawing on expert knowledge during routine pavement structural evaluation or overlay design requires easy access to expertise. Development of expert system technology has made possible the capture of specialized knowledge and the incorporation of this knowledge into numerical computation schemes. An expert system can assist pavement engineers in analyzing pavement deflections and obtaining effective layer moduli for evaluation and design purposes (*14,15*).

STRUCTURE OF A BACKCALCULATION EXPERT SYSTEM

The knowledge in a backcalculation expert system may include the following:

1. General knowledge of the properties of paving materials—for example, the possible range of modulus values and Poisson's ratios for particular types of material, nonlinearity (stress dependency), the effect of temperature on asphalt layer modulus, and the effect of moisture on base and subgrade moduli;
2. General knowledge of pavement structures, such as variation of layer thickness resulting from construction practices and the possible depth to bedrock according to local topography;
3. Knowledge of pavement behavior—for example, that deflections under or closer to the load are influenced more by the upper layer modulus, whereas deflections at greater distances from the load are affected more by the subgrade modulus; that moduli of thin layers usually have a small influence on the surface deflection; that the effect on surface deflections of a soft layer under a much stiffer layer (e.g., a flexible subbase under a cement-stabilized base) is often masked by the stiffer layer; and that stabilized layers may have warping induced by a temperature gradient;
4. Knowledge of the backcalculation computer program—for example, the sensitivity of input parameters, assumptions and limitations of the mathematical model, accuracy of the numerical solution of the model, and accuracy and sensitivity of the numerical search scheme;
5. Knowledge of the sources and approximate sizes of errors introduced because of instrumentation, differences between the model and reality, and the search scheme; and
6. Knowledge of the variability of paving material properties.

The knowledge may be separated into two parts: a pre- and a postprocessor. Figure 13 shows a general flow diagram of the backcalculation process assisted by an expert system. Details of the knowledge stored in the pre- and postprocessors will be reported in another paper.

Although expert judgment may be useful in providing general guidelines, it cannot substitute for essential data. The

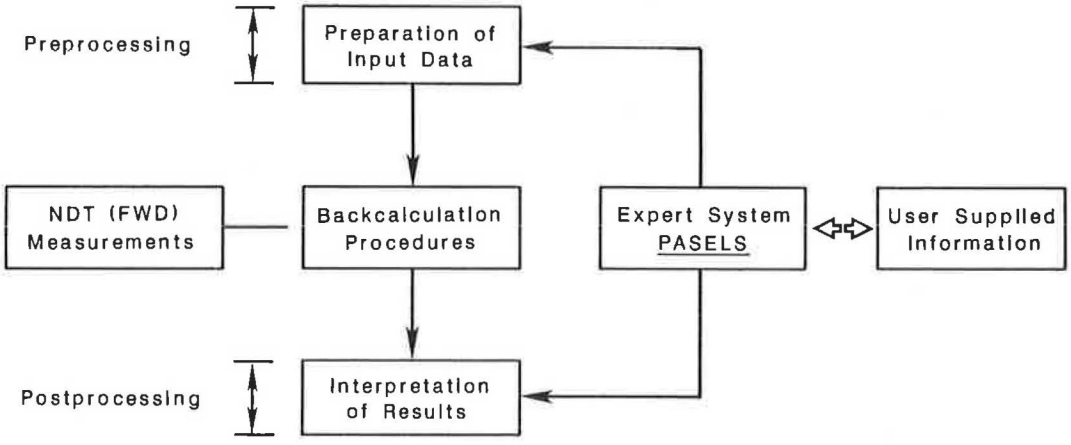

FIGURE 13 Concept of using expert systems in backcalculation.

availability and accuracy of input data such as layer thickness and depth to bedrock are still critical to the success of backcalculation. The preprocessors, however, may help to estimate reasonable input data that are not available from measurement or that are judgmental.

The results of the expert system analysis should be viewed as a probable estimation rather than as a "correct" solution. Improvements in backcalculation procedures, such as better constitutive relationships, more accurate modeling of dynamic loading, and so forth, may provide more accurate solutions than those of expert systems.

SUMMARY

Pavement layer materials are characterized by their elastic modulus, which can be estimated from surface deflections through backcalculation. A comparative survey of backcalculation procedures was conducted. The major findings are as follows:

1. Results from algorithmic backcalculation methods must be examined carefully for correctness. Large discrepancies may be found among different analysis methods and among different analysts.
2. Differences in input parameters may produce significantly different backcalculation results. Some parameters (e.g., subgrade depths and Poisson's ratios) are seldom measured; the analyst's judicious estimates must be relied on.
3. Backcalculated surface layer and base layer moduli are usually less reliable than backcalculated subgrade moduli.
4. An automated basin-by-basin scrutiny of backcalculation results can be achieved through the use of expert systems.
5. Knowledge and experience of pavement experts can be acquired and stored as rules in a knowledge base. A knowledge-based expert system can help perform mechanistic analysis by modeling the pavement structure more accurately and by recognizing possible errors in the results.
6. The use of expert systems reduces the expertise required to perform a difficult and tedious task and enables pavement experts to devote their time to more creative work.
7. Further improvements in backcalculation methods are needed.

REFERENCES

1. R. L. Lytton. Backcalculation of Pavement Layer Properties. In *Nondestructive Testing of Pavements and Backcalculation of Moduli*. STP 1026, ASTM, Philadelphia, Pa., 1988, pp. 1–38.
2. L. H. Irwin. *User's Guide to MODCOMP 2*. Cornell Local Roads Program Report 83-8. Cornell University, Ithaca, N.Y., 1983.
3. A. J. Bush III and D. R. Alexander. Pavement Evaluation Using Deflection Basin Measurements and Layered Theory. In *Transportation Research Record 1022*, TRB, National Research Council, Washington, D.C., 1985, pp. 16–29.
4. R. L. Lytton, F. P. Germann, Y. J. Chou, and S. M. Stoffels. *NCHRP Report 327: Determining Asphaltic Concrete Pavement Structural Properties by Nondestructive Testing*. TRB, National Research Council, Washington, D.C., 1990.
5. J. Uzan and R. L. Lytton. General Procedure for Backcalculating Layer Moduli. *First Symposium on Nondestructive Testing of Pavements and Backcalculation of Moduli*, ASTM, Baltimore, Md., 1988.
6. P. Ullidtz, G. Battiato, B. K. Larsen, and R. N. Stubstad. Verification of the Analytical-Empirical Method of Pavement Evaluation Based on FWD Testing. *Proc., 6th International Conference on Structural Design of Asphalt Pavements*, University of Michigan, Ann Arbor, Mich., Vol. 1, 1987, pp. 521–532.
7. S. P. Timoshenko and J. N. Goodier. *Theory of Elasticity*. McGraw-Hill, New York, 1970.
8. J. N. Siddall. *Analytical Decision-Making in Engineering Design*. Prentice-Hall, Englewood Cliffs, N.J., 1972.
9. A. Ralston and P. Rabinowitz. *A First Course in Numerical Analysis*. McGraw-Hill, New York, 1978.
10. T. Rwebangira, R. G. Hicks, and M. Truebe. Sensitivity Analysis of Selected Backcalculation Procedures. In *Transportation Research Record 1117*, TRB, National Research Council, Washington, D.C., 1987.
11. J. P. Mahoney, N. F. Coetzee, R. N. Stubstad, and S. W. Lee. A Performance Comparison of Selected Backcalculation Computer Programs. In *Nondestructive Testing of Pavements and Backcalculation of Moduli*, STP 1026, ASTM, Philadelphia, Pa., 1988, pp. 452–467.
12. W. Yang. *Mechanistic Analysis of Nondestructive Pavement Deflection Data*. Ph.D. thesis. Cornell University, Ithaca, New York, 1988.
13. P. Ullidtz. *Pavement Analysis*. Elsevier, New York, 1987.
14. Y. J. Chou, J. Uzan, and R. L. Lytton. Backcalculation of Layer Moduli from Nondestructive Pavement Deflection Data Using an Expert System Approach. In *Nondestructive Testing of Pavements and Backcalculation of Moduli*, STP 1026, ASTM, Philadelphia, Pa., 1988, pp. 341–354.
15. Y. J. Chou and R. L. Lytton. Use of Expert System in Pavement Structural Evaluation. *Proc., International Conference on Application of Advanced Technologies in Transportation Engineering*, San Diego, Calif., ASCE, New York, 1989.

Comparison of Dynamic and Static Backcalculation Moduli for Three-Layer Pavements

CHENG LING ONG, DAVID E. NEWCOMB, AND RAJ SIDDHARTHAN

Deflection data collected from the falling weight deflectometer (FWD) have mostly been analyzed by using the static layered elastic analysis method. Analysis might be improved by including dynamic effects, such as inertia, damping, and resonance. Results from a finite element backcalculation program developed to account for these factors are discussed. The program can perform both static and dynamic backcalculation analyses. Dashpots or dampers are installed at the boundary nodes (bottom and lateral) to simulate half-space conditions, thus avoiding the need to specify a rigid base (say at 20 ft) at the bottom of the subgrade. Such dashpots absorb propagating waves in the dynamic analysis, thus preventing wave reflection off the rigid boundary. Backcalculation results computed from two existing methods and the proposed method using FWD data obtained at four sites in Nevada are compared. The results indicate that the moduli of the asphalt layers are not affected by the type of analysis (static or dynamic) for any of the sites. Lower base and higher subgrade moduli were consistently computed in the dynamic analysis compared with the static analysis.

Backcalculation of layer moduli from dynamic deflection measurements is becoming an accepted means of estimating in situ material properties (*1*). This is commonly done by matching deflections measured under a known dynamic load with theoretical deflections generated in an analytical model of the pavement by varying the elastic moduli of the layers. Most backcalculation procedures use linear elastic layered models. Though such models are simple and useful, they have limitations. One major limitation is that the applied load is assumed to be static. This is not the case in modern deflection testing where an impulse load is used.

According to previous research (*2,3*), dynamic instead of static analysis should be performed on nondestructive testing data obtained through dynamic loading. Pavement deflection under a static load is different from that under a dynamic or impulse load because of viscoelastic pavement properties and dynamic effects such as inertia, damping, and resonance. Dynamic analysis would therefore provide a more accurate estimate of the pavement modulus from backcalculation.

PAST RESEARCH USING DYNAMIC ANALYSIS

One of the more recent and well-known research efforts using dynamic analysis was performed by Mamlouk (*2,4*). The elastodynamic method was used to calculate the deflection of pavement subjected to cyclic (road rater) loading. That model has a rock or rigid layer at some depth (about 15 ft) in the subgrade. Roesset and Shao (*5*) determined that the rigid layer has to be located at least 70 ft from the surface to prevent boundary effects for a dynamic analysis. Mamlouk's research also included material and radiation damping in its elastodynamic analysis. (The characteristics of radiation damping will be discussed later.) The viscoelastic theory determines the change in strain of a material under load with time.

Roesset and Shao (*5*) also studied pavement response using dynamic analysis and determined that calculated deflections are different from those in static analysis. However, theirs was not a backcalculation model and did not provide modulus values for the pavement layers.

C. L. Ong, Texas Research and Development Foundation, 6811 Kenilworth Avenue, Suite 230, Riverdale, Md. 20737. D. E. Newcomb, University of Minnesota, Minneapolis, Minn. 55455. R. Siddharthan, University of Nevada, Reno, Nev. 89512.

OBJECTIVE OF RESEARCH

The major objective of this paper is to show the difference in backcalculated moduli between dynamic and static analyses using falling weight deflectometer (FWD) data. A dynamic backcalculation program that can closely simulate the FWD impulse load and perform analysis for a three-layer pavement has been developed. The program, called FEDPAN, uses the finite element method and can simulate the behavior of the pavement under the FWD load. It includes both the effect of pavement inertia and damping in the dynamic analysis and can perform static backcalculation analysis. One of the major advantages of a finite element–based analysis is that the nonlinear material property characterization can be easily incorporated in the study. Such a study is currently under way.

APPROACH TO PROGRAM DEVELOPMENT

The Structural Analysis Program IV (SAP IV) (*6*), a widely used and accepted linear finite element program, was used as the base program in FEDPAN to calculate theoretical deflections. SAP IV can perform axisymmetric and other types of analyses. The axisymmetric analysis was chosen for FEDPAN because of the symmetrical deflection basin due to the FWD load. The response of an axisymmetric problem can be obtained by analyzing only a radial section. This type of analysis also greatly reduces memory requirements and computing time. To further reduce the mesh size, dashpots or dampers

were added to the model to absorb radiating waves created by the FWD loading.

The purpose of installing dashpots at boundary nodes is to reduce the size of the finite element domain that should be discretized. A smaller domain reduces the number of elements, which in turn reduces the memory storage and computation time required. The dashpots located at the boundary absorb the radiating waves [P waves (compression waves) and S waves (shear waves)] caused by the impulse loading. This viscous boundary simulates the presence of similar pavement layer materials beyond the boundary and gives the effect of a continuum layer for the waves to propagate away from the source, even though the actual discretized domain is small. Without the dashpots, the waves reflect off the rigid boundary and back into the domain. The boundary dashpot characteristics depend on wave velocities, material properties, and the area of the boundary elements. The relationships are as follows (*7*):

Dashpot forces = stress (compression or shear)

* area of element

Here,

$$\text{stress} = \rho V_{c/s} \dot{w}_{n/t} \tag{1}$$

where

ρ = mass density of element,
$V_{c/s}$ = compression or shear wave velocity,
$\dot{w}_{n/t}$ = normal or tangential wave velocity,
$V_c = (G/\rho)^{1/2}$,
$V_s = (1/S)V_c$,
G = shear modulus,
$S = [(1 - 2\nu)/2(1 - \nu)]^{1/2}$, and
ν = Poisson's ratio.

The dashpots are used to simulate a continuum condition, but they can be removed to simulate the presence of a rigid or rock layer.

The dynamic analysis is performed in the time domain incrementally. This method is suitable for impact loading problems in which the time of loading is short. In the dynamic analysis with dashpots, the equation of motion is

$$[M]\ddot{x} + ([C] + \text{dashpots})\dot{x} + [K]x = F(t) \tag{2}$$

where

[M] = mass matrix,
$\ddot{x}$ = acceleration,
[C] = Rayleigh damping matrix,
$\dot{x}$ = velocity,
[K] = stiffness matrix,
x = displacement, and
$F(t)$ = applied force as a function of time.

The Rayleigh damping matrix used in Equation 2 will be explained in the next section. The closure algorithm used in this program is the CHEVDEF algorithm (*8*), which is used in many other backcalculation programs.

CHARACTERISTICS OF PHYSICAL MODEL

In this study, the finite element pavement mesh is made up of four node rectangular elements, as shown in Figure 1 (top). The nodes at the boundaries of the mesh are either fixed (hinged) or on rollers. None of the fixed nodes at the bottom boundary can move, either vertically or laterally, which simulates a rigid boundary. The right and the left boundary nodes are on rollers and can move vertically but not laterally. Figure 1 (bottom) indicates that dashpots are installed at these boundary nodes except for the left boundary, because of the axisymmetric loading. For clarity, only the dashpots that absorb compressional waves are shown in the figure. A boundary with dashpots installed at the nodes will be referred to as a viscous boundary, and fixed nodes at the bottom nodes, which simulate the presence of a rock or rigid layer, will be referred to as a rigid boundary. The zone of influence at the surface caused by a load is typically 10 to 12 times the radius of the footing (the radius of the FWD loading plate is approximately 6 in.), and, therefore, the right boundary of the mesh was located approximately 15 ft (30 times the radius) to the right of the load. Deflections were recorded on the surface of the pavement at 0.0, 7.9, 11.8, 23.6, and 39.4 in. from the center of the load, which correspond to the locations of geophones in the field test.

Though FEDPAN can estimate moduli of a three-layer pavement, the pavement layers can be subdivided into thinner layers, up to a total of eight. Memory allocation in the program can be increased to accommodate more sublayering, if required.

The FWD impulse loading curve is simulated in the model by using a Haversine equation. With this equation, the nodes

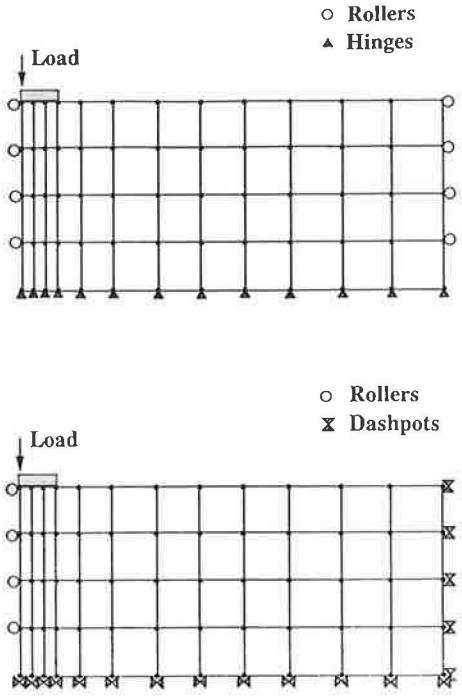

FIGURE 1 Finite element method representation: *top*, four node elements; *bottom*, dashpots installed at boundary nodes.

under the FWD loading plate will experience a change in load with time. The FWD load is spread over the plate, and the nodal forces are computed on the assumption of uniform stress distribution under the plate. This type of stress distribution is commonly used in foundation engineering. The duration of the simulated impulse loading is 30 msec, with peak load at 15 msec. The response of the pavement is observed for 90 msec. Any peak in deflections during the 90-msec period is recorded. This ensures that delays in peak deflections at the nodes due to damping or other dynamic effects of the pavement are accommodated. The material damping used in the model is characterized by the Rayleigh damping equation, which gives the damping matrix as a sum of mass and stiffness proportional components:

$$[C] = \alpha[M] + \beta[K] \quad (3)$$

where

[C] = Rayleigh damping matrix,
α = mass proportional coefficient, and
β = stiffness proportional coefficient.

In FEDPAN, the mass proportional coefficient is set to zero. When α is zero, undesirable high-frequency components of the response will be filtered out [see Figure 2 (*9*)].

VERIFICATION OF COMPUTER PROGRAM—FEDPAN

To test the FEDPAN program, pavement moduli values obtained after a few iterations with FEDPAN were used in the original SAP IV. The programs produced the same deflection results, as expected. The tests were performed for both the static and dynamic analyses. The computed static stress and deformation results were checked against classical solutions available in the literature (*10*), and the responses observed were similar.

The values of the dashpot coefficients generated by the program were also verified by hand calculations. To check whether the dashpots were working correctly, the dashpot coefficients of the bottom boundary were gradually increased. The surface deflections of the pavement model decreased and approached the deflections obtained using a rigid layer, as shown in Figure 3. This indicates that the dashpots were functioning correctly. Researchers also concluded that these types of dashpots are good absorbers for both harmonic and nonharmonic waves (*6*).

FEDAT, an input data generator program, was written to help create the data file for FEDPAN. FEDAT generates the nodal coordinates and other data required in the backcalculation. It is interactive and prompts for layer thicknesses and number of sublayers in each layer. It also prompts for the type of analysis (static or dynamic) and generates dashpots for the dynamic analysis if so desired. The β value used in material damping and other material properties are specified by the user. Stress values in any element or in rows of elements can be determined if they are requested by the user. Hundreds of input items required to set up any finite element–based analysis are therefore reduced to a minimum by FEDAT. This substantially reduces extensive and, often, time-consuming data preparation.

LIMITATIONS AND ASSUMPTIONS

In FEDPAN, the pavement materials are assumed to be homogeneous and isotropic in each layer. FEDPAN performs only a linear analysis, even though behavior in the unbound pavement materials may be nonlinear. An effort to incorporate nonlinear analysis into FEDPAN is currently being made. The material damping ratio (ζ) in this study was assumed to be 5 percent, a value commonly used in pavement response analysis (*2*). This may be achieved by selecting the β value used in Rayleigh damping by the following equation:

$$\beta = 2\zeta/\omega_n \quad (4)$$

where

ζ = critical damping ratio,
ω_n = natural angular frequency = $2\pi f$, and
f = fundamental frequency of the pavement (Hz).

The fundamental frequency of the pavement was assumed to be 14 Hz. The fundamental frequency of the pavement

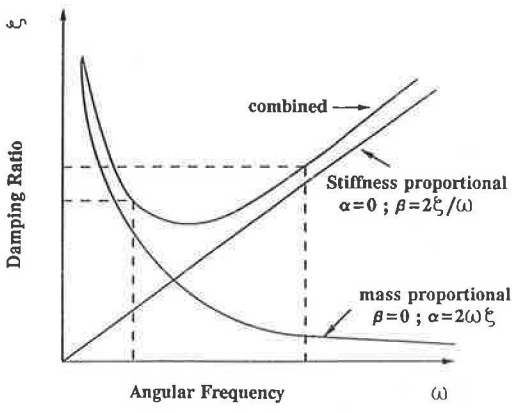

FIGURE 2 Rayleigh damping (*9*).

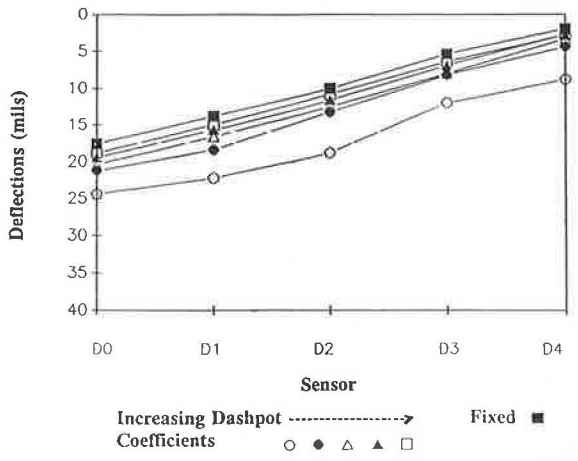

FIGURE 3 Results from dashpot tests.

structure is a function of structural mass and stiffness. Researchers showed that typical pavement sections with 20 ft of subgrade have fundamental frequencies in the vicinity of 14 Hz (*2,3*). On the other hand, if the fundamental frequencies for the test sections are known, they can be used in Equation 4.

Other assumptions used in this study, such as unit weights and initial guess moduli (seed moduli), are given in Table 1. The procedure adopted uses an overall damping ratio of 5 percent for the pavement section. On the other hand, if evidence exists that damping in the asphalt layer is substantially different from that in the bottom layers, the damping matrix can be constructed element by element using the steps outlined by Idriss et al. (*11*). They generated a damping matrix for seismic soil response studies that takes into account the variable damping in soil elements.

Observations of trial tests showed that the CHEVDEF (*8*) closure algorithm used in this program is not very sensitive to the seed moduli or the maximum and minimum moduli range, as long as the moduli calculated fall within the range. Lee (*12*) reported that the backcalculation program EVERCALC (layered elastic program), which he developed, showed the same lack of sensitivity. The upper limit of the layer moduli values has been selected to be quite high, but this does not affect the computed results. The algorithm will converge as long as the field data are good. If the percent summation of the absolute differences between the calculated and the measured deflections is less than or equal to 6 percent (tolerance), convergence in the backcalculation procedure is achieved. When this happens, the assumed moduli values are considered the corresponding pavement layer modulus.

TEST SITE DESCRIPTION

The sites used in the study are located in Nevada. FWD tests were performed by the Nevada Department of Transportation (NDOT) using a Dynatest 8000 FWD. Initially, five sites were chosen for the study, but one site was dropped when layer thickness data from the construction record were found to be questionable. The remaining four were Sites 11, 12, 16, and 31. The thickness profiles for these sites are shown in Table 2. Deflections used in the backcalculation were obtained on the same marked spots during different seasons.

RESULTS AND ANALYSIS

The results obtained are subject to the limitations and assumptions described earlier. The results also do not reflect the stress sensitivity of the unbound materials. Three backcalculation analyses were performed using FEDPAN: static analysis with rigid boundary, dynamic analysis with rigid boundary, and dynamic analysis with viscous boundary.

Parametric Tests

Two parametric tests were conducted using FEDPAN with data from Site 12. The first was to determine the thickness of elements to be used in the subgrade. The moduli values calculated for four equal sublayers in the 240-in. subgrade were compared with the moduli values calculated for six equal sublayers using the same 240-in. subgrade for all three methods of analysis. The results are presented as ratios of moduli

TABLE 1 MATERIAL PROPERTIES USED IN STUDY

	Layer 1	Layer 2	Layer 3
Maximum (psi)	5,000,000	500,000	250,000
Minimum (psi)	100,000	2,000	2,000
Poisson's Ratio	0.35	0.35	0.40
Seed Moduli (psi)	500,000	25,000	20,000
Unit Weight (lb/ft^3)	144	125	115

TABLE 2 PAVEMENT PROFILES FOR TEST SITES

Site	Thickness (inches)			No. of Layers		
	AC	Base	Subgrade	AC	Base	Subgrade
11	4.25	11.00	240.00	1	1	4
12	8.25	16.00	240.00	1	1	4
16	9.75	11.00	240.00	1	1	4
31	16.25	13.00	240.00	2	1	4

in Figure 4. The ratios were obtained by dividing the pavement layer moduli by the corresponding moduli computed with the six-layer characterization for the subgrade.

Figure 4 indicates only a small difference in moduli given by the static analysis in both the four- and six-layer sublayering of the subgrade, and the difference in moduli using dynamic analysis with dashpots was even smaller. The dynamic analysis with rigid bottom yielded the greatest difference, up to 12 percent in the base.

This test showed that the 240 in. of subgrade can be divided into four sublayers and still provide a good estimate compared with division into six sublayers, which requires more computation time.

The second parametric test determined the influence of the location of the bottom boundary. Moduli values computed for all three layers by FEDPAN for subgrade thicknesses (D_s's) of 240 and 120 in. (both with four equal subgrade sublayers) were compared. Figure 5 shows the ratio of moduli values normalized using the moduli values computed with 120 in. of subgrade. Figure 5 indicates that the modulus of asphalt concrete (AC) is not affected by either the location of the rigid bottom or the type of analysis. However, the moduli values of base and subgrade were substantially affected.

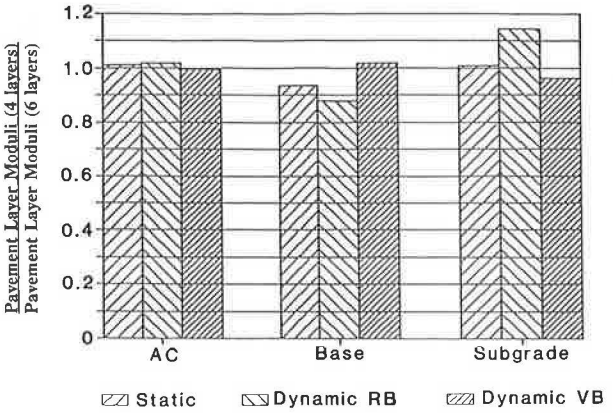

FIGURE 4 Sensitivity of backcalculated moduli to sublayering of subgrade (RB indicates rigid boundary; VB indicates viscous boundary).

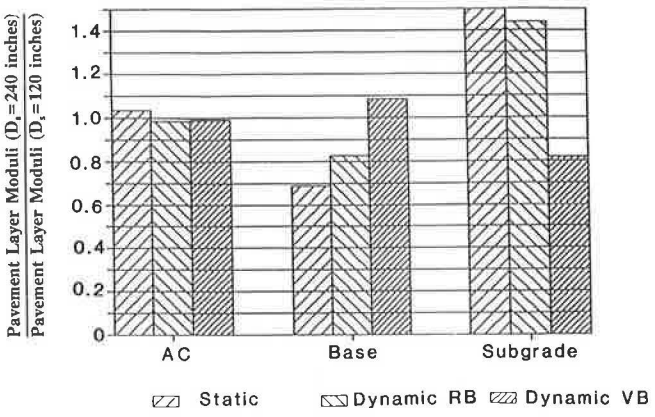

FIGURE 5 Sensitivity of backcalculated moduli to subgrade thickness (RB indicates rigid boundary; VB indicates viscous boundary).

The static analysis with rigid boundary at 120 in. in the subgrade indicated a stronger base and a weaker subgrade. The dynamic analysis with rigid boundary showed the same trend. On the other hand, results from the dynamic analysis with dashpots (viscous boundary) indicated the opposite trend. After the parametric tests, the location of the bottom boundary was set at 240 in. in the subgrade with four equal sublayers in all subsequent analyses.

Backcalculation of Field Test Results

The backcalculation was performed for the static analysis, dynamic analysis with viscous boundary, and dynamic analysis with rigid boundary using the FWD data collected by NDOT for the selected sites. Results obtained were averaged for Sites 11 (two seasons), 12 (four seasons), 16 (three seasons), and 31 (two seasons). Comparisons between the different analyses are shown in Figures 6 through 10. The ratio method of comparison was used in order to evaluate the effects of the different analyses without addressing seasonal effects, even though the strength of the pavement layers varies with the season. For all three analyses, an examination of the backcalculated moduli results obtained for different seasons indicated that

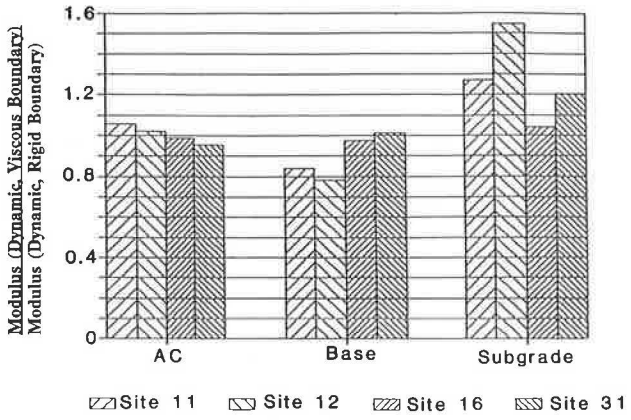

FIGURE 6 Ratio of moduli for dynamic viscous boundary to moduli for dynamic rigid boundary.

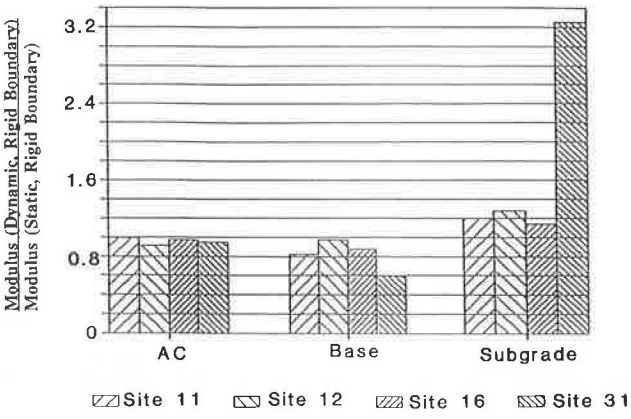

FIGURE 7 Ratio of moduli for dynamic rigid boundary to moduli for static analysis using FEDPAN.

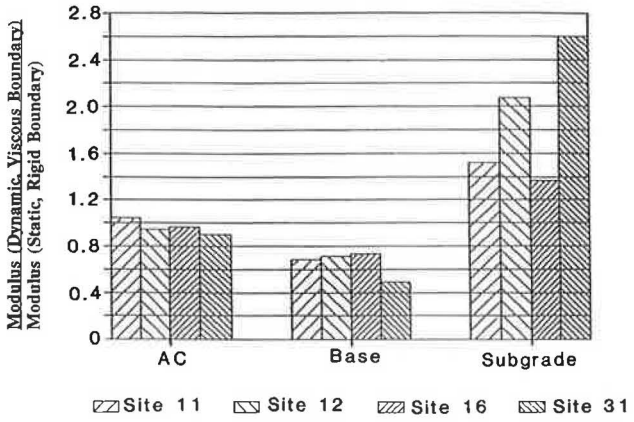

FIGURE 8 Ratio of moduli for dynamic viscous boundary to moduli for static analysis using FEDPAN.

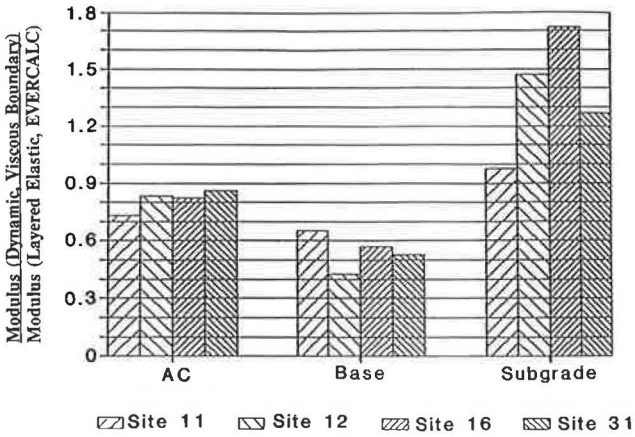

FIGURE 9 Ratio of moduli for FEDPAN dynamic viscous boundary to moduli for EVERCALC.

the same trend existed, so the results were averaged and reported. The average percent difference for the backcalculated results (last iteration) and the average number of iterations used to reach convergence are given in Table 3.

Comparison of Results for Dynamic Viscous Boundary and Dynamic Rigid Boundary

Figure 6 compares dynamic backcalculated moduli values for viscous and rigid boundary models. The figure indicates that the AC moduli were not affected by the inclusion of dashpots at the boundaries at any of the sites. In particular, the asphalt moduli at Sites 16 and 31 (with thick AC layers of 9.75 and 16.2 in., respectively) were not significantly affected by the presence of dashpots. But for base and subgrade layers, the backcalculated moduli values were substantially affected by the backcalculation procedure, except at Site 16.

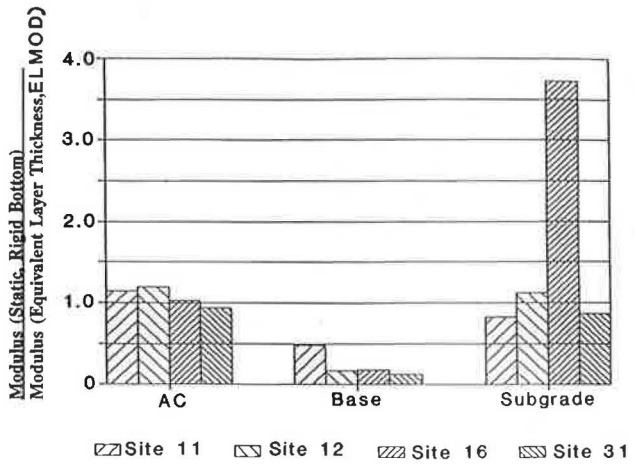

FIGURE 10 Ratio of moduli for FEDPAN (static) to moduli for ELMOD.

Comparison of Dynamic Results with Static Results

Comparisons of results obtained using FEDPAN for the two dynamic analyses and the static analysis are presented in Figures 7 and 8. Again, the static and dynamic analyses yield very similar results in the estimate of AC modulus. However, the subgrade and base moduli values can be substantially affected by the type of analysis. These results indicate that the static backcalculation procedure, which neglects inertia and other dynamic effects, may lead to an underestimation of the subgrade moduli. The base moduli, on the other hand, may be overestimated by the static analysis.

TABLE 3 AVERAGE CONVERGENCE RESULTS FOR 11 DEFLECTION SITES

	Iteration	Difference (%)
EVERCALC	3.0	3.47
FEDPAN Static	3.0	4.17
Dynamic Rigid Boundary	3.3	4.12
Dynamic Viscous Boundary	3.2	3.26

Comparison of FEDPAN Results with EVERCALC and ELMOD Results

Figure 9 compares the results obtained from dynamic analysis with viscous boundary and EVERCALC (*12*). Moduli ratios of FEDPAN (static) to ELMOD (which uses the Equivalent Thickness Method) are shown Figure 10. In general, the two figures indicate that the backcalculated moduli are quite different. The base modulus is overestimated by both EVERCALC and ELMOD when compared with FEDPAN, and the subgrade modulus estimates vary. The main reasons are the differences in the methods of analysis and the assumptions used by the backcalculation programs. In the case of FEDPAN, when the rigid bottom boundary option was used, the rigid bottom was located at a depth of 20 ft into the subgrade, whereas EVERCALC can consider only a semi-infinite subgrade.

CONCLUSIONS AND RECOMMENDATIONS

This paper describes a dynamic model (FEDPAN) for backcalculation of FWD deflection data to obtain pavement layer moduli values. Dashpots introduced at the bottom and lateral right boundaries allow the size of the finite element domain to be reduced, providing for efficient analysis. The dashpots also reduced the effects of reflection waves by simulating half-space conditions without having to use a rigid boundary at a distance from the load (say at 20 ft in the subgrade). The conclusions to be presented are subject to the limitations and assumptions discussed throughout this paper. The conclusions are as follows:

1. If bedrock (or a stiff layer) exists near the surface, the bottom boundary of the mesh can be located there when using FEDPAN. If the stiff layer does not exist, the rigid bottom boundary may be located at some distance (at least 20 ft in the subgrade) with dashpots connected to the nodes. When dashpots are provided, the waves that reach the viscous boundary are absorbed, and wave reflection does not take place. This case represents a semi-infinite subgrade.
2. The study indicates that four sublayers are sufficient in the 20 ft of subgrade when a static analysis or a dynamic analysis with dashpots is used. A subgrade with six sublayers can improve the accuracy of the results, especially in the dynamic analysis when a rigid boundary at approximately 20 ft is required.
3. AC layer moduli were not affected by either the static or the dynamic analyses. The sites considered represent different combinations of asphalt and base layer thicknesses. The thickness of the asphalt layers used in this study varied from 4.25 to 16.2 in.
4. The dynamic analysis produced higher subgrade moduli and lower base moduli than the static analysis. For pavements with thick asphalt layers, the dynamic analysis produced much higher subgrade moduli. However, because of the thick asphalt layers at Sites 16 and 31, further research is recommended to determine whether the reading from the outermost sensor can adequately represent the stress experienced by the subgrade only, and not a combination of stresses from other layers.
5. When the dynamic backcalculation analysis with viscous boundary was performed, the computed subgrade moduli values were higher and the base moduli values were lower than those computed by the dynamic analysis with rigid boundary or the static analysis.
6. The results obtained from two static analysis programs, one with FEDPAN and another with EVERCALC, confirmed that the location of a rigid boundary is extremely important. Comparison of the two analysis programs ELMOD and EVERCALC indicated that different programs and methods of analysis can produce quite different results.
7. Limitations of the proposed method include the inability to model nonlinear soil properties and lateral variation in moduli values, which should be overcome in future models.
8. Comparisons of the backcalculated moduli from FEDPAN with the pavement moduli obtained from laboratory tests should also be made.

ACKNOWLEDGMENT

This research was made possible by a grant from the National Science Foundation. Other financial support was provided by NDOT. The authors also gratefully acknowledge Dynatest, Inc., for providing the ELMOD program and the Washington Department of Transportation for providing the EVERCALC program used in this study.

REFERENCES

1. *Nondestructive Testing of Pavements and Backcalculation of Moduli*. Special Technical Paper 1026. ASTM, Philadelphia, Pa., 1988.
2. M. S. Mamlouk. Use of Dynamic Analysis in Predicting Field Multilayer Pavement Moduli. In *Transportation Research Record 1043*, TRB, National Research Council, Washington, D.C., 1985, pp. 113–121.
3. T. G. Davies and M. S. Mamlouk. Theoretical Response of Multilayer Pavement Systems to Dynamic Nondestructive Testing. In *Transportation Research Record 1022*, TRB, National Research Council, Washington, D.C., 1985, pp. 1–7.
4. B. Sebaaly, T. G. Davies, and M. S. Mamlouk. Dynamics of Falling Weight Deflectometer. *Journal of Transportation Engineering*, ASCE, Vol. 111, No. 6, Nov. 1985, pp. 618–632.
5. J. M. Roesset and K.-Y. Shao. Dynamic Interpretation of Dynaflect and Falling Weight Deflectometer Tests. In *Transportation Research Record 1022*, TRB, National Research Council, Washington, D.C., 1985, pp. 7–16.
6. K. J. Bathe, E. L. Wilson, and F. E. Paterson. *A Structural Analysis Program for Static and Dynamic Response of Linear Systems*. Report EERC 73-11. Earthquake Engineering Research Center, University of California at Berkeley, Berkeley, 1973 (revised 1974).
7. J. Lysmer and R. L. Kuhlemeyer. Finite Dynamic Model for Infinite Media. *Journal of Engineering Mechanics*, ASCE, Aug. 1969, pp. 859–877.
8. A. J. Bush III. *Nondestructive Testing for Light Aircraft Pavements, Phase I: Evaluation of Nondestructive Testing Devices*. Report FAA-RD-80-9. Federal Aviation Administration, U.S. Department of Transportation, 1980.
9. R. W. Clough and J. Penzien. *Dynamics of Structures*. McGraw-Hill, New York, 1975.
10. H. G. Poulos and E. H. Davies. *Elastic Solutions for Soil and Rock Mechanics*. John Wiley and Sons, Inc., New York, 1974.
11. I. M. Idriss, H. B. Seed, and N. Serff. Seismic Response by Variable Damping Finite Elements. *Journal of Geotechnical Engineering*, ASCE, Vol. 100, No. GT1, Jan. 1974, pp. 1–13.
12. S. W. Lee. *Backcalculation of Pavement Moduli by Use of Pavement Surface Deflections*. Ph.D. dissertation. University of Washington, Seattle, 1988.

Advanced Backcalculation Using a Nonlinear Least Squares Optimization Technique

N. SIVANESWARAN, STEVEN L. KRAMER, AND JOE P. MAHONEY

In recent years the analysis of pavement structures has relied increasingly on characterizing material properties (such as resilient modulus) by use of nondestructive deflection testing and backcalculation procedures. An important element common to all backcalculation procedures—the technique used to achieve a "convergence" of the measured and calculated deflection basins—will be described. A convergence method based on the use of nonlinear least squares is described. The method was adapted to a layered elastic program (CHEVRON N-layer). This convergence approach improves moduli estimates over prior procedures; however, the most important element is the ability to efficiently backcalculate not only layer moduli but also layer thicknesses. This ability is illustrated by using hypothetical two- and three-layer pavement sections and by using real data for a three-layer section.

In recent years the design and rehabilitation of pavement structures has relied increasingly on accurate characterization of the mechanical properties of the materials that compose them. A number of nondestructive testing techniques have been developed to evaluate some of these mechanical properties. The falling weight deflectometer (FWD) method has seen widespread use, in large part because of its ability to impose dynamic loading on a pavement structure similar to the loading imposed by truck traffic.

Conventional interpretation of the results of an FWD test generally involves backcalculation of estimates of the elastic moduli of the various layers of the pavement section. Backcalculation procedures seek to define a set of elastic moduli that best describe the pavement deflections observed from the FWD test in the framework of a particular pavement model. A number of pavement models and backcalculation procedures have been employed to interpret FWD tests. Some of the issues involved in accurate and reliable FWD test interpretation are discussed, and a versatile backcalculation procedure that has exhibited improved performance characteristics relative to many previously used procedures is presented. This procedure is then extended to allow backcalculation of other parameters, namely layer thicknesses, in addition to layer moduli.

In the FWD test, a transient impulse load is applied to a pavement surface by a cushioned falling weight. The response of the pavement surface is measured at a number of points at different distances from the weight. The response is generally measured by velocity transducers, with the velocity time history integrated to provide a time history of pavement deflection. The test may be repeated several times at a particular location and the results averaged to reduce random errors, or the test may be repeated with different loads to evaluate stress dependence of layer moduli.

For current methods of interpretation of the results of FWD tests, the maximum displacement at each velocity transducer is used to define a deflection basin, which is interpreted as having resulted from a statically applied load. This approach discards a great deal of potentially useful information contained in the load and displacement signals. Using a solution for a layered system of linear, elastic materials and assuming that layer thicknesses and Poisson's ratios are accurately known, the moduli of the individual layers providing the best agreement with the observed deflection basin are considered to represent the stiffness of the various materials.

Department of Civil Engineering, FX-10, University of Washington, Seattle, Wash. 98195.

BACKCALCULATION

Problems of backcalculation, sometimes referred to as parameter identification or system identification, are common in many areas of science and engineering. Basically, they involve situations where an input is transformed by some process to an output. An analytical or numerical model is used to describe the process. Usually, the input and the output are known, and the backcalculation problem becomes one of identifying the model parameters. Such methods were formalized by electrical engineers who identified model parameters for various electrical components by matching a known input signal to the component with the measured output signal.

Backcalculation of FWD Test Results

In FWD test interpretation, the input is the impulse load applied to the pavement surface by the falling weight, the output is the measured deflection basin, and the process is the mechanical transfer of the kinetic energy of the falling weight at the point of impact to the work done in deforming the pavement. The input, related to the particular FWD apparatus and weight being used, is generally well known. The output, expressed in terms of the deflection basin, is measured and therefore also known. The process, which is typically described by a layered elastic mechanical model, depends on model parameters, which include the modulus, thickness, and Poisson's ratio of each layer. For most current FWD test

interpretation procedures, the layer thicknesses and Poisson's ratios are assumed to be accurately known, leaving the layer moduli as the only unknown variables. The FWD backcalculation problem is shown schematically in Figure 1, where the layer moduli are contained in the vector **E**. The problem is to find the model parameters that best describe the known deflection basin produced by the known FWD load, using the layered elastic model.

Requirements of a Backcalculation Method

A variety of different methods have been used for backcalculation of layer moduli in the interpretation of FWD test results. In this paper, the term backcalculation will refer to the numerical process by which the layer moduli are calculated rather than the more broadly defined problem of pavement analysis. These methods have ranged from simple, largely manual methods to more sophisticated numerical methods. To be useful to practicing pavement engineers, a good backcalculation method must possess certain characteristics.

First, and most obvious, it must be accurate. Satisfactory performance of pavement overlays or other rehabilitative measures designed by a mechanistic-empirical process depends on accurate characterization of layer moduli. Consequently, a suitable backcalculation method must be able to recognize and correct even small errors in layer moduli in order to develop an accurate solution.

Second, it must converge rapidly. Under production conditions the interpretation of large numbers of FWD tests is usually required. Under other conditions it is desirable to interpret the results of an FWD test in the field immediately after its completion. In either case, important decisions often must be made quickly on the basis of the backcalculated layer moduli. It is therefore important that the backcalculation procedure allow processing of large amounts of data in the shortest possible time. However, in the future, rapid increases in computational capabilities resulting from advances in computer hardware may allow some sacrifice of computational efficiency for robustness or versatility.

Third, the backcalculation method must be robust—it must converge to a correct solution, even under difficult circumstances. Such circumstances arise from errors and uncertainty in the measured test results, pavement structures that cause the backcalculation problem to be ill-conditioned, and poor initial estimates of the layer moduli.

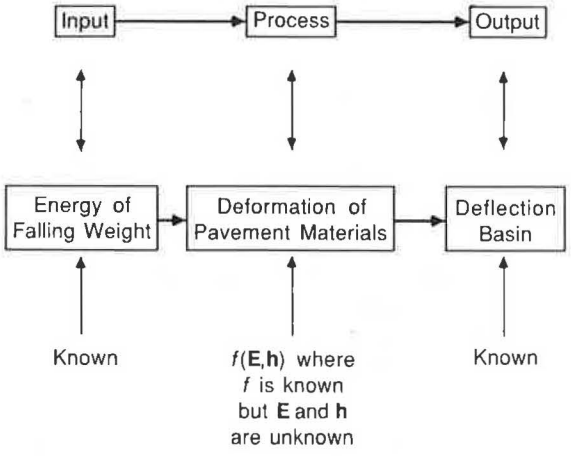

FIGURE 1 Schematic view of backcalculation process.

Fourth, the backcalculation method should be versatile. In looking toward the future, it is desirable to base FWD backcalculation on methods that can account for parameters other than layer moduli alone. Future FWD backcalculation methods may, for example, use the entire time history of motion at each sensor with dynamic modeling to backcalculate dynamic moduli and damping, as described in a frequency domain approach by Lytton (*1*). The advanced procedure described in this paper can backcalculate both layer thickness and layer moduli simultaneously and is being adapted to include other parameters as well.

Current Backcalculation Methods

A number of computer programs have been developed for analysis of FWD test results. Many of these programs have been patterned after the DEF series of programs (CHEVDEF, BISDEF) developed by the U.S. Army Corps of Engineers (*2*). These programs employ a gradient search technique for iteration toward the correct set of layer moduli. In the formulation used in these programs, a successive linear least squares approach is used, taking advantage of empirically linearized model parameters. The linearization of model parameters allows a system of simultaneous equations to be solved for the layer moduli at each iteration. If the parameters were truly linear, only one iteration would be required; however, the linearization is only approximate, so successive iterations are required to approach the correct solution. This approximate linearity simplifies the FWD interpretation problem to the point where satisfactory accuracy and efficiency can be obtained for many data sets by a limited optimization method.

A different approach is used by the program MODULUS (*3*) developed at Texas A&M University. Before the actual backcalculation process, MODULUS computes a series of normalized deflection basins using the BISAR program with layer moduli that cover the range of moduli anticipated in the field. The number of normalized deflection basins increases rapidly with the number of unknown parameters in the backcalculation problem. The deflection basins are stored in a data base for subsequent comparison with measured deflection basins. By using this data base, a Hooke-Jeeves pattern search algorithm, and three-point Lagrangian interpolation, a reasonable set of moduli can be attained quickly. The Hooke-Jeeves algorithm is a direct search technique that relies only on function values, neglecting first- and second-derivative information. It can handle nonlinear problems, but it often requires significantly more iterations to reach a solution than more recently developed nonlinear optimization techniques. The approach taken by MODULUS is distinctly faster than other approaches for production cases in which many deflection basins in the same pavement geometry are to be evaluated. When pavement conditions change, however, the time-consuming task of generating normalized deflection basins must be repeated.

In summary, currently available backcalculation procedures seek only to evaluate pavement layer moduli. The accuracy

and efficiency of most rely on the empirically observed linear dependence of pavement deflection on the logarithm of layer modulus. These methods generally perform satisfactorily within the limited framework of conventional FWD test interpretation. In order to broaden the scope and capabilities of the FWD test, however, improved backcalculation procedures must be used.

NONLINEAR LEAST SQUARES OPTIMIZATION

A nonlinear least squares optimization approach for FWD backcalculation problems is proposed in this paper. The nonlinear least squares approach has certain advantages over current procedures for conventional FWD backcalculation, but it has many more advantages when viewed in the light of more advanced FWD backcalculation procedures. The advantages will be illustrated by using the proposed approach to backcalculate layer moduli and layer thickness at the same time.

Criterion Function

After selection of a model to represent the system and the quantities to be measured, the backcalculation problem can be expressed as an optimization problem in which the objective is to estimate a set of model parameters that best describes the measured quantities. How well the model describes the measured quantities can be evaluated by defining a criterion function as a function of the differences between measured and model-predicted quantities. The optimization process then seeks to minimize the value of the criterion function. Selection of the criterion function can strongly influence the accuracy and efficiency of the optimization process.

In backcalculating layer moduli from FWD data, the measured quantities are the pavement deflections at the various sensor locations. Hence the criterion function should represent the discrepancy between the measured deflections and those predicted by the model. Several criterion functions can be defined. For the FWD backcalculation problem involving n deflection measurements on a pavement section of M layers with unknown modulus and thickness, the most common criterion functions can be expressed as follows:

- Sum of absolute differences:

$$f(\mathbf{E},\mathbf{h}) = \frac{1}{n}\sum_{i=1}^{n}|d_i^c(\mathbf{E},\mathbf{h}) - d_i^m| \tag{1}$$

- Sum of absolute relative differences:

$$f(\mathbf{E},\mathbf{h}) = \frac{1}{n}\sum_{i=1}^{n}\left|\frac{d_i^c(\mathbf{E},\mathbf{h}) - d_i^m}{d_i^m}\right| \tag{2}$$

- Sum of squared differences:

$$f(\mathbf{E},\mathbf{h}) = \frac{1}{n}\sum_{i=1}^{n}[d_i^c(\mathbf{E},\mathbf{h}) - d_i^m]^2 \tag{3}$$

- Sum of squared relative differences:

$$f(\mathbf{E},\mathbf{h}) = \frac{1}{n}\sum_{i=1}^{n}\left[\frac{d_i^c(\mathbf{E},\mathbf{h}) - d_i^m}{d_i^m}\right]^2 \tag{4}$$

where

$d_i^c(\mathbf{E},\mathbf{h})$ = calculated deflection at Location i based on $\mathbf{E}$ and $\mathbf{h}$,
$\mathbf{E}$ = $\{E_1, E_2, E_3, \ldots, E_M\}$ (unknown moduli of the layers),
$\mathbf{h}$ = $\{h_1, h_2, h_3, \ldots, h_{M-1}\}$ (unknown layer thicknesses), and
d_i^m = measured deflection at Location i.

Each criterion function defined above has its own advantages and disadvantages, and the quality of its performance is problem dependent. The first two functions are nonsmooth, meaning that their slopes are not necessarily continuous, and consequently optimization techniques that use first-derivative (either analytical or numerical) information cannot be used for estimation. This is a major disadvantage, because optimization methods that use first-derivative information often perform much better than methods that use only function values. From a statistical standpoint, the preferred form of the criterion function depends on the nature of the random error of the measurements, as summarized in Table 1.

The measured deflections contain errors arising from the accuracy of the deflection-measuring system. The specified accuracy of most available FWD devices is on the order of ±2 percent of the measured deflection for commonly used ranges of loading (*4*). The random error can therefore be approximated, for criterion function selection, as normally distributed with zero mean and a constant coefficient of variation. Table 1 indicates that the sum of squared relative differences (Equation 4) is the preferred criterion function for use in backcalculating layer moduli from FWD data.

TABLE 1 SELECTION OF PREFERRED CRITERION FUNCTION FORM

Random Error Characteristics				
Distribution	Mean	Standard Deviation	Coefficient Variation	Preferred Criterion Function
Laplace	Zero	Constant	-	Sum of Absolute Differences
Laplace	Zero	-	Constant	Sum of Relative Differences
Normal	Zero	Constant	-	Sum of Squared Differences
Normal	Zero	-	Constant	Sum of Squared Relative Differences

Nonlinear Least Squares Optimization Method

A number of optimization methods are available to minimize the sum of squared relative differences, that is, to solve the following problem:

$$\text{minimize } f(\mathbf{E},\mathbf{h}) = \frac{1}{n}\sum_{i=1}^{n}\left[\frac{d_i^c(\mathbf{E},\mathbf{h}) - d_i^m}{d_i^m}\right]^2 \quad (5)$$

Optimization methods developed for general minimization problems, including direct search and quasi-Newton methods, can be used to solve this problem. However, methods that take into account the special structure of the sum of squared relative differences converge substantially faster than general minimization methods. If the relative error at Location i is represented by

$$r_i(\mathbf{E},\mathbf{h}) = \frac{d_i^c(\mathbf{E},\mathbf{h}) - d_i^m}{d_i^m} \quad (6)$$

the criterion function can be expressed, after multiplying by the constant n for convenience, as

$$f(\mathbf{E},\mathbf{h}) = \sum_{i=1}^{n}[r_i(\mathbf{E},\mathbf{h})]^2 = \mathbf{r}^T\mathbf{r} \quad (7)$$

where $\mathbf{r} = \{r_1, r_2, r_3, \ldots, r_n\}$, the relative error (residual).

Then the gradient of the criterion function is

$$\nabla f = 2\mathbf{A}\mathbf{r} \quad (8)$$

where $\mathbf{A} = \{\nabla r_1, \nabla r_2, \ldots, \nabla r_n\}$, and the Hessian can be written as

$$\mathbf{H} = \nabla^2 f = 2\mathbf{A}\mathbf{A}^T + 2\sum_{i=1}^{n} r_i\nabla^2 r_i \quad (9)$$

The gradient and Hessian are the respective multidimensional equivalents of the slope and curvature of a one-dimensional function. In this formulation, the first part of the Hessian is known as soon as the gradient ∇f has been evaluated. Because $\mathbf{r}^T\mathbf{r}$ is being minimized, the relative errors are often small. Consequently, the second part of the Hessian may be negligibly small, so that a good approximation to the Hessian may be made by neglecting the second part, which gives

$$\mathbf{H} \approx 2\mathbf{A}\mathbf{A}^T \quad (10)$$

A solution can then be obtained iteratively by incorporating the approximated Hessian into the Levenberg-Marquardt algorithm (*5*,*6*).

Numerical studies have indicated that the residuals vary approximately linearly with the logarithm of layer moduli. This behavior can be exploited to speed convergence by choosing log E_i as the parameter to be determined instead of E_i. As previously noted, many existing backcalculation methods rely on this behavior; they would not perform satisfactorily without linearization of this aspect of the problem. Because of this linearity, the ∇r_i^2 terms are very small (zero if the relationship is linear) when layer moduli are the only unknowns, and the second part of the Hessian becomes smaller yet, further improving the Hessian approximation used above. With the nonlinear least squares approach, the structure of the selected criterion function allows the Hessian to be easily and rapidly approximated, resulting in a more efficient search for the parameters that minimize the criterion function.

The nonlinear least squares approach has two main advantages in addition to its ability to handle nonlinear problems. First, an optimization method that uses the above approximation to the Hessian will converge much faster than other methods. An approximation to the Hessian is obtained as soon as the gradient is calculated in each iteration; other nonlinear optimization methods may require several iterations to obtain a satisfactory estimate of the Hessian. Second, because $2\mathbf{A}\mathbf{A}^T$ is always positive definite, the criterion function is convex and will have a unique minimum. It should be noted, however, that the criterion function is not proven to be convex. The claim that the neglected term in the Hessian is very small compared with the term retained in the approximation is only supported by numerical experiments, and no theoretical evaluation of the claim is possible because of the complex nature of the problem.

VERIFICATION OF NONLINEAR LEAST SQUARES OPTIMIZATION APPROACH

The nonlinear least squares optimization approach meets all the requirements of a good backcalculation method and has a number of advantages over other methods. The advantages were explored by incorporating the approach into an existing backcalculation program. The LMDIF routine, available in the MINPACK collection of FORTRAN programs developed at the Argonne National Laboratory (*7*), is a well-tested nonlinear least squares routine that takes advantage of the least squares problem structure. This optimization routine was used for the studies described in this paper and has been incorporated into EVERCALC, a layered elastic pavement analysis program developed for the Washington State Department of Transportation. The revised version of the program, EVERCALC 3.0, and the previous version, EVERCALC 2.0, will be compared in terms of the requirements of a good backcalculation method.

Accuracy and Efficiency

The nonlinear least squares optimization approach leads to accurate solutions. It can recognize small differences between computed and measured deflection basins and make the layer modulus adjustments necessary to reduce the differences to an acceptable value. However, most other backcalculation methods also lead to accurate solutions when error tolerances are set at low values, at least when the problem is well conditioned and the seed moduli are reasonably close to the actual moduli.

In order to achieve accurate solutions, however, many iterations may be required. Because of the ease with which the

conventional backcalculation problem (i.e., evaluation of layer moduli alone) can be linearized, nearly all backcalculation methods are reasonably efficient when circumstances are not difficult—when errors and uncertainty are minimal, the backcalculation problem is well conditioned, and seed moduli are close to the actual moduli. In the absence of these conditions the efficiency of backcalculation methods is closely related to their robustness.

Robustness

The principal advantage of the nonlinear least squares optimization approach for conventional FWD test interpretation is in robustness. The approach offers distinct improvements in accuracy and speed when the backcalculation problem is complicated by errors and uncertainty in deflection measurements, very sharp or very small modulus contrasts, or poor seed moduli. Because these complications are not uncommon in practice, the benefits of using the nonlinear least squares optimization approach can be considerable.

Several sources contribute to uncertainty in the measured deflections and thus to uncertainty in the backcalculated layer moduli. One of the most common is the limited accuracy of the deflection-measuring system of available FWD devices. To evaluate the effects of such errors on backcalculated layer moduli, a simulation was carried out with the hypothetical four-layer pavement system used in a study of measurement error effects by Irwin et al. (*4*) and shown in Figure 2.

In the simulations by Irwin et al., the instrument error was assumed to be normally distributed with a standard deviation of 1.95 μm. The true deflection basin, characterized by six deflections at offsets of 0, 8.86, 11.8, 20.7, 29.5, and 53.2 in., was first computed for the pavement shown in Figure 2 for a load of 10,000 lb and a plate of radius 5.9 in. using the CHEVRON N-layer program. Thirty deflection basins were then created by adding randomly generated errors to the computed deflections. The layer moduli for each of the 30 deflection basins were backcalculated with EVERCALC 3.0. The results are presented in Table 2, along with those obtained with EVERCALC 2.0 and MODCOMP 2 (*4*). The mean EVERCALC 3.0 moduli were generally somewhat closer to the true moduli, but the variability in backcalculated moduli, reflected in the coefficient of variation of the modulus for each layer, was significantly lower for EVERCALC 3.0. The improvement in the performance of EVERCALC 3.0 (small in this case) is largely attributed to the robust nonlinear least squares optimization routine, though some may be due to differences in the modeling approaches used in the two programs.

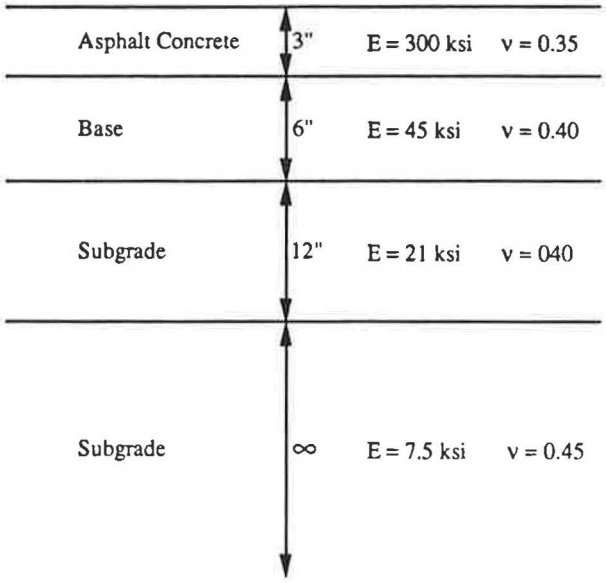

FIGURE 2 Four-layer pavement structure analyzed by Irwin et al. (*4*).

Versatility

The nonlinear least squares optimization approach has capabilities beyond those of conventional backcalculation procedures. This versatility is described in the following section.

ADVANCED BACKCALCULATION BY NONLINEAR LEAST SQUARES OPTIMIZATION APPROACH

All currently available FWD interpretation programs require the thickness of each pavement layer to be specified before backcalculation. These layer thicknesses can be measured accurately from core samples but are usually obtained from design and construction records. However, as-built layer thicknesses can vary significantly from those described in the design and construction records. Measured asphalt thicknesses have been observed to differ from those in design and construction records by up to 128 percent (*8*). Because pave-

TABLE 2 COMPARISON OF EFFECTS OF MEASUREMENT ERRORS ON BACKCALCULATED LAYER MODULI

		MODCOMP 2 Moduli		EVERCALC 2.0 Moduli		EVERCALC 3.0 Moduli	
Layer	Actual (ksi)	Mean (ksi)	COV (%)	Mean (ksi)	COV (%)	Mean (ksi)	COV (%)
AC	300.0	306.0	16.3	290.5	18.6	295.2	12.2
Base	45.0	44.6	13.2	46.0	13.3	45.5	9.0
Subbase	21.0	21.3	6.6	20.5	7.3	21.0	4.8
Subgrade	7.5	7.5	1.2	7.5	1.2	7.5	0.8

ment deflections are sensitive to layer thicknesses, even modest errors in assumed layer thicknesses can lead to large errors in backcalculated layer moduli.

An advanced backcalculation procedure that uses the nonlinear least squares optimization approach has been developed to backcalculate both layer moduli and layer thickness from the same set of FWD data. Currently used optimization procedures may not be capable of solving such nonlinear problems accurately and efficiently.

Problem Characteristics

Some insight into the FWD moduli backcalculation problem can be obtained from examination of a simple, hypothetical two-layer backcalculation problem. Consider the pavement section of Figure 3, in which a 10-in. layer of asphalt concrete (AC) is underlain by an infinitely thick subgrade. The actual moduli of the AC and subgrade are 500 and 20 ksi, respectively. If the deflection basin predicted for this section by the CHEVRON N-layer program is considered the measured deflection basin, values of the sum of squared relative differences criterion function can be computed for other combinations of layer moduli. The values of the criterion function for other layer moduli will reflect how close they are to the actual moduli. Figure 4a shows contours of the sum of squared relative differences criterion function for this hypothetical problem with a 10-in. AC thickness. Figure 4b shows the sensitivity of the criterion function to the AC layer thickness at the actual layer moduli.

Certain characteristics of the FWD moduli backcalculation problem are apparent from Figure 4. The criterion function is relatively sensitive to subgrade modulus and relatively insensitive to AC modulus. These observations are not unexpected, because most of the pavement surface deflection results from deformation of the subgrade soils. The size of the 0.01 criterion function contour [which corresponds to 10 percent root-mean-square (RMS) of the relative error] is also of note. It encompasses an AC modulus range of 300 to 800 ksi and a subgrade modulus range of 18 to 24 ksi. Clearly, a criterion function tolerance of much less than 0.01 or an RMS relative error tolerance less than 10 percent is necessary to ensure reasonable accuracy of backcalculated moduli. As the number of layers in the pavement section increases while the number of deflection measurements remains the same, this range (i.e., the volume encompassed by a fixed value of the criterion function or the RMS relative error) also increases, requiring much tighter error tolerances. The criterion function is also sensitive to the thickness of the AC layer. Hence, accurate knowledge of layer thickness is necessary for accurate backcalculation of layer moduli. This sensitivity of layer moduli to layer thickness was well illustrated by Irwin et al. (*4*).

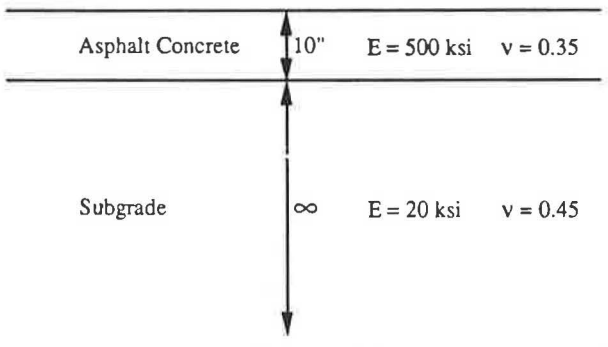

FIGURE 3 Hypothetical two-layer pavement structure.

Illustration of Advanced Backcalculation Procedure

When the assumed layer thicknesses specified in a conventional backcalculation problem are incorrect, the resulting backcalculated layer moduli will be incorrect. Whether the backcalculated layer moduli are too high or too low will depend on whether the layer thicknesses were underestimated or overestimated. The effect of such errors can be illustrated by introducing incorrect layer thicknesses into a conventional analysis of a pavement section of known properties. The benefits of the advanced backcalculation procedure can then be illustrated by considering the layer thicknesses as unknowns and iterating toward a set of layer moduli and layer thicknesses that best matches the measured deflection basins.

Two-Layer Case

Using the CHEVRON N-layer program, a deflection basin was generated for the two-layer pavement section of Figure 3, which consists of a 10-in.-thick AC layer with modulus E_1 = 500 ksi overlying a subgrade with modulus E_2 = 20 ksi. A 10 percent error in AC thickness could lead to the specification of a 9- or 11-in. thickness in a conventional backcalculation analysis. Assuming either of these incorrect AC thicknesses, a conventional backcalculation procedure would converge to an incorrect set of layer moduli. Using EVERCALC 3.0 with fixed values of AC thickness (conventional mode), a backcalculated AC modulus of 648.2 ksi was obtained from four different sets of seed moduli when the AC thickness was assumed to be 9 in. Thus a 10 percent underestimation of AC thickness resulted in a 29.6 percent overestimation of AC modulus. When the AC thickness was incorrectly assumed to be 11 in., the AC modulus was backcalculated to be 402.6 ksi, again from four different sets of seed moduli. The subgrade modulus was accurately predicted for all cases. The optimization process is shown graphically in Figure 5a. The actual solution is represented by the large point at the center of the cube, the initial conditions by the medium-size points along the edges of the cube, and the conditions at the end of each iteration by the small points at the kinks in the optimization "paths." As can be seen, the conventional mode of backcalculation requires that the optimization paths remain in the same AC thickness plane, so the actual solution cannot be reached.

The advanced mode of EVERCALC 3.0 was then used, starting from the same seed values of layer modulus and AC layer thickness, with the AC layer thickness also considered an independent variable. The results are shown graphically in Figure 5b. The optimization paths converge, in two or three iterations, to values close to the actual solution. The numerical results are presented in Table 3. In each case, the advanced

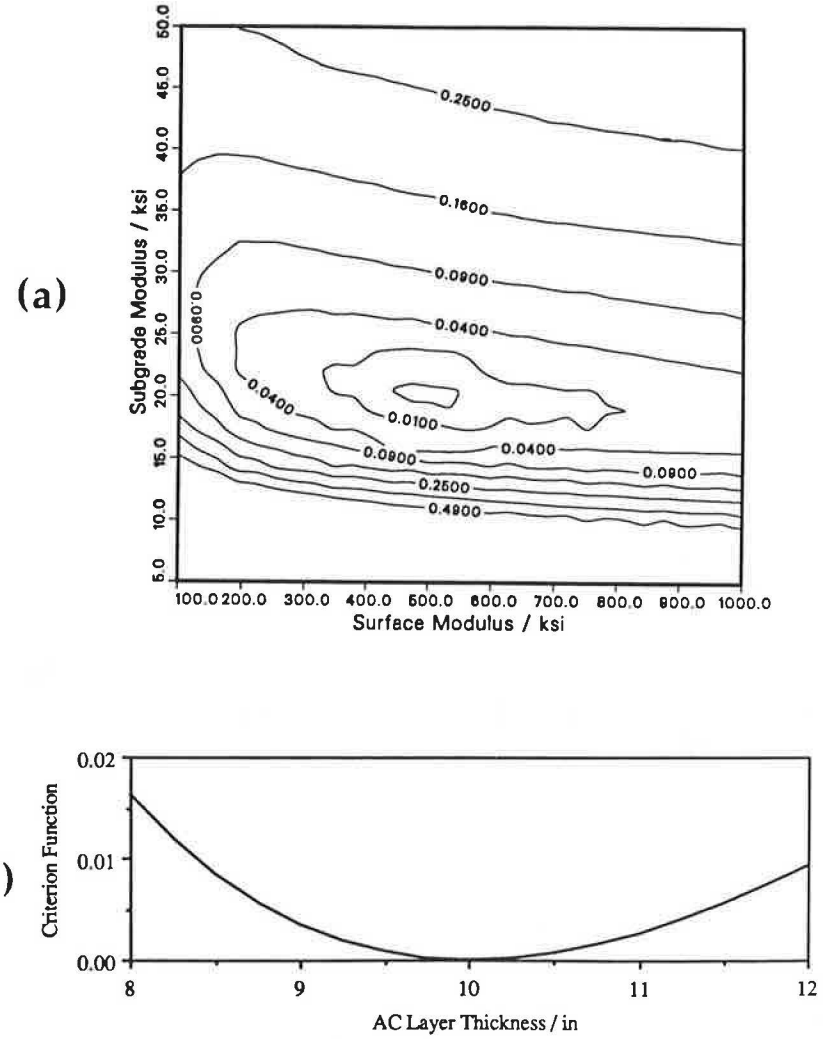

FIGURE 4 (a) Criterion function contours with AC thickness set at actual value; (b) variation of criterion function with AC thickness with moduli set at actual values. [Criterion function value = (RMS error)^2.]

backcalculation procedure of EVERCALC 3.0 converged to the correct moduli for the AC and subgrade layers and to the correct thickness of the AC layer. Averaging the modulus and thickness values from eight sets of seed values (seed moduli and seed thickness) gave differences between the actual and backcalculated values of less than 0.1 percent.

Three-Layer Case

A similar analysis was performed for the three-layer pavement structure shown in Figure 6. This pavement structure consisted of 5 in. of AC (E_1 = 500 ksi) over 10 in. base material (E_2 = 40 ksi) over subgrade (E_3 = 20 ksi). In the three-layer analyses, pavement thickness errors of ±20 percent were assumed. Four sets of incorrect layer thickness assumptions were evaluated, corresponding to (h_1, h_2) values of (4, 8), (4, 12), (6, 8), and (6, 12), where h_1 and h_2 are the AC and base layer thicknesses in inches, respectively. Each set was evaluated once from seed moduli twice as large as the actual moduli and once from seed moduli half as large as the actual moduli. The sections were analyzed with EVERCALC 3.0, first in the conventional mode and then in the advanced mode starting from the ending point of the conventional analysis. The results for the eight cases are presented in Table 4. Again, it can be seen that errors in assumed pavement layer thickness resulted in significant errors in backcalculated layer moduli, with the exception of the subgrade modulus, when conventional backcalculation techniques were used. When the layer thicknesses were released as independent variables in the advanced mode of EVERCALC 3.0, the program again converged rapidly toward the correct modulus and thickness for all layers. Averaging the modulus and thickness values from each of the eight sets of seed values gave errors no larger than 0.3 percent.

During each iteration, both layer moduli and layer thicknesses are adjusted at the same time, as shown in Figure 5b. Consequently, the increase in the number of parameters required for the advanced approach does not lead to a proportional increase in the number of iterations or the total com-

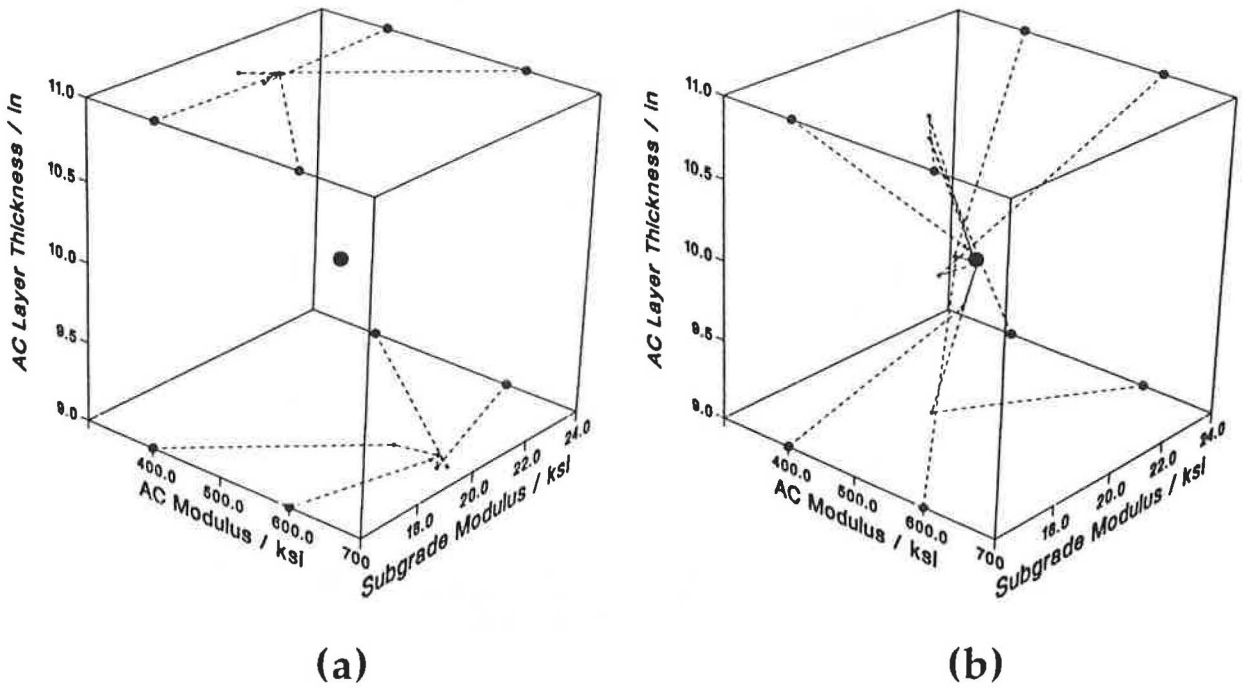

FIGURE 5 Optimization paths taken by EVERCALC 3.0 during backcalculation of hypothetical two-layer problem: a, conventional mode; b, advanced mode.

TABLE 3 COMPARISON OF BACKCALCULATED MODULI AND LAYER THICKNESS—TWO-LAYER CASE

	Seed Values			Calculated Values*			Calculated Values**			
Case	E1	E2	h	E1	E2	RMS Error (%)	E1	E2	h	RMS Error (%)
1	400	24	9.000	648.2	20.1	0.8	500.0	20.0	10.002	0.01
2	600	24	9.000	648.2	20.1	0.9	501.0	20.0	9.990	0.07
3	400	15	9.000	648.2	20.1	0.8	500.0	20.0	10.002	0.08
4	600	16	9.000	648.2	20.1	0.9	500.1	20.0	10.001	0.08
5	400	24	11.000	402.6	19.9	0.8	500.6	20.0	9.994	0.00
6	600	24	11.000	402.6	19.9	0.9	501.0	20.0	9.990	0.04
7	400	16	11.000	402.6	19.9	0.8	500.7	20.0	9.995	0.08
8	600	16	11.000	402.6	19.9	0.9	500.0	20.0	10.001	0.00
					Average Values		500.4	20.0	9.997	
					Error (%)		0.08	0.00	0.03	

*h fixed at seed value (conventional mode of backcalculation)
**h freed as independent variable (advanced mode of backcalculation)

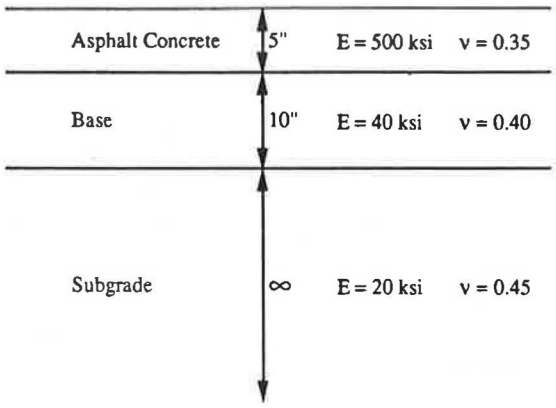

FIGURE 6 Hypothetical three-layer pavement structure.

puting time. In fact, the time required to reach a solution in the advanced mode was typically only 10 percent greater than in the conventional mode.

Application to Real Data

The advanced backcalculation procedure was applied to actual deflection basin data obtained by a Washington State Department of Transportation FWD (Dynatest Model 8000) at a test site (Milepost 20.85 on SR-11) in northwestern Washington State. AC and base thicknesses were measured at three locations in the 1,000-ft-long test section; average values were 5.2 in. and 28.8 in., respectively. The deflection basin and the results of conventional backcalculation by five different backcalculation programs were described by Mahoney et al.

TABLE 4 COMPARISON OF BACKCALCULATED MODULI AND LAYER THICKNESS—THREE-LAYER CASE

	Seed Values					Calculated Values*				Calculated Values**					
Case	E1	E2	E3	h1	h2	E1	E2	E3	RMS Error (%)	E1	E2	E3	h1	h2	RMS Error (%)
1	1000	80	40	4	8	696.2	58.7	20.0	0.8	500.7	40.0	20.0	4.995	9.992	0.01
2	1000	80	40	4	12	877.7	39.4	19.9	0.5	500.5	40.1	20.0	4.996	9.985	0.01
3	1000	80	40	6	8	347.1	39.6	20.1	0.5	501.0	40.4	20.0	4.995	9.990	0.01
4	1000	80	40	6	12	373.4	31.3	20.1	0.2	499.3	40.1	20.0	5.000	9.960	0.06
5	250	20	10	4	8	696.4	58.6	20.0	0.8	501.3	40.2	20.0	4.981	9.975	0.03
6	250	20	10	4	12	877.4	39.4	19.9	0.5	496.3	40.2	20.0	5.010	9.861	0.06
7	250	20	10	6	8	347.2	39.6	20.0	0.5	500.0	40.0	20.0	4.999	10.010	0.02
8	250	20	10	6	12	373.1	31.4	20.1	0.2	500.0	40.0	20.0	4.996	9.985	0.05
									Average Values	499.9	40.1	20.0	4.997	9.970	
									Error (%)	0.02	0.25	0.00	0.06	0.30	

*h fixed at seed value (conventional mode of backcalculation)
**h freed as independent variable (advanced mode of backcalculation)

(*9*). The conventional backcalculation programs used the measured AC and base thicknesses to backcalculate moduli for each of the three layers. The programs exhibited considerable variability in backcalculated AC modulus, ranging from 518 to 761 ksi with an average of 621 ksi, but much more consistent base and subgrade moduli (25.0 ksi and 26.4 ksi, respectively). The average RMS error at convergence for the five programs was 2.7 percent.

Advanced backcalculation was performed with gross errors in assumed layer thickness. Seed thicknesses of 4.0 in. for the AC layer (77 percent of measured thickness) and 32.8 in. for the base layer (114 percent of measured thickness) were used. The results are summarized in Table 5. The advanced procedure iterated to backcalculated thicknesses of 5.4 in. for the AC and 26.3 in. for the base and, simultaneously, to backcalculated layer moduli of 656, 22, and 27 ksi for the AC, base, and subgrade layers, respectively. The RMS error for the advanced backcalculation procedure was 0.8 percent. The backcalculated thicknesses are in good agreement with the measured thicknesses, and the backcalculated moduli are in good agreement with those backcalculated by the conventional backcalculation programs.

POTENTIAL LIMITATIONS

The verification of the advanced backcalculation procedure described in this paper is based on one real deflection basin and two hypothetical pavement sections with calculated deflection basins. The probability of the parameters backcalculated with the nonlinear least squares optimization approach being close to the actual parameters increases with increasing system overdeterminism (ratio of number of independent data points to number of unknown parameters). Therefore, increasing the number of unknowns by adding layer thicknesses to the list of unknown parameters implies that additional data points may be necessary, particularly for many-layered pavement structures. In the three-layer structures considered here, five unknowns (three moduli and two thicknesses) were accurately calculated from deflection basins

TABLE 5 COMPARISON OF BACKCALCULATED MODULI AND LAYER THICKNESS—SR-11 FIELD SITE

Method	AC	Base	Subgrade	RMS Error (%)
ELMOD	518	28	23	1.9
ELSDEF	550	27	25	5.8
EVERCALC 2.0	761	23	27	1.2
ISSEM4	592	25	28	n.a.
MODCOMP2	686	22	29	1.8
Average	**621**	**25.0**	**26.4**	**2.7**
EVERCALC 4.0	**656**	**22**	**27**	**0.8**

Layer	Measured Thickness (in)	Seed Thickness (in)	Backcalculated Thickness (in)
AC	5.2	4.0	5.4
Base	28.8	32.8	26.3

defined by six deflections. Whereas the advanced backcalculation procedure worked well in these cases, the effects of large measurement errors that may exist in real data on the confidence intervals of backcalculated parameters have not yet been fully investigated.

Increasing the overdeterminism of the FWD backcalculation problem (with consequent improvement in confidence intervals), however, can easily be accomplished. By representing the stress-dependent layers with more fundamental parameters—for example, k_1 and k_2 [from $E = k_1(\theta)^{k2}$]—the data from multiple load drops can be combined in a single backcalculation analysis. As an example, consider a four-layer system subjected to four load drops. If two parameters are necessary to describe the load-dependent modulus for each layer except the AC, the total number of unknowns will be 10, including the thicknesses of the upper three layers. If the FWD apparatus is configured to make six deflection measurements, a total of 24 independent data points will be generated. With 10 unknowns calculated from 24 data points, the backcalculation problem is highly overdetermined and the advanced procedure is likely to converge to an accurate solution. Investigation of this approach is continuing.

SUMMARY

An improved optimization technique for backcalculating pavement layer moduli has been described. The optimization technique (nonlinear least squares) can converge to a solution more quickly using wide ranges of input data, such as seed moduli. Further, the technique can be used to backcalculate layer thicknesses.

Data were presented in Tables 3 and 4 illustrating the effect of incorrect layer thicknesses on backcalculated moduli. Clearly, the ability to determine both the layer moduli and thicknesses represents an improvement in backcalculation technique.

FUTURE ACTIVITIES

In an extension of the work described in this paper, an advanced version of EVERCALC, EVERCALC 4.0, will be tested on actual field data. The data will include FWD deflection basins on pavement sections that have been cored for thickness determination and for which the samples have been tested in the laboratory for resilient moduli (AC by ASTM D4123 and unstabilized base and subgrade materials by a modified triaxial test similar to AASHTO T274). Though laboratory resilient moduli do not necessarily represent the "true" moduli, this information will allow evaluation of the procedure. The ability of the proposed technique to estimate depths to rock (rigid) layers and material parameters, such as k_1 and k_2 [from $E = k_1(\theta)^{k2}$], for unstabilized layers will also be evaluated. The nonlinear least squares optimization technique will also be used to examine the minimum number of deflection sensors, sensor spacings, and FWD load levels necessary to accurately backcalculate both layer moduli and layer thicknesses from surface deflections.

REFERENCES

1. R. L. Lytton. Backcalculation of Pavement Layer Properties. In *Nondestructive Testing of Pavements and Backcalculations of Moduli* (A. J. Bush III and G. Y. Baladi, eds.). ASTM STP 1026. American Society for Testing and Materials, Philadelphia, Pa., 1989, pp. 7–38.
2. A. J. Bush III. *Nondestructive Testing for Light Aircraft Pavements, Phase II: Development of the Nondestructive Evaluation Methodology*. Report FAA-RD-80-9-II. Federal Aviation Administration, U.S. Department of Transportation, 1980.
3. J. Uzan, R. L. Lytton, and F. P. Germann. General Procedure for Backcalculating Layer Moduli. In *Nondestructive Testing of Pavements and Backcalculations of Moduli* (A. J. Bush III and G. Y. Baladi, eds.). ASTM STP 1026. American Society for Testing and Materials, Philadelphia, Pa., 1989, pp. 217–228.
4. L. H. Irwin, W. S. Yang, and R. N. Stubstad. Deflection Reading Accuracy and Layer Thickness Accuracy in Backcalculation of Pavement Layer Moduli. In *Nondestructive Testing of Pavements and Backcalculations of Moduli* (A. J. Bush III and G. Y. Baladi, eds.). ASTM STP 1026. American Society for Testing and Materials, Philadelphia, Pa., 1989, pp. 229–244.
5. K. Levenberg. A Method for the Solution of Certain Nonlinear Problems in Least Squares. *Quarterly of Applied Mathematics*, Vol. 2, 1944, pp. 164–168.
6. D. W. Marquardt. An Algorithm for Least Squares Estimation of Nonlinear Parameters. *SIAM Journal*, Vol. 11, 1963, pp. 431–441.
7. J. J. More, B. S. Garbow, and K. E. Hillstrom. *User Guide for MINPACK-1*. Argonne National Laboratory, Argonne, Ill., 1980, 261 pp.
8. S. W. Lee. Backcalculation of Pavement Moduli by Use of Pavement Surface Deflections. Ph.D. dissertation. University of Washington, Seattle, 1988, 247 pp.
9. J. P. Mahoney, N. F. Coetzee, R. N. Stubstad, and S. W. Lee. A Performance Comparison of Selected Backcalculation Computer Programs. In *Nondestructive Testing of Pavements and Backcalculations of Moduli* (A. J. Bush III and G. Y. Baladi, eds.). ASTM STP 1026. American Society for Testing and Materials, Philadelphia, Pa., 1989, pp. 452–469.

Relating Deflection Data to Pavement Strain

CARL A. LENNGREN

Much effort has been made to verify backcalculated moduli based on deflections. However, pavement strain is of more interest to the pavement design engineer. A comparison of recorded strain at an instrumented road section with the strain obtained from backcalculation based on data from a falling weight deflectometer is presented. The agreement between the two methods is good, even if the backcalculated moduli show some discrepancy.

In mechanistic design the calculated or estimated strain is crucial. A common procedure for determining the strain is to measure the surface deflection of a pavement with a falling weight deflectometer (FWD). The elastic moduli of the pavement layers are then surmised and used as input in computer programs.

Most evaluation techniques employ backcalculation of linear elastic layer analysis programs (e.g., BISAR and CHEVRON). There are also programs based on finite element analyses, like ILLI-PAVE, that require more input data on soil characteristics and therefore must be used with care (*1*). In either case, to initiate the process, the elastic moduli of the pavement layers are assumed, and the resulting deflections are compared with the measured ones. Adjustments of the estimated moduli are made until the agreement between the two deflection sets is within a given tolerance. The strain in the matching deflection basin is then taken as the strain exerted in the pavement. Algorithms to get the program to converge are crucial. Kilareski and Anani (*2*) pointed out that the subgrade is affected by all sensors and adjustments should work accordingly.

There are presently a number of computer programs available for backcalculation—BISDEF, ELMOD, ISSEM4, SEARCH, WESDEF, and EVERCALC, to mention a few (*3–6*). Most studies indicate that the *E*-modulus of the subgrade can be readily determined. Bound layers must be sufficiently thick to be assessed an appropriate modulus. The unbound granular layers appear to be the most difficult to determine. Their resilient E-moduli are known to depend on the stress and hence the load (*7*). The stress sensitivity could be determined by using different load levels. Usually, pavements are tested with a second load level corresponding to half the standard one (e.g., 50 and 25 kN).

Most efforts to validate backcalculation techniques have compared derived moduli with those obtained in the field (*8*). However, strain should be of much more interest than moduli. The Road and Traffic Laboratory in Finland has an instrumented asphalt pavement road in operation for studies of truck wheel configurations and tires (*9*). Strain gauges are glued to 6-in.-diameter cores, which in turn are glued back into the pavement. Hence, this facility appeared ideal to verify the backcalculated strains from an FWD measurement by comparing them with the measured response from the strain gauges.

Department of Highway Engineering, Royal Institute of Technology, S-100 44 Stockholm, Sweden. Current affiliation: Department of Civil and Mineral Engineering, University of Minnesota, 500 Pillsbury Drive SE, Minneapolis, Minn. 55455.

FIELD MEASUREMENT

The FWD deflection measurements took place in September 1989 on a clear, sunny day that allowed the pavement to warm up. A pavement temperature range from 15°C to 27°C (59°F to 81°F) was achieved by first measuring in the morning and then repeating the measurements in the afternoon as the pavement temperature peaked around 3 p.m. Thus a wide range of asphalt concrete (AC) elastic moduli was obtained. A KUAB 50 FWD equipped with seven sensors was provided by RST-Sweden. The sensors were spaced 0, 20, 30, 45, 60, 90, and 120 cm from the center of the loading plate, which had a radius of 15 cm. Three load levels were used: 50, 25, and 12.5 kN, and each drop was repeated at least once.

Care was taken to center the loading plate over the strain gauge so that the maximum strain would occur under the D_0 sensor. Because the purpose of the facility is to study the effect of moving trucks, the sampling is normally triggered by the vehicle's breaking a photocell beam. However, the FWD is stationary, so the photocell could not be used. Instead, a lamp on the FWD signaled the initiation of the drop to the strain gauge operator, so that the 2-sec-long "window" of sampling could be used.

Measurements were made on AC thicknesses of 8 and 15 cm. The AC mix consisted of a penetration 80 binder and a densely graded aggregate, with a lime filler content of 6 percent. The maximum aggregate size was 16 mm. The binder content was 5.9 percent. The mix design was the same for both thicknesses. Each drop of the FWD was labeled with a three-digit number, which is used in the tables and figures that follow.

The unbound base consisted of crushed gravel and sand; the maximum aggregate size was 32 mm. The subbase consisted of gravel and sand with a maximum aggregate size of 64 mm. The subgrade consisted of sand, which was well drained and dry at the time of measurement. Because the two locations were close, little variation of the properties of these layers and the subgrade might be expected. The maximum deflections recorded were 545 μm on the 8-cm-thick AC layer and 360 μm on the 15-cm-thick layer. The deflections on the

warmer pavements were about 20 percent higher than those on the colder pavements.

The sampling rate of the strain gauges is 16 kHz, well above the resolution needed for recording the rising pulse of the FWD, which is roughly 25 msec. The FWD records the maximum deflections only, which correspond to the maximum strain, although the deformation lags somewhat. Only tension was recorded from the drops. For a moving truck, the tension peak is surrounded by two compression stages (*9*).

BACKCALCULATION OF FIELD DATA

The program CLEVERCALC was used for the backcalculation. CLEVERCALC is a modified version of EVERCALC developed in the state of Washington, adapted to metric units and equipment. These programs stop the iteration process when the sum of the relative errors of the backcalculated deflection basin compared with the measured basin stay within a given tolerance *or* when the change of moduli from one iteration to the next is less than some other given tolerance (*6*). The sum of the relative errors for each sensor of the deflection basin is referred to as the deflection error in the following.

A three-layer system was assumed for the calculations. The thicknesses were known to be 8 and 15 cm for the bound AC layer. The base and subbase combined were 62 cm for the thinner pavement and 55 cm for the corresponding thicker pavement. The subgrade was considered semi-infinite. The Poisson's ratios used were 0.35, 0.40, and 0.45 for the three layers, the topmost mentioned first. The program needs six sensors for an initiation routine (*10*). The version used first employed only five sensors in the backcalculation, spaced either at 0, 20, 30, 60, and 90 cm, or at 0, 20, 60, 90, and 120 cm. Both settings were used in this study for comparison, and they are indexed "20" or "120" in the following, designating the sensor that was used. Recent versions of the program use all seven sensors in the evaluation. Depending on the choice of sensors, different moduli were obtained, but only slight differences in strain were observed.

SELECTING VALID DATA

All of the basins recorded on the 15-cm asphalt pavement were solved within a few iterations for the stipulated tolerance of 3 percent. Most calculated basins matched the measured ones well, the deflection error defined above being smaller than 5 percent. The worst error was 10.8 percent for the D_{20} calculation and 22 percent for the D_{120} calculation. (The change of modulus was smaller than 3 percent.) Figure 1 shows afternoon deflection measurements for the 15-cm asphalt pavement at three load levels.

However, difficulties were encountered in reaching good agreement with the deflection basin of the thinner pavement. The measurements made in the morning were particularly troublesome. The program was unable to find a reasonable match for the 50-kN loads, and the deflection error for most of the others hovered around 30 to 40 percent when D_{20} was used in the backcalculation. The afternoon measurements agreed much better, with one exception.

D_0 and D_{20} values were almost the same where the difficulties were encountered. For this type of pavement, one would anticipate D_0 to be about 20 percent higher than D_{20}. A discontinuity might be suspected in the asphalt pavement, such as the core slipping somewhat relative to the original pavement. The sectioned loading plate of the KUAB 50 should rule out any unevenness of the surface. The effect was not seen for most measurements made in the afternoon (see Table 1).

A correlation study of load and deflections was made to find inconsistencies and thus locate the deflections that had to be excluded from the study. The deflections are strongly correlated with each other for each of the four sets of measure-

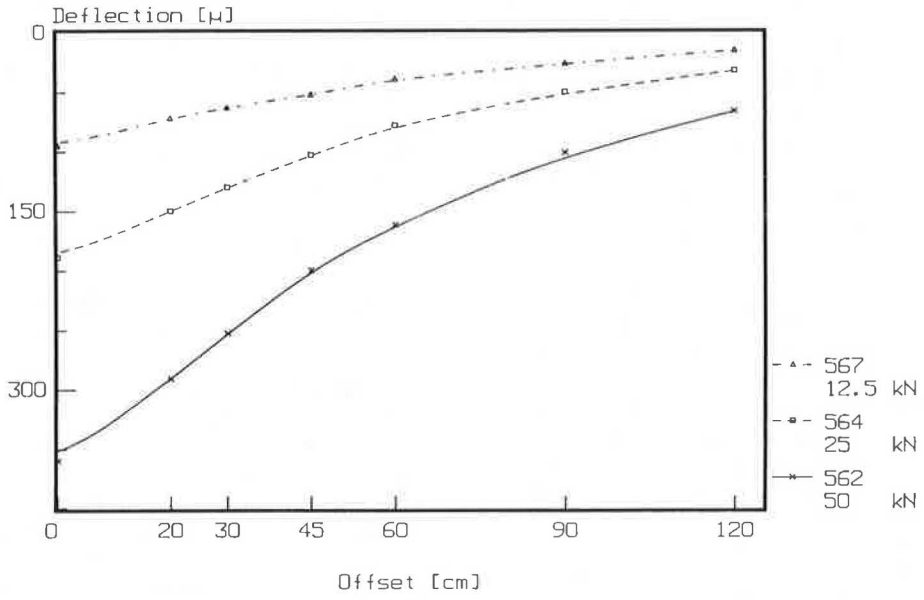

FIGURE 1 Deflection basins.

TABLE 1 D_0/D_{20} RATIO OF THE 8-cm AC LAYER

Ref.No	Time	Load [kN]	D_0 [μ]	D_0/D_{20}	Remark
530	am	50	488	.97	Skip
531	am	50	491	.97	Skip
532	am	26	272	1.05	Skip
533	am	26	273	1.04	Skip
534	am	13	146	1.12	Skip
535	am	13	146	1.12	Skip
569	pm	50	545	1.06	Skip
570	pm	50	541	1.29	O.K.
571	pm	25	299	1.38	O.K.
572	pm	25	301	1.33	O.K.
573	pm	13	158	1.36	O.K.
574	pm	13	149	1.30	O.K.
575	pm	50	533	1.35	O.K.

ments (i.e., thin and thick asphalt layer and morning and afternoon). Within these four groups the load was varied by a factor of four, between 12.5 and 50 kN. The deflections were strongly linearly correlated with the load. However, the number of data points for each set is only six or seven, and the data are spread over a wide range on three levels only, so high coefficients of determination are to be expected. Therefore, in addition to the coefficient of determination (r^2), the reasonableness of the regression line, like the slope and intercept, was scrutinized.

All 15-cm AC layer measurements yielded coefficients of determination near 1.00 for all cases. The regression line intercepts for load and deflection were all close to zero, and consequently the data were accepted in the study.

However, the D_0–D_{20} regression line for the 8-cm AC morning measurement showed the impossibility of D_{20} being higher than D_0. The intercept of regression lines involving sensors at 0 and 30 cm was as high as 51 μm, indicating unreasonable but consistent relationships. The afternoon measurements also exhibited some less comforting results, but by excluding the first measurement, reasonable slopes and intercepts were attained. Therefore, these measurements were considered valid in the study, even if the lighter load levels could be solved by excluding D_{20} in the calculations.

Only more testing on the site using other strain gauges could verify whether poor adhesion between core and pavement was the problem. Another plausible reason is faulty sensors on the FWD. However, none of these explanations fully clarifies why only the first of the seven measurements in the afternoon was incorrect.

BACKCALCULATED MODULI

The backcalculated moduli (rounded to two significant digits) and the corresponding deflection error are given in Tables 2 through 5. Table 6 summarizes the mean and standard de-

TABLE 2 BACKCALCULATED MODULI FOR D_{20} ON 15-cm PAVEMENT

Ref	Time	LOAD [kN]	Error [%]	AC Temp. [°C]	********** Modulus ********** AC [MPa]	Base [MPa]	Subgrade [MPa]
528	a.m.	50	5	15	8700	190	150
529	a.m.	50	3	15	9800	170	150
524	a.m.	25	2	15	7800	200	150
525	a.m.	25	6	15	7200	210	150
526	a.m.	25	3	15	6700	230	150
527	a.m.	12.5	11	15	4800	360	130
562	p.m.	50	7	27	5700	160	150
563	p.m.	50	1	26	5800	160	160
565	p.m.	25	5	26	5300	140	170
567	p.m.	12.5	9	24	4100	190	150
568	p.m.	12.5	8	24	3500	230	140

TABLE 3 BACKCALCULATED MODULI FOR D_{120} ON 15-cm PAVEMENT

Ref	Time	LOAD [kN]	Error [%]	AC Temp. [°C]	********** Modulus ********** AC [MPa]	Base [MPa]	Subgrade [MPa]
528	a.m.	50	7	15	10000	140	170
529	a.m.	50	5	15	11000	120	170
524	a.m.	25	10	15	10000	120	180
525	a.m.	25	10	15	8800	150	170
526	a.m.	25	15	15	9900	130	190
527	a.m.	12.5	18	15	6600	250	150
562	p.m.	50	8	27	6600	120	170
563	p.m.	50	3	26	6200	140	160
565	p.m.	25	2	26	5300	130	170
567	p.m.	12.5	22	24	5500	130	180
568	p.m.	12.5	12	24	4800	140	180

TABLE 4 BACKCALCULATED MODULI FOR D_{20} ON 8-cm PAVEMENT

Ref	Time	LOAD [kN]	Error [%]	AC Temp. [°C]	********** Modulus ********** AC [MPa]	Base [MPa]	Subgrade [MPa]
570	p.m.	50	4	26	7400	170	140
571	p.m.	25	3	25	6000	150	140
572	p.m.	25	5	25	5900	150	140
573	p.m.	12.5	11	25	5400	150	150
574	p.m.	12.5	5	24	7100	140	140

TABLE 5 BACKCALCULATED MODULI FOR D_{120} ON 8-cm PAVEMENT

Ref	Time	LOAD	Error	AC	********** Modulus **********		
				Temp.	AC	Base	Subgrade
		[kN]	[%]	[°C]	[MPa]	[MPa]	[MPa]
570	p.m.	50	11	26	8400	150	150
571	p.m.	25	14	25	6900	140	150
572	p.m.	25	19	25	7100	140	150
573	p.m.	12.5	23	25	7100	120	160
574	p.m.	12.5	8	24	7400	140	140

TABLE 6 MEAN AND STANDARD DEVIATION OF BACKCALCULATED MODULI (MPa)

Variable	Mean	Standard Deviation	Mean	Standard Deviation
	***** D_{20}	******	***** D_{120}	*****
Asphalt Concrete	6325	1650	7600	1880
Base	188	55	141	31
Subgrade	148	9	165	14

viation of the moduli for the two sensor locations. A wide range of AC moduli was achieved by the temperature variation, with a coefficient of variation of about 0.25. Use of the outer sensor location yielded higher AC moduli, and a regression equation between methods indicated an intercept of 1000 MPa and a slope of 1.04 (i.e., use of the outer sensor resulted in about 1 GPa higher modulus).

The base layer modulus also showed variability, which might be explained by stress sensitivity. However, no relation between load and base modulus was seen (r^2 = .08), and the variability is more likely to be an effect of the many possible solutions of finding a fitting basin. The subgrade modulus showed little variability and no noticeable stress sensitivity. The overall stress level was low, however, even for the 50-kN load. Depending on the sensors employed, the result was different—165 MPa for the outer sensor at 120 cm and 150 MPa for the inner sensor at 20 cm. No effort was made to determine the moduli by laboratory testing. The results using the sensor at 20 cm appear more realistic, because the base is stiffer than the subgrade, which is what would be expected for these materials. The mean error of the backcalculated basin was also lower for the sensor at 20 cm, or 5.5 percent versus 11.7 percent. However, later versions of CLEVERCALC using all seven sensors complied better with the five-sensor D_{120} setting.

BISAR CHECK OF MODULI, DEFLECTION, AND STRAIN

Many studies have compared results from different elastic layer programs. Most of these investigations appear to conclude that there is no significant difference between CHEVRON and BISAR. The former is used by CLEVERCALC. To check whether the conditions were prevalent for the present study, the BISAR program was used as a control of the backcalculated moduli and strains, and the CLEVERCALC moduli were used as input values.

Practically all deflections measured were retrieved with the BISAR program. An example, Reference 562, a 50-kN load on the thicker pavement, is given in Table 7. The largest discrepancy was found for the D_{120} sensor when comparing with the moduli yielded with the 0-20-30-60-90 sensors.

However, in this case the AC modulus differs 16 percent, the base modulus 33 percent, and the subgrade modulus 13 percent, depending on which sensors are used. Consequently, despite variability of the derived moduli, the deflections are well matched, as is the asphalt strain. Figure 2 shows a plot of strain versus center deflection. Because all material properties but the AC are constant, the relation is truly linear. The backcalculated strains, the BISAR-derived strains, and the measured strains are given in Tables 8 and 9. The tables also contain the deviation between gauge and CLEVERCALC as [(CLEVERCALC/Gauge) − 1] * 100.

DISCUSSION OF RESULTS

As Table 7 indicates, the deflection basin based on the backcalculated moduli shows a solid fit with the original measurement even though only five sensors were used in the backcalculation. There is a small discrepancy, though, for the outermost sensor when not employed itself. The backcalculated moduli constitute only one of many solutions to the deflection basin, and the great variability of the base and subbase suggests this fact. As pointed out above, the deflections correlated strongly with the load and with each other, indicating a linear relationship between stress and elastic response of the layers involved.

TABLE 7 DEFLECTIONS OBTAINED IN THE BISAR PROGRAM (μ)

Sensor	D_0	D_{20}	D_{30}	D_{45}	D_{60}	D_{90}	D_{120}
FWD-measurement	360	291	253	200	162	101	66
Backcal:d D20	357	295	254		158	103	
BISAR 20	357	297	256	202	160	105	75
Backcal:d D120	356		258		159	99	67
BISAR 120	356	300	260	207	162	102	69

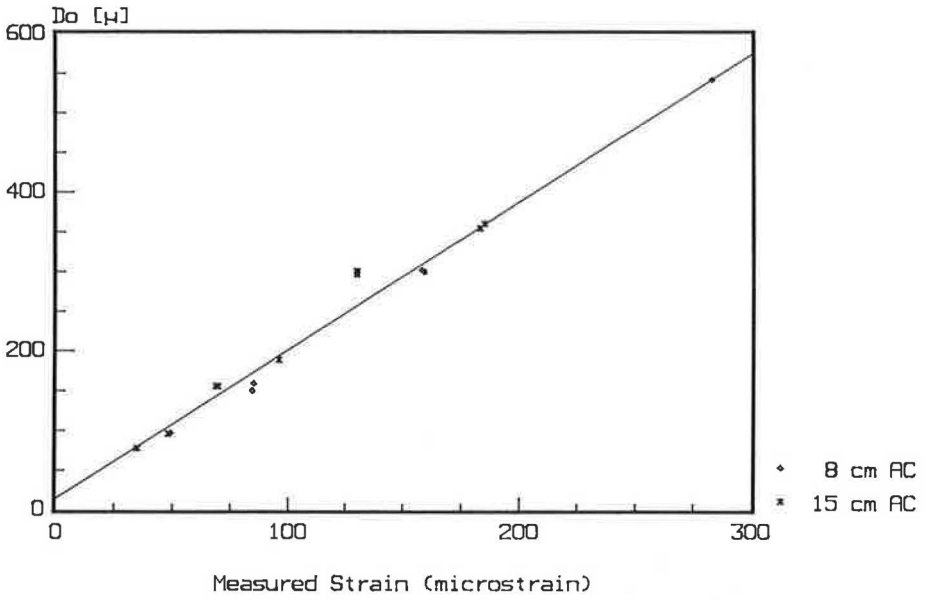

FIGURE 2 Strain versus center deflection ($Y = 14.5 + 1.88X$; $r^2 = .98$).

TABLE 8 FIFTEEN-cm AC PAVEMENT ASPHALT STRAIN

Ref	Time	Load [kN]	BISAR [μ/m]	CLEVERCALC [μ/m]	Gauge [μ/m]	Deviation [%]
524 - 20	am	25.6	72	72	69.5	+ 3
524 -120	am	25.6	66	66	69.5	- 6
525 - 20	am	25.7	75	75	69.0	+ 9
525 -120	am	25.7	71	71	69.0	+ 3
526 - 20	am	25.7	77	77	68.7	+12
526 -120	am	25.7	67	68	68.7	- 1
527 - 20	am	12.8	40	40	34.7	+14
527 -120	am	12.8	38	38	34.7	+ 9
528 - 20	am	50.3	133	133	130	+ 2
528 -120	am	50.3	127	127	130	- 2
529 - 20	am	50.2	125	125	130	- 4
529 -120	am	50.2	119	119	130	- 8
562 - 20	pm	50.1	189	189	185	+ 2
562 -120	pm	50.1	179	178	185	- 4
563 - 20	pm	50.3	186	186	183	+ 2
563 -120	pm	50.3	183	182	183	- 1
565 - 20	pm	25.4	103	103	95.9	+ 7
565 -120	pm	25.4	104	104	95.9	+ 8
567 - 20	pm	12.8	58	57	48.0	+19
567 -120	pm	12.8	51	51	48.0	+ 6
568 - 20	pm	12.8	59	58	48.5	+18
568 -120	pm	12.8	56	56	48.5	+14

TABLE 9 EIGHT-cm AC PAVEMENT ASPHALT STRAIN

Ref	Time	Load [kN]	BISAR [μ/m]	CLEVERCALC [μ/m]	Gauge [μ/m]	Deviation [%]
570 - 20	pm	50.1	296	295	283	+ 4
570 -120	pm	50.1	284	284	283	0
571 - 20	pm	25.4	175	174	159	+ 9
571 -120	pm	25.4	168	167	159	+ 5
572 - 20	pm	25.5	176	176	158	+11
572 -120	pm	25.5	167	167	158	+ 6
573 - 20	pm	12.8	95	95	84.8	+12
573 -120	pm	12.8	87	87	84.8	+ 2
574 - 20	pm	12.8	82	82	84.2	- 2
574 -120	pm	12.8	81	81	84.2	- 4

The modulus of a granular layer is a function of density, gradation, degree of saturation, angularity of the particles, and stress state (*7*). In this case the base, subbase, and subgrade were all made up of granular materials, but no dependency of load was derived, implying that a linear response could be anticipated.

However, the derived moduli may indicate some stress sensitivity, as in Figure 3, which shows the base modulus as a function of the AC modulus for the 15-cm AC layer, using the D_{120} sensor. Two temperature and hence modulus groups are clearly seen for the AC. Within each group the base modulus tends to increase slightly with decreasing AC modulus, which complies with the stress dependency. However, a test for independence indicates that the regression curve could be regarded as horizontal; thus, the two variables are independent of each other at the 1 percent level of significance. The regression line is

$$E_{base} = E_{asphalt} * 0.0032 + 168 \qquad (r^2 = .047) \qquad (1)$$

The extreme base modulus of 250 MPa is Blow 527, which did not solve better than 18 percent deflection error. The load was a 12.5-kN drop, a load level that generally rendered the most scatter. Omitting this point does not alter the regression much other than to lower the intercept:

$$E_{base} = E_{asphalt} * 0.00087 + 140 \qquad (r^2 = .049) \qquad (2)$$

At the 1 percent significance level, r^2 should be more than .585 to reject independence.

Figure 4 shows a plot of the load versus the AC modulus. The afternoon D_{120} measurement shows only slight dependence of the load, whereas the morning measurement exhibits increasing modulus with increasing load. The AC strain measured correlated almost perfectly with load for three stress levels at each combination of thickness and temperature.

Figure 5 shows a plot of load versus base modulus. Disregarding Blow 27 at the upper left part of the figure, no stress dependence is seen. The stress state is completely dominated by the load. The influence of the AC modulus is small.

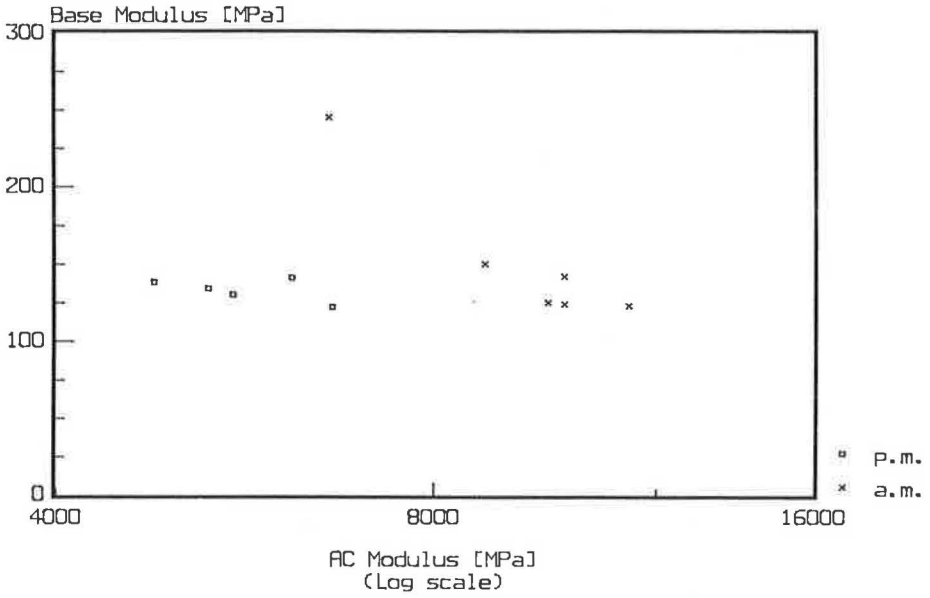

FIGURE 3 AC versus base modulus.

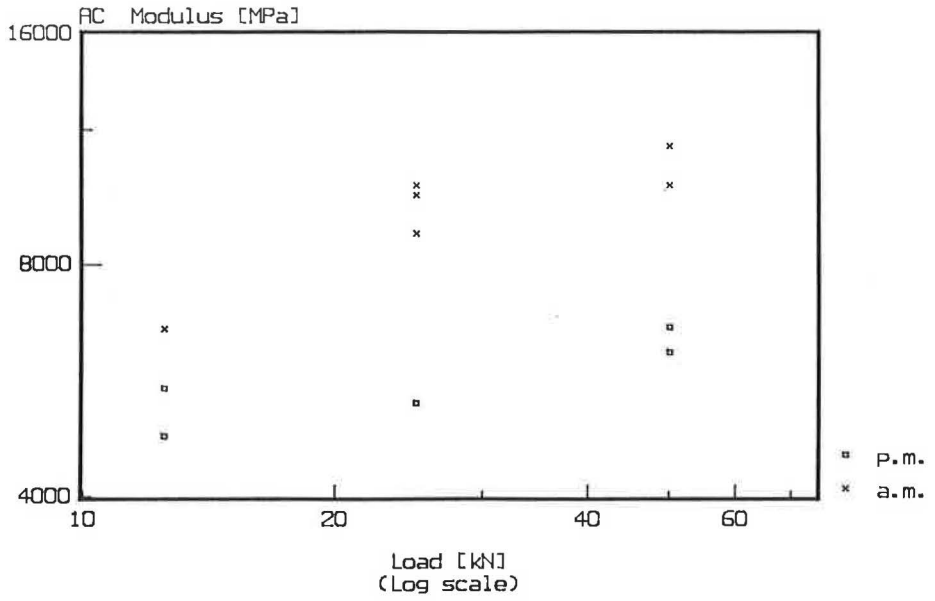

FIGURE 4 Load versus asphalt modulus.

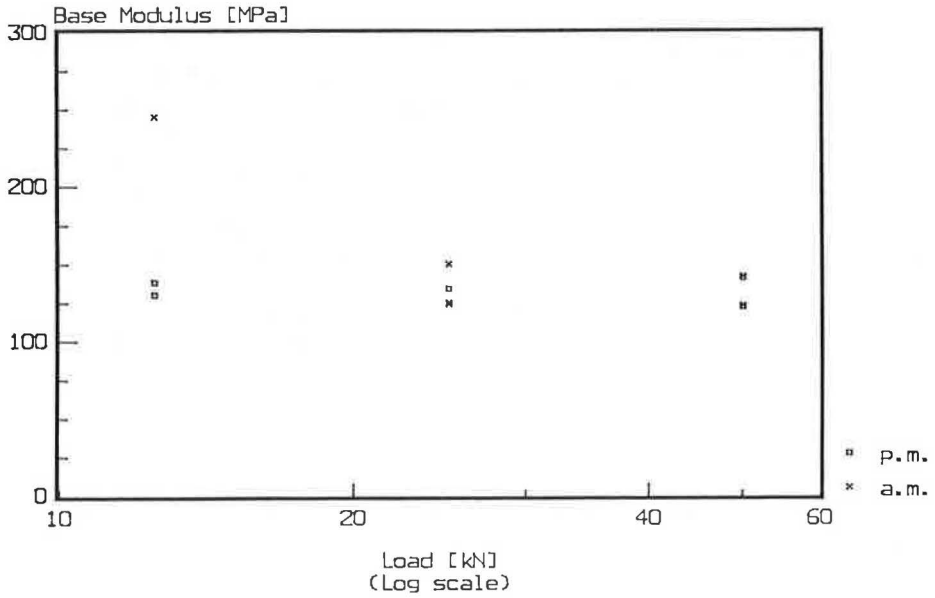

FIGURE 5 Load versus base modulus.

The stress state varied linearly with the load. Therefore, the scatter of the base modulus seen is probably an artifact of the program.

The same conclusions were drawn for several test sites, most of them with thin asphalt surfacings leading to higher stress states in the granular materials than in the present case, from a study in Norway (*11*). It challenges the benefit of using finite element methods, because they involve more material properties characterization than does the linear elastic, which in turn increases the uncertainties about the specimen tested.

Figure 6 shows a plot of the load versus the subgrade modulus. It is much less scattered, especially for the 50-kN loads. Note also the standard deviation in Table 6.

Despite the small variation of deflections from repeated loading, the program was unable to achieve consistent moduli. The base/subbase modulus varied by as much as a factor of 2.6, D_{20} calculations included. The subgrade, however, varied by only 28 percent. By excluding basins with a poorer fit than 10 percent deflection error, the variability of the base drops to 70 percent, still a high value.

It appears from experience that a common error of linear elastic program backcalculation is to underestimate the base layer modulus, which results in AC or subgrade moduli that are too high. That error appears to be more common if the outer 120-cm sensor is used in the process. The farther away a sensor, the more it is affected by deeper layers and naturally

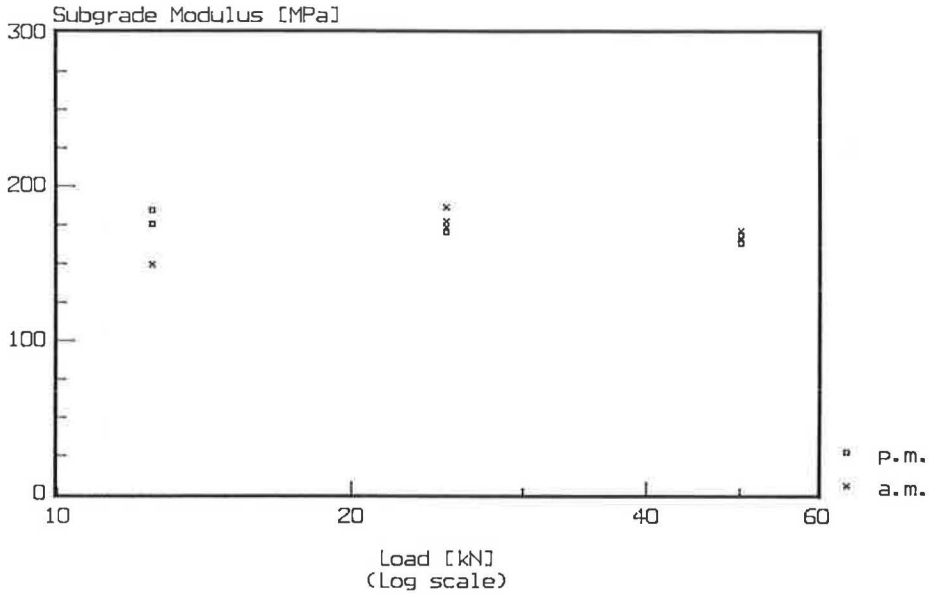

FIGURE 6 Load versus subgrade modulus.

at some point a rigid base, which may disrupt the semi-infinite subgrade model.

It may be argued that the moduli are not inherently that important as long as the parameters used for overlay design criteria are fairly accurate. Indeed, the agreement between the measured and backcalculated strains is surprisingly good (see Figure 7 and Tables 8 and 9). The coefficient of determination is as high as .99 for both the D_{20} and D_{120} solutions. This is also the case for the newer program employing all seven sensors. All three display intercepts near zero and slopes near 1 in their respective regression lines. The mean deviation for all 32 basins is 4.6 percent with a slight overestimate of the strain. If design life is considered according to the fourth power of the strain, it translates to an overestimate of 20 percent, still within a reasonable tolerance.

By breaking down the material in subgroups, it can be seen that the 12.5-kN load solved for the 120-cm sensor shows the highest mean deviation, 12.2 percent (see Table 10). The 50-kN load most commonly used for routine measurements actually displays a slight underestimate of the strain. No other clear trend among the subgroups can be seen, partly because of an insufficient number of observations. However, the D_{120} solutions are closer to the strain gauge measurements, the mean deviation being only 1.7 percent as opposed to 7.4 percent with the 20-cm sensor or -3.1 percent for all seven sensors used.

The thickness of the pavement layers was accurately known in the present field study. Further, the construction materials were homogeneous, something that is not always encountered in routine work, especially dealing with overlays. Even if

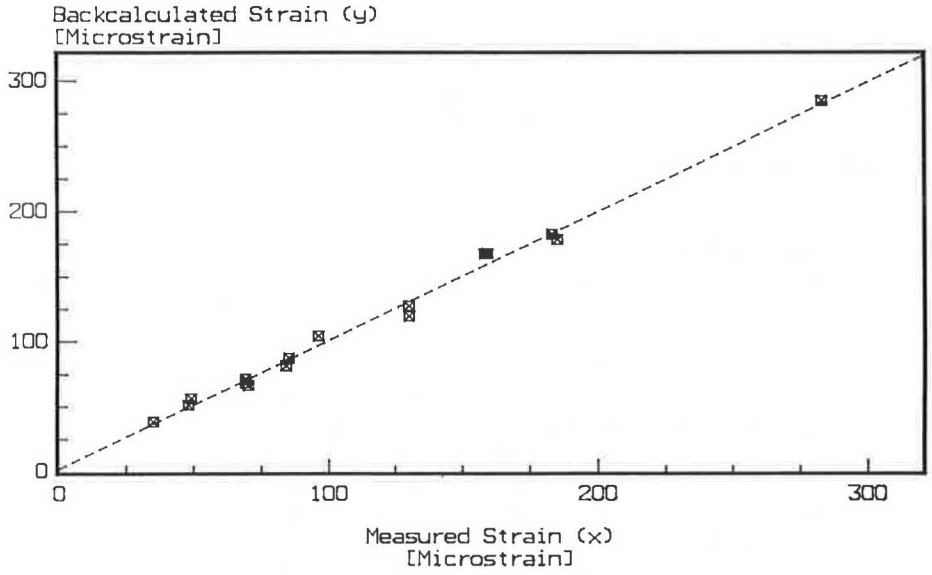

FIGURE 7 D_{120} regression line ($Y = 2.11 + 0.989X$; $r^2 = .992$).

TABLE 10 MEAN RELATIVE ERROR FOR VARIOUS COMBINATIONS OF BACKCALCULATED STRAIN

Group	N	Mean	Standard Deviation
ALL, $D_{20}+D_{120}$	32	.045	.069
15 cm	22	.046	.077
8 cm	10	.043	.054
12 kN	10	.088	.081
12 kN-20	5	.122	.084
12 kN-120	5	.054	.068
25 kN	12	.055	.052
25 kN-20	6	.085	.032
25 kN-120	6	.025	.052
50 kN	10	-.009	.037
50 kN-20	5	.014	.032
50 kN-120	5	-.030	.079
D_{20}	16	.074	.068
D_{120}	16	.017	.060
Seven sensors	16	-.031	.060
D_{20} 15cm	11	.077	.074
D_{120} 15cm	11	.016	.070
D_{20} 8cm	5	.069	.058
D_{120} 8cm	5	.018	.041

normal conditions do not always allow for detailed surveying, it is encouraging that the calculated strains match the measured strains under these controlled conditions.

CONCLUSIONS

Good agreement was obtained between the asphalt pavement strain established by a backcalculation procedure and the measured strain in the pavement.

The 12.5-kN loading showed higher variability of the derived moduli, perhaps because of proportionally less resolution of the deflection readings.

The relation between deflections and strains for the program used based on the CHEVRON N-layer elastic analysis did not differ from BISAR for the loading conditions and pavements tested.

Even if the asphalt strain compared well, repeated loading yielded less compliant moduli. The latter may be caused by the change of modulus routine allowing a solution where the deflection basins do not match. The convergence of backcalculation programs should perhaps employ more sophisticated routines in the iteration process (*12*).

ACKNOWLEDGMENTS

The author wants to acknowledge RST-Sweden AB, which sponsored the FWD measurements. The Road and Traffic Laboratory in Finland provided the data from the strain gauges, and its cooperation is also deeply appreciated.

REFERENCES

1. M. R. Thompson. ILLI-PAVE Based NDT Analysis Procedures. In *Nondestructive Testing of Pavements and Backcalculation of Moduli*, STP 1026, ASTM, Philadelphia, Pa., 1988, pp. 487–502.
2. W. P. Kilareski and B. A. Anani. Evaluation of In-Situ Moduli and Pavement Life from Deflection Basins. *Proc., 5th International Conference on the Structural Design of Asphalt Pavements*, Delft, the Netherlands, Vol. 1, 1982, pp. 349–366.
3. J. P. Mahoney, N. F. Coetzee, R. N. Stubstad, and S. W. Lee. A Performance Comparison of Selected Backcalculation Computer Programs. In *Nondestructive Testing of Pavements and Backcalculation of Moduli*, STP 1026, ASTM, Philadelphia, Pa., 1988, pp. 452–467.
4. T. Rwebangira, R. G. Hicks, and M. Truebe. Sensitivity Analysis of Selected Backcalculation Procedures. In *Transportation Research Record 1117*, TRB, National Research Council, Washington, D.C., 1987, pp. 25–37.
5. A. J. Bush III. *Nondestructive Testing of Light Aircraft Pavements, Phase II: Development of the Nondestructive Evaluation Methodology*. Report FAA-RD-80-9-II. Federal Aviation Administration, U.S. Department of Transportation, 1980.
6. *EVERCALC User's Guide*. University of Washington and Washington State Department of Transportation, 1987.
7. R. G. Hicks and C. L. Monismith. Factors Influencing the Resilient Response of Granular Materials. In *Highway Research Record 345*, HRB, National Research Council, Washington, D.C., 1971, pp. 15–31.
8. S. W. Lee, J. P. Mahoney, and N. C. Jackson. Verification of Backcalculation of Pavement Moduli. In *Transportation Research Record 1196*, TRB, National Research Council, Washington, D.C., 1988, pp. 85–95.
9. M. Huhtala, J. Pihlajamäki, and M. Pienimäki. Effects of Tires and Tire Pressures on Road Pavements. In *Transportation Research Record 1227*, TRB, National Research Council, Washington, D.C., 1989, pp. 107–114.
10. D. Newcomb. Development and Evaluation of Regression Method To Interpret Dynamic Pavement Deflections. Ph.D. dissertation. University of Washington, Seattle, 1986.
11. H. Mork. Analyse av lastresponsrar for vegkonstruksjonar. Doktor Ingeniöravhandling. 1988:6 Institutt for veg- og jernbanebyggning. Universitetet i Trondheim, Trondheim, Norway, NTH 1990 (Norwegian).
12. F. W. Jung. Interpretation of Deflection Basin for Real-World Materials in Flexible Pavements. Presented at 69th Annual Meeting of the Transportation Research Board, Washington, D.C., 1990.

Backcalculation of Asphalt Concrete–Overlaid Portland Cement Concrete Pavement Layer Moduli

KATHLEEN T. HALL AND ALAEDDIN MOHSENI

The United States currently has a large and growing mileage of portland cement concrete (PCC) highway pavement overlaid with asphalt concrete (AC). Evaluation of existing AC/PCC pavements and selection of second rehabilitation strategies are thus becoming increasingly pressing concerns of state highway agencies. Use of deflection test data to interpret the condition of the underlying PCC is crucial to a structural evaluation and second overlay design for this type of pavement. However, interpretation of deflection measurements is perhaps more difficult for AC/PCC pavement than for any other pavement type. Many of the available tools for backcalculation of pavement layer moduli are limited in their ability to successfully analyze AC/PCC pavement. A simple and straightforward procedure for backcalculation of AC/PCC pavement layer moduli is described. The approach is built on available closed-form solutions to backcalculation for bare PCC pavement, with adjustments made to measured deflections to account for the influence of the AC layer. An example using deflection data collected on an AC-overlaid PCC Interstate highway section indicates that the backcalculation procedure produces reasonable results that are consistent with those obtained from other backcalculation methods and with the known condition of the pavement.

The most widely used rehabilitation technique for portland cement concrete (PCC) pavements is resurfacing with asphalt concrete (AC). Many states have already overlaid substantial portions of their PCC highway pavement mileage with AC and plan to overlay more in the near future. Thus, the mileage of AC-overlaid PCC is growing. Evaluation and rehabilitation of AC/PCC pavements are becoming increasingly prominent and pressing concerns of state highway agencies.

Much of the distress seen in AC/PCC pavements is reflected from deterioration in the underlying PCC slab. The PCC distresses that are most responsible for AC overlay deterioration are slab cracking, punchouts, joint deterioration, deterioration resulting from poor PCC durability ("D" cracking and reactive aggregate distress), and deterioration of PCC and AC patches. The deterioration will also reflect through a second AC overlay unless it is identified and corrected. This requires a coordinated effort of distress surveying, nondestructive deflection testing (NDT), and coring for materials samples. The information obtained is valuable in establishing a profile of condition along the length of the project, which may then be used to identify areas requiring repair and to determine second rehabilitation options.

Department of Civil Engineering, University of Illinois at Urbana-Champaign, Urbana, Ill.

Analysis of deflections measured at locations where the underlying PCC is severely deteriorated, as in the case of "D" cracking, will invariably produce extremely low backcalculated PCC modulus values. They should not be interpreted as the true stress-strain response of the PCC as a homogeneous elastic layer, but rather as an indication of the extent to which its behavior departs from that of a sound slab (i.e., the extent of the PCC's deterioration). The ability to diagnose the condition of the PCC from deflection measurements is particularly valuable in evaluation of AC/PCC pavements, because the extent of the deterioration of the PCC is often not fully evident from visible distress. In some cases, the deterioration of the PCC may be so severe and widespread that the only feasible rehabilitation alternatives are substantial structural improvements, such as a very thick AC overlay, an unbonded PCC overlay, or reconstruction.

Structural evaluation using NDT data is perhaps more difficult for AC/PCC pavements than for all other pavement types. The available computer programs for backcalculation of pavement layer moduli possess a variety of theoretical and practical limitations, which hinder their usefulness in AC/PCC pavement analysis. Valid and repeatable results are typically only obtained from even the best of these tools by knowledgeable pavement engineers with considerable experience in backcalculation.

Previous research (*1*,*2*) has demonstrated that a closed-form solution exists for backcalculation of PCC and subgrade moduli for slab-on-grade systems. One of the advantages of this direct approach to determination of pavement layer properties is its efficiency in processing deflection data. However, the direct approach applies only to two-layer systems in which the top layer behaves like a plate (e.g., a PCC slab). This approach is not directly applicable to analysis of AC-overlaid PCC pavements, because it does not account for the influence of the AC overlay on deflections. The adaptations to the closed-form approach that are required for backcalculation of AC/PCC pavement layer moduli are described in this paper.

LIMITATIONS OF AVAILABLE BACKCALCULATION TOOLS

Most of the tools currently used for backcalculation of pavement moduli are computer programs based on multilayer elastic theory. The programs determine the elastic moduli of pavement layers by matching deflection basin measurements to

deflections predicted by multilayer elastic theory, given the layer thicknesses and Poisson's ratios and the magnitude and area of the applied load. A few backcalculation programs exist that use the equivalent thickness concept (i.e., reduction of a multilayer elastic system to an equivalent system of fewer layers for which a solution is more easily obtainable). Backcalculation may also be done using plate theory [i.e., two-layer elastic theory for the special case of a rigid upper layer that exhibits pure bending (without shear deformation) in response to load].

In backcalculation programs based on multilayer elastic theory, actual deflections are matched to predicted deflections in one of two ways: by iterative numeric integration of elastic layer equations or by searching a data base of deflection basins that have been generated for ranges of layer thicknesses and moduli. Backcalculation by the equivalent thickness method may also be done by iteration or by data base search. Iteration was used in the first plate theory backcalculation routines, but has since been replaced by direct solution of closed-form equations.

Iterative Backcalculation Programs

BISDEF (*1*), CHEVDEF (*2*), WESDEF (*3*), and ELSDEF are examples of iterative backcalculation programs that make repetitive calls to an elastic layer analysis subroutine [e.g., BISAR (*4*) for BISDEF] in order to match measured deflections to deflections predicted for program-selected layer moduli. The process stops when the measured and predicted deflections match within tolerance levels set by the user or when the maximum number of iterations set by the user is reached. A detailed description of the solution algorithm used in these programs is given by Anderson (*5*).

One limitation of iterative elastic layer backcalculation programs is that they require the user to enter starting values and ranges for the layer moduli. Unless appropriate starting values are selected, the program may never converge to a solution within the selected ranges. Some researchers have noted that there is no unique solution to the set of moduli that will produce a given deflection basin. Rather, there are as many solutions as there are layers in the pavement structure (*6-8*). As a result, the solution toward which the program converges depends on the initial or "seed" modulus values selected. The boundary values must also be selected judiciously. Limits that are too narrow may prevent the program from converging to the correct solution. Limits that are too broad may allow the program to converge to an incorrect solution, particularly if inappropriate seed moduli are selected. Success with these programs thus requires not only a good knowledge of pavements but also experience in backcalculation for the specific pavement type in question. It has even been suggested that iterative elastic layer backcalculation can never be truly automated until an expert system is developed to guide decisions such as selection of seed moduli (*6,9*).

A second limitation of iterative elastic layer backcalculation is that it is time-consuming, increasingly so for increasing number of layers. Convergence to a solution may require several iterations for a pavement system of three or more layers. The iterative backcalculation programs available today cannot process deflection data at a rate even close to that at which deflection data may be collected in the field.

In general, the iterative elastic layer backcalculation programs available do not perform well in analyzing AC/PCC pavements, for both of the reasons cited above. Frequently they are unable to match predicted and actual deflection basins within reasonable tolerance levels even when given broad ranges of moduli and permitted to run several iterations. Their tendency is to underpredict the modulus of the AC surface, often going to the lower limit of the AC modulus range allowed by the user, and consequently overpredicting the modulus of the PCC slab. As a result, it is necessary to confine the AC modulus to a narrow range bracketing an appropriate value [determined by independent means (e.g., as a function of AC mix temperature)] to obtain meaningful backcalculated modulus values for the PCC layer. The long execution time required for backcalculation of AC/PCC pavement layer moduli is also a significant limitation. Analysis of several dozen AC/PCC pavement deflection basins, such as might be measured on a highway section a few miles in length, may require several hours of program execution even on a high-end personal computer.

BOUSDEF (*10*) is an iterative backcalculation program similar to BISDEF, except that deflections for trial layer moduli combinations are computed not by an elastic layer subroutine but rather an equivalent thickness subroutine. This dramatically reduces execution time, which is BOUSDEF's major advantage over the BISDEF class of programs. However, the appropriateness of BOUSDEF for backcalculation of AC/PCC pavement layer moduli is questionable because of violation of assumptions of the equivalent thickness method. These include the assumptions that the pavement layers above the subgrade exhibit pure bending behavior, that all layers are fully bonded at their interfaces, that the layer moduli decrease with depth, and that the equivalent thickness of any layer (with respect to the layer below) is larger than the radius of the applied load.

Data Base Backcalculation Programs

Data base backcalculation programs run much more quickly than iterative programs but require a large amount of computer storage. Furthermore, a data base backcalculation program can only be applied to situations comparable with that for which the data base was generated (i.e., number of layers, material types, ranges of thicknesses and elastic moduli, interface bonding conditions, magnitude and geometry of loading, and number and spacing of sensors).

Of the backcalculation programs currently available, the data base–type program COMDEF (*11*) is the only one developed specifically for AC/PCC pavements. COMDEF's data base of deflection basins contains the results of more than 40,000 elastic layer program (BISAR) runs. As a result, the complete COMDEF data base occupies more than 4 megabytes of hard disk space on a personal computer. It is possible to load portions of the data base corresponding to the specific cross sections of interest to conserve hard disk space. A second and more serious limitation of COMDEF is that it requires deflections for seven sensors at 12-in. spacings; it cannot accommodate fewer sensors or other spacings. COMDEF

does not permit the user to choose whether to model the AC/PCC interface condition as bonded or unbonded, and the program's documentation does not indicate which interface condition (presumably bonded) was used in the development of the data base.

MODULUS (*12*) is a data base backcalculation program in which the deflection basin data base is produced by a factorial of elastic layer program (CHEVRON) runs. MODULUS was developed for analysis of flexible pavements, but it may be used to analyze AC/PCC pavements. This process may take 15 min to 1 hr, depending on the pavement structure and the capabilities of the computer used, and must be repeated for every cross section of interest. At least 1 megabyte of hard disk space must be available to store the generated data base. Once the data base is generated, analysis of deflection data proceeds quickly.

Closed-Form Backcalculation

ILLIBACK (*13,14*) is a backcalculation program based on closed-form solution of plate theory equations, intended for use in analysis of bare PCC pavements. ILLIBACK executes more quickly than any other available backcalculation program and could conceivably be used for real-time analysis of deflection data in the field. It is the only available backcalculation program that determines a modulus of subgrade reaction (k value, psi/in.) as well as an elastic modulus for the subgrade. However, the current version of ILLIBACK can only be used for bare PCC pavements. Work is under way to modify ILLIBACK to address two-layer plate systems, for example, a PCC pavement with a bonded or unbonded PCC overlay, or a PCC pavement with a stabilized base.

Even with these modifications, however, ILLIBACK would not be an appropriate tool for analysis of AC/PCC pavement, because modeling the AC as a plate would fail to account for the significant compression that occurs in an AC overlay of a PCC slab. Nonetheless, for the purposes of AC/PCC pavement backcalculation, the efficiency and repeatability of the closed-form approach to backcalculation make it the most appealing of the available backcalculation schemes, if it can be modified to account for the behavior of the AC surface.

CLOSED-FORM BACKCALCULATION FOR BARE PCC PAVEMENT

For a bare PCC pavement, the PCC slab's elastic modulus (E_{pcc}) and the subgrade k value or elastic modulus (E_s) may both be backcalculated from the maximum deflection d_0 and the *AREA* of the deflection basin as defined by the following equation:

$$AREA = 6 * \left[1 + 2\left(\frac{d_{12}}{d_0}\right) + 2\left(\frac{d_{24}}{d_0}\right) + \left(\frac{d_{36}}{d_0}\right)\right] \quad (1)$$

where d_0 is the maximum deflection at the center of the load plate in inches and d_{12}, d_{24}, and d_{36} are the deflections at 12, 24, and 36 in. from the plate center, respectively, in inches.

AREA has units of length, rather than area, because each of the deflections is normalized with respect to d_0 in order to remove the effect of different load levels and to restrict the range of values obtained. *AREA* and d_0 are thus independent parameters from which the two unknown values E_{pcc} and k or E_s may be determined for a known slab thickness. This approach to direct backcalculation of slab and subgrade properties was first proposed by Hoffman and Thompson (*15*) and further validated by ERES (*16*) and Foxworthy (*17*). Further investigation of this concept by Ioannides (*13,14*) has produced a closed-form solution procedure to replace the iterative and graphical procedures used previously, as well as the computer program ILLIBACK for rapid analysis of deflection basin data for slab-on-grade pavement systems.

AREA Versus ℓ

Research by Ioannides (*13,14*) has demonstrated that for a given load radius and sensor arrangement, a unique relationship exists between *AREA* and the "dense liquid" radius of relative stiffness of the pavement, in which the subgrade is characterized by a k value (*18*):

$$\ell_K = \left[\frac{E_{pcc} D_{pcc}^3}{12(1 - \mu_{pcc}^2) k}\right]^{1/4} \quad (2)$$

where

ℓ_k = dense liquid radius of relative stiffness (in.),
E_{pcc} = PCC elastic modulus (psi),
D_{pcc} = PCC thickness (in.),
μ_{pcc} = PCC Poisson's ratio, and
k = k value (psi/in.).

A separate unique relationship exists between *AREA* and the "elastic solid" radius of relative stiffness of the pavement, in which the subgrade is characterized by an elastic modulus and a Poisson's ratio (*19*):

$$\ell_e = \left[\frac{E_{pcc} D_{pcc}^3 (1 - \mu_s^2)}{6(1 - \mu_{pcc}^2) E_s}\right]^{1/3} \quad (3)$$

where

ℓ_e = elastic solid radius of relative stiffness (in.),
μ_s = subgrade Poisson's ratio, and
E_s = subgrade elastic modulus (psi).

The equations for deflection of a PCC slab resting on a dense liquid foundation or an elastic solid foundation have been summarized by Ioannides (*13*). For this study, these equations were solved for radial distances of 0, 12, 24, and 36 in. and for ℓ_k and ℓ_e values from 15 to 80 using the IMSL (*20,21*) library of functions available on the Apollo network of UNIX workstations at the University of Illinois. The deflections computed were used to obtain an *AREA* corresponding to each value of ℓ_k and ℓ_e. The results are shown in Figure 1.

Because the curves asymptotically approach an *AREA* value of 36 in., an appropriate and meaningful equation form for modeling the relationship of *AREA* to ℓ is that of an asymptotic regression model, also called a monomolecular growth model (*22*). Such a model has the following general form:

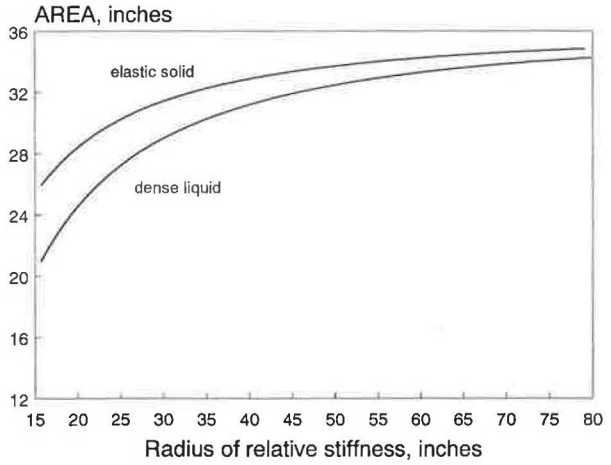

FIGURE 1 Relationship of *AREA* to radius of relative stiffness ℓ_k and ℓ_e for load radius a = 5.9 in.

$$AREA = k_1 - k_2\, e^{-k_3 \ell^{k_4}} \tag{4}$$

where

k_1 = the asymptotic y value,
k_2 = parameter for the range of *AREA* values, and
k_3, k_4 = scale parameters that govern the rate of growth.

The model must be rearranged to predict ℓ_k or ℓ_e as a function of *AREA*. The SAS statistical analysis software (*23*) was used to determine the parameters for each model by nonlinear regression.

$$\ell_k = \left[\frac{\ln\left(\frac{36 - AREA}{1812.279}\right)}{-2.559}\right]^{\frac{1}{0.228}} \tag{5}$$

[residual R^2 = 99.99 percent (predicted versus actual values), σ_Y = 0.097 in., n = 63, and residual range = 0.996 to 1.018].

$$\ell_e = \left[\frac{\ln\left(\frac{36 - AREA}{4521.676}\right)}{-3.645}\right]^{\frac{1}{0.187}} \tag{6}$$

[residual R^2 = 99.99 percent (predicted versus actual values), σ_Y = 0.118 in., n = 83, and residual range = 0.996 to 1.023].

Subgrade k or E_s

With *AREA* calculated from measured deflections, ℓ_k or ℓ_e may be obtained from Equations 5 or 6 or from Figure 1. The k value may then be obtained from Westergaard's (*18*) deflection equation:

$$k = \left(\frac{P}{8 d_0\, \ell_k^2}\right) \times \left\{1 + \left(\frac{1}{2\pi}\right)\left[\ln\left(\frac{a}{2\ell_k}\right) + \gamma - 1.25\right]\left(\frac{a}{\ell_k}\right)^2\right\} \tag{7}$$

where

P = applied load (lb),
d_0 = maximum deflection at center of load (in.),
a = load radius, and
γ = Euler's constant, 0.57721566490.

Figure 2 was developed from Equations 5 and 7 for load P = 9,000 lb and load radius a = 5.9 in. For loads within about 2,000 lb of this value, the deflections d_0, d_{12}, d_{24}, and d_{36} may be scaled linearly to 9,000-lb deflections.

The elastic modulus of the subgrade (E_s) may be obtained from Losberg's (*19*) deflection equation:

$$E_s = \left[\frac{2P(1 - \mu_s^2)}{d_0\, \ell_e}\right]\left[0.19245 + 0.0272 \times \left(\frac{a}{\ell_e}\right)^2 + 0.0199\left(\frac{a}{\ell_e}\right)^2 \ln\left(\frac{a}{\ell_e}\right)\right] \tag{8}$$

Figure 3 was developed from Equations 6 and 8 for load P = 9,000 lb, load radius a = 5.9 in., and subgrade Poisson's ratio μ_s = 0.50. For loads within about 2,000 lb of this value, the deflections d_0, d_{12}, d_{24}, and d_{36} may be scaled linearly to 9,000-lb deflections.

PCC Elastic Modulus

Once the k value or elastic modulus of the subgrade is known, the elastic modulus of the PCC slab may be determined using the appropriate (dense liquid or elastic solid) definition of the radius of relative stiffness. Figure 4 was developed from Equations 2 and 5 for PCC Poisson's ratio μ_{pcc} = 0.15 and load radius a = 5.9 in. Figure 5 was developed from Equations 3 and 6 for PCC Poisson's ratio μ_{pcc} = 0.15, subgrade Poisson's ratio μ_s = 0.5, and load radius a = 5.9 in. For either support characterization, the PCC elastic modulus E_{pcc} may be determined for a known value of slab thickness, D_{pcc}.

BACKCALCULATION FOR AC/PCC PAVEMENT

AC Elastic Modulus

To remove the effect of the AC surface from the NDT data, the elastic modulus of the AC layer must be determined. The recommended method for determining E_{ac} is to monitor the temperature of the AC mix during deflection testing and to use a relationship between E_{ac} and temperature. The AC mix temperature may be measured directly or estimated from surface or air temperatures using procedures developed by Southgate (*26*), Shell (*27*), the Asphalt Institute (*28*), or Hoffman and Thompson (*15*). Air temperature data may be recorded during deflection testing or obtained from a local weather station.

The relationship between AC modulus and temperature is shown in Figure 6, developed by Thompson and Cation (*29*) for typical Illinois Department of Transportation mixes. The curves shown in Figure 6 apply to new AC mixes. AC that has been in service for some years may have a different modulus for any given temperature. The third line in Figure 6 is drawn for the AC cores used in the example described later.

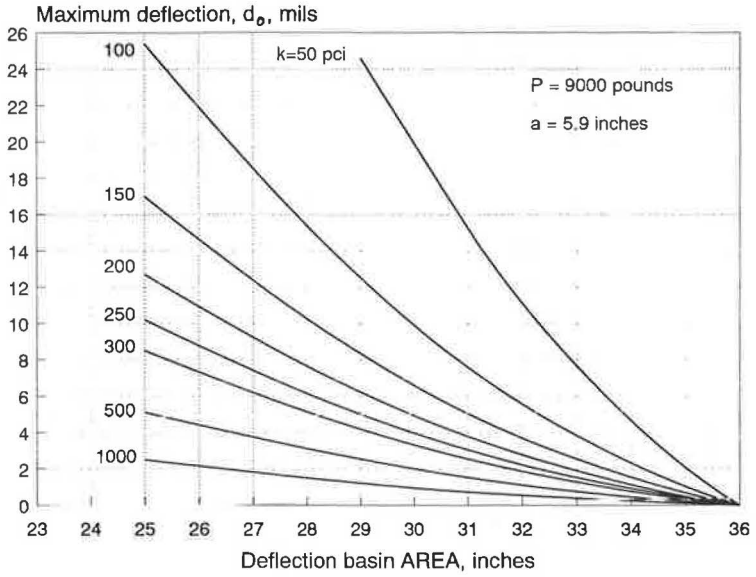

FIGURE 2 Effective k value determination from d_0 and *AREA*.

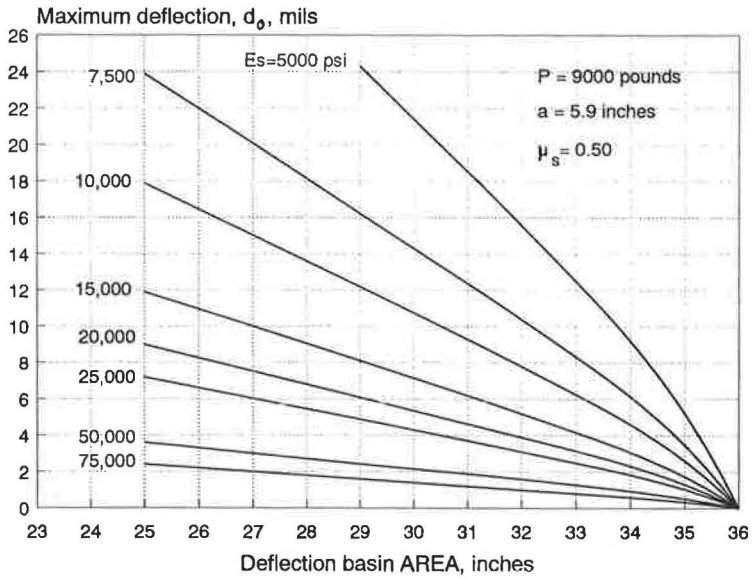

FIGURE 3 E_s determination from d_0 and *AREA*.

Diametral resilient modulus testing (ASTM D 4123) may be conducted at one or more temperatures on AC cores taken from the pavement in order to establish points for a curve for the E_{ac} versus temperature. However, because it may not be feasible to conduct this type of testing, correlations may be established between AC resilient modulus and indirect tensile strength, which may be more readily determined. Equation 13, developed by Carpenter and VanDam (*30*) for 4-in.-diameter samples of AC mixes at 72°F with typical Illinois Department of Transportation gradations and ranges of asphalt contents, asphalt stiffnesses, and compaction efforts, is an example of such a correlation:

$$M_R = 35{,}632 + 4{,}446\ (S_{IT}) \quad (9)$$

(R^2 = 85 percent and n = 56) where M_R is AC resilient modulus (psi) and S_{IT} is AC indirect tensile strength (psi).

This particular relationship is specific to the AC mixes tested. Similar relationships could be developed for other AC mixes.

d_0 of PCC Layer

The elastic layer program BISAR was used to model AC/PCC pavement structures over a broad range of parameters:

Parameter	*Values*
AC thickness	2, 4, and 6 in.
AC modulus	100, 500, and 1,000 ksi
PCC thickness	6, 8, and 12 in.
PCC modulus	3 million and 7 million psi
Subgrade modulus	6, 24, and 42 ksi
AC/PCC interface	bonded and unbonded

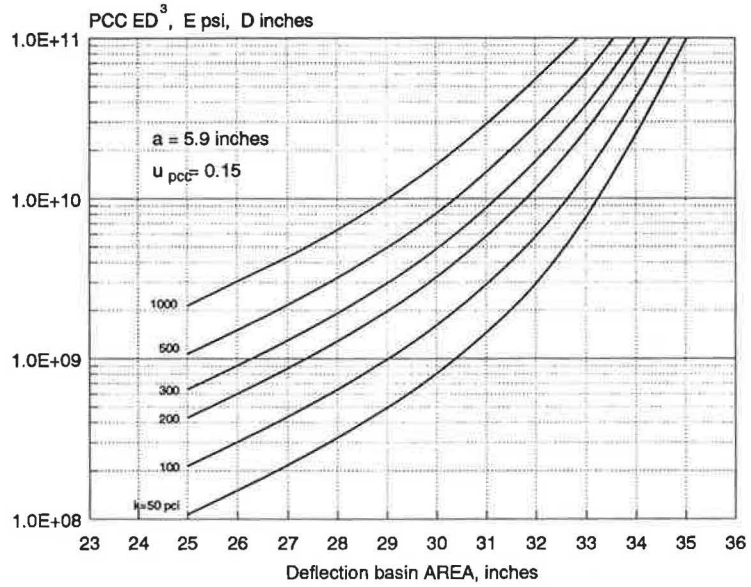

FIGURE 4 PCC elastic modulus determination from *k* value, *AREA*, and slab thickness.

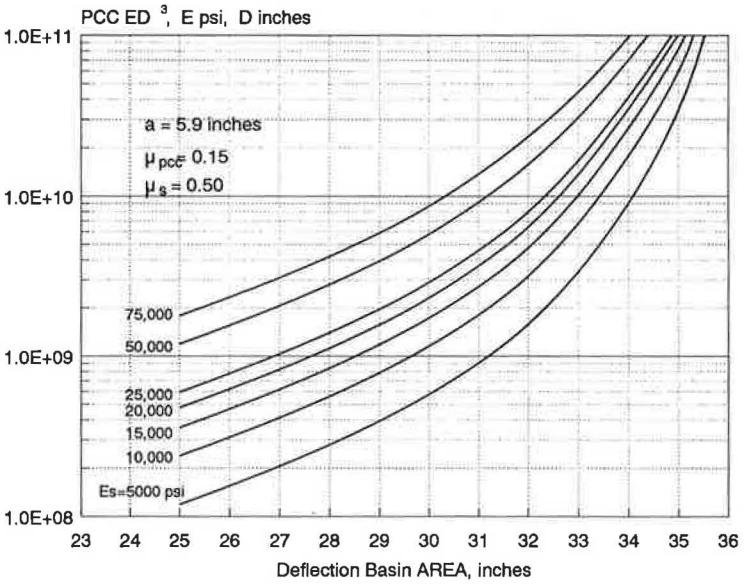

FIGURE 5 PCC elastic modulus determination from E_s, *AREA*, and slab thickness.

A load magnitude of 9,000 lb and a load radius of 5.9 in. were used. Poisson's ratio values used for the AC, PCC, and subgrade were 0.35, 0.15, and 0.5, respectively. The PCC/subgrade interface was modeled as unbonded.

Deflections were computed at the surface of the AC and the surface of the PCC at radial offsets of 0, 12, 24, and 36 in. Compression in the AC layer, as indicated by the change in d_0 between the AC and PCC surfaces, often accounted for a significant portion of the total deflection, depending primarily on the thickness and modulus of the AC and the stiffness of the subgrade, and to a lesser extent on the interface condition and the thickness and stiffness of the PCC slab. For example, in systems with a stiff subgrade (42 ksi), low AC modulus (100 ksi), and thick AC layer (6 in.), more than 50 percent of the total deflection in the pavement occurred in the AC layer.

The change in d_0 is significantly greater when the AC is not bonded to the PCC than when it is bonded. For each interface bonding condition, it was found that the change in d_0 could be predicted reliably as a function of the ratio of the AC thickness to AC modulus (D_{ac}/E_{ac}). These relationships were found to be insensitive to the ranges of other parameters

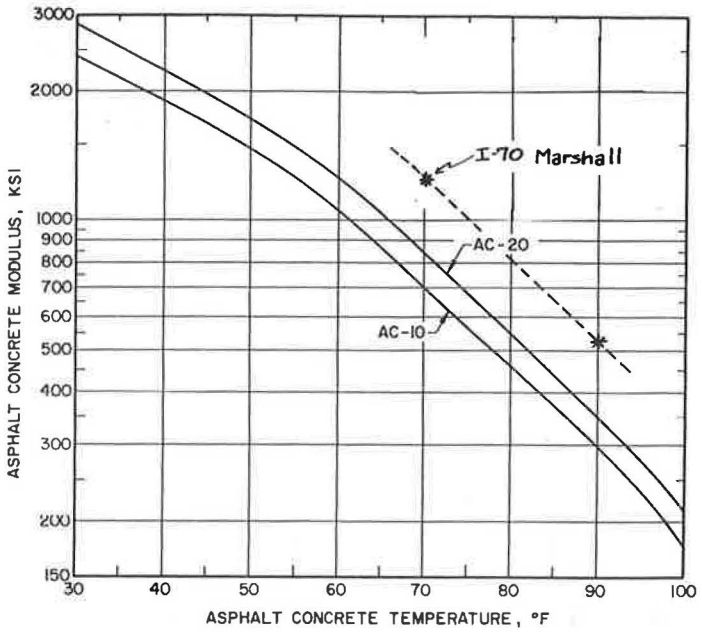

FIGURE 6 Asphalt concrete modulus–temperature relations for typical Illinois Department of Transportation Class I mixtures (*29*).

investigated. Equation 10 was obtained for AC/PCC bonded, and Equation 11 was obtained for AC/PCC unbonded:

$$d_{0\ \text{compress}} = -0.04524 + 63269.74\left(\frac{D_{ac}}{E_{ac}}\right)^{1.02138} \quad (10)$$

(residual R^2 = 99.94 percent, σ_Y = 0.047 mils, and n = 225)

$$d_{0\ \text{compress}} = -0.02149 + 27058.01\left(\frac{D_{ac}}{E_{ac}}\right)^{0.91878} \quad (11)$$

(residual R^2 = 99.89 percent, σ_Y = 0.074 mils, and n = 225)

where

$d_{0\ \text{compress}}$ = AC compression at center of load (mils),
D_{ac} = AC thickness (in.), and
E_{ac} = AC elastic modulus (psi).

The d_0 of the PCC slab in the AC/PCC pavement may be determined by subtracting the compression occurring in the AC surface from the d_0 measured at the AC surface.

The interface condition is a significant unknown in the backcalculation problem. The AC/PCC interface is assumed to be fully bonded when the AC layer is first placed, but how well that bond is retained is not known. Examination of cores taken at a later time may show that the bond has been reduced or completely lost. This is particularly likely if stripping occurs at the AC/PCC interface. Because in most cases the true interface bonding condition is not known, it is recommended that the change in d_0 be determined for both conditions.

AREA of PCC

In the elastic layer analyses conducted, only d_0 was found to change significantly between the AC and PCC layers; differences in d_{12}, d_{24}, and d_{36} were very close to zero over the entire range of parameters. Therefore, the *AREA* of the PCC slab may be computed from Equation 1 using the d_0 of the PCC slab determined as described above and d_{12}, d_{24}, and d_{36} measured at the AC surface. This computed *AREA* of the PCC will always be larger than the *AREA* of the AC surface's deflection basin. This is due to the form of Equation 1, in which *AREA* is normalized by dividing all of the deflections by d_0. If the denominator of each term decreases while the numerators remain unchanged, a larger *AREA* value will be computed.

Correction to d_0 and *AREA* of PCC

The computed d_0 and *AREA* of the PCC slab's deflection basin in the AC/PCC pavement are not the same d_0 and *AREA* that would be obtained if the AC layer were not present and deflections were measured on the bare PCC surface. To determine the PCC elastic modulus and the subgrade k value or elastic modulus independent of the AC overlay, the computed d_0 and *AREA* of the PCC slab must each be corrected to represent the bare PCC pavement condition. Furthermore, different corrections must be applied depending on the subgrade characterization (dense liquid or elastic solid) assumed in the backcalculation. This is because the different characterizations produce different deflection basins for the same input modulus values or, conversely, different backcalculated modulus values for the same input deflection basin.

Deflections were calculated for a factorial of bare PCC slabs on grade using the Apollo computer system to solve the Westergaard and Losberg equations for the dense liquid and elastic solid characterizations. The PCC slabs ranged from 6 to 12 in. in thickness and 3 million to 7 million psi in elastic modulus. The subgrade modulus or k value was held to a constant value to produce a wide range of ℓ_k or ℓ_e values.

The PCC slabs were then modeled in BISAR with AC overlays from 1 to 9 in. and E_{ac} values from 250 ksi to 1.25 million psi. The bare PCC deflection basins were compared with the deflection basins of the overlaid PCC slabs, and the needed correction equations were obtained. The general form used for all of the models is given in Equation 12. The values of the coefficients are given in Table 1. There are a total of eight models: a d_0 correction and an *AREA* correction for each of two AC/PCC bonding conditions and two subgrade characterizations. The corrections obtained are applied to the PCC d_0 and *AREA*, as shown in Equations 13 and 14.

$$\text{correction} = g + h * [D_{ac}^{a} * E_{ac}^{b} * D_{pcc}^{c} * d_{0\,pcc}^{d} * AREA_{pcc}^{e} * 10^{f}]^{i} \quad (12)$$

$$d_{0\ \text{bare}} = d_{0\ \text{pcc}} + d_0 \text{ correction} \quad (13)$$

$$AREA_{\text{bare}} = AREA_{\text{pcc}} + AREA \text{ correction} \quad (14)$$

The bare PCC d_0 and *AREA*, determined as described above, are the appropriate values to use to determine the PCC elastic modulus and dynamic k value or elastic modulus. It must be emphasized that the moduli determined in this manner (i.e., as if the AC surface were not present) are not the same moduli that the PCC and foundation layers exhibit in the actual AC/PCC pavement structure. The slab E and subgrade k and E are not intrinsic properties of either layer, but rather are influenced by the entire pavement structure's response to load. The purpose of this correction is to remove the effect of different AC overlay thicknesses and stiffnesses so that backcalculated PCC modulus values can be correlated to the extent of deterioration.

Sensitivity to Rigid Layer Beneath Foundation

This backcalculation method is based on an assumption of an infinite subgrade depth. Other researchers (*31*,*32*) have noted the sensitivity of various backcalculation procedures to the depth and stiffness of a rigid foundation layer. The sensitivity of this procedure to a rigid foundation layer was investigated by taking one of the weakest cross sections previously studied (2-in. AC, E_{ac} = 100,000 psi; 6-in. PCC, E_{pcc} = 3 million psi; and subgrade E_s = 6,000 psi) and determining the effect of BISAR-computed deflections at the AC and PCC surfaces with a rigid layer (modulus 250,000 psi) at depths of 5 to 20 ft. The rigid layer had no effect on the change in d_0 between the AC and PCC and only a slight effect on the change in *AREA*. The depth to a rigid layer was therefore judged to be not sufficiently significant to AC/PCC pavement analysis to require an additional correction.

EXAMPLE OF AC/PCC BACKCALCULATION PROCEDURE

Project Description

Deflection testing was conducted in September 1989 on a 9-mi section of I-70 near Marshall, Illinois, on an 8-in. CRCP pavement with a 4.5-in. AC overlay. The CRCP was constructed in 1968 and carried more than three times its design traffic by the time it was overlaid in 1980. Because of the heavy traffic and "D"-cracking aggregate used in the PCC, the pavement was severely deteriorated when it was rehabilitated.

The original pavement had a 4-in. bituminous-aggregate mixture base, but coring showed that the base was largely disintegrated and permeated by subgrade (silty clay) fines. Modeling the base and subgrade as a single layer thus appeared to reasonably represent the foundation conditions.

The first four basins were measured 10 ft apart in an eastbound section of the project that was rated in good condition on the basis of ride quality and visible distress. The second four, also 10 ft apart, were measured westbound at the same milepost, in a section of the project that was rated in fair to poor condition.

TABLE 1 COEFFICIENTS FOR d_0 AND *AREA* CORRECTION MODELS

	a	b	c	d	e	f	g	h	i	Obs	SEE	R^2
BDLD0 *	7.7888	3.6934	0.8548	14.9214	-10.7881	-2.2577	-1.5648	2.5484	0.2707	135	0.0547	0.9950
BDLAREA	1.1524	0.5378	-0.2374	2.0897	2.5639	9.4702	-0.5021	1.7250	1.3439	180	0.0138	0.9949
BESD0	2.3693	1.1245	0.4104	3.3122	-4.0414	-5.0151	-0.0477	0.7400	0.9850	180	0.0056	0.9990
BESAREA	2.8670	1.3189	-0.7492	3.4096	-5.8091	7.0101	0.5569	184.5114	0.5698	180	0.0145	0.9948
UDLD0	12.9885	4.3260	-17.4702	29.6353	-70.8581	51.6622	-1.8480	3.0444	0.0675	135	0.0538	0.9940
UDLAREA	1.7455	0.5138	-2.5830	0.7585	1.5610	4.9433	-0.3607	0.3118	0.8434	180	0.0202	0.9924
UESD0	2.2074	1.0511	-0.5542	2.0054	-1.5275	-7.7880	-0.2292	2.7547	1.2127	180	0.0070	0.9988
UESAREA	3.4949	1.4440	-1.4457	3.8288	-5.7058	8.9962	0.6607	35.0914	0.4809	180	0.0275	0.9902

* For BDLD0 Eac, in million psi

AC Elastic Modulus

The AC mix temperature was monitored during deflection testing by drilling holes to the middepth of the overlay, inserting liquid and a temperature probe, and allowing the temperature to stabilize before reading. The mix temperature varied from 66°F at 9 a.m. to 90°F at 3 p.m., as shown in Figure 7. Resilient modulus testing done later on cores from the AC surface indicated modulus values of about 1.2 million psi at 70°F and 520,000 psi at 90°F. The temperature-modulus relationship shown in Figure 6 was used to assign a modulus of 670,000 psi (at 84°F) to the first four basins and 615,000 psi (at 86°F) to the second four basins.

Backcalculation of PCC and Foundation Moduli

Table 2 gives the backcalculation results for the eight deflection basins (with all deflections scaled to a 9,000-lb load).

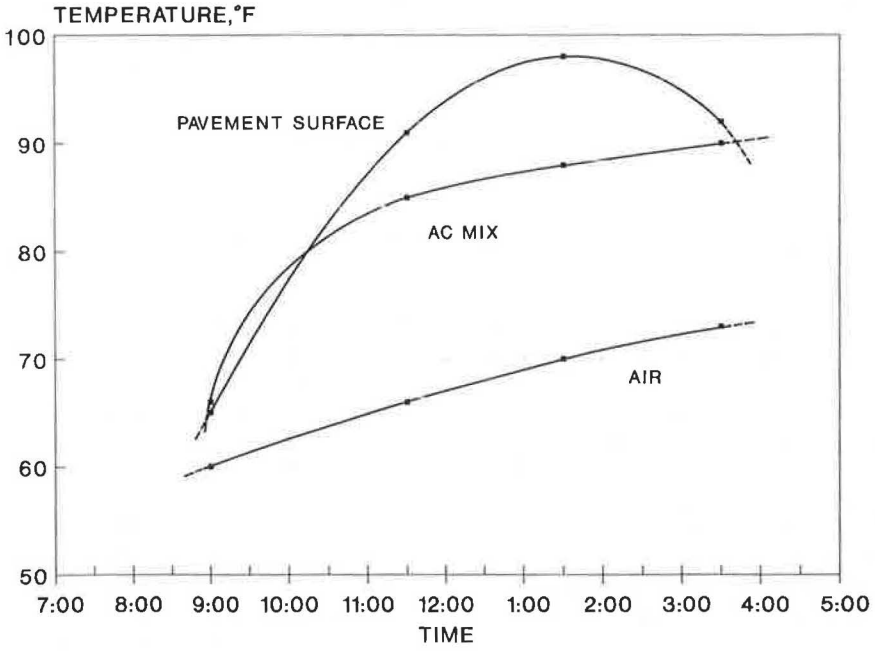

FIGURE 7 Variation in air, surface, and AC mix temperature during deflection testing for I-70 example.

TABLE 2 BACKCALCULATION RESULTS FOR I-70 EXAMPLE

							DENSE LIQUID			ELASTIC SOLID			DENSE LIQUID		ELASTIC SOLID	
							CORRECTED			CORRECTED						
MP & DIR	AC/PCC	AC d0 (mils)	AC AREA (in)	change in d0 (mils)	PCC d0 (mils)	PCC AREA (in)	PCC d0 (mils)	PCC AREA (in)	lk (in)	PCC d0 (mils)	PCC AREA (in)	le (in)	Epcc (M psi)	k (pci)	Epcc (M psi)	Es (psi)
154 E	BONDED	4.54	27.16	0.28	4.26	28.57	3.00	28.24	27.62	4.55	29.67	23.18	6.40	480	4.69	24661
		4.98	27.96	0.28	4.70	29.29	3.56	29.03	30.10	5.07	30.45	25.77	6.43	342	5.20	19872
		5.88	28.24	0.28	5.60	29.37	4.90	29.27	30.94	6.29	30.77	27.01	4.94	235	4.60	15287
		5.82	28.40	0.28	5.54	29.55	4.79	29.45	31.58	6.18	30.92	27.61	5.27	231	4.89	15201
154 E	UNBONDED	4.54	27.16	0.46	4.08	29.52	2.47	29.31	31.08	3.88	30.25	25.05	9.91	463	6.42	26753
		4.98	27.96	0.46	4.52	30.18	2.93	29.98	33.74	4.32	30.92	27.61	9.85	332	7.00	21759
		5.88	28.24	0.46	5.42	30.12	3.95	29.94	33.55	5.23	30.89	27.48	7.23	249	5.72	18048
		5.82	28.40	0.46	5.36	30.31	3.87	30.13	34.39	5.17	31.07	28.29	7.76	242	6.13	17734
154 W	BONDED	7.58	22.97	0.31	7.27	23.71	10.01	23.58	18.59	10.92	26.93	17.16	0.85	312	1.07	13919
		7.51	21.79	0.31	7.20	22.48	10.47	22.28	17.02	11.58	26.16	15.99	0.68	354	0.88	14109
		8.78	22.65	0.31	8.47	23.27	15.33	23.31	18.25	14.97	27.65	18.41	0.54	211	0.90	9450
		7.39	23.94	0.31	7.08	24.74	8.93	24.64	20.10	9.89	27.50	18.14	1.13	301	1.32	14525
154 W	UNBONDED	7.58	22.97	0.50	7.08	24.16	7.03	23.95	19.10	6.96	25.12	14.65	1.29	421	1.23	25681
		7.51	21.79	0.50	7.01	22.90	7.44	22.69	17.49	6.90	23.91	13.33	1.01	472	1.03	28578
		8.78	22.65	0.50	8.28	23.65	9.16	23.46	18.44	8.22	24.74	14.20	0.92	347	0.98	22460
		7.39	23.94	0.50	6.89	25.23	6.43	25.03	20.73	6.76	26.15	15.98	1.66	394	1.51	24192

Because the AC and PCC were debonded in 15 of the 16 cores taken on this project, the backcalculated values corresponding to the unbonded interface assumption are, in this case, considered to be more realistic.

It is evident that the PCC in the eastbound section is in much better condition than in the westbound section. The eastbound CRCP modulus values are about 5.5 million to 8.5 million psi, whereas the westbound CRCP modulus values are all less than 1.5 million psi. Obviously, such low modulus values are unreasonable for sound PCC, and they suggest that the PCC is severely deteriorated because of "D" cracking. Although this entire mile of the project was rated in fair condition on the basis of ride quality and distress observations, the deflections shown in Table 2 were measured at locations where the AC overlay was uncracked. This is consistent with the results of the subsequent coring operation: at locations where exceptionally high deflections were measured, the underlying PCC was invariably deteriorated. This was true even at locations with little or no distress visible at the AC surface.

Comparison with Other Backcalculation Results

Table 3 gives the backcalculation results obtained for the eight deflection basins using MODULUS, a program recently developed at the Texas Transportation Institute under NCHRP Project 10-27 (*12*), which generates a matrix of solutions for ranges of layer moduli and selects the combination that produces deflections most closely matching the measured deflections.

The AC modulus was restricted in MODULUS to a fairly narrow range of 600 to 700 ksi, which encompasses the values used before: 670 ksi for the first four deflection basins and 615 ksi for the second four basins. The version of MODULUS used to analyze these data assumed full bond between the AC and PCC layers.

MODULUS consistently assigned the minimum allowable value of 600 ksi to theAC layer. The values obtained for the PCC are similar to those obtained before when the AC and PCC were assumed bonded: about 2 million to 4 million psi for the eastbound basins, and less than 1 million psi for the westbound basins. These values are of interest for comparison with those obtained by the new procedure, but the higher PCC modulus values backcalculated under the assumption that the AC and PCC are not bonded are considered to be more realistic.

An attempt to allow MODULUS to backcalculate the AC modulus within a broader range produced significantly lower moduli for the AC (about 450 ksi for the first four basins and 125 ksi for the second four basins) and correspondingly higher PCC moduli (in excess of the selected maximum of 4 million psi for several basins). The 325-ksi drop in modulus attributed to the AC by the MODULUS program was not considered reasonable considering (*a*) the rise of only 2°F in measured AC mix temperature that occurred during the time that the deflections were measured and (*b*) the modulus values obtained for the same temperature range from laboratory tests on the AC cores.

TABLE 3 BACKCALCULATION RESULTS FROM MODULUS FOR I-70 EXAMPLE

AC/PCC	mp	dir	no	Eac (psi)	Epcc (million psi)	Esub (psi)
Bonded	154.0	E	1	600,000	2.9	27,200
			2	600,000	4.2	21,500
			3	600,000	3.2	17,800
			4	600,000	2.6	18,700
Bonded	154.0	W	1	600,000	0.51	22,900
			2	600,000	0.60	24,300
			3	600,000	0.39	20,100
			4	600,000	0.81	20,800

Assumptions in Backcalculation

The results of backcalculation by any method should be viewed in the light of the inherent assumptions concerning the pavement layers. For the AC/PCC backcalculation procedure described here, the assumptions include characterization of the AC as an elastic layer, the PCC as a plate (an elastic layer that exhibits pure bending without shear deformation), and the foundation as either a bed of springs or an elastic solid. These are certainly simplifications of the true nature of the layer properties. The most obvious violation of these assumptions is the attribution of plate bending behavior to severely "D" cracked PCC, which may have more in common with a granular base than with a sound PCC slab. The extremely low backcalculated values that result should not be interpreted as the true stress-strain response of the PCC as a homogeneous elastic layer, but rather as an indication of the extent to which its behavior departs from that of a sound slab (i.e., the extent of the PCC's deterioration). The ability to diagnose the condition of the PCC from deflection measurements is particularly valuable in evaluation of AC/PCC pavements, because the extent of the deterioration of the PCC is often not fully evident from visible distress.

SUMMARY AND CONCLUSIONS

The development of a simple and straightforward procedure for backcalculation of AC/PCC pavement layer moduli was described. The procedure relies on knowledge of the AC surface modulus based on AC mix temperature at the time of deflection testing. Adjustments to the deflection basin measured at the AC surface are made to determine the deflection basin induced in the PCC layer. The PCC deflection basin may then be used to predict the deflection basin that would be measured without the AC layer present. The backcalculated PCC modulus determined in this manner, independent of the effect of the AC overlay, may then be used as an indicator of the extent of deterioration in the PCC.

Assignment of the AC modulus on the basis of mix temperature at the time of deflection testing is necessary to avoid

backcalculating incorrect values for the PCC modulus and thus misinterpreting the condition of the PCC. Other researchers have noted that the solutions to multilayer backcalculation problems are not unique. Thus, it is possible to obtain good matches between measured and predicted deflections for AC modulus values that are clearly inconsistent with the conditions existing at the time of deflection testing.

The example presented indicates that the AC/PCC backcalculation procedure described produces reasonable results that are consistent with those obtained using another backcalculation routine considered to be reliable.

An important feature of the AC/PCC pavement backcalculation procedure described here is its ability to identify areas in which the underlying PCC is deteriorated. This information is crucial to decisions that must be made for second rehabilitation, including division of the project into uniform sections, identification of areas requiring repair, selection of an overlay type or other rehabilitation alternative, and second overlay design.

ACKNOWLEDGMENTS

This paper is based on the results of Project IHR-517, "Development and Field Testing of an Illinois Pavement Feedback System." IHR-517 was sponsored by the Illinois Department of Transportation (Division of Highways) and the U.S. Department of Transportation (FHWA). The authors are grateful for the encouragement and direction of Michael Darter and the generous input of many other individuals, including Robert Elliott, Sam Carpenter, Barry Dempsey, Marshall Thompson, and Anastasios Ioannides. The cooperation and assistance of Max Rexroad of the University of Illinois, as well as personnel in the Illinois Department of Transportation's Bureau of Materials and Physical Research and in District 5, are also gratefully acknowledged.

REFERENCES

1. A. J. Bush III. *Computer Program BISDEF*. U.S. Army Corps of Engineers Waterways Experiment Station, Vicksburg, Miss., 1985.
2. A. J. Bush III. *Nondestructive Testing for Light Aircraft Pavements, Phase II: Development of the Nondestructive Evaluation Methodology*. Report FAA-RD-80-9-II. Federal Aviation Administration, U.S. Department of Transportation, 1980.
3. F. J. Van Cauwelaert, D. R. Alexander, T. D. White, and W. R. Barker. Multilayer Elastic Program for Backcalculating Layer Moduli in Pavement Evaluation. In *Nondestructive Testing of Pavements and Backcalculation of Moduli* (A. J. Bush III and G. Y. Baladi, eds.). ASTM STP 1026. ASTM, Philadelphia, Pa., 1989.
4. D. L. DeJong, M. G. F. Peutz, and A. R. Korswagen. *Computer Program BISAR*. Koninklijke/Shell-Laboratorium, Amsterdam, the Netherlands, 1973.
5. M. Anderson. *Evaluation of Models for Backcalculation of Pavement Layer Moduli*. Applied Research Associates, Inc., Nov. 1990.
6. R. L. Lytton. Backcalculation of Layer Moduli. In *Nondestructive Testing of Pavements and Backcalculation of Moduli* (A. J. Bush III and G. Y. Baladi, eds.). ASTM STP 1026. ASTM, Philadelphia, Pa., 1989.
7. F. H. Scrivner, C. H. Michalak, and W. M. Moore. Calculation of the Elastic Moduli of a Two-Layer Pavement System from Measured Surface Deflections. In *Highway Research Record 431*, HRB, National Research Council, Washington, D.C., 1973.
8. T. Y. Hou. *Evaluation of Layered Material Properties from Measured Surface Deflections*. Ph.D. dissertation. University of Utah, Salt Lake City, 1977.
9. Y. J. Chou, J. Uzan, and R. L. Lytton. Backcalculation of Layer Moduli from Nondestructive Pavement Deflection Data Using the Expert System Approach. In *Nondestructive Testing of Pavements and Backcalculation of Moduli* (A. J. Bush III and G. Y. Baladi, eds.). ASTM STP 1026. ASTM, Philadelphia, Pa., 1989.
10. H. Zhou, R. G. Hicks, and C. A. Bell. BOUSDEF: A Backcalculation Program for Determining Moduli of a Pavement Structure. In *Transportation Research Record 1260*, TRB, National Research Council, Washington, D.C., 1990, pp. 166–179.
11. M. Anderson. A Data Base Method for Backcalculation of Composite Pavement Layer Moduli. In *Nondestructive Testing of Pavements and Backcalculation of Moduli* (A. J. Bush III and G. Y. Baladi, eds.). ASTM STP 1026. ASTM, Philadelphia, Pa., 1989.
12. R. L. Lytton, F. P. Germann, Y. J. Chou, and S. M. Stoffels. *NCHRP Report 327: Determining Asphaltic Concrete Pavement Structural Properties by Nondestructive Testing*. TRB, National Research Council, Washington, D.C., 1990.
13. A. M. Ioannides. Dimensional Analysis in NDT Rigid Pavement Evaluation. *Transportation Engineering Journal*, ASCE, Vol. 116, No. TE1, 1990.
14. A. M. Ioannides, E. J. Barenberg, and J. A. Lary. Interpretation of Falling Weight Deflectometer Results Using Principles of Dimensional Analysis. *Proc., Fourth International Conference on Concrete Pavement Design and Rehabilitation*, Purdue University, West Lafayette, Ind., 1989.
15. M. S. Hoffman and M. R. Thompson. *Mechanistic Interpretation of Nondestructive Pavement Testing Deflections*. Transportation Engineering Series No. 32, Illinois Cooperative Highway and Transportation Research Series No. 190. University of Illinois at Urbana-Champaign, Urbana, 1981.
16. *Nondestructive Structural Evaluation of Airfield Pavements*. ERES Consultants, Inc., 1982.
17. P. T. Foxworthy. *Concepts for the Development of a Nondestructive Testing and Evaluation System for Rigid Airfield Pavements*. Ph.D. thesis. University of Illinois at Urbana-Champaign, Urbana, 1985.
18. H. M. Westergaard. Stresses in Concrete Runways of Airports. *HRB Proc.*, Vol. 19, 1939.
19. A. Losberg. *Structurally Reinforced Concrete Pavements*. Doktorsavhandlingar Vid Chalmers Tekniska Högskola, Göteborg, Sweden, 1960.
20. *IMSL SFUN/LIBRARY User's Manual*. Version 2.1. IMSL, Inc., 1989.
21. *IMSL MATH/LIBRARY User's Manual*. Version 1.1. IMSL, Inc., 1989.
22. G. A. F. Seber and C. J. Wild. *Nonlinear Regression*. John Wiley and Sons, Inc., New York, 1989.
23. *SAS User's Guide: Statistics*. Version 5 edition. SAS Institute, Inc., Cary, N.C., 1985.
24. D. M. Burmister. The Theory of Stresses and Displacements in Layered Systems and Applications to the Design of Airport Runways. *HRB Proc.*, Vol. 23, 1943.
25. D. M. Burmister. The General Theory of Stresses and Displacements in Layered Systems. Parts I, II, and III. *Journal of Applied Physics*, Vol. 16, 1945.
26. H. F. Southgate. *An Evaluation of Temperature Distribution Within Asphalt Pavements and Its Relationship to Pavement Deflection*. Research Report KYHPR-64-20. Kentucky Department of Highways, 1968.
27. *Pavement Design Manual*. Shell International Petroleum Company, London, England, 1978.
28. *Research and Development of the Asphalt Institute's Thickness Design Manual (MS-1) Ninth Edition*. Research Report 82-2. Asphalt Institute, College Park, Md.,1982.
29. M. R. Thompson and K. A. Cation. *A Proposed Full-Depth Asphalt Concrete Thickness Design Procedure*. Transportation Engineering Series No. 45, Illinois Cooperative Highway and Transportation Program Series No. 213. University of Illinois at Urbana-Champaign, Urbana, 1986.

30. S. H. Carpenter and T. VanDam. Laboratory Performance Comparisons of Polymer-Modified and Unmodified Asphalt Concrete Mixtures. In *Transportation Research Record 1115*, TRB, National Research Council, Washington, D.C., 1987.
31. T. Rwebangira, R. G. Hicks, and M. Truebe. Sensitivity Analysis of Selected Backcalculation Procedures. In *Transportation Research Record 1117*, TRB, National Research Council, Washington, D.C., 1987.
32. R. C. Briggs and S. Nazarian. Effects of Unknown Rigid Subgrade Layers on Backcalculation of Pavement Moduli and Projections of Pavement Performance. In *Transportation Research Record 1227*, TRB, National Research Council, Washington, D.C., 1989.

Detection and Determination of Depth of Rigid Bottom in Backcalculation of Layer Moduli from Falling Weight Deflectometer Data

A. S. M. Mustaque Hossain and John P. Zaniewski

A new approach has been developed to detect the presence of a rigid layer at a shallow depth below the pavement using falling weight deflectometer (FWD) deflection data. A parameter, SLOPE, has been derived from the sixth and seventh sensor deflection values by applying Boussinesq's linear elastic idealization to pavement systems under quasi-concentrated FWD load. Typical values of SLOPE have been determined that indicate the presence of a rigid bottom at a shallow depth. The depth of such a rigid layer was determined by matching the outer sensor deflections corresponding to an estimated subgrade modulus with an elastic layer analysis program and a gradient-based optimization routine. The detection and depth determination procedure were verified using FWD measurements, cone penetration results and drilling records on 13 in-service pavements in Arizona, and existing results from manual backcalculation analysis. Satisfactory agreement was observed between the results of this study and results from manual backcalculation analysis. The rigid layer detection and depth determination procedures have been coded in a computer program, Arizona Deflection Analysis Method.

Most backcalculation methods for determination of layer moduli from deflection basins assume a semi-infinite subgrade. McCullough and Taute (*1*) showed that the presence of a rock layer at a finite depth below the pavement can significantly affect theoretical Dynaflect deflection basins. Bush and Alexander (*2*) assumed a rigid bottom at a depth of 240 in. for evaluation of in situ moduli from their deflection basin matching program. Wiseman et al. (*3*) used finite subgrade thickness for their study of nondestructive testing evaluation of pavements. Mamlouk (*4*) and Sebaaly (*5*) arbitrarily selected the depth of the rigid bottom for dynamic analysis of Road Rater, Dynaflect, and falling weight deflectometer (FWD) deflection basins. Uddin et al. (*6*) proposed a method for estimation of the depth of the rigid bottom by dynamic analysis of FWD deflection data. However, no further use of Uddin's method has been reported in the literature. Ullidtz (*7*) reported that ELMOD can detect and estimate the depth of the rigid bottom. Yazdani and Scullion (*8*) reported an experimental program at Texas Transportation Institute using a multidepth deflectometer for monitoring pavement response. A comparison of measured deflections with calculated deflections indicated that a better match was obtained between the two sets when the calculated deflections for the pavement system with a rigid bottom at 240 in. were used.

College of Engineering and Applied Sciences, Arizona State University, Tempe, Ariz. 85287.

Thus, it is apparent that detection and determination of the depth of the rigid bottom, when present at a relatively shallow depth, is an important part of a backcalculation scheme. An approach is presented for the detection of a rigid layer and the estimation of its depth from the top of the subgrade using an FWD deflection basin.

DEFINITION OF RIGID BOTTOM

The rigid bottom, in general, implies the presence of a very stiff layer at some depth below the pavement. In backcalculation, the subgrade is usually characterized as a single uniform layer of infinite thickness in the vertical direction. However, subgrades usually consist of layers of different materials. Mamlouk et al. (*9*) found, through an analysis of cone penetration data on a number of in-service pavement subgrades, that for several of the pavements there was a rigid bottom or "hard rock" basalt or limestone layer underlying the pavement at a finite depth. In most cases the cone penetration data exhibited "medium hard" layers at various depths, sometimes reverting to relatively soft layers beneath the medium hard layers. In a few cases, nothing that could even be called medium hard was encountered within 25 ft of drilling or cone penetration. Figure 1 shows the typical layered profile of subgrade modulus versus depth determined from cone penetration data using the concept of a minimum modulus calculated from cone penetration resistance (*9*). The moduli values were calculated on the basis of correlation among modulus, soil type, and cone tip resistance. The minimum modulus refers to the minimum subgrade modulus encountered in the profile. Figure 1 indicates a remarkable variation of subgrade modulus with depth. Thus, treatment of the subgrade as a single layer in backcalculation requires representing the moduli of several strata in the subgrade with a single composite or equivalent modulus value.

In this study, the rigid bottom refers to the layer in the subgrade in which deformation due to the applied FWD load is essentially zero. The situation might occur because of the presence of an incompressible rock layer or a very hard clay layer in the subsurface. The interface between the subgrade and the rigid layer is considered to be rough (i.e., full continuity exists across such an interface).

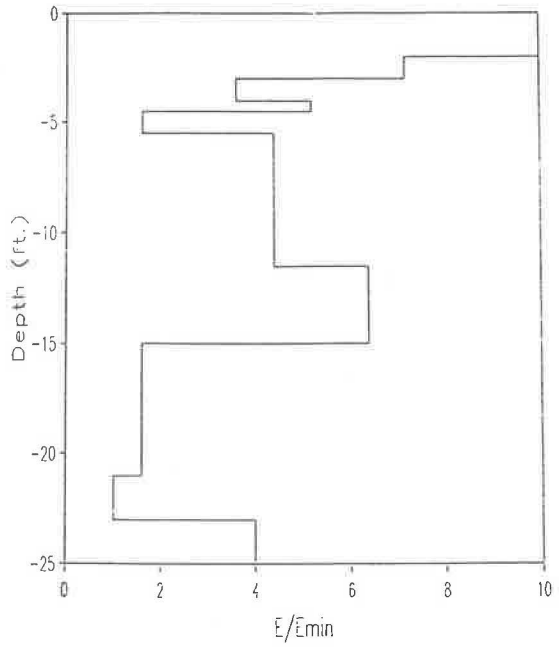

FIGURE 1 Typical layered profile of the subgrade (*9*).

CONSIDERATION OF RIGID BOTTOM IN BACKCALCULATION

The semi-infinite subgrade is an inherent assumption in elastic layer theory for a number of backcalculation processes. For example, the BKCHEVM (*9*) backcalculation program uses CHEVRON (*10*) as the elastic layer analysis program. In this scheme the subgrade is usually assumed to be semi-infinite. However, the BKCHEVM program automatically introduces a rigid bottom 240 in. below the top of the subgrade whenever it detects a rigid bottom on the basis of the seventh sensor deflection value. This detection procedure is arbitrary and not rational.

The BKCHEVM program was used to backcalculate layer moduli for three typical pavements (weak, medium, and stiff) with finite depths of subgrade. Inputs to the program were the simulated deflection basins obtained from CHEVRON for a 9,000-lb load applied on a plate 11.8 in. in diameter on pavements with layer moduli and thicknesses given in Tables 1 and 2. Poisson's ratios of 0.30, 0.40, 0.40, and 0.45 for the asphalt concrete (AC), base, subbase, and subgrade layer materials were assumed.

Tables 1 and 2 show the layer types, thicknesses, and actual and backcalculated layer moduli for different pavement types with finite and infinite depth of subgrade, respectively. Table 1 indicates that the differences between the BKCHEVM-backcalculated and known layer moduli for different layers vary from 14 to 167 percent for pavements with finite depth of subgrade. Table 2 indicates that for infinite depth of subgrade, the differences between backcalculated and known layer moduli are relatively small. For medium and weak pavements, the differences range only from 0.0 to 7.0 percent, whereas for stiff pavement, a 100 percent difference was encountered. Thus, it is evident that for infinite depth of subgrade, BKCHEVM can predict layer moduli with reasonable accuracy for weak and medium pavements.

Jung (*11*) has shown that the accuracy in the calculation of the moduli of the layers above the subgrade is not important as long as the combined effect of the moduli in transmitting forces to the subgrade remains unchanged. To verify the re-

TABLE 1 COMPARISON OF KNOWN AND BACKCALCULATED LAYER MODULI FOR PAVEMENTS WITH FINITE DEPTH OF SUBGRADE

Pavement Type	Layer/ Type[1]	Thickness (in)	Known Modulus (ksi)	Seed Modulus (ksi)	Backcalc. Modulus (ksi)	Diff.[2] (%)
Weak	1/AC	3.0	250	350	70	72.0
	2/AB	4.0	20	40	44	-120.5
	3/SM	9.0	10	30	7	30.0
	4/SG	240	5	8.6	6.7	-33.6
Medium	1/AC	4.0	450	350	100	77.8
	2/AB	4.0	30	40	80	-166.7
	3/SM	12.0	20	30	17.2	14.1
	4/SG	240	10	16.5	13.6	-36.1
Stiff	1/AC	6.0	650	350	1,000	-53.9
	2/AB	4.0	40	40	80	-100.0
	3/SM	9.0	25	30	10	60.0
	4/SG	120	7	20.2	13.2	-88.7

[1] AC: Asphalt Concrete, AB: Aggregate Base, SM: Select Material, SG: Subgrade.

[2] Diff (%) = (Eknown - Ebackcalc)/Eknown x 100

TABLE 2 COMPARISON OF KNOWN AND BACKCALCULATED LAYER MODULI FOR PAVEMENTS WITH INFINITE DEPTH OF SUBGRADE

Pavement Type	Layer/ Type[1]	Thickness (in)	Actual Modulus (ksi)	Seed Modulus (ksi)	Backcalc. Modulus (ksi)	Diff.[2] (%)
Weak	1/AC	3.0	250	350	235.8	6.0
	2/AB	4.0	20	40	21.4	7.0
	3/SM	9.0	10	30	10	0.0
	4/SG	s-i	5	4.99	5	0.0
Medium	1/AC	4.0	450	350	450.4	0.08
	2/AB	4.0	30	40	30.1	0.33
	3/SM	12.0	20	30	19.9	0.50
	4/SG	s-i	10	9.6	10.0	0.00
Stiff	1/AC	6.0	650	350	591.1	9.06
	2/AB	4.0	40	40	80	100.0
	3/SM	9.0	25	30	17.8	28.8
	4/SG	s-i	7	6.8	7.1	2.1

s-i; semi-infinite subgrade

[1] AC: Asphalt Concrete, AB: Aggregate Base, SM: Select Material, SG: Subgrade.

[2] Diff (%) = (Eknown - Ebackcalc)/Eknown x 100

sponse of the pavement at the critical location, horizontal tensile strain was calculated with CHEVRON at the bottom of the AC layer corresponding to an 18-kip axle load and 100-psi tire pressure for the known and backcalculated pavement systems. Table 3 shows the comparison of tensile strains calculated at the bottom of the AC layer for known and backcalculated pavement layer moduli for different pavement types and subgrade conditions. The table also shows the number of 18-kip equivalent single-axle loads (ESALs) to be carried by the pavement before fatigue failure, computed from the fatigue criteria developed by Mamlouk et al. (*9*):

$$N = 9.33 \times 10^{-7} (1/e_{ac})^{3.84}$$

where N is the theoretical number of 18-kip ESAL repetitions until fatigue failure and e_{ac} is the tensile strain at the bottom of the AC layer (in microinches per inch).

It is evident that the difference between the asphalt strain corresponding to known layer moduli and the asphalt strain corresponding to backcalculated layer moduli was smaller for infinite depth of subgrade. Consequently, the number of 18-kip ESALs to be carried by the backcalculated pavement systems before fatigue failure does not vary widely from values corresponding to known layer moduli. The maximum difference of 14 percent was for stiff pavement. For finite subgrades, however, the differences between the strain corresponding to backcalculated layer moduli and the strain corresponding to known layer moduli vary from 30 to 49 percent. The differences are magnified when the number of 18-kip ESALs that can be carried by the pavements is computed by using the fatigue criteria developed by Mamlouk et al. (*9*). The differences in computed traffic range between 288 and 1,249 percent. The large differences are attributable to the error resulting from inaccurate determination of the thickness of the subgrade. Detection and accurate prediction of the depth of rigid bottom are important prerequisites for a better backcalculation scheme.

DETECTION OF RIGID BOTTOM

Ullidtz (*7*) has shown that at distances larger than twice the load radius, a distributed uniform load may be treated as a point load. Then, by using Boussinesq's equation, the surface modulus or the "weighted mean modulus" of the elastic half-space idealization of the pavement system can be computed from the surface deflections:

$$E_{sm}(0) = 2(1 - \nu^2)\sigma a/d(0) \quad (1)$$

and

$$E_{sm}(r) = (1 - \nu^2)\sigma a^2/[rd(r)] \quad (2)$$

where

$E_{sm}(r)$ = surface modulus at distance r from the center of the loading plate,
ν = Poisson's ratio (0.35),
σ = contact stress under the loading plate,
a = radius of the loading plate,
$d(r)$ = deflection at distance r, and
r = radial distance from the center of the loading plate.

The surface modulus at distance r roughly reflects the surface modulus at the equivalent depth. In FWD testing, it is assumed that the outermost deflections (sixth and seventh sensors at 12-in. spacing of sensors) are completely controlled by the subgrade. Therefore, the computed surface moduli corresponding to these sensor deflections reflect the contribution of the subgrade. According to Ullidtz (*7*), if the surface moduli (E_{sm6} and E_{sm7}) calculated at the sixth and seventh sensor locations are identical, the subgrade response is linear, that is,

$$\text{SLOPE} = (E_{sm7} - E_{sm6})/E_{sm7} \times 100 \approx 0 \quad (3)$$

This equality implies that the response of subgrade material is linear with depth and that there is no rigid layer at a shallow depth. But if $(E_{sm7} - E_{sm6})/E_{sm7} \times 100 \neq 0$, the response is nonlinear. The nonlinearity might occur because of the nonlinear behavior of subgrade material, the presence of a rigid layer at a shallow depth, or both.

The subgrade material is generally known to be nonlinear (*12*). But it is hypothesized that if the applied load is repeated several times, the effect of nonlinear response due to the

TABLE 3 COMPARISON OF AC STRAIN AND NUMBER OF 18-KIP ESALs CORRESPONDING TO KNOWN AND BACKCALCULATED LAYER MODULI FOR DIFFERENT PAVEMENT TYPES AND SUBGRADE THICKNESSES

Pavement Type	Subgrade Type	Known Strain (micro in/in)	Backcalc Strain (micro in/in)	Diff* (%)	Nknown (millions)	Nbackcalc (millions)	Diff* (%)
Weak	Finite	739.0	375.97	49.12	0.98	13.23	-1249
	Infinite	739.0	730.04	1.2	0.98	1.03	-5.10
Medium	Finite	354.3	235.33	33.58	16.6	80.00	-382.0
	Infinite	354.3	356.57	-0.64	16.6	16.20	2.41
Stiff	Finite	186.73	131.2	9.73	194.3	753.1	-287.6
	Infinite	186.73	170.42	8.73	194.3	166.8	14.41

* Diff (%) = (Known-Backcalc)/Known x 100

subgrade material will be reduced. Kasianchuck and Argue (*13*) showed that the nonlinear load-deflection behavior of a subgrade during the initial loading of a repeated plate load test becomes linear when the load is repeated (Figure 2). This is evidence that the stress-strain behavior of the subgrade becomes linear after repeated traffic loadings.

Mamlouk et al. (*9*) studied the material nonlinearity and stress sensitivity due to FWD loads of the materials of several in-service pavements in Arizona. They found that within the stress range of the FWD tests, the effect of material nonlinearity is negligible compared with the effect of spatial variability in material properties. In other words, the "error" in an FWD deflection measurement resulting from assuming linearity would be insignificant compared with random variability for the subgrades studied. However, for this study the behavior of subgrade and pavement materials was assumed to be linear and elastic. Even with these assumptions, the nonlinearity in the subgrade response due to the presence of a rigid layer at a shallow depth can be significant. Figure 3 shows the effect of the presence of a rigid layer at a shallow depth on the surface moduli for different categories of pavements with assumed linear subgrade material. The effect of the presence of a rigid layer decreases as the depth of the rigid layer increases. At a certain depth, the rigid layer no longer influences pavement response. This critical depth varies with the pavement stiffness.

Table 4 shows the values of SLOPE for linear subgrade material corresponding to different depths of the rigid layer. It is evident that for all pavement types, as the depth of the rigid layer increases, SLOPE decreases. For shallow rigid layers and very stiff pavements, SLOPE becomes negative. The negative SLOPE value implies a positive nonlinearity of the subgrade response, and it happens often with thick pavement structures in which the FWD sensors are too close to the load. This was observed by Ullidtz (*7*). For a very deep layer, SLOPE should be zero (Figure 4). SLOPE values for different pavements vary depending on the thickness and moduli of the layers, especially the subgrade modulus.

Figure 5 shows the relationships between SLOPE and depth of rigid layer for different subgrade moduli for a medium stiff pavement. It is evident that the same pavement has different SLOPE values corresponding to a single depth of rigid layer but different subgrade moduli. Thus, the SLOPE value is a nonunique parameter for detection of a rigid layer, because it is also affected by the subgrade modulus. However, it is possible to develop typical values of SLOPE to detect the rigid bottom empirically.

Table 5 shows the matrix of pavements used in the analysis. The matrix has eight factors each at three levels, yielding 3^8 = 6,561 pavement structures. These structures were used to generate values of SLOPE for different pavement types with semi-infinite subgrade. A calculated SLOPE from any FWD basin falling outside this range would be attributed to the presence of a rigid layer at a relatively shallow depth. To generate simulated deflection basins, a uniform circular loading of 9,000 lb with a diameter of 11.8 in. was used. Deflections were calculated with CHEVRON (*10*) at the load center and at six other locations at a uniform spacing of 12 in.

SLOPE for each pavement was calculated from Equation 3. Pavements with a subgrade modulus of 3,000 psi were excluded from the analysis because none of the pavements in Arizona analyzed by Mamlouk et al. (*9*) has subgrade modulus

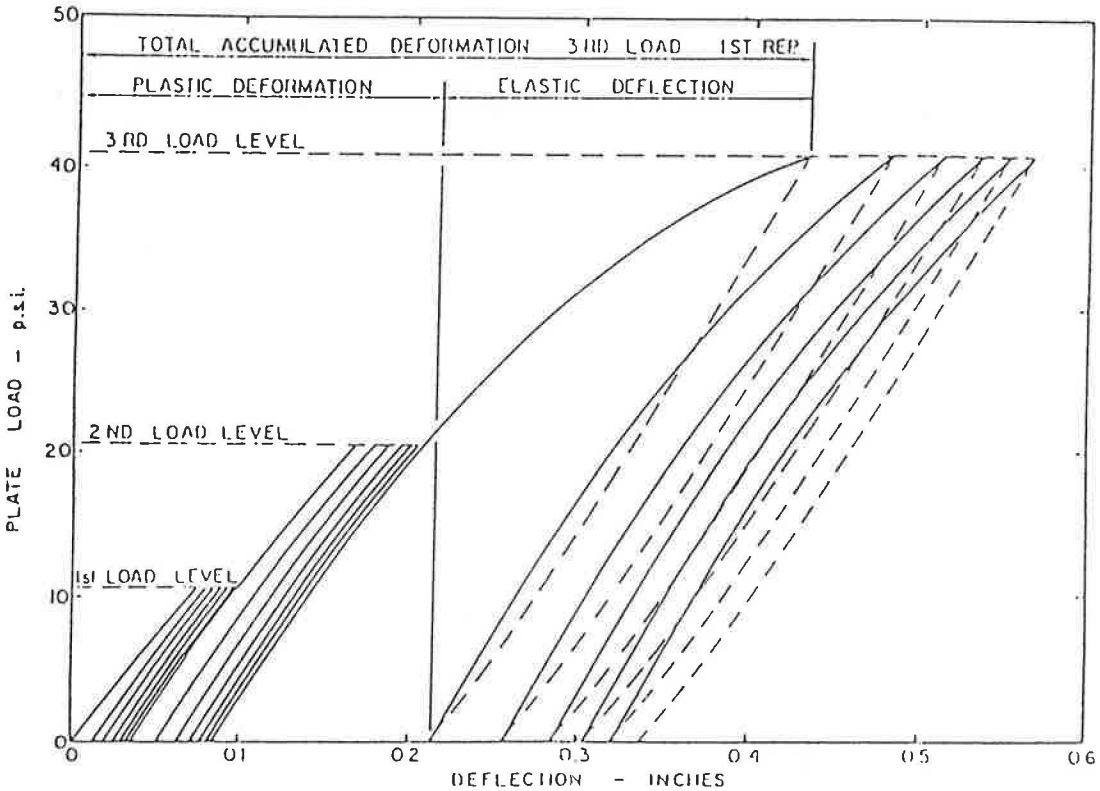

FIGURE 2 Typical load-deflection diagram from repetitive plate load test (*13*).

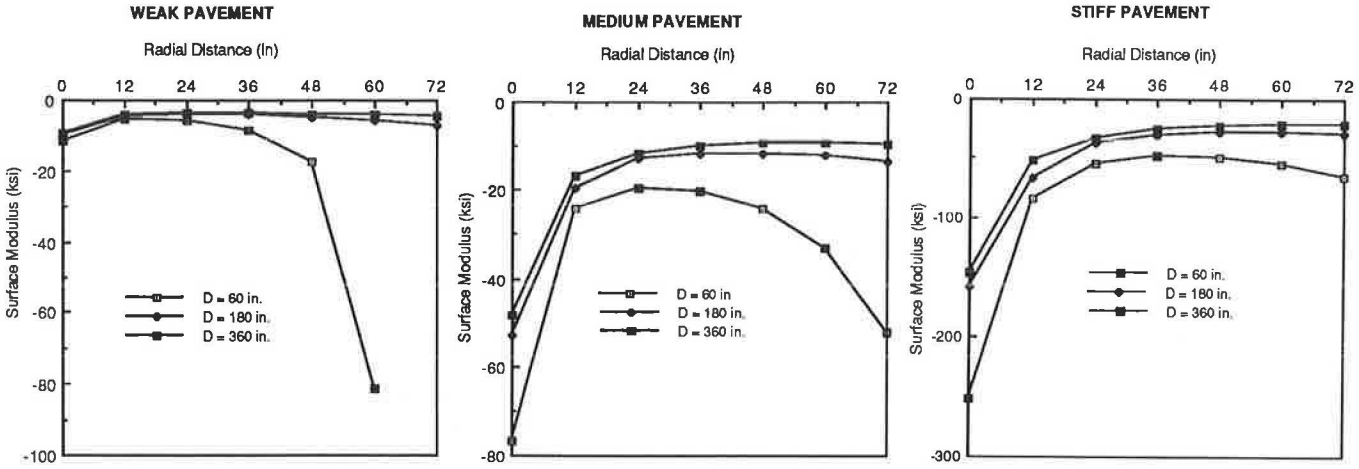

FIGURE 3 Effect of the presence of a rigid layer on the surface moduli of different types of pavements.

TABLE 4 VALUES OF SLOPE FOR DIFFERENT PAVEMENT TYPES AND DEPTHS OF RIGID LAYER

Pavement Type	D[1](inch)	SLOPE(%)
Weak	60	
(3" AC)	120	33.16
	180	18.98
	240	13.74
	300	11.02
	360	9.38
Medium	60	36.7
(7" AC)	120	15.91
	180	9.3
	240	6.26
	300	4.45
	360	3.58
Stiff	60	16.3
(14" AC)	120	6.56
	180	2.55
	240	0.35
	300	-1.19
	360	-1.63

[1] Depth to the rigid layer.

less that 6,500 psi and because the frequency analysis of the seventh sensor deflections from FWD measurements on the Arizona highway system indicated stiffer subgrades for Arizona (*14*). Table 6 shows the summary statistics for SLOPE for different pavement types. On the basis of the range of values in Table 6, the following guidelines were selected to indicate semi-infinite subgrade or linear subgrade response:

For 3 in. $\leq T_{AC} < 6$ in., $0.22 \leq$ SLOPE < 4.47

For 6 in. $\leq T_{AC} < 10$ in., $-0.65 \leq$ SLOPE < 7.27

For 10 in. $\leq T_{AC}$, $-3.16 \leq$ SLOPE < 7.80

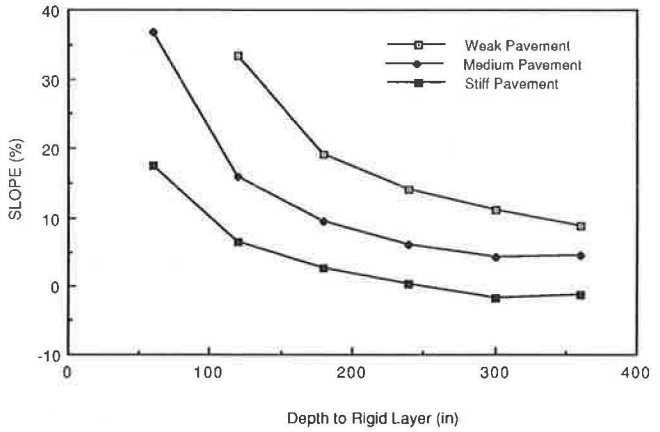

FIGURE 4 Influence of depth of rigid layer on SLOPE for different types of pavements.

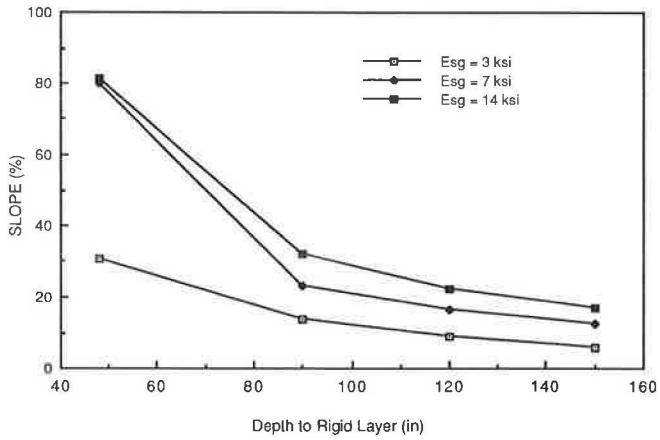

FIGURE 5 Relationship between SLOPE and depth of rigid layer for different subgrade moduli for medium stiff pavement.

For any pavement, if the SLOPE calculated from the sixth and seventh sensor deflections in FWD testing falls outside these ranges, there must be a rigid layer below the pavement at a shallow depth. The presence of this layer makes the subgrade response nonlinear, as the SLOPE value shows.

TABLE 5 PAVEMENT MATRIX USED FOR SIMULATED DEFLECTION BASIN GENERATION

	FACTORS							
LEVELS	T_{AC} (in)	T_{AB} (in)	T_{SM} (in)	D (in)	E_{AC} (ksi)	E_{AB} (ksi)	E_{SM} (ksi)	E_{SG} (ksi)
(1) LOW	3.0	4.0	9.0	120	100	15	10	3
(2) MED	6.0	4.0	12.0	240	450	30	20	7
(3) HIGH	10.0	6.0	18.0	s-i	850	50	30	14

Note: 1) D: Depth to Rigid Layer, s-i: semi-infinite subgrade

2) AC: Asphalt Concrete, AB: Aggregate Base, SM: Select Material/ Subbase, SG: Subgrade

TABLE 6 SUMMARY STATISTICS FOR SLOPE FOR PAVEMENTS WITH SEMI-INFINITE SUBGRADE

Pavement Type	Statistic	SLOPE
Weak (3"AC)	Mean	2.83
	Std. Dev.	0.807
	C.V.(%)	37.0
	Range	0.22 - 4.47
Medium (6"AC)	Mean	3.41
	Std. Dev.	1.40
	C.V.(%)	64.0
	Range	-0.65 - 7.27
Stiff (10"AC)	Mean	2.69
	Std. Dev.	2.24
	C.V.(%)	101.0
	Range	-3.16 - 7.8

TABLE 7 TEST SITES AND PAVEMENT TYPES

Site	Location	Route	Mile Post	Pavement Type
1	Benson	I10W	300.07	5-layer
3	Winslow	I40E	260.21	4-layer
4	Minnetonka	I40E	261.78	4-layer
5	Dead River	I40E	317.06	4-layer
6	Flagstaff	I17N	337.00	4-layer
7	Crazy Creek	I40E	323.78	4-layer
9	Sunset Point	I17N	251.41	5-layer
10	Seligman	I40W	131.71	4-layer
12	Benson East	I10W	303.00	4-layer
14	Jacob Lake	US89AN	578.00	4-layer
18	Morristown	US60W	120.00	4-layer
19	McNary	US260E	369.00	5-layer
20	Kingman	I40E	59.00	4-layer

However, a negative SLOPE value should be treated with caution. Positive nonlinearity, evident from the negative SLOPE value, might indicate that the pavement is too stiff to apply the "surface modulus" concept and that the remote deflection sensors should be moved further away from the load.

VERIFICATION WITH FIELD DATA

The recommended values of SLOPE for detection of a rigid bottom were tested by using FWD deflection data for the Arizona pavements given in Tables 7 and 8. Table 9 shows the results of the analysis. The method accurately predicted the presence of a rigid layer in almost all cases. Of the 22 deflection basins evaluated, 19 were correctly classified with respect to the rigid bottom determination. This is acceptable because of the empirical nature of the approach. Site 7/1 was identified as having semi-infinite subgrade, and the depth of the rigid layer computed by manual matching was 300 in. Because this pavement has an AC thickness of 8.0 in. with a 6-in. cement-treated base, 300 in. of subgrade can be interpreted as a semi-infinite subgrade.

DETERMINATION OF DEPTH OF RIGID BOTTOM

As defined earlier, the depth of the rigid layer refers to the depth of a stiff layer below the subgrade. The subgrade modulus is assumed to reflect the composite modulus or equivalent

TABLE 8 LAYER TYPE AND THICKNESS AT DIFFERENT SITES

Site/ Sta	Layer 1		Layer 2		Layer 3		Layer 4		Layer 5	
	Mat	Thk (in)	Mat	Thk (in)	Mat	Thk (in)	Mat	Thk (in)	Mat	Thk (in)
1/1	AC	7	BS	2.5	AB	2	SB	12	SC-SM*	
3/1	AC	12	BTB	3	SB	5	SM*	-	-	-
4/1	AC	11.5	BTB	2	SB	3	SM*	-	-	-
5/1	AC	8	CTB	4.5	SB	7	SM*	-	-	-
6/1	AC	9	AB	4	SB	12	-	-	-	-
7/1	AC	8	CTB	6	SB	6	SM*	-	-	-
9/1	AC	6	BS	4	SB	26	SGS	6	CL-CH*	-
10/1	AC	6	AB	6	SB	24	CH*	-	-	-
12/1	AC	6	AB	6	SB	18	SC-SM*	-	-	-
14/1	AC	9	BS	4	AB	4	SC-CH*	-	-	-
18/1	AC	4.25	AB	4	SB	15	-	-	-	-
19/1	AC	4.8	BS	2.2	AB	3	SB	6		
20/1	AC	9.5	AB	4	SB	15	-	-		

* Subgrade Classification based on Unified Method.
Note: AC: Asphalt Concrete, BS: Bituminous Surface, BTB: Bituminous Treated Base, CTB: Cement Treated Base, AB: Aggregate Base, SGS: Subgrade Seal, SB: Sub Base (Select Material)

TABLE 9 RESULTS OF USING SLOPE TO DETECT RIGID BOTTOM (FWD DEFLECTION DATA)

Site/Sta	T_{AC}(in)	SLOPE(%)	Rigid Bottom[1]	D^2(in)
1/1	7.0	10.00	YES	140
3/1	12.0	-7.37	YES	S.inf
3/7	12.5	2.86	NO	S.inf
4/1	11.5	2.86	NO	S.inf
5/1	8.0	20.00	YES	85
5/4	8.0	17.89	YES	82
6/1	9.0	20.00	YES	60
7/1	8.0	3.23	NO	300
7/4	6.25	0.69	NO	S.inf
9/1	6.0	15.29	YES	72
10/1	6.0	12.70	YES	S.inf
10/7	6.5	0.80	NO	S.inf
12/1	6.0	7.69	YES	100
14/4	9.0	7.57	YES	120
18/1	4.25	0.0	NO	S.inf
18/4	4.25	6.15	YES	120
19/1	4.8	8.15	YES	240
19/4	4.8	10.93	YES	240
20/1	9.5	-2.58	YES	150

[1] Rigid bottom detected based on the value of SLOPE

[2] Values are after Mamlouk et al. (9)

modulus of the materials between the bottom of the pavement structure and the rigid layer. The moduli of the pavement layers above the subgrade do not contribute much toward the deflections measured at the outermost sensors (*7*). Again, deflections at the sixth and seventh sensor locations calculated from elastic layer theory are highly affected by the presence of a rigid layer at a shallow depth, as shown in Table 10. Thus, when finding the depth of rigid layer corresponding to an equivalent subgrade modulus, estimated values from regression equations can be assigned to the upper layer moduli (*14*).

The thickness of subgrade can be found by minimizing the error between the measured and calculated deflection values at the sixth and seventh sensor locations. An objective function can be defined as

$$\text{minimize } f = \sum_{i=1}^{n} W_i[(\Delta_i^m - \Delta_i^c)/\Delta_i^m]^2 \tag{4}$$

with

$$D^L \leq D \leq D^U$$

where

f = squared error,
W_i = weighting factor for Sensor i (1 for Sensor 6 and 2 for Sensor 7),
Δ_i^m = measured deflection at Sensor i,
Δ_i^c = calculated deflection at Sensor i,
D = thickness of the subgrade,
D^L = lower limit of thickness of the subgrade,
D^U = upper limit of thickness of the subgrade, and
n = number of sensors = 2 (i.e., the sixth and seventh).

TABLE 10 EFFECT OF RIGID BOTTOM ON SIMULATED DEFLECTION VALUES

Pavement Type	D (in.)	Difference in Deflections for Sensor No.(%) 1	2	3	4	5	6	7
Weak	360*	0	0	0	0	0	0	0
	180	6	9	8	15	22	29	37
	60	20	26	40	59	78	95	-
Medium	360*	0	0	0	0	0	0	0
	180	9	15	9	15	20	24	29
	60	37	31	40	51	62	72	82
Stiff	360*	0	0	0	0	0	0	0
	180	8	23	10	15	21	24	27
	60	42	39	36	47	55	61	68

* Deflections corresponding to D = 360 in. have been taken as standards.

Equation 4 can be rewritten as

$$\text{minimize } f = \sum_{i=1}^{n} W_i(1 - \Delta_i^c/\Delta_i^m)^2 \tag{5}$$

with

$$D^L \leq D \leq D^U$$

Equation 5 is minimized by OPTECH (*15*), a powerful and efficient gradient-based technique for constrained nonlinear function optimization that converges rapidly and uses both function and gradient of the function information.

Because the effect of subgrade modulus on the sixth and seventh sensor deflection values is significant, an accurate estimation of subgrade modulus is required before calculating the thickness of the subgrade or depth of the rigid layer. Two approaches were investigated for estimating the equivalent subgrade modulus: (*a*) empirical study of simulated deflection basins and (*b*) correlation with the resistance or R values of subgrade soils determined in the laboratory (AASHTO T190).

Empirical Study of Simulated Deflection Basins

Uddin et al. (*6*) estimated the subgrade modulus from the fifth sensor deflection of the Dynaflect, and Ullidtz (*7*) estimates subgrade modulus with the seventh sensor deflection value of the Dynatest FWD, which is valid only for semi-infinite subgrade. Because the deflection value measured by the seventh sensor is very small in magnitude, a small variation in measurement at this location results in a large error in the estimation of subgrade modulus (*7*). In this study, an exponential curve of the form $Y = Ae^{BX}$ was fitted to deflection basins consisting of all seven sensor deflections. Y is the deflection in mils, and X is the radial distance from the load in inches. A and B are the regression constants that define the shape of the deflection basin (*14*). The A and B values were computed over 6,000 simulated deflection basins from elastic layer analysis, and regression equations were developed for estimating subgrade modulus from A and B. Because, depending on the pavement type, 70 to 95 percent of the total surface deflections are contributed by the subgrade layer (*12*), the estimation of subgrade modulus from the parameters A and B is more rational than using a single sensor deflection value.

The pavements used in the development of regression equations for subgrade modulus were those described in Table 5. Separate equations were developed for subgrades with finite and infinite thickness. The equations were developed by stepwise forward multiple linear regression using STATPAK (*16*). The logarithm of the subgrade modulus was the dependent variable, and A and B were the independent variables. A log transformation of A was used to achieve linearity in the relationship.

The equation for pavements with finite subgrade thickness is

$$y = 4.508 - 0.986\log_{10}A - 19.896B \qquad R^2 = 0.89$$

$$\text{Esubgrade} = 10^y \qquad n = 4{,}374 \tag{6}$$

For infinite subgrade thickness, the equation is

$$y = 4.639 - 1.019\log_{10}A - 24.467B \qquad R^2 = 0.994$$

$$\text{Esubgrade} = 10^y \qquad n = 2{,}187 \tag{7}$$

Correlation with Laboratory Resistance or *R* Values of Soil

The ADOT *Preliminary Engineering Design Manual* (*17*) estimates the subgrade modulus with the equation

$$\text{Esubgrade} = \frac{[1{,}815 + 225(\text{Rmean}) + 2.40(\text{Rmean})^2]}{0.6(\text{SVF})^{0.6}} \tag{8}$$

In Equation 8, SVF is the seasonal variation factor and

$$\text{Rmean} = \frac{\text{Nt Rt } \sigma c^2 + \text{Nc Rc } \sigma t^2}{\text{Nt}\sigma c^2 + \text{Nc}\sigma t^2}$$

where

Nt = number of actual *R* values,
Nc = number of correlated *R* values (from PI and percentage of material passing a No. 200 sieve),
Rt = mean of the actual *R* values,
Rc = mean of the correlated *R* values,
σt = standard deviation of the actual *R* values, and
σc = standard deviation of the correlated *R* values.

Calculation Scheme

The calculation scheme to find the depth of the rigid layer corresponding to an estimated subgrade modulus is as follows:

1. FWD-measured deflections are normalized to a 9,000-lb load assuming linear response of the subgrade, and an exponential curve of the form $Y = Ae^{BX}$ is fitted to the deflection basin.
2. The subgrade modulus is calculated both by the regression equations involving *A* and *B* and the *R*-value approach. The layer moduli of other layers are calculated from appropriate regression equations from Table 11. An initial estimate of subgrade thickness is 240 in.
3. CHEVRON is used to compute the theoretical surface deflection at each sensor location corresponding to the FWD test load, and the objective function (f^{old}) is calculated corresponding to the FWD-measured deflection values.
4. The thickness of the subgrade is perturbed by an amount ΔD, the deflections are again calculated by using CHEVRON, and a new value of the objective function (f^{new}) is computed.
5. The gradient of the objective function is computed by the following formula:

$$\partial f/\partial D = (f^{\text{new}} - f^{\text{old}})/\Delta D$$

6. The gradient and thickness values are fed into an optimization routine (OPTECH), which estimates a new thickness value corresponding to the minimized objective function.

TABLE 11 REGRESSION EQUATIONS FOR ESTIMATING PAVEMENT LAYER MODULI

Layer	Equation for Modulus (psi)	R^2	Ref.
AC	$E = 1{,}377{,}559\text{-}49{,}389\ t_{ac}\text{-}7{,}868\ t_{sb}\text{-}1.02\ E_{sg}\text{-}25{,}470\ d_1$	0.71	14
(for finite subgrade)			
	$E = -254{,}809\text{-}13{,}761.5\ t_{ac} + 26.33\ E_{sg} + 12{,}192.54\ d_1$	0.74	14
(for infinite subgrade)			
	$90{,}0000 \le E \le 1{,}500{,}000$		
CTB, BTB, BS	$E = 388{,}522\text{-}8023\ t_{sb}\text{-}9701\ d_1$	0.74	14
	$60{,}000 \le E \le 450{,}000$		
AB	$E = E_{sm}\ (1 + 10.52\ \text{Log}(t_{ab})\text{-}1.56\ \text{Log}(E_{sm})\ \text{Log}(t_{ab}))$	-	18
	$10{,}000 \le E \le 2\ E$ (calculated)		
SM	$E = E_{sg}\ (1 + 7.18\ \text{Log}(t_{subbase})\text{-}1.56\ \text{Log}(E_{sg})\ \text{Log}(t_{sm}))$	-	18
	$10{,}000 \le E \le 2\ E$ (calculated)		

Note: AC: Asphalt Concrete, BS: Bituminous Surface, BTB: Bituminous Treated Base, CTB: Cement Treated Base, AB: Aggregate Base, SM: Select Material, t: thickness (in); d_1: FWD First sensor deflection (mils).

7. Steps 4 through 6 are repeated until the objective function stabilizes or the calculated thickness value in successive iterations does not change by more than 5 percent. The thickness value corresponding to the minimized objective function is the calculated depth of the rigid bottom.

Figure 6 shows a flowchart of the calculation scheme. This scheme and the rigid layer detection procedure have been coded in the computer program Arizona Deflection Analysis Method (ADAM). Convergence of the objective function usually requires three to five iterations on a Digital VAX 6000-410 machine. A typical rigid bottom detection and determination scheme usually requires 30 to 70 sec of CPU time. The program is coded in ANSI FORTRAN77 and should work on microcomputers.

ANALYSIS WITH FIELD DATA

The procedure for determining the depth of the rigid layer was tested with the FWD deflection data for the sites in Table 7. The subgrade moduli were computed by using Equations 6 or 7 and Equation 8. Table 12 shows the subgrade modulus and the depth of the rigid layer computed by ADAM and by manual matching of the deflection basins (*9*). In most cases the modulus of the subgrade and the depth of the rigid layer determined from A and B in this study agree well with those computed by manual matching. The calculation scheme developed in this study appears to have captured the "intelligence" in the manual matching of deflection basins.

The subgrade modulus computed from the R values of the subgrade soil and the corresponding depth of the rigid layer are not in good agreement with those from manual matching. The modulus of the subgrade is a measure of the elasticity of the material, whereas the R value is an index value representing the deformation of the material under certain prescribed conditions. The correlation between the two cannot be expected to be good in all cases, because these properties are not directly related to each other. In addition, the laboratory R-value determination is done on a small amount of disturbed subgrade material, whereas the composite subgrade modulus from backcalculation represents a large volume of undisturbed material (*9*).

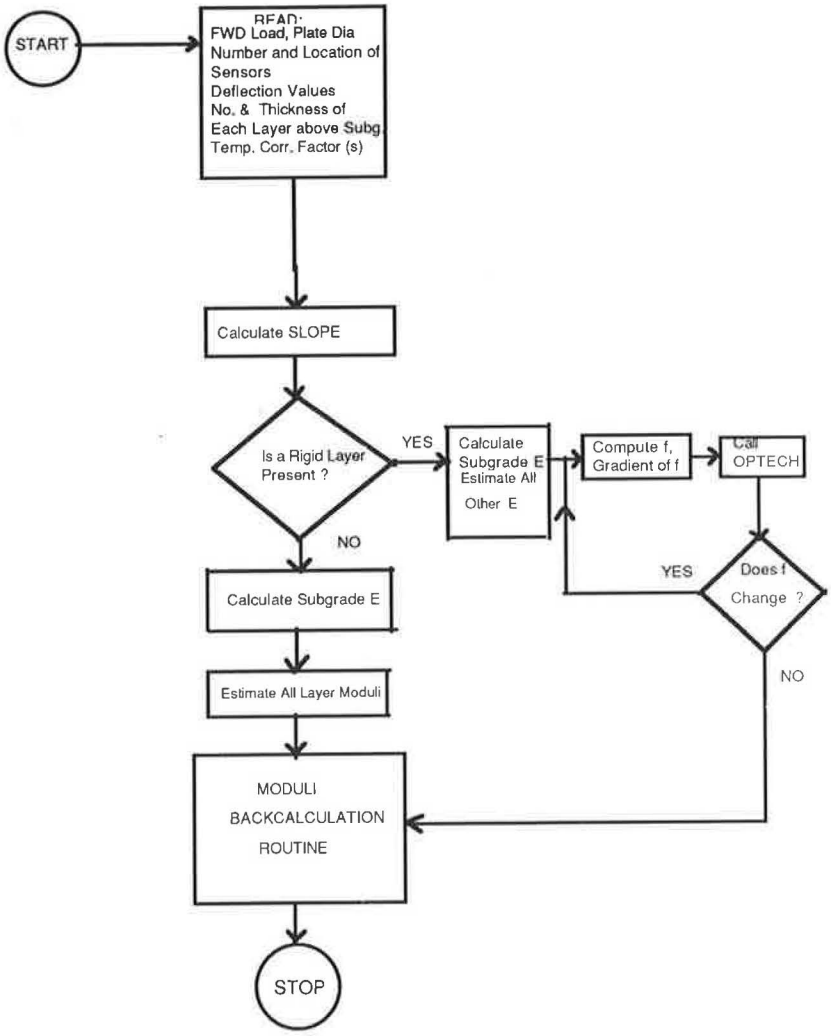

FIGURE 6 Flowchart of rigid layer detection and depth estimation scheme.

TABLE 12 COMPARISON OF SUBGRADE MODULI AND THICKNESSES CALCULATED BY ADAM WITH THOSE COMPUTED FROM MANUAL MATCHING OF DEFLECTION BASINS

Site/Station	Regression Eqn. Esg (ksi)	Regression Eqn. D (in)	"R"-Value Eqn Esg (ksi)	"R"-Value Eqn D (in)	Manual Matching* Esg (ksi)	Manual Matching* D (in)
1/1	18.8	124	20.0	131	18.0	140
3/7	18.4	s-inf	12.2	195	20.0	s-inf
4/1	18.9	s-inf	5.2	69	20.5	s-inf
5/4	12.5	143	31.6	s-inf	7.0	82
6/1	14.8	128	-	-	6.5	60
7/4	12.4	s-inf	20.2	s-inf	13.5	s-inf
9/1	12.0	126	6.6	73	8.5	72
10/4	7.6	165	-	-	10.0	240
10/7	15.9	s-inf	-	-	16.0	s-inf
12/1	13.7	135	22.4	300	10.5	100
14/4	24.9	146	5.7	56	25	120
18/1	48.5	s-inf	30.5	251	50	s-inf
18/4	4.7	150	-	-	22	120
19/1	7.8	150	-	-	10	240
19/4	8.7	150	-	-	11	240
20/1	29.8	127	36.4	150	45	150

* After Mamlouk et al. (9)

TABLE 13 COMPARISON OF CALCULATED DEPTH OF RIGID BOTTOM WITH DRILLING AND CONE PENETRATION RESULTS

Site/ Station	Regr. Eqn. Depth (in)	R-val. Eqn. Depth (in)	Manual* Matching Depth (in)	Drilling & Cone Results** (in)
1/1	124	131	140	Drilling stopped @ 300. Cone Refusal at: >180.
3/7	s-inf	s-inf	s-inf	Drilling stopped @ 300. Cone pen. stopped @ 300.
4/1	s-inf	69	s-inf	Drilling stopped @ 144. Cone pen. stopped @ 144. Presence of Ground Water.
5/4	143	s-inf	82	Drilling stopped @ 300 Cone refusal @ 72.
6/1	128	-	60	None
7/4	s-inf	s-inf	s-inf	Drilling stopped @ 300 Cone refusal @ 120.
9/1	126	73	72	Drilling stopped @ 60 Cone refusal @ 60. Basalt at 60 in.
10/4	165	-	240	Drilling stopped @ 300 Cone refusal @ 144.
10/7	s-inf	-	s-inf	None
12/1	135	300	100	Drilling stopped @ 300. Cone Refusal @ 300 Vry hrd drill: 120-300.
14/4	146	56	120	Drilling stopped @ 90. Cone refused @ 90. Limestone at 90 in.

* After Mamlouk et al. (9)
** After project HPR-PL-1(33) Item 254, Rational Characterization of Pavement Structures Using Deflection Analysis, Arizona Department of Transportation.

Table 13 compares the depths of the rigid layers, or subgrade thicknesses, computed in this study with the drilling and cone penetration test results obtained on several existing pavement subgrades in Arizona (*9*). The manual matching and modulus from the *R*-value approach predicted the existence of a rigid rock layer fairly accurately for Sites 9 and 14. However, when the results of calculations for all the sites are considered, it is evident that no set of calculated depths is in excellent agreement with the drilling and penetration results.

Because both subgrade modulus and thickness determine the surface deflections of the outermost sensors, the ADAM results indicate a compensating effect compared with manual matching. In other words, if the subgrade modulus is lower than the manual matching values, there is a corresponding decrease in subgrade thickness. The subgrade moduli calculated corresponding to *A* and *B* and the corresponding depths of the rigid layer are in good agreement with the manual matching procedure.

SUMMARY

A method has been developed for detection and determination of the depth of a rigid layer from an empirical study of the simulated deflection basins from elastic layer theory. The method uses the outermost sensor deflections from FWD testing. It has been verified with field data and shown to be accurate for practical purposes in predicting the presence of a rigid layer at a shallow depth below the pavement. Agreement with a manual matching method was also observed. On the basis of the algorithm for this method, a computer program, ADAM, was developed for detection and estimation of the depth of a rigid layer. The program has been implemented on a Digital VAX 6000-410 mainframe.

REFERENCES

1. B. F. McCullough and A. Taute. Use of Deflection Measurements for Determining Pavement Material Properties. In *Transportation Research Record 852*, TRB, National Research Council, Washington, D.C., 1982, pp. 8–15.
2. A. J. Bush III and D. R. Alexander. Pavement Evaluation Using Deflection Basin Measurements and Layered Theory. In *Transportation Research Record 1022*, TRB, National Research Council, Washington, D.C., 1985, pp. 16–22.
3. G. Wiseman, J. Greenstein, and J. Uzan. Application of Simplified Layered System to NDT Pavement Evaluation. In *Transportation Research Record 1022*, TRB, National Research Council, Washington, D.C., 1985, pp. 29–36.
4. M. S. Mamlouk. Use of Dynamic Analysis in Predicting Field Multilayer Pavement Moduli. In *Transportation Research Record 1043*, TRB, National Research Council, Washington, D.C., 1985, pp. 113–120.
5. B. E. Sebaaly. *Dynamic Models for Pavement Analysis*. Ph.D. dissertation. Department of Civil Engineering, Arizona State University, Tempe, 1987.
6. W. Uddin, A. H. Meyer, W. R. Hudson, and K. H. Stokoe II. *A Structural Evaluation Methodology for Pavements Based on Dynamic Deflections*. Research Report 387-1. Center for Transportation Research, University of Texas at Austin, Austin, 1985.
7. P. Ullidtz. *Pavement Analysis*. Elsevier, New York, 1987.
8. J. I. Yazdani and T. Scullion. Comparing Measured and Theoretical Depth Deflections Under a Falling Weight Deflectometer Using a Multidepth Deflectometer. In *Transportation Research Record 1260*, TRB, National Research Council, Washington, D.C., 1990, pp. 216–225.
9. M. S. Mamlouk, W. N. Houston, S. L. Houston, and J. P. Zaniewski. *Rational Characterization of Pavement Structures Using Deflection Analysis*. Report FHWA-AZ87-254, Vol. 1. Center for Advanced Research in Transportation, Arizona State University, Tempe, 1988.
10. L. J. Painter. *CHEVRON N-Layer Program—Improved Accuracy*. California Research Corporation, Richmond, Calif., 1980.
11. F. W. Jung. Interpretation of Deflection Basin for Real-World Materials in Flexible Pavements. Presented at 69th Annual Meeting of the Transportation Research Board, Washington, D.C., 1990.
12. E. J. Yoder and M. W. Witczak. *Principles of Pavement Design*, 2nd ed. John Wiley and Sons, Inc., New York, 1975.
13. D. A. Kasianchuck and G. H. Argue. A Comparison of Plate Load Testing with the Wave Propagation Technique. *Proc., 3rd International Conference on the Structural Design of Flexible Pavements*, London, 1972, pp. 444–454.
14. A. S. M. M. Hossain. *Deflection Analysis of Flexible Pavements Using Nondestructive Test Data*. Ph.D. dissertation. Department of Civil Engineering, Arizona State University, Tempe, 1990.
15. S. D. Rajan. *A User's Guide to OPTECH*. Technical Report. Department of Civil Engineering, Arizona State University, Tempe, 1985.
16. *STATPAK User Guide*. Northwest Analytical, Inc., Portland, Oreg., 1983.
17. *Materials Preliminary Engineering Design Manual*, 3rd ed. Arizona Department of Transportation, Phoenix, 1989.
18. J. P. Zaniewski, W. R. Hudson, S. B. Seeds, and L. Moser. *Pavement Performance Model Development*. Report FHWA/RD-84/103, Vol. 2. ARE Inc., Austin, Tex., 1984.